AMAP Assessment 2015:
Methane as an Arctic climate forcer

AMAP

Arctic Monitoring and Assessment Programme (AMAP)

AMAP Assessment 2015:
Methane as an Arctic climate forcer

AMAP Assessment 2015: Methane as an Arctic climate forcer

MIX
Paper from
responsible sources
FSC
www.fsc.org   FSC™ C010651

Acknowledgments

Contents

Preface

This assessment report presents the results of the 2015 AMAP Assessment of Methane as an Arctic climate forcer. This is the first AMAP assessment dealing with this issue and complements a second assessment of black carbon and tropospheric ozone as Arctic climate forcers.

The Arctic Monitoring and Assessment Programme (AMAP) is a group working under the Arctic Council. The Arctic Council Ministers have requested AMAP to:

- produce integrated assessment reports on the status and trends of the conditions of the Arctic ecosystems;
- identify possible causes for the changing conditions;
- detect emerging problems, their possible causes, and the potential risk to Arctic ecosystems including indigenous peoples and other Arctic residents; and to
- recommend actions required to reduce risks to Arctic ecosystems.

This report provides the accessible scientific basis and validation for the statements and recommendations made in the *Summary for Policy-makers: Arctic Climate Issues 2015* report[i] that was delivered to Arctic Council Ministers at their meeting in Iqaluit, Canada in April 2015. It is also the basis for a related AMAP State of the Arctic Environment report *Arctic Climate Issues 2015: Overview*[ii] . It includes extensive background data and references to the scientific literature, and details the sources for figures reproduced in the overview report. Whereas the Summary for Policy-makers report contains recommendations that focus mainly on policy-relevant actions concerned with addressing short-lived climate forcers, the conclusions and recommendations presented in this report also cover issues of a more scientific nature, such as proposals for filling gaps in knowledge, and recommendations relevant to future monitoring and research work.

This assessment of methane as an Arctic climate forcer was conducted between 2012 and 2014 by an international group of over 40 experts. Lead authors were selected based on an open nomination process coordinated by AMAP. A similar process was used to select international experts who independently reviewed this report.

Information contained in this report is fully referenced and based first and foremost on peer-reviewed and published results of research and monitoring undertaken since 2010. It also incorporates some new (unpublished) information from monitoring and research conducted according to well-established and documented national and international standards and quality assurance/quality control protocols. Care has been taken to ensure that no critical probability statements are based on non-peer-reviewed materials.

Access to reliable and up-to-date information is essential for the development of science-based decision-making regarding ongoing changes in the Arctic and their global implications.

The methane assessment summary reports[i, ii] have therefore been developed specifically for policy-makers, summarizing the main findings of the assessment. The methane assessment lead authors have confirmed that both this report and its derivative products accurately and fully reflect their scientific assessment. The methane assessment reports are freely available from the AMAP Secretariat and on the AMAP website: www.amap.no, and their use for educational purposes is encouraged.

AMAP would like to express its appreciation to all experts who have contributed their time, efforts and data, in particular the lead authors who coordinated the production of this report. Thanks are also due to the reviewers who contributed to the methane assessment peer-review process and provided valuable comments that helped to ensure the quality of the report. A list of contributors is included in the acknowledgements at the start of this report and lead authors are identified at the start of each chapter. The acknowledgements list is not comprehensive. Specifically, it does not include the many national institutes, laboratories and organizations, and their staff, which have been involved in various countries in methane-related monitoring and research. Apologies, and no lesser thanks are given to any individuals unintentionally omitted from the list.

The support from the Arctic countries and non-Arctic countries implementing research and monitoring in the Arctic is vital to the success of AMAP. The AMAP work is essentially based on ongoing activities within these countries, and the countries that provide the necessary support for most of the experts involved in the preparation of the AMAP assessments. In particular, AMAP would like to acknowledge Canada and the United States for taking the lead country role in this assessment and thank Canada, Norway and the Nordic Council of Ministers for their financial support to the methane assessment work.

The AMAP Working Group is pleased to present its assessment to the Arctic Council and the international science community.

Marjorie Shepherd (Methane Assessment Co-lead, Canada)

J. Michael Kuperberg (Methane Assessment Co-lead, USA)

Morten Olsen (AMAP Chair, April 2015)

Lars-Otto Reiersen (AMAP Executive Secretary)

Oslo, September 2015

---

i. AMAP, 2015. Summary for Policy-makers: Arctic Climate Issues 2015. Arctic Monitoring and Assessment Programme (AMAP), Oslo, Norway. 16 pp.

ii. AMAP, 2015. Climate Issues 2015: Overview report. Arctic Monitoring and Assessment Programme (AMAP), Oslo, Norway. 16 pp.

1. Introduction

Authors: Elizabeth Bush, Mike Kuperberg, Marjorie Shepherd

1.1 Background

This chapter sets out the context and motivation for undertaking this assessment of methane and the Arctic climate, and provides a guide for readers to the chapters that follow. The overarching context for this assessment is the concern of Arctic nations for the consequences of the large and rapid changes in regional climate that are already underway – evident in observational records and projected to continue. This concern has resulted in two major assessments of Arctic climate change under the auspices of Arctic Council: *The Arctic Climate Impact Assessment* (ACIA 2005) and *Snow, Water, Ice and Permafrost in the Arctic (SWIPA): Climate Change and the Cryosphere* (AMAP 2011a). These assessments documented the widespread changes already occurring across the physical landscapes and ecosystems of the Arctic, and highlighted risks associated with the projected continuation and potential acceleration of observed changes if anthropogenic drivers of Arctic warming continue. An anthropogenic contribution to Arctic warming over the last 50 years has been established (Bindoff et al. 2013) and future scenarios of Arctic and global climate change generally assume additional emissions of anthropogenic greenhouse gases, although these emissions vary in timing and magnitude across scenarios. The challenges that future climate-related risks present to people living in the Arctic were also comprehensively described in the aforementioned Arctic assessment reports.

Reducing the rate and magnitude of Arctic warming during this century will require global comprehensive strategies to address the suite of greenhouse gases and other substances driving anthropogenic climate change. As is clear from Fig. 1.1 (Collins et al. 2013), carbon dioxide will dominate radiative forcing under a range of future scenarios, as it does currently, accounting for about 80–90% of total anthropogenic forcing in the year 2100. Carbon dioxide is the main persistent (long-lived[1]) greenhouse gas contributing to anthropogenic climate change and it is now well established that total cumulative emissions of carbon dioxide are the main determinant of long-term global warming (Collins et al. 2013). Therefore, reducing emissions of carbon dioxide is the backbone of any meaningful effort to limit global and Arctic warming. However, emissions of other substances also contribute substantially to present-day radiative forcing and as long as such emissions continue, these substances will continue to contribute to total radiative forcing and thus to global warming and associated climate changes (Fig. 1.1). Comprehensive climate-change mitigation would encompass strategies to reduce emissions of all climate forcing agents. Any ongoing anthropogenic methane emissions, for example, would elevate climate warming above that induced by carbon dioxide alone. Reducing emissions of methane (with an atmospheric lifetime of about a decade; see Ch. 2) and other substances with shorter atmospheric lifetimes than carbon dioxide (e.g. from days to decades) provides an opportunity to reduce radiative forcing in the near term (i.e. in the years immediately following the reduction in emissions) since atmospheric concentrations of short-lived substances can be lowered more quickly through emission reductions. The timescale of the response, in terms of lowering atmospheric concentrations, is dependent on the atmospheric lifetime of the particular substance (see Ch. 2). Indeed, it has already been shown that reducing emissions of methane and black carbon can help reduce projected global and Arctic warming in the near term (UNEP and WMO 2011; Shindell et al. 2012) and this work provided a foundation for the Arctic Council to initiate some targeted work directed towards understanding the role of short-lived climate forcers in Arctic climate and the potential benefits of mitigating such substances.

The Arctic Council, through its Arctic Monitoring and Assessment Programme (AMAP) working group, has undertaken scientific work directed at understanding the role of short-lived climate forcers in Arctic climate change, targeting black carbon, ozone and methane for focused study[2]. It is in this context that the Short-Lived Climate Forcers Expert Group on Methane (henceforth referred to as the Methane Expert Group) was established and tasked by AMAP to provide scientific information to inform methane mitigation planning by Arctic nations. The intent of this work is to better understand the contribution methane mitigation can make to reducing the rate of Arctic warming in the near term. Methane is a globally well-mixed greenhouse gas meaning levels of methane in the atmosphere are similar around the globe. In turn, this means that reductions in emissions anywhere contribute to reducing atmospheric methane levels. Assessing methane mitigation benefits will provide information about the ability of Arctic nations to influence methane levels, putting potential mitigation by Arctic nations in context with global methane mitigation potential.

Atmospheric methane levels are, however, influenced by natural as well as anthropogenic emission sources. Therefore, whether or not Arctic (and global) methane concentrations can be lowered depends not only on mitigation of anthropogenic methane sources but also on future changes in natural methane sources. In the Arctic, rising temperatures have the potential to enhance the release of methane from natural sources.

There are known to be very large reservoirs of methane and organic carbon in the Arctic Ocean seabed, and on land in the

1 Carbon dioxide is removed from the atmosphere through a variety of biogeochemical processes operating on different timescales. Some portion of emitted carbon dioxide stays in the atmosphere for millennia (Ciais et al. 2013).

2 AMAP established a Short-Lived Climate Forcer Expert Group in 2009. Initially, this group focused on understanding the role of black carbon in Arctic climate and produced an assessment report in 2011 (AMAP 2011b). The first expert group is now focusing on both black carbon and ozone while a second expert group, focusing on methane, has been established.
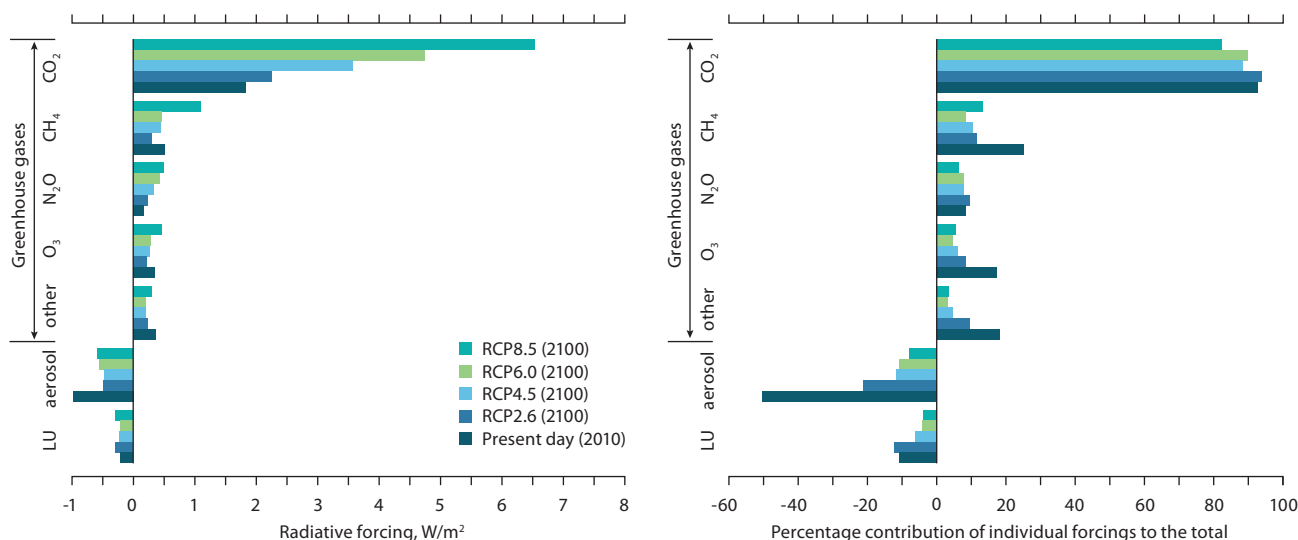
Fig. 1.1 The left-hand panel shows the contribution of individual anthropogenic forcings to the total radiative forcing in 2100 for four RCPs (representative concentration pathways[3]) and at present day. The individual forcings comprise: the greenhouse gases carbon dioxide (CO_2), methane (CH_4), nitrous oxide (N_2O), ozone (O_3) and others; aerosols; and land use (LU). The right-hand panel shows the individual forcings relative to the total radiative forcing (i.e. RF_x/RF_{tot}, with RF_x individual radiative forcings and RF_{tot} total radiative forcing). Adapted from Collins et al. (2013: fig. 12.3).

soils and lake sediments of the Arctic. Decomposition of the carbon in these reservoirs can lead to the emission of either carbon dioxide or methane, depending on the conditions under which decomposition occurs, with wet, anaerobic conditions favoring methane production (see Ch. 3). These reservoirs are contained (completely or partially) by ice, frozen soil and frozen sediment, and the surface–air exchange is partially mediated by ice cover. The Arctic Council led SWIPA report (AMAP 2011a; Callaghan et al. 2011) and other recent major scientific assessments (Ciais et al. 2013; NRC 2013) drew attention to the risks associated with warming, thawing and destabilizing of land and subsea permafrost in the Arctic, particularly with regard to the potential for enhanced fluxes of methane to the atmosphere. As methane is a powerful greenhouse gas, and given the sheer size of Arctic carbon reservoirs, there is a recognized potential for climatically significant methane emissions from the Arctic, which would represent a positive, amplifying feedback on the global climate system (i.e. warming increases methane emissions which in turn drive further warming…, and so on). While recent comprehensive reviews of the published literature have concluded that gradual rather than abrupt increases in Arctic methane emissions over the 21st century are more likely, with a moderate positive feedback on climate (Ciais et al. 2013; NRC 2013), these same studies also emphasized that scientific understanding of the topic is immature with many uncertainties about the controlling processes and timescales for enhanced methane releases from the ocean and land. In recognition of the status of this area of science as an emerging issue, the Methane Expert Group was also tasked to provide an in-depth report on potential future increases in methane from natural sources in the Arctic in response to projected regional warming. While such emissions are not under the direct control of Arctic nations, understanding the contributions of these sources to changing atmospheric methane levels will influence Arctic nations' ability to attribute reductions in atmospheric methane levels to any anthropogenic methane mitigation they, or other countries, may undertake.

This document is a report on the work completed by the Methane Expert Group in the two and a half years since its inception. The report is developed from a review of relevant literature as well as targeted scientific analyses designed to help fulfill the mandate of providing policy-relevant science advice to the Arctic Council, through AMAP, to inform discussions of actions on short-lived climate forcers. This work was directed at answering two major questions:

What is the potential benefit, in terms of reduced Arctic warming, of methane emissions mitigation by Arctic nations?

How does the magnitude of potential emission reductions from anthropogenic sources compare to potential changes in methane emissions from natural sources in the Arctic?

Clearly, future Arctic warming will be influenced not only by actions taken by Arctic nations to reduce anthropogenic emissions of methane and other climate forcers, but also by actions taken by the rest of the world. Therefore, it is important to understand the potential benefit of methane mitigation by Arctic nations in this larger context. While the methane mitigation potential of Arctic nations is put in context with global methane mitigation potential in this report, an integrated consideration of the benefits of mitigation measures in a multi-pollutant framework was outside the mandate of the Methane Expert Group. Similarly, it is recognized that there is also a larger context or backdrop to the question about natural methane emissions addressed by the group as major natural sources of methane also exist outside the Arctic, most notably in the tropics. Changes in natural methane emissions both within and outside the Arctic will respond to climate changes that ensue in response to total radiative forcing changes, driven primarily by carbon dioxide (see earlier). The focus on methane mitigation and on Arctic methane sources in this report reflects the task given to the Methane Expert Group and the expertise among its members.

---

3   The four RCPs are described in Ch. 5. In brief, these four scenarios were the basis for future climate change projections under the Coupled Model Intercomparison Project Phase 5 (CMIP5), with these projections featured in the Working Group I contribution to the IPCC Fifth Assessment (Collins et al. 2013c). The four RCPs span a range of potential future radiative forcing, from a high emission scenario (RCP8.5) to one that aims to limit global warming to about 2°C (RCP2.6).

1.2 The Arctic climate context: Past and future warming

To set the stage for the technical chapters that follow and to demonstrate the basis for concern about contemporary and future Arctic climate change, this section presents an updated estimate of recent Arctic warming and some illustrative maps of observed and potential future Arctic warming. It was not the intent to repeat the comprehensive analysis of Arctic climate undertaken as part of the AMAP SWIPA project (Overland et al. 2011b; Walsh et al. 2011). Previous analyses of long-term surface temperature data consistently show evidence of a strong amplification of warming in the Arctic region of about twice that of the rest of the world (Trenberth et al. 2007; Bekryaev et al. 2010; Overland et al. 2011a; Christensen et al. 2013; Jeffries and Richter-Menge 2013). Over the period 1950–2012, mean annual surface temperature (combined land and sea-surface temperatures) for the region north of 60°N has increased by about 1.6°C based on analysis of three data sets[4] (see Fig. 1.2). All three data sets indicate that warming has been strongest in spring (March–May), with mean increases in spring surface temperature of about 2°C (HadCRUT4: 1.95°C; GISS: 2.02°C; MLOST: 1.83°C). Warming in autumn (Sept–Nov) and winter (Dec–Feb) has been only slightly less than that observed over the spring season (data not shown), while the weakest warming has been during summer (June–Aug). Maps of the seasonal warming trends for winter and summer (1950–2012) based on the NASA GISS data set (which has greater coverage over Arctic land areas than the other two data sets due to the method of interpolation used to fill in data between monitoring stations) are shown in Fig. 1.3. Winter mean temperature has risen 2.01°C (90% confidence interval: 1.26–2.76°C); while summer mean temperature has risen only 1.10°C (90% confidence interval: 0.68–1.45°C).

Looking forward, robust features of global model projections of climate change over the 21st century include a continuation of the observed large-scale trends for the Arctic, with strong regional warming about twice the global mean increase in annual surface temperature and with seasonally strongest warming in autumn and winter and weakest warming in summer (Collins et al. 2013).

For illustrative purposes, selected maps (Fig. 1.4) of average projected temperature changes, relative to the period 1986–2005, have been drawn from the recently published Working Group I contribution to the Fifth Assessment Report of the Intergovernmental Panel on Climate Change (IPCC 2013c). The selection illustrates projected changes over high latitude areas under two contrasting scenarios. With the RCP2.6 scenario, global temperature has stabilized or is declining from peak level (depending on the model) by the latter decades of the 21st century, with a mean rise in global average surface temperature, relative to the reference period, of 1.0°C over the period 2081–2100. With the RCP8.5 scenario, global
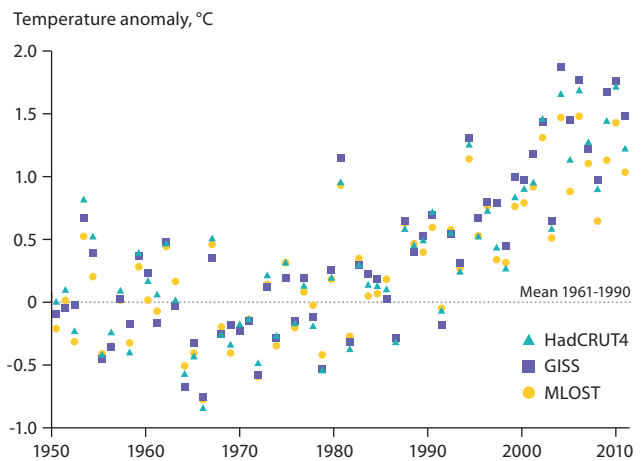
Fig. 1.2 Annual average combined land and sea-surface temperature anomalies, 1950–2012 (relative to the mean over 1961–1990) for the area north of 60°N for three data sets: the Hadley Centre and Climate Research Unit dataset (HadCRUT4), the NASA Goddard Institute for Space Studies dataset (GISS), and the National Atmospheric and Oceanic Administration merged land-ocean surface temperature dataset (MLOST). Trends (mean and 90% confidence intervals) over the 63-year period are 1.56°C (1.06–2.10°C) HadCRUT4; 1.73°C (1.15–2.32°C) GISS; and 1.46°C (1.06–1.83) MLOST.

temperature is still rising by the end of the century, with a mean rise in global average surface temperature of 3.7°C over the period 2081–2100. While average future Arctic warming under the RCP2.6 scenario appears to be roughly comparable in magnitude to that observed since 1950, the high greenhouse gas emission assumptions of scenario RCP8.5 are projected to lead to dramatic changes in regional climate.

To further illustrate the potential for changes across the Arctic landscape under future warming, Fig. 1.5 shows how the locations around the circumpolar North, where the average annual air temperature is zero degrees centigrade, shifts northward under future climate change scenarios. The diminishing size of the zero isotherm area over the progressively warmer climate scenarios, suggests regions where there is potential for permafrost degradation and release of carbon (as carbon dioxide or methane) from permafrost thaw, contributing to positive climate feedbacks. While permafrost distribution and thermal state are affected by other factors besides air temperature, and a wide variety of future permafrost states can be more rigorously diagnosed from climate models (e.g. Slater and Lawrence 2013), the figure is illustrative of the implications for natural ecosystem methane emissions (discussed in Ch. 3 and 4).

1.3 Report structure

There are significant challenges in acquiring and presenting an integrated understanding of the impact of changing methane emissions on Arctic climate. The approach taken in this report is to first present the group of chapters that deal with natural

---

4   This temperature analysis is based upon the Hadley Centre and Climate Research Unit dataset (HadCRUT4), the NASA Goddard Institute for Space Studies dataset (GISS), and the National Atmospheric and Oceanic Administration merged land-ocean surface temperature dataset (MLOST). Temperature anomalies in the three datasets are relative to different base periods. They are adjusted to a common base period 1961–1990 for time series plotting. The linear trend was computed using Mann-Kendall in combination with the Theil-Sen approach following Wang and Swail (2001) to account for auto-correlation in the time series. For robust trend analysis, selection criteria were applied such that only sites with at least 50 years of data over the 63-year period, and at least six months of each year or two months of each season are used to compute annual or seasonal averages. Environment Canada, Climate Research Division, August, 2014.

HadCRUT4 annual

GISS annual

NOAA MLOST annual

GISS summer

GISS winter

0   0.5   1   1.25 1.5 1.75 2   2.5   3   4

Observed temperature change, °C
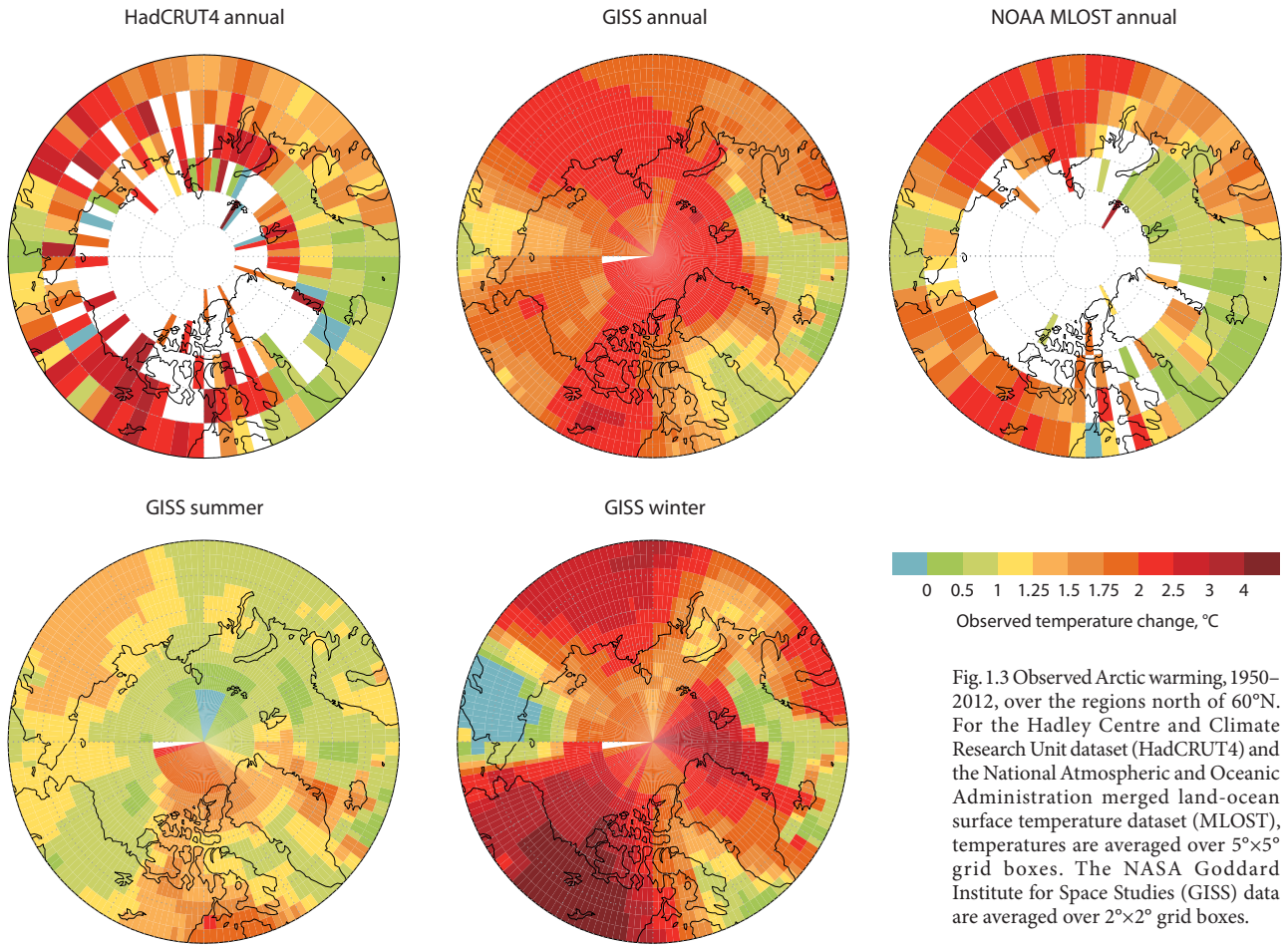
Fig. 1.3 Observed Arctic warming, 1950–2012, over the regions north of 60°N. For the Hadley Centre and Climate Research Unit dataset (HadCRUT4) and the National Atmospheric and Oceanic Administration merged land-ocean surface temperature dataset (MLOST), temperatures are averaged over 5°×5° grid boxes. The NASA Goddard Institute for Space Studies (GISS) data are averaged over 2°×2° grid boxes.

RCP2.6 Winter (DJF)

RCP2.6 Summer (JJA)

RCP8.5 Winter (DJF)

RCP8.5 Summer (JJA)

0   0.5   1   1.5   2   3   4   5   7   9   11

Projected temperature change, °C
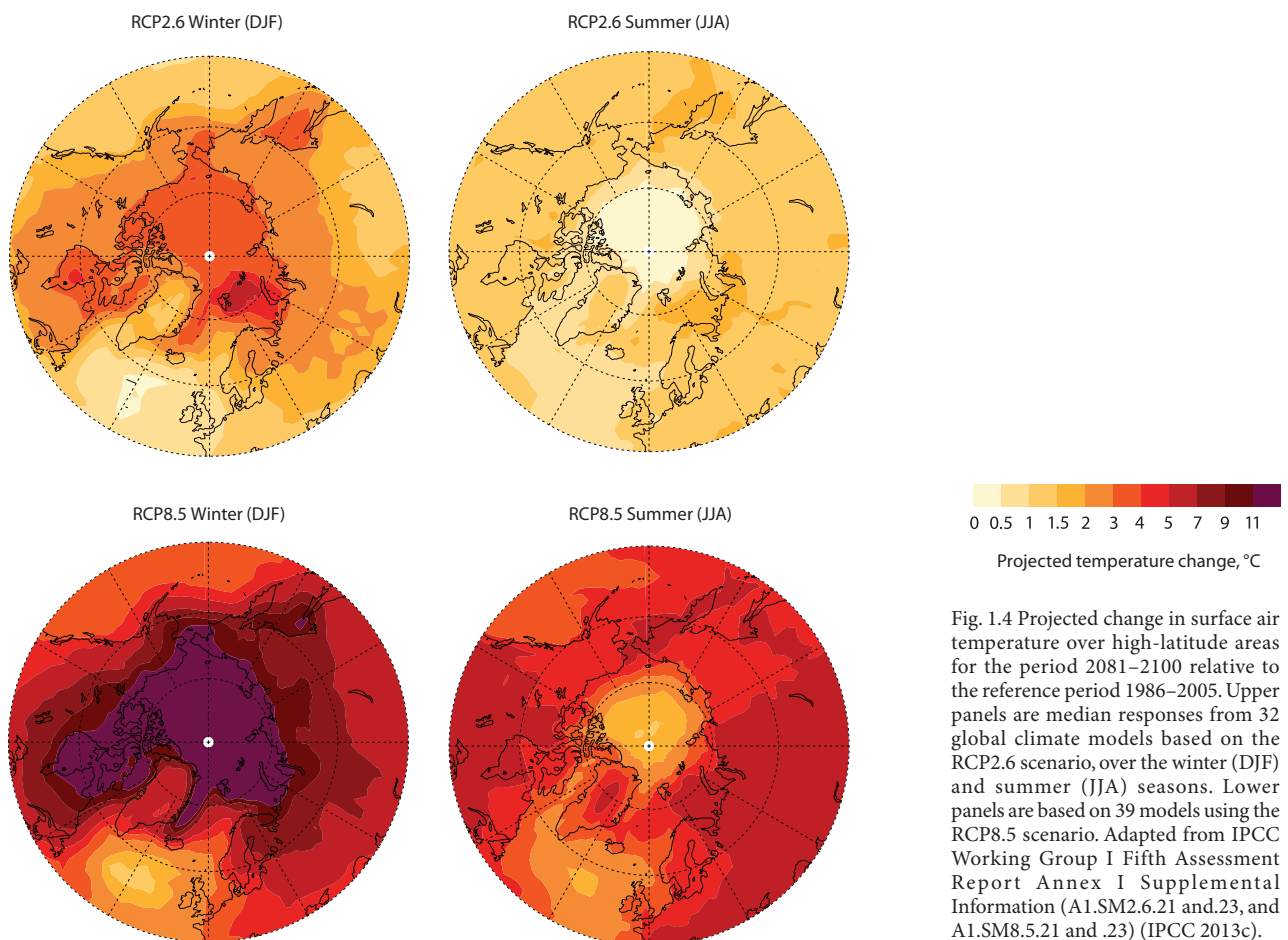
Fig. 1.4 Projected change in surface air temperature over high-latitude areas for the period 2081–2100 relative to the reference period 1986–2005. Upper panels are median responses from 32 global climate models based on the RCP2.6 scenario, over the winter (DJF) and summer (JJA) seasons. Lower panels are based on 39 models using the RCP8.5 scenario. Adapted from IPCC Working Group I Fifth Assessment Report Annex I Supplemental Information (A1.SM2.6.21 and.23, and A1.SM8.5.21 and .23) (IPCC 2013c).

Position of 0°C near-surface air temperature isotherm

— Historical (1996-2005)
— RCP2.6 (2081-2100)
— RCP8.5 (2081-2100)
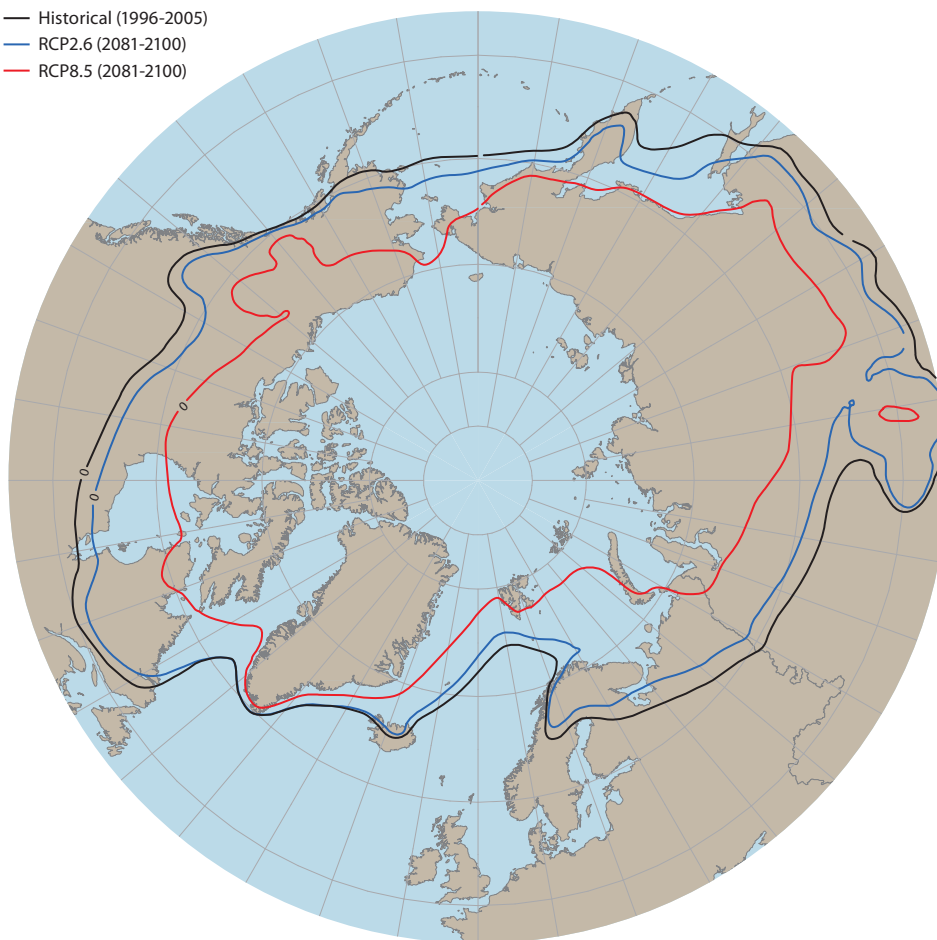
Fig. 1.5 The location of the zero degree near-surface air temperature isotherm for the historical 1996–2005 period and the future 2081–2100 period for the RCP2.6 and RCP8.5 scenarios. The zero degree isotherm is based on ensemble-mean annual air temperature simulated by 29 models (see below) that participated in the CMIP5 and averaged over the 10-year period centered on 2000 and 2090. Map created by Environment Canada's Climate Research Division, December, 2014.

The 29 models from which results are used are BNU-ESM, CCSM4, CESM1-CAM5, CESM1-WACCM, CNRM-CM5, CSIRO-Mk3-6-0, CanESM2, EC-EARTH, FGOALS-g2, FIO-ESM, GFDL-CM3, GFDL-ESM2G, GFDL-ESM2M, GISS-E2-H, GISS-E2-R, HadGEM2-AO, HadGEM2-ES, IPSL-CM5A-LR, IPSL-CM5A-MR, MIROC-ESM, MIROC-ESM-CHEM, MIROC5, MPI-ESM-LR, MPI-ESM-MR, MRI-CGCM3, NorESM1-M, NorESM1-ME, bcc-csm1-1, and bcc-csm1-1-m.

and anthropogenic methane sources, then present chapters that address atmospheric concentrations (as the atmosphere integrates emissions from all sources) and finally to present the results of modeling work that explicitly evaluates how changing sources will influence atmospheric concentrations and climate. As per the mandate to the Methane Expert Group, the scope of analysis is primarily Arctic-focused. While some AMAP assessments use a delineation of the Arctic region as defined by AMAP (land and marine areas north of the Arctic Circle, and north of 62°N in Asia and 60°N in North America, modified to include the marine areas north of the Aleutian chain, Hudson Bay, and parts of the North Atlantic Ocean including the Labrador Sea; AMAP 2011a, Fig. 1.1), for this assessment, no specific definition of an Arctic boundary was assumed and each chapter articulates boundaries suitable to the analysis within that chapter. Readers should note that while many of the chapters focus on the Arctic as a northern latitude region, where there is discussion of anthropogenic emissions of methane, the perspective is of Arctic nations as political entities, including all areas within their national borders. Given that methane is a global greenhouse gas, the technical chapters begin with an overview of the global methane budget (sources and sinks), and the role of methane as a greenhouse gas and climate forcer (Ch. 2). This provides essential background scientific information as well as the global context for understanding the subsequent chapters of the report, which are more Arctic focused. As Ch. 2 is provided for context, no key findings or conclusions are provided for that chapter.

Chapters 3 and 4 summarize current understanding of the natural processes that produce methane in Arctic environments and that may lead to enhanced emissions of methane from major terrestrial (Ch. 3) and marine (Ch. 4) sources. This work assesses the available published literature on these topics, drawing on both observational studies using flux measurements of methane to the atmosphere, and modeling studies. Emissions of methane from human activity are also changing and may also be contributing to recent changes in atmospheric methane levels. An assessment of available global methane emissions inventories is provided in Ch. 5 along with information specific to Arctic nations. In addition, Ch. 5 presents two scenarios of potential future anthropogenic methane emissions. One assumes no additional methane mitigation beyond existing legislation; the other is based on maximum technically feasible emission reductions with current abatement technologies. This scenario is global, but information specific to Arctic nations is extracted from the scenario.

Chapters 6 and 7 address the issue of how atmospheric concentrations of methane respond to changing emissions. Chapter 6 presents an overview of the current atmospheric methane monitoring network over the Arctic region. Data from these sites are then analyzed and combined with previously published information to characterize trends and changes in atmospheric methane levels over time, on seasonal and longer time scales. Isotopic and trajectory analyses are explored as potential tools for detecting changes in methane emissions

Table 1.1 Policy-relevant science questions guiding the work of the AMAP Methane Expert Group.

What is the potential benefit, in terms of reduced Arctic warming, of methane emissions mitigation by Arctic nations?

How does the magnitude of potential emission reductions from anthropogenic sources compare to potential changes in methane emissions from natural sources in the Arctic?

Chapters 3 & 4	Chapter 5	Chapters 6 & 7	Chapter 8	Various chapters
What are the current and potential future natural emissions from the Arctic region?	*What are the current and potential future anthropogenic emissions of Arctic and non-Arctic nations?*	*Are the current monitoring activities (of atmospheric concentrations and fluxes) sufficient to capture anticipated source changes?*	*What is the historical and future Arctic climate response to changes in methane emissions, from Arctic and from global sources?*	*What are the uncertainties in understanding the Arctic climate response to methane?*
What are the current methane emissions from Arctic terrestrial and marine sources?	*What are current global anthropogenic methane emissions, and those of Arctic nations?*	*What are the trends and variability in Arctic methane concentrations and what are the primary drivers of this variability?*	*What is the contribution of historical changes in global atmospheric methane to Arctic climate warming?*	*Related to anthropogenic emissions characterization/ quantification/projection?*
What are the controlling processes and factors that strongly influence natural emissions?	*How will the magnitude of emissions change in the future under different policy assumptions?*	*How much of a trend in atmospheric methane abundance can be detected with the current monitoring network?*	*What impact will increasing atmospheric concentrations of methane have on climate and will Arctic nations have the ability to influence that impact through mitigation of anthropogenic methane emissions?*	*Related to natural emissions characterization/ quantification/projection from terrestrial and marine sources?*
How may these emissions from natural sources in the Arctic change in the future?	*What percentage of global methane mitigation potential is controlled by Arctic Council nations?*	*Are emission estimates consistent with atmospheric concentrations?*	*How will atmospheric methane concentrations change in response to potential changes in natural methane emissions and how do these changes compare to those that might result from mitigation of anthropogenic methane emissions?*	*Related to climate response?*
What are the uncertainties or limitations in these estimates?	*What are the principal sources of uncertainty in these estimates of current and future anthropogenic emissions?*	*Is there evidence of increasing Arctic methane emissions in the atmospheric observations?*	*Does the location of anthropogenic methane emissions matter?*	*Related to measuring changes in atmospheric methane concentrations?*

from different sources. Chapter 7 more explicitly integrates information on both atmospheric methane levels and emissions by taking a top-down inverse modeling approach to assess the extent to which changes in atmospheric methane in the Arctic can be explained and reconciled with estimates of natural and anthropogenic emissions in the Arctic. This information is also used to assess whether or not the atmospheric observations provide any indication of a trend in Arctic methane emissions.

In Ch. 8, the importance of past and potential future changes in methane emissions or concentrations on Arctic climate are discussed. In particular, the results of dedicated climate modeling experiments using the emission estimates from Ch. 3, 4, and 5 are presented, aimed at answering the overarching questions posed to the Methane Expert Group. Earth System Models are used to evaluate the benefit of anthropogenic methane emissions abatement in terms of reduced global and Arctic warming. Scenarios of natural emission change, founded on the analyses in Ch. 3 and 4, are used to calculate resulting changes in atmospheric methane concentration, allowing an estimate of warming resulting from such changes.

Each of the chapters in this report address a number of more specific policy-relevant science questions than the overarching questions presented at the end of Sect. 1.1. As a guide to the scope of work undertaken as part of this assessment, and to where readers can find information of particular interest, these questions are presented in Table 1.1. Key findings that respond to the questions in Table 1.1 are presented at the end of each chapter, along with recommendations for ongoing scientific work needed to address gaps in understanding. Chapter 9 presents a synthesis of these key findings and science recommendations.

The report concludes with a detailed summary of the strategies used for modelling the climate response. This annex is a common

contribution to the AMAP assessments on methane (the present report) and black carbon and ozone (AMAP 2015) and has been produced to facilitate an integrated understanding of the separate climate modelling exercises undertaken by the two AMAP expert groups on short-lived climate forcers (SLCFs).

Acknowledgments

2. The global methane budget and the role of methane in climate forcing

Authors: David Plummer, Andrei Kiselev

2.1 Background

Methane is emitted into the atmosphere from a large variety of sources and removed from the atmosphere predominately by chemical reactions. Since the lifetime of methane is approximately nine years (Prather et al. 2012), it is relatively well mixed throughout the troposphere and a simple global budget can be constructed as:

$$\Delta B_{CH_4} = E_m - L \qquad \text{Eq. 2.1}$$

where ΔB_{CH4} is the change in the global amount of methane in the atmosphere, E_m is the global total of emissions and L is the global total of methane losses. As discussed in more detail in Sect. 2.3, observations of the atmospheric concentration of methane and estimates of the rate of loss allow for tightly constrained estimates of ΔB_{CH4} and L, respectively. Given these two terms and the associated uncertainties, the global total methane emission source can be constrained to approximately 10% (Prather et al. 2012). While the total emissions of methane are fairly well constrained, the division of the total among the individual sources and, in particular, the variability of individual sources and the contribution of changes in sources to the observed record of methane concentration is the subject of considerable research (e.g. Kai et al. 2011; Bergamaschi et al. 2013).

This chapter focuses primarily on the role of atmospheric chemistry in removing methane from the atmosphere, including current understanding of the magnitude and stability of this sink and the factors and mechanisms that influence it. A discussion of the radiative forcing of climate by methane is also presented, including the influence of methane on tropospheric ozone, through atmospheric chemical processes, that accounts for a significant component of the radiative forcing due to methane. Only a brief overview of the current understanding of the magnitude of different methane sources is presented here. The reader is referred to subsequent chapters for a more in-depth discussion on this topic.

2.2 Overview of natural and anthropogenic methane sources

The dominant sources of methane can be assigned to one of three categories – biogenic, thermogenic or pyrogenic. *Biogenic methane* is produced by micro-organisms during the decomposition of organic carbon in anaerobic (low oxygen) environments (e.g. natural wetlands, flooded rice fields, landfills, termites, guts of ruminant animals) as well as in some natural-gas formations. *Thermogenic methane*, produced on geological timescales when deposits of organic material are exposed to high heat and pressure to form fossil fuels, is released (vented or leaked) when natural gas, oil and coal are extracted, processed and transported. Thermogenic methane may also enter the

atmosphere through naturally occurring pathways such as seeps and mud volcanoes. For an overview of biogenic and thermogenic sources see Cicerone and Oremland (1988). *Pyrogenic methane* is produced by the incomplete combustion of organic matter and includes sources such as biofuel burning, agricultural fires and wildfires (Andreae and Merlet 2001). A fourth category, *abiogenic methane*, results from chemical reactions involving inorganic carbon in the Earth's crust. While the magnitude of emissions from abiogenic sources is very poorly known, it is not believed to be significant and is discussed further in Ch. 4.

For the purposes of this assessment, the three process-based categories of methane emission are further classified as either natural or anthropogenic sources. This is to delineate clearly both the ways in which anthropogenic activities have perturbed the methane cycle and the possible scope of mitigation measures to reduce anthropogenic methane emissions. Table 2.1 provides a recent synthesis of global methane source estimates. The estimates presented in Table 2.1 show anthropogenic activities to account for approximately 50% of the global total methane emissions, while other estimates suggest anthropogenic emissions may account for over 60% of the global total (e.g. Prather et al. 2012).

Table 2.1 Estimated annual average emissions for the major methane sources over the period 2000–2009 from Kirschke et al. (2013). The estimate for each source is calculated as the mean of a variable number of individual studies for each source. The range (in brackets) is defined as the maximum and minimum values from the studies reviewed.

Global sources	No. studies	Annual average emission, Tg CH_4
Natural sources		
Natural wetlands	3	217 (177–284)
Freshwater (lakes and rivers)	3	40 (8–73)
Wild animals (ruminants)	1	15 (15–15)
Wildfires	5	3 (1–5)
Termites	4	11 (2–22)
Geological	3	54 (33–75)
Marine	3	6 (2–9)[a]
Permafrost (excl. lakes and wetlands)	1	1 (0–1)
Total		349 (238–492)
Anthropogenic sources		
Rice cultivation	4	36 (33–40)
Domesticated animals (ruminants)	3	89 (87–94)
Landfills and waste	3	75 (67–90)
Biomass burning (incl. biofuels)	6	35 (32–39)
Fossil fuels	3	96 (85–105)
Total		331 (304–368)

[a] More recent estimates are provided in Ch. 4.

The estimates presented in Table 2.1 are derived from 'bottom-up' studies. These are studies where the emissions from a sample of a particular source type are estimated, often based on measurements taken in the real world. The measured emissions from the sample are then extrapolated to derive the global total using estimates of the global extent of the source. As such, the global total of the independently estimated sources is not constrained by estimates of the global total of emissions. Indeed, the sum of the best-guess estimates for each source from the bottom-up studies yields a global total emission of 680 Tg CH_4/y (Table 2.1), which falls outside the uncertainty range of the 'top-down' estimate of global total emissions of 554 ± 56 Tg CH_4/y derived from the methane abundance and estimates of atmospheric lifetime (Prather et al. 2012). Comparison with the top-down estimate suggests global total methane emissions towards the lower end of the range given by the bottom-up studies, where the two estimates overlap, however, the comparison does not provide information on where the net overestimate in the bottom-up studies may originate.

In addition to the bottom-up estimates and the constraints from the atmospheric lifetime and observed concentration, some additional methods to estimate emissions have been used, including atmospheric inversion (discussed further in Ch. 7) and the analysis of methane isotopes (discussed further in Ch. 6). These methods provide additional information on the broad regional (continental-scale) distribution of sources or source categories (biogenic versus thermogenic).

The significant contribution of anthropogenic sources to the global total of methane emissions provides an indication of the degree to which anthropogenic activities have perturbed the methane budget. Ice cores provide robust evidence that atmospheric concentrations[5] were around 720 ppb in 1750 (Ciais et al. 2013), while atmospheric measurements show a global average methane concentration of 1819 ppb in 2012 (WMO 2014). Most of the increase in methane is believed to be due to increased emissions resulting from anthropogenic activities, notably rice cultivation, ruminant livestock, landfills and fossil fuel extraction and use.

In terms of the more recent past, the rate of increase in the atmospheric concentration of methane has decreased since the mid-1980s, approaching a near-zero growth rate over 1999–2006 (see Fig. 2.1), before resuming a slower increase from 2007 onwards. The considerable year-to-year variability in the rate of increase in the atmospheric concentration over the 1990s has been attributed to the eruption of Mt. Pinatubo and the collapse of the Soviet Union in 1991/92 (Dlugokencky et al. 1996; Bousquet et al. 2006) and a strong El Niño in 1997/98 (Bousquet et al. 2006). The longer-term stability of the atmospheric methane concentration over 1999–2006 indicates a rough balance between sources and sinks during this period. Current understanding of methane sinks suggests these are fairly stable with time (discussed further in Sect. 2.3) and argues for changes in methane sources as the main reason behind recent changes in methane concentration growth rates, although attributing the changes in emissions to particular sources has proved challenging. Some studies have suggested that methane
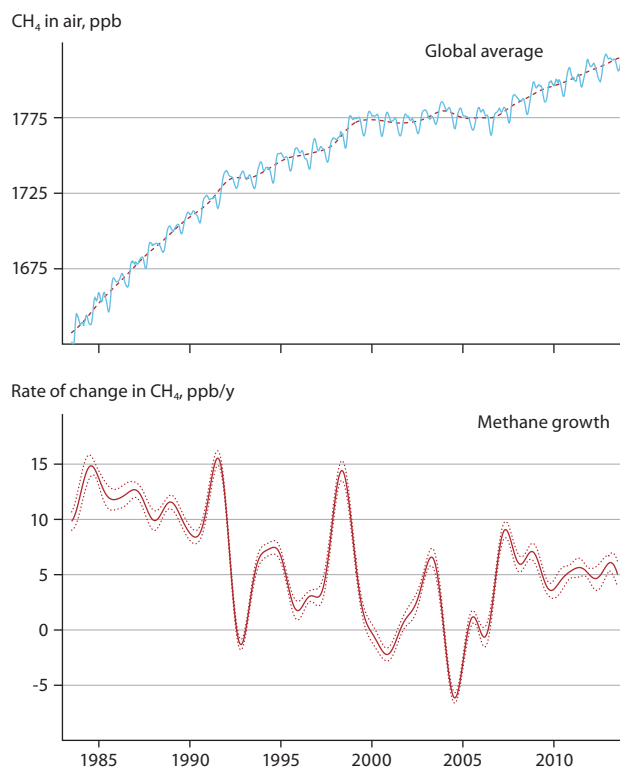
Fig. 2.1 The global-average methane concentration derived from surface observations by the US National Oceanic and Atmospheric Administration (NOAA) Cooperative Air Sampling Network (upper panel; the dashed red line is the trend line fitted to the deseasonalized data) and (lower panel) the annual rate of change in methane concentration (full red line) calculated from the dashed line in the upper panel, along with the 1-sigma uncertainty (hatched red lines). Updated from Dlugokencky et al. (2011).

emissions from fossil fuel extraction and distribution decreased by 10 to 30 Tg CH_4/y between the 1980s and 2000s, with much of this decrease occurring before 2000 (Aydin et al. 2011; Simpson et al. 2012). It has also been suggested that decreases in microbial emissions, particularly due to changes in the practice of rice cultivation, could be responsible for a ~15 Tg CH_4/y decrease over roughly the same time period (Kai et al. 2011). Uncertainty in the observations used to derive the decrease in microbial emissions (Levin et al. 2012) and the possibility of an offsetting increase in microbial emissions from sources such as natural wetlands or ruminants (Kirschke et al. 2013) further complicate an understanding of the causes of the stabilization of methane concentrations in the early 2000s.

A rise in atmospheric methane concentration resumed in 2007, albeit at a slower rate than in the 1980s. Figure 2.2 presents the latitudinally-resolved growth rate in the near-surface concentration of methane over 2000 to 2014. Clearly evident are strong increases in methane in 2007 at high latitudes in the northern hemisphere and in tropical latitudes in both 2007/08 and 2010/11. The increases are believed to be driven by increased emissions from wetlands due to year-to-year variability in meteorological conditions (Bousquet et al. 2011). The contribution of these anomalous years to the resumption of growth in the global-average methane concentration, including the possibility of additional contributions from changes in anthropogenic emissions, are discussed in Ch. 5 and 6.

---

5   Throughout this report the atmospheric concentration of methane will be given as the volume mixing ratio, also referred to as the molar mixing ratio, defined as the number density of methane relative to the number density of dry air. For simplicity, the term 'concentration' is used throughout.
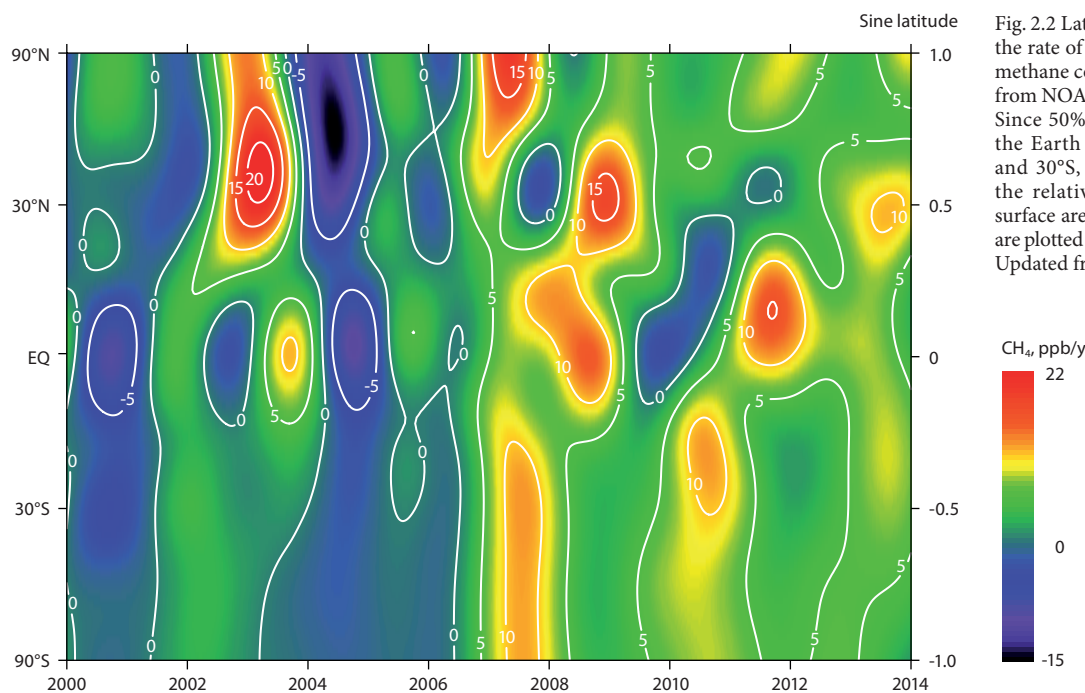
Fig. 2.2 Latitudinal distribution of the rate of change in near-surface methane concentration calculated from NOAA surface observations. Since 50% of the surface area of the Earth occurs between 30°N and 30°S, to correctly represent the relative distribution of the surface area with latitude the data are plotted as sine of latitude (-1,1). Updated from Nisbet et al. (2014).

2.3 Overview of methane sinks

The dominant (~80%) removal process for methane (CH_4) in the atmosphere is by chemical reaction with the hydroxyl radical, OH, in the troposphere. The reaction

$$OH + CH_4 \longrightarrow H_2O + CH_3· \qquad \text{Eq. 2.2}$$

involves the abstraction of a hydrogen atom from the methane molecule. The methyl radical ($CH_3·$) will then very rapidly, within seconds, react with an oxygen molecule to produce a methyl peroxy radical:

$$CH_3· + O_2 \longrightarrow CH_3O_2 \qquad \text{Eq. 2.3}$$

This is the beginning of the atmospheric oxidation process of methane. The methyl peroxy radical and all subsequent products undergo additional chemical reactions or are removed from the atmosphere by deposition on timescales ranging from a few seconds to several weeks, depending on the environmental conditions. Since methane has an average lifetime against initial reaction with tropospheric OH of 11.2 years (Prather et al. 2012), the subsequent steps that lead to either complete oxidation to carbon dioxide (CO_2) or deposition of intermediate products to the Earth's surface are, in comparison, very rapid. The rate of methane oxidation and removal from the atmosphere is controlled by the initial reaction of methane with OH.

Reaction with OH in the troposphere is estimated to remove 440 ± 52 Tg CH_4/y (Prather et al. 2012, discussed further in Sect. 2.4.1), but it is not the only removal mechanism. Methane is transported into the stratosphere where it can also undergo reaction with OH, as well as atomic oxygen ($O(^1D)$) and atomic chlorine (Cl), with each of these reactions contributing approximately equally to the stratospheric loss (McCarthy et al. 2003). The contribution of stratospheric loss to the total loss is limited by the small amount of global mass residing in the stratosphere and is estimated to be 30–40 Tg CH_4/y (Allan et al. 2007; Denman et al. 2007). Methane can also react with chlorine

in the troposphere, predominately near the surface over oceans where small amounts of chemically reactive chlorine can be produced (Singh et al. 1996), accounting for an estimated removal of 25 ± 12 Tg CH_4/y (Allan et al. 2007). In addition to atmospheric oxidation, uptake by methane-consuming bacteria in dry soils, discussed further in Ch. 3, is estimated to remove approximately 25–40 Tg CH_4/y (Curry 2007; Spahni et al. 2011). The sum of these removal mechanisms yields an estimated sink of methane of 540 ± 56 Tg CH_4/y (Prather et al. 2012).

Since the dominant methane loss processes are through chemical reactions, and the absolute rate of these chemical losses are directly proportional to the amount of methane in the atmosphere, the magnitude of these methane sinks will change with the methane concentration. It can therefore be helpful to analyze methane loss from the standpoint of the atmospheric lifetime of the gas – the average time methane will remain in the atmosphere after emission. The atmospheric lifetime, τ_{CH4}, can be defined as:

$$\tau_{CH4} = B_{CH4} / L_{CH4} \qquad \text{Eq. 2.4}$$

where B_{CH4} is the total mass, or burden, of methane in the atmosphere and L_{CH4} is the loss rate of methane, here expressed as the mass of methane removed per year. Following Prather et al. (2012), using a global average methane concentration for 2010 of 1795 ppb, the atmospheric burden of methane is estimated as 4932 Tg CH_4. Together with the estimated methane sink of 540 ± 56 Tg CH_4/y, a methane lifetime of 9.1 ± 0.9 years is derived. The methane lifetime calculated from the rate of loss by individual processes and the total lifetime from the sum of all loss processes, quoting the full range of estimates from the literature, is presented in Table 2.2. Note that while there are significant uncertainties for the magnitude of minor loss processes, because reaction with OH in the troposphere accounts for approximately 80% of the methane loss the uncertainties for minor loss processes do not contribute substantially to the overall uncertainty.

Table 2.2 Summary of methane loss processes expressed as the loss rate per year and as atmospheric lifetime. The atmospheric burden used in the calculation of lifetime is 4932 Tg CH_4 (Prather et al. 2012). The estimate of loss to tropospheric OH is from Prather et al. (2012) with their stated uncertainties. Other estimates are as described in the early part of Sect. 2.3.

Loss process	Magnitude of sink, Tg CH_4/y	Lifetime to sink, years
Tropospheric OH	390–490	10.1–12.6
Tropospheric chlorine	15–40	125–330
Uptake in dry soils	25–40	125–200
Chemical loss in stratosphere	30–40	125–165
Total loss	460–610	8.1–10.7

The atmospheric lifetime is also instructive as it provides an estimate of the amount of time required for the atmospheric concentration to respond to a decrease in emissions, thus, it is an important factor to connect changes in emissions and climate forcing. The relationship between atmospheric lifetime and the response of global average methane concentration to changes in emissions is complicated by the fact that changes in methane concentration will feed back onto processes that control methane removal – discussed further in Sect. 2.4. Modelling studies have estimated a decrease in global average tropospheric OH, weighted to account for reaction with methane, of 0.31 ± 0.04% for a 1% increase in the global average methane concentration (Holmes et al. 2013; Myhre et al. 2013). Assuming the rates of the other methane loss processes are insensitive to the methane concentration, a 1% increase in global average methane concentration will result in a 0.25% decrease in the loss rate of methane ($1/\tau_{CH4}$). The effect of a small perturbation in methane concentration on the loss rate of all methane in the atmosphere generates a secondary effect that additionally perturbs the evolution of the methane concentration, increasing the time needed for the global average methane concentration to respond to changes in emissions. The time constant for the methane concentration to adjust to a perturbation in emissions is a factor $1/(1-s)$ of the methane lifetime τ_{CH4}, where s is the sensitivity of methane loss to changes in the methane concentration. The 0.25% change in methane loss per 1% change in methane concentration gives a value of s of 0.25, and yields a time constant for the methane concentration to adjust to a change in emissions of 12.4 ± 1.4 years. The implications of differences in time constants for how climate gases respond to changes in emissions is explored in Box 2.1.

2.4 Methane and the hydroxyl radical

Atmospheric oxidation by OH in the troposphere is the dominant removal mechanism for methane. The atmospheric concentration of OH will, therefore, be the dominant factor controlling the lifetime of methane. The primary source of hydroxyl in the troposphere results from the photolysis (the absorption of a photon of solar radiation, hv, with sufficient energy to break the molecule) of ozone producing an electronically excited atomic oxygen,

$$O_3 + hv \longrightarrow O_2 + O(^1D) \qquad \text{Eq. 2.5}$$
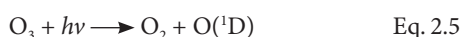
The excited atomic oxygen will predominantly react with molecular oxygen (O_2) or nitrogen (N_2) to relinquish the extra energy it carries, however a small fraction will react with water vapor to produce hydroxyl:

$$O(^1D) + H_2O \longrightarrow 2OH \qquad \text{Eq. 2.6}$$

Note that only the excited form of atomic oxygen can react with water vapor (H_2O) to produce OH. Thus the production of hydroxyl is favored by high levels of incident solar radiation and higher concentrations of water vapor making the tropical lower troposphere a globally important region for OH.

In addition to the primary production of OH from water vapor, OH can be recycled. The reaction of OH with methane, seen above, produces methyl peroxy radicals which may then react with nitrogen monoxide (NO) by:

$$NO + CH_3O_2 \,(+O_2) \longrightarrow CH_2 + HO_2 + NO_2 \qquad \text{Eq. 2.7}$$

Note that this reaction implicitly includes a second, separate reaction (the addition of O_2) that happens almost instantaneously after the first. The hydroperoxyl radical (HO_2), produced above can then be recycled back to OH by further reaction with NO,

$$NO + HO_2 \longrightarrow NO_2 + OH \qquad \text{Eq. 2.8}$$
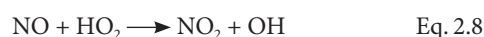
Alternatively, and increasingly important when concentrations of NO are low, the HO_2 can react with itself by,

$$HO_2 + HO_2 \longrightarrow H_2O_2 + O_2 \qquad \text{Eq. 2.9}$$
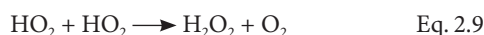
The hydrogen peroxide (H_2O_2) produced is relatively long-lived to further chemical reactions (on the order of days). It is, however, quite soluble meaning H_2O_2 is readily removed from the atmosphere by either wet or dry deposition processes, with the consequence that the OH is not recycled. In addition to self-reaction, HO_2 may also react with the methyl peroxy radical (CH_3O_2) and generate products that similarly lead to an inefficient recycling of OH. The balance between the self-reaction of peroxy radicals and the recycling of OH through reaction with NO illustrates the important role the concentration of NO plays in affecting the concentration of OH in the atmosphere.

In addition to reaction with methane, OH can also react with a wide variety of organic compounds found in the atmosphere; it is referred to as the 'detergent' of the atmosphere for the role it plays in initiating atmospheric oxidation and the eventual removal of compounds from the atmosphere. Of note, OH may react with carbon monoxide (CO) by:

$$OH + CO \,(+O_2) \longrightarrow CO_2 + HO_2 \qquad \text{Eq. 2.10}$$

Carbon monoxide is one of the intermediate products of methane oxidation and is also emitted into the atmosphere in

Box 2.1 Relationship between atmospheric lifetime and the response of atmospheric concentration to changes in emissions

Control of short-lived climate forcers is of interest for climate change mitigation because their atmospheric concentration, and hence the radiative forcing of the constituents (gas or particle) on climate, responds rapidly to changes in emissions due to their short atmospheric lifetimes. To illustrate this point, results from a simple box model are used to investigate the response of the atmospheric concentration to changes in emissions for two gases with different atmospheric lifetimes. The first is methane, with a lifetime that is sufficiently long (9.1 years) that it has only small spatial variations in concentration, relative to the global average, due to local or regional processes. Because methane is well-mixed, the response of the global average methane concentration to changes in emissions can be estimated by assuming that the atmosphere (the troposphere) behaves like a single well-mixed box. The response of methane will be compared with that of nitrous oxide (N_2O), a long-lived greenhouse gas with a lifetime of ~ 130 years (Prather et al. 2012; SPARC 2013). Note that for methane, the feedback of changes in the concentration of methane on the methane lifetime has been included using an assumed 0.25% decrease in the loss rate for a 1% increase in concentration (Myhre et al. 2013), with the 9.1 year lifetime specified for the concentration of methane in 2010. Although there is a similar, though weaker, feedback of concentration on lifetime for N_2O it has not been considered here – a constant lifetime of 131 years has been used.

Figure 2.3 presents the results from the box model simulations of the global average concentration of N_2O and methane as a function of time. The emissions for both species increase with time to maintain a constant 0.25% per year increase in concentration up to 2010, close to the currently observed rate of increase for both methane and N_2O. At 2010, three scenarios are explored: a case where emissions remain constant at the 2010 rate; an instantaneous decrease of the 2010 emission rate by 10%; and an instantaneous decrease of the 2010 emission rate by 20%. Methane establishes a new steady-state concentration

reflecting the change in emissions after approximately 40 years, with much of the adjustment occurring within 20 years of the change. In contrast, the N_2O concentration continues to change (increase) past 2100. The different time scales to establish a new steady state concentration in balance with the constant emissions is one aspect of the different atmospheric lifetimes.

A second aspect of the different behavior is the level at which the new steady-state is established. For the case with constant emissions after 2010, methane stabilizes at a concentration approximately 3% higher than the 2010 concentration while the concentration of N_2O at 2100 is 16% higher than at 2010 and still increasing. The initial 0.25% per year increase in concentration represents the same relative increase in atmospheric burden for each species. Although the much smaller fractional loss of N_2O each year, due to the much longer atmospheric lifetime, means that the annual increase in N_2O is much greater relative to removal compared with methane. As a result, to establish a balance between constant emissions after 2010 and atmospheric removal the N_2O loss must increase by a larger relative amount than for CH_4. Since the annual loss is proportional to the concentration, the N_2O concentration must increase more than the concentration of methane to establish a new steady state.

The results show that for species with atmospheric lifetimes similar to that of methane (i.e. years to one or two decades), the atmospheric concentration will stabilize rapidly after any increase in emissions stops and decreases in emissions will rapidly be reflected in decreased atmospheric concentrations, with the atmospheric lifetime being indicative of the timescales for the concentration to adjust. For long-lived species, the period of time over which atmospheric concentrations adjust to changes in emissions will be longer. Additionally, the change in emissions required to stabilize increasing concentrations will be greater than for short-lived species, assuming the same relative rates of increase in atmospheric concentration.
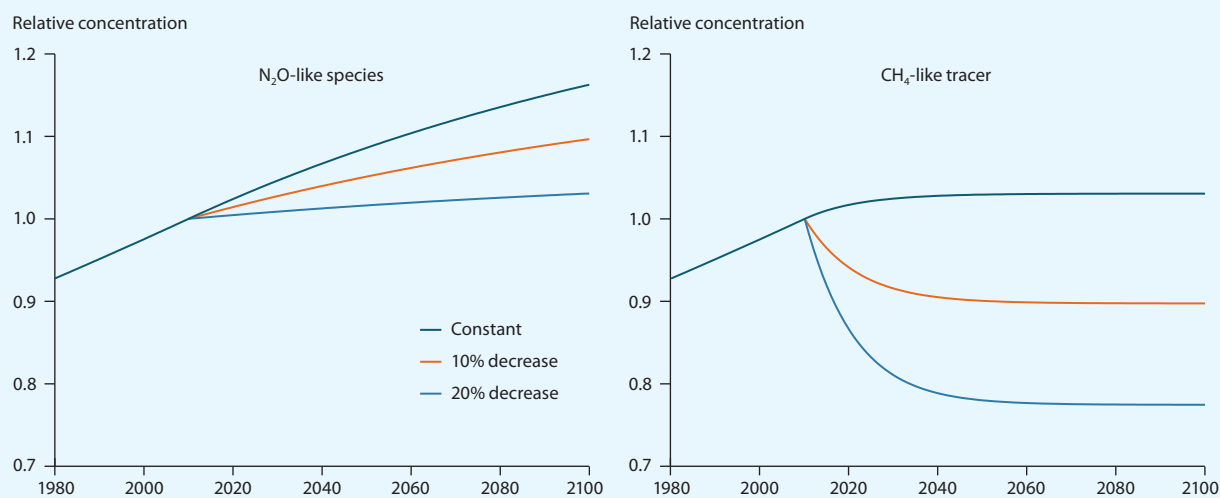
Fig. 2.3 Evolution of the global average concentration of two chemical species with time calculated using a simple one-box model of the atmosphere. The left-hand panel shows the evolution of a nitrous oxide (N_2O)-like species with an assumed lifetime of 131 years and the right-hand panel shows the evolution of a methane (CH_4)-like tracer with a lifetime of 9.1 years. The methane tracer includes the effect of changes in concentration on its own lifetime, where the total loss decreases by 0.25% for a 1% increase in concentration. Both tracers increase at a rate of 0.25% per year until 2010, at which point the emissions are assumed to either remain constant, instantaneously decrease by 10% or instantaneously decrease by 20%. The concentrations of both species are normalized to their value at the beginning of 2010.

large quantities by incomplete combustion processes, including industrial processes, internal combustion engines and biomass burning (Duncan et al. 2007).

The broad outline of OH production and cycling in the atmosphere given above illustrates how the primary production of OH is sensitive to ozone, solar radiation and water vapor concentrations.

Box 2.2 The photochemical production of ozone

Methane also has important impacts on climate through the role it plays in the photochemical production of ozone (O_3) in the troposphere and lower stratosphere (Crutzen and Zimmermann 1991). During sunlit conditions, the chemical species nitrogen monoxide (NO) and nitrogen dioxide (NO_2) rapidly pass through a cycle given by the following two reactions:

$$NO + O_3 \longrightarrow NO_2 + O_2$$
$$NO_2 + h\nu \; (+O_2) \longrightarrow NO + O_3$$
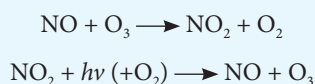
Of note, the sum of these two reactions does not result in any change of concentration for any of the participating species. Where NO_2 is produced by the reaction of NO with ozone, the subsequent photolysis of NO_2 merely regenerates ozone. However, NO_2 may be produced by the reaction of NO with HO_2 and with other peroxy radicals; in the case of methane, CH_3O_2. In this case, the subsequent photolysis of NO_2 will result in the net production of ozone. This sequence of reactions gives rise to the photochemical production of ozone due to the atmospheric oxidation of organic compounds in the presence of nitrogen oxides (NO_X; due to the rapid interconversion, NO_X is frequently used to refer to the sum of NO and NO_2).

Although the discussion of organic compounds that undergo atmospheric oxidation is limited here to methane, there is a tremendous variety of organic compounds present in the atmosphere from both anthropogenic and natural sources (e.g. Houweling et al. 1998). The details of the chemistry vary from compound to compound, sometimes in important ways, but the underlying process by which the atmospheric oxidation of organic compounds interact with NO_X to photochemically produce ozone is similar. It is usual to differentiate between methane and the group of much shorter-lived organic compounds by referring to the latter as non-methane volatile organic compounds (nmVOCs).

Over industrialized regions of the world, the combination of intense sunshine, warm temperatures and high concentrations of NO_X and organic compounds from anthropogenic and natural sources can result in the rapid photochemical generation of ozone in the atmosphere and give rise to large concentrations of ozone near the surface, creating air quality problems (Crutzen 1974). While more broadly, emissions of anthropogenic NO_X and organic compounds, including methane, affect the concentration of ozone throughout the troposphere. Atmospheric oxidation of methane in the lowermost stratosphere can also lead to photochemical production of ozone in that region, although the NO_X is likely to be of stratospheric origin (Portmann and Solomon 2007; Fleming et al. 2011).

The reactions also show that increasing concentrations of methane and CO will act to depress the concentration of OH, while increased concentrations of NO will generally have the effect of increasing OH through more efficient recycling. As discussed in Box 2.2, increased concentrations of NO will also lead to the photochemical production of ozone, which will further increase OH concentration since the products of ozone photolysis participate in the primary production mechanism of OH. These general aspects of atmospheric chemistry are important to understand how climate change and emissions may influence methane lifetime.

2.4.1 Observation-based estimates of hydroxyl

While challenging, the concentration of OH can be directly measured in the atmosphere (e.g. Wennberg et al. 1995). However, due to the high reactivity of OH it is extremely short-lived, with a lifetime on the order of seconds (Lelieveld et al. 2004), and the atmospheric concentration is therefore strongly dependent on local rates of production and destruction, which are highly variable in space and time. For example, the concentration of OH has been found to vary by a factor of two between measurements made under a cloud and measurements made beside the cloud, with the variation matching the observed variation in the rate of ozone photolysis (Mauldin et al. 2001). Therefore, it is not possible to extrapolate measurements of OH to derive a global average concentration that would be useful for constraining methane losses.

Observations of methyl chloroform (MCF), a chemical with no known natural sources, that depletes stratospheric ozone and whose use was subsequently phased-out under the Montreal Protocol, has provided an opportunity to estimate the global abundance of OH. Like methane, the dominant removal mechanism of MCF from the atmosphere is through reaction with OH and when the continued production and use of MCF was discontinued, atmospheric abundances began to decrease. Surface observations, shown in Fig. 2.4, demonstrate the exponential decay of the MCF concentration with the rate

MCF in air, parts per trillion
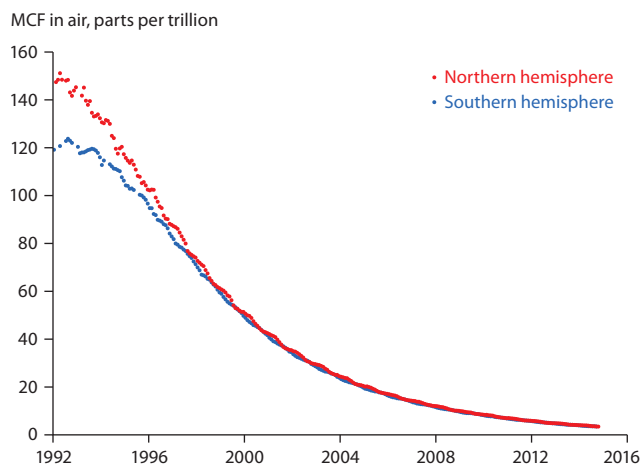
Fig. 2.4 Observed hemispheric monthly average concentration of methyl chloroform (MCF). The hemispheric average concentrations are derived from flask samples taken approximately weekly at nine remote surface sites operated by the US National Oceanic and Atmospheric Administration (NOAA)/Global Monitoring Division following the method described by Montzka et al. (2011).

of decay reflecting the atmospheric lifetime. Until ~1997 a significant inter-hemispheric gradient was observed, with higher concentrations in the northern hemisphere reflecting the predominance of emissions in that hemisphere. As emissions decreased to levels that were insignificant compared to the burden and removal processes, the inter-hemispheric difference became small and the global average removal rate (the exponential first-order loss rate) stabilized at around -0.181 ± 0.005/y (Montzka et al. 2011). Accounting for other (minor) loss processes, loss in the stratosphere and uptake by the oceans, it is possible to derive the MCF loss rate to OH in the troposphere from the observed rate of decrease. The MCF loss to OH can then be scaled to that of methane using the relative reaction rates of MCF and methane with OH. In this way, estimates of methane loss to OH (440 ± 52 Tg CH_4/y) with relatively small estimated uncertainties have been calculated (Prather et al. 2012).

The observed decay rate of MCF can also be used to provide an estimate of the amount of interannual variability in the global average concentration of OH. Earlier estimates suggested interannual variability in OH of 7–9%, with maximum year-to-year changes on the order of 20% (Prinn et al. 2005). It is now believed that these earlier estimates of large interannual variability were complicated by the fact that ongoing emissions of MCF were still considerable. Estimates derived from MCF observations for the post-1998 period show an interannual variability of less than 3% (Montzka et al. 2011).

2.4.2 Photochemical modelling estimates of hydroxyl

Global chemical models also provide estimates of present-day OH concentrations. These models include a representation of emissions, transport, chemistry and removal of a suite of chemical compounds that captures the important chemical processes of the troposphere. A suite of current-generation models that participated in the Atmospheric Chemistry Climate Model Intercomparison Project (ACCMIP) estimated the present-day chemical lifetime of methane to reaction with tropospheric OH to be 9.3 ± 0.9 years, which corresponds to a methane sink of 530 ± 50 Tg CH_4/y (Voulgarakis et al. 2013). While an earlier multi-model study, based on a substantially different set of global models and conducted for the Task Force on Hemispheric Transport of Air Pollution (TF-HTAP), estimated a tropospheric OH methane sink of 480 ± 80 Tg CH_4/y (Fiore et al. 2009). Both of these estimates were calculated as the mean of the participating models, with the ranges given as one standard deviation of the individual model estimates. The model estimates can be compared with the methane loss of 440 ± 52 Tg CH_4/y derived from the observed decay of MCF. While some individual models calculate a tropospheric OH sink that is in agreement with the observationally-derived estimate, and in fact the multi-model mean from the TF-HTAP study falls within the stated uncertainty of the observational estimate, models in general tend to overestimate methane loss to OH. Factors contributing to the range of model estimates include uncertainties in the chemistry (Dillon and Crowley 2008; Lelieveld et al. 2008; Fuchs et al. 2013) and the representation of non-methane hydrocarbons in the models (Voulgarakis et al. 2013). Differences in temperature, water vapor, stratospheric

ozone column or the concentration of ozone in the troposphere have also been shown to play a role (Holmes et al. 2013; Naik et al. 2013). The effect of clouds on photolysis has been shown to have only minor effects on methane lifetime on a global scale (Voulgarakis et al. 2009), although the general treatment of photolysis appears to be an important factor driving the spread in simulated present-day methane lifetime between models (Voulgarakis et al. 2013).

2.4.3 Long-term changes in hydroxyl

While model estimates of present-day methane loss to OH remain uncertain, they still provide critical insight into how tropospheric OH, and methane loss by reaction with OH, may have changed in the past and how it may change in the future. As the magnitude of the methane sink to OH is proportional to the methane abundance, for longer-term changes in the methane budget it is necessary to analyze changes in the methane lifetime, introduced in Sect. 2.3. For changes from preindustrial to present-day conditions, the suite of ACCMIP models analyzed by Naik et al. (2013) suggest a slight decrease in the methane lifetime to tropospheric OH between 1850 and 2000, from 10.1 to 9.7 years. The small change in methane loss from 1850 to present-day is the result of a balance of positive and negative influences on OH. Changes that tended to enhance the OH concentration between 1850 and 2000 include increased water vapor and temperature (owing to climate change), increased tropospheric ozone, decreased stratospheric ozone (which allows more ultraviolet radiation into the troposphere) and increased concentrations of NO (which act to recycle OH). Factors that depressed the concentration of OH between 1850 and 2000 include the factor of 2.2 increase in the concentration of methane and higher concentrations of CO from anthropogenic emissions, both of which react directly with OH (Naik et al. 2013). Note that although the multi-model mean showed a slight decrease in the methane lifetime to tropospheric OH, individual models showed changes that ranged between an increase of one year and a decrease of one year. The range of changes in methane lifetime found for the ACCMIP models is similar to the range of changes found in earlier studies, with individual studies showing both small increases in methane lifetime (Wang and Jacob 1998; Wild and Palmer 2008) and small decreases (Berntsen et al. 1997). It is worth noting, however, that these earlier studies did not account for changes in climate, which would have affected OH through changes in temperature and water vapor.

Projections of how the methane lifetime may change to 2100 were also made as part of ACCMIP. As for the historical period, generally small changes in methane lifetime were projected between 2000 and 2100 with individual models showing changes that ranged from small increases to small decreases for each of the four future scenarios investigated – the four Representative Concentration Pathways, or RCPs, specified for the Fifth Assessment of the Intergovernmental Panel on Climate Change. For the three RCPs with the lowest radiative forcing (RCP2.6, RCP4.5, RCP6.0), the models generally showed small decreases in the methane lifetime to OH loss of less than one year for RCP4.5 and decreases of less than one-half year for RCP2.6 and RCP6.0. The clearest signal in the model projections was found for RCP8.5, where nine of the

12 models showed an increase in the methane lifetime although with a small average change of +0.8 years. The dominant factor behind the increased methane lifetime for RCP8.5 has been shown to be the increase in methane concentrations specified for this scenario (Voulgarakis et al. 2013). For 2100, RCP8.5 prescribes a global average methane concentration of 3750 ppb, while the other three RCPs all prescribe year 2100 methane concentrations that are 100–500 ppb lower than the year 2000 values of approximately 1750 ppb.

2.5 Methane radiative forcing

Methane is well-mixed throughout the troposphere and has increased in concentration significantly since the pre-industrial period. Methane itself is a greenhouse gas with an estimated tropospheric radiative forcing due to the change in concentration between pre-industrial (~1750) and present-day of +0.48 W/m^2 (IPCC 2013a). This can be compared to the estimated radiative forcing from all well-mixed greenhouse gases (CO_2, CH_4, N_2O and halocarbons) of 2.83 W/m^2 (IPCC 2013a). The direct radiative forcing from methane is, however, only one of the ways in which methane can affect climate.

As discussed in Box 2.2, the atmospheric oxidation of hydrocarbons, including methane, in the presence of sufficient concentrations of reactive nitrogen compounds will lead to the photochemical production of ozone in the troposphere and lower stratosphere. Models calculate an increase of tropospheric ozone of approximately 30–40% between pre-industrial (1850) and present-day, predominately due to increased methane and increased anthropogenic emissions of CO, other hydrocarbons and NO_X (Gauss et al. 2006; Young et al. 2013). Very limited observations in the late-1800s suggest that ozone concentrations near the surface were, in fact, considerably lower than the models estimate (Volz and Kley 1988; Cooper et al. 2014), although possible interferences and significant uncertainties in the measurement techniques has meant the significance of the discrepancy has not yet been ascertained (Pavelin et al. 1999).

The increase in tropospheric ozone from the pre-industrial period is of concern because of the negative impacts ozone has on vegetation and human health (USEPA 2013). Ozone also absorbs at infra-red wavelengths and, as such, can change the radiative balance of the troposphere and change surface and tropospheric temperatures. Ozone is most effective as a radiative forcer in the vicinity of the tropopause (Forster and Shine 1997). In its latest assessment the IPCC estimates radiative forcing from increased ozone due to ozone precursor emissions (methane, CO, NO_X and nmVOCs) at +0.50 W/m^2 for the period 1750–2010 (Myhre et al. 2013). Experiments performed as part of ACCMIP, where the effects on ozone of individually varying the emissions of CO, NO_X, nmVOCs and the concentration of methane between 1850 and 2000 levels, allows for the radiative forcing due to the changes in ozone to be attributed to each of these emissions (Stevenson et al. 2013). Scaling the individual effects to the total forcing of +0.50 W/m^2, the change in ozone from increased methane alone is estimated at +0.24 W/m^2, with additional contributions from NO_X emission (+0.14 W/m^2), CO (+0.07 W/m^2) and nmVOCs (+0.04 W/m^2).

A complication arises because changes in ozone precursors affect the concentration of OH in the atmosphere and, by extension, the removal of methane from the atmosphere. For example, emissions of NO_X will produce a positive radiative forcing from increased ozone through the role it plays in the photochemical production of ozone. Emissions of NO_X will also contribute a negative radiative forcing through increased OH that removes methane from the atmosphere more rapidly. When these secondary effects are accounted for, including the important influence of the methane concentration on methane lifetime, the total radiative forcing of methane emissions on methane concentrations is estimated to be +0.64 W/m^2. Emissions of NO_X, due to the increase in methane removal, produces a radiative forcing of -0.25 W/m^2, while emissions of CO (+0.07 W/m^2) and nmVOCs (+0.02 W/m^2) contribute small additional terms to the radiative forcing (Myhre et al. 2013). The total of the four effects is equal, by design, to the +0.48 W/m^2 radiative forcing calculated from the change in atmospheric methane concentration from 1750 to 2010.

The atmospheric oxidation of methane produces water vapor as one of the end products. One molecule of methane will produce two molecules of H_2O. The additional water has a vanishingly small effect in the troposphere where fluxes into and out of the atmosphere through evaporation and precipitation are very large compared to the water vapor produced from methane. In the stratosphere, however, where concentrations are on the order of several parts per million, water vapor from methane oxidation is an important contribution. The IPCC reports that the increase in stratospheric water vapor due to the increase in methane emissions from the pre-industrial period to present-day has resulted in an additional +0.07 W/m^2 radiative forcing (Myhre et al. 2013).

The latest estimate of the IPCC is that the total radiative forcing from methane is +0.97 W/m^2, given as the sum of the change in ozone due to the increase in methane (+0.24 W/m^2), the increase in the atmospheric concentration of methane including the effect of the increased methane concentration on methane lifetimes (+0.64 W/m^2) and the increase in stratospheric water vapor (+0.07 W/m^2). An additional small contribution to CO_2 that results from the oxidation of methane (+0.02 W/m^2) brings the total to +0.97 W/m^2.

Acknowledgments

3. Natural terrestrial methane sources in the Arctic

Authors: Torben R. Christensen, Ko van Huissteden, Torsten Sachs

3.1 Introduction

The natural terrestrial sources of methane include wetlands, freshwaters (lakes and rivers), wild animals (ruminants), termites, wildfires and geogenic sources such as volcanic emissions and natural seeps. Most of the emissions from termites and volcanos take place outside the Arctic region. While wildfires may play an important role and increasingly so (Jenkins et al. 2014) both globally, and in particular in the Arctic, wetlands and freshwaters represent by far the largest terrestrial sources. In a world without anthropogenic methane emissions, the dynamics of global wetland emissions would be the primary source of variability in atmospheric methane concentrations. Hence, wetlands are a focus of studies on past greenhouse gas concentrations (Chappellaz et al. 1993a; Loulergue et al. 2008). Temperature and soil wetness-driven variations in tropical wetland emissions and periglacial development of northern wetlands have strongly impacted atmospheric methane concentrations over the past 10000 years or so, both directly (Loulergue et al. 2008) and indirectly, through the emissions of volatile organic compounds that affected the oxidizing capacity of the atmosphere and so the atmospheric capacity to break down methane (see Sect. 2.4) (Harder et al. 2007). The balance between these processes has determined past natural dynamics of atmospheric methane and there is evidence that these, in turn, have driven major climate change events by influencing the strength of the Earth's natural greenhouse effect (DeConto et al. 2012).

The presence of a greenhouse effect was first proposed in the early part of the 19th century by French authors Fourier and (later) Pouillet (Handel and Risbey 1992). Tyndall (1861) was the first to note that changes in atmospheric carbon dioxide concentrations might influence climate. In an apparently little noticed paper by Hunt (1863) it was first suggested that other gases, including 'marsh gas' (methane), could also affect climate (Handel and Risbey 1992). Arrhenius (1896) provided the first quantitative discussion of the effect of carbon dioxide on climate and later made the suggestion that manmade emissions of this gas could cause changes in climate (Arrhenius 1908). Although the emission of 'marsh gas' had been well known for decades, methane was unambiguously identified in the atmosphere before the middle of the past century (Migeotte 1948). It took another 38 years before the earlier spectral data collected in Arizona and Germany were translated into atmospheric mixing ratios of about 1.4–1.5 ppm (Rinsland et al. 1985). In the 1970s and 1980s, various authors gave the first accounts of atmospheric methane (see Wahlen 1993).

Ehhalt (1974) made the first estimation of global methane emissions including from wetlands, tundra and freshwaters, although very few ecosystem–atmosphere flux measurements were available at that time. The first wetland methane flux measurements were carried out in connection with the International Biological Program (IBP) in the late 1960s and early 1970s. These studies included the work of Clymo and

Reddaway (1971) at Moor House in Britain, and Svensson (1976) who investigated a subarctic mire in northern Sweden. These studies were carried out as purely biological investigations with no intent to put such work in a climate change context. More recently, interest in climate change has spurred a dramatically increasing number of studies of wetland methane emissions over the past decades, the results of which are reviewed briefly in this chapter. Interestingly, the most recent compilation of data on global methane emissions (Kirschke et al. 2013) does not differ in its range for wetland emissions from that of the first budget by Ehhalt (1974). The early estimates of uncertainty seem to mirror the natural variability in fluxes as they are understood today (Christensen 2014).

The policy relevance of estimating natural methane emissions is mainly that this provides a baseline against which to compare the magnitude of current anthropogenic emissions and thus to identify the potential for Arctic countries (and countries worldwide) to influence future levels of atmospheric methane through mitigation. Also, anthropogenically-caused global warming may lead to higher natural emissions, particularly in the Arctic region (Ch. 1). This chapter reviews the processes governing Arctic wetland methane emissions, discusses the specifics of the currently available data on the extent of such emissions, and provides an overview of the carbon dynamics of tundra soils (see Box 3.1 for key terminology). The chapter concludes with projections of possible future changes in these emissions. This information addresses the following questions posed in Chapter 1 (see Table 1.1):

What are the current methane emissions from Arctic terrestrial sources?

What are the controlling processes and factors that strongly influence natural emissions?

How may these emissions from Natural sources in the Arctic change in the future?

What are the uncertainties or limitations in these estimates?

Answers to these questions will help to address one of the two overarching questions posed to the Methane Expert Group:

How does the magnitude of potential emission reductions from anthropogenic sources compare to potential changes in methane emissions from natural sources in the Arctic?

3.2 Description of natural terrestrial methane sources

3.2.1 Processes

Wetland environments have long been known to be significant contributors to atmospheric methane through microbial breakdown (decomposition) of organic material in saturated soils (Ehhalt 1974; Fung et al. 1991; Bartlett and Harriss 1993).

Box 3.1 Key terminology

Active layer	The top part of a permafrost soil which thaws annually in summer and refreezes in winter.
Anaerobic environment	Living environment with no free oxygen available. Often found in sediments and wetland soils.
Cryoturbation (frost churning)	Refers to the mixing of materials from various horizons of the soil due to freezing- and thawing-induced expansion and contraction of soil.
Drained thermokarst lake basin	Lake that has been drained naturally by contact with a river system or other lower-lying lakes.
Ebullition	In this context, associated with the bubbles that cause sudden and erratic release of gas (with a large content of methane) from wet soils and sediments.
Peatland	Can be both dry and wet ecosystems but characterized by a substantial accumulation of organic material, peat. This means peatlands must in a past or present perspective have been considered as mires where there is a surplus of organic matter produced that accumulated in the ground. According to the International Peat Society the definition of a peatland is simply "an area with or without vegetation with a naturally accumulated peat layer at the surface".
Permafrost table	The top of the frozen soil horizons below the active layer.
Taiga	A biome characterized by being dominated by coniferous forest consisting mostly of spruce, pine and larch.
Talik	A layer of year-round unfrozen ground that lies in permafrost areas. In regions of continuous permafrost, taliks often occur underneath lakes and rivers, where the deep water does not freeze in winter, and thus the soil underneath will not freeze either.
Thermokarst	Subsidence and erosion processes created by thawing of ice-rich permafrost.
Thermokarst lake	Lake created by subsidence of the soil by thawing of permafrost that is oversaturated with ice.
Tundra, wet and dry	Tundra is a biome where the tree growth is hindered by low temperatures and short growing seasons. The term *tundra* comes from the Sami word *tuntuuri* meaning 'treeless mountain tract'. Tundra is present in vast areas of the Arctic as wet tundra overlapping with the global wetland category. Medium-wet (mesic) and dry tundra comprise the rest of the biome.
Wetland	'Wetland' is a very broad characterization of an ecosystem where the vegetation has adapted to constant inundation. According to the RAMSAR Convention a wetland is "a land area that is saturated with water, either permanently or seasonally, such that it takes on the characteristics of a distinct ecosystem". The main wetland types include swamps, marshes, bogs and fens. Tundra wetlands may include all types.
Yedoma deposits	Ice-rich Pleistocene loess deposits of mixed origin with labile but frozen organic carbon that may have a total ice volume content of 30–90%.

In wet, anaerobic (oxygen-free) environments, methane is formed through the microbial process of methanogenesis. Methane formation follows from a complex set of ecosystem processes that begins with the primary fermentation of organic macromolecules to acetic acid, other carboxylic acids, alcohols, carbon dioxide, and hydrogen. Primary fermentation is followed by secondary fermentation of the alcohols and carboxylic acids to acetate, hydrogen, and carbon dioxide, which are fully converted to methane by methanogenic bacteria (Cicerone and Oremland 1988; Conrad 1996). Many factors affect this sequence of events, including temperature, the persistence of anaerobic conditions, gas transport by vascular plants, changes in microbial community composition, and supply of easily decomposable organic substrates (Whalen and Reebugh 1992; Davidson and Schimel 1995; Joabsson and Christensen 2001; Ström et al. 2003). Also, substances such as nitrate and, in particular, sulfate, may competitively inhibit methanogenesis and support anaerobic methane oxidation. Figure 3.1 shows the variety of controls on methane formation rates at different spatial and temporal scales.

The net release of methane from wetland soils is the result of transport and the competing soil processes of methane production and methane consumption. While methane is produced in anaerobic soils, it is consumed (oxidized) in aerobic parts of the soil. This oxidation takes place through the microbial process of methanotrophy, which can even take place in dry soils by bacteria oxidizing methane transported from the atmosphere (Whalen and Reeburgh 1992; Moosavi and Crill 1997; Christensen et al. 1999). Microbial methane oxidation in soils can represent a terrestrial sink for atmospheric methane and a process that to some extent can counterbalance net methane production in areas where dry tundra landscapes dominate (Emmerton et al. 2014). Nevertheless, the total estimated soil sink of such dry landscapes, even globally, remains small compared with the overwhelming importance of hydroxyl radical (OH) oxidation in the atmosphere (Ch. 6) but also compared with the large wetland and freshwater emissions (Kirschke et al. 2013). However, methanotrophy is responsible for the oxidation of an estimated 50% of the methane produced at depth in the soil column in wet areas with net emissions

Controls on methanogenesis
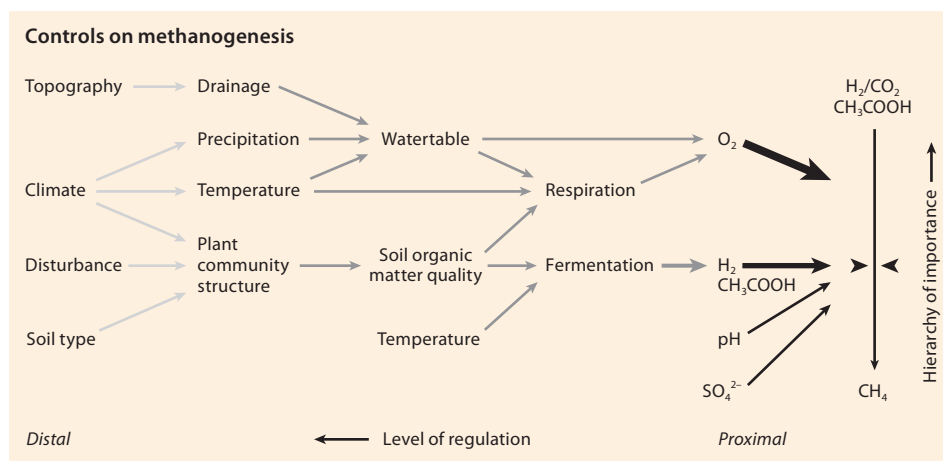
Fig. 3.1 Major controls on the pathways to methane formation. Distal (climate/environmental) and proximal (chemical) controlling parameters are indicated as well as a hierarchy of importance in a complex ecosystem context. Based on Schimel (2004).

(Reeburgh et al. 1994) and, in terms of controlling net methane emissions, is as important a process as methanogenesis.

The anaerobic process of methanogenesis (methane production) is far more responsive to changes in temperature than the aerobic process of methanotrophy (methane consumption/oxidation) (Conrad 2009). The mechanistic basis for this difference is not clear, but the ecosystem consequences are straightforward: soil warming in the absence of any other changes will accelerate methane emission (which is the difference between production and consumption), in spite of the simultaneous stimulation of the two opposing processes (Ridgwell et al. 1999). Therefore, in the absence of other changes, warming favors increasing production and net emission of methane on a short-term basis (Yvon-Durocher et al. 2014). Over the longer term, indirect effects of warming may result in changes in the water balance, vegetation, and overall soil carbon dynamics, making the overall outcome less certain. In permafrost environments undergoing thaw, in addition to the effect of temperature on the microbial processes themselves, warming has been shown to favor increasing emission through a combination of the stimulating effects of increased vascular plant coverage and the availability of thawing old organic material (Klapstein et al. 2014). This finding corresponds well with landscape-scale analysis of changes in Scandinavian permafrost wetlands over decades where increasing emissions have been documented due to changes in community structure following permafrost thaw (Johansson et al. 2006; Bosiö et al. 2012).

Analysis of growing-season methane fluxes for a large number of boreal sites across permafrost zones (Olefeldt et al. 2013) illustrates not only strong relationships between methane flux and water-table position, soil temperature, and vegetation composition but also their interacting effects on fluxes. For example, emissions from wetlands with water tables at or above the soil surface are more sensitive to variability in soil temperature than are drier ecosystems, whereas drier wetlands are more sensitive to changes in water-table position. Methane storage and transport issues may disturb the described picture of temperature, water table and plant mediated controls on net emission. At certain time scales, episodic releases of stored gases may be triggered by physical pressure build-up in permafrost soil when the active layer starts freezing from the top downwards toward the permanently frozen soil in the autumn (Mastepanov et al. 2008, 2013). There may also be sudden methane emissions during the growing season related to atmospheric pressure change (Klapstein et al. 2014). In a related ecosystem, but more

strictly freshwater setting, Wik et al. (2014) showed how the transport of methane to the atmosphere in bubbles of gas from subarctic lakes shows a highly predictable relationship with energy input, suggesting increasing emissions as the duration of lake ice cover diminishes. The bottom line is that ebullition (bubble emission) and storage/transport issues as well as microbial community shifts may complicate seasonal emission patterns such they do not always follow simple relationships with variations in temperature and plant productivity.

The controls on methane emissions are, therefore, a rather complex set of processes, often working in opposing directions. Early empirical models of wetland methane exchanges suggested sensitivity to climate change (Roulet et al. 1992; Harriss et al. 1993). A simple mechanistic model of tundra methane emissions, including the combined effects of the driving parameters (temperature, moisture, and active layer depth), also suggested significant changes in methane emissions as a result of climate change (Christensen and Cox 1995). Since then, wetland methane emission models have grown in complexity (Panikov 1995; Cao et al. 1996; Christensen et al. 1996; Walter and Heimann 2000; Granberg et al. 2001; Wania 2007; Riley et al. 2011; Zhang et al. 2012, 2013; Watts et al. 2014) as the mechanistic understanding of the most important processes controlling methane fluxes has improved. Autumn and winter processes have also been found to have a strong influence on net annual emissions of methane, in addition to summer/growing season processes (Panikov and Dedysh 2000; Mastepanov et al. 2008, 2013). In northern wetlands, variations in methane emission at the regional to global scale are found to be driven largely by temperature (Crill et al. 1992; Harriss et al. 1993), but with important modulating effects of vascular plant species composition superimposed (Christensen et al. 2003; Ström et al. 2003). Thus, from the perspective of empirical studies of northern wetlands, an initial warming is expected to lead to increased methane emissions, but the scale of this increase depends on associated changes in soil moisture conditions, and the secondary effects of changes in vegetation composition.

The highest tundra methane emissions are generally associated with wetland conditions combined with highly organic soils (often peat). Plant productivity can amplify the source strength of methane production, and this interaction has been studied at scales ranging from below-ground microbial investigations (Panikov 1995; Joabsson et al. 1999) to large-scale vegetation models linked to methane parameterizations (Cao et al. 1996; Christensen et al. 1996; Walter and Heimann 2000; Zhuang et al.
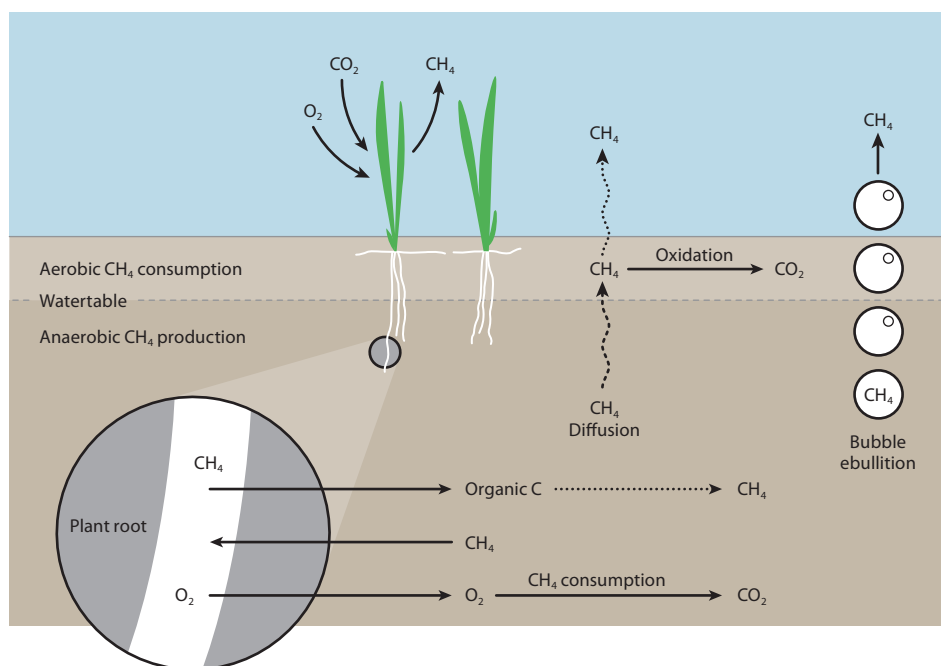
Fig. 3.2 Means by which vascular plants can influence net methane emission from wetland soils. Modified from Joabsson and Christensen (2001).

2004; Sitch et al. 2007a; Zhang et al. 2013). Various studies have attributed the relationship between living plants and methane emissions to different mechanisms, such as: stimulation of methanogenesis by increasing C-substrate availability (input of organic substances to soil through root exudation and litter production); build-up of plant-derived peat deposits that retain water and provide an anaerobic soil environment; removal from the soil by plants of mineral nutrients such as nitrate and sulfate, which are competitive inhibitors of methanogenesis (competitive electron acceptors); and enhancement of gas transport from methanogenic soil layers to the atmosphere via root aerenchyma acting as gas conduits that bypass zones of potential methane oxidation in the soil. In addition to these stimulatory effects on net methane emissions, certain plants may also reduce emissions through actively oxidizing the root vicinity (rhizospheric oxidation), which can enhance methane consumption, while *Sphagnum* and other peat mosses can also possibly increase oxidation through a symbiotic relationship with methanotrophs (Kip et al. 2010; Parmentier et al. 2011). Figure 3.2 summarizes the ways in which plants may affect methane emissions from wetlands.

3.3 Methods for measuring methane fluxes

Direct surface flux measurements of methane exchange with the atmosphere rely primarily on closed chamber and eddy covariance methods, with the latter usually deployed on ground-based flux towers. Most recently, airborne eddy covariance flux measurements were conducted in the North American, Canadian, and Siberian Arctic (Box 3.2). In boreal and Arctic ecosystems, methane flux measurements are still predominantly performed with chambers, which usually cover <1 m^2 (Whalen and Reeburgh 1990a; Christensen et al. 1995; Corradi et al. 2005; Mastepanov et al. 2008; Sachs et al. 2010). Ecosystem-scale eddy covariance observations of integrated fluxes over larger areas (typically hectares) have become available relatively recently due to advances in laser

and infrared absorption technology (Friborg et al. 2000; Sachs et al. 2008; Wille et al. 2008; Jackowicz-Korczyński et al. 2010; Parmentier et al. 2011; see Box 3.2). In spite of the rapid advances in technology, ecosystem-scale observations of northern wetland methane fluxes still remain sparse and geographically fragmented, due to the logistical challenges and often harsh environmental conditions accompanying fieldwork in the Arctic environment. Also, measurements with year-round coverage are still extremely rare and most available data cover the growing season only.

Direct flux measurements of ecosystem–atmosphere exchange of methane are pivotal for understanding the spatial and temporal dynamics of the emissions. However, flux measurements outside the growing season are very rare in Arctic environments due to logistical and operational difficulties during winter. Mastepanov et al. (2008) showed high emissions during autumn related to active layer freezing but the general lack of autumn and winter measurements introduces much uncertainty into annual methane emission estimates. The contribution of episodic and spatially variable bubble emissions of methane (ebullition), from both land surfaces and lakes, is also uncertain and might be a stronger source of emission than previously appreciated (Walter et al. 2006; Goodrich et al. 2011). Recent advances in quantifying ebullition seep fluxes have been made by coupling long-term continuous measurements of ebullition using submerged bubble traps placed over discrete ebullition seeps with spatially extensive surveys of the distributions of ebullition seeps across lakes. The technique, first introduced by Walter et al. (2006), utilizes the ice-cover season to identify locations of point-source ebullition seep in lakes, as bubbles released from sediments in winter get trapped as vertical stacks in downward growing lake ice. Traps are then placed under the ice, above the bubbling point-source to monitor ebullition fluxes continuously, year round throughout the ice-cover and ice-free seasons. The technique has been used to estimate regional-scale methane emissions in Alaska and Greenland (Walter Anthony et al. 2012). Statistical analyses suggested that estimates of whole-lake methane ebullition emissions using a stratified sampling design that quantifies point-source ebullition emissions are more accurate than distributed placement of bubble

Box 3.2 Measuring methane fluxes

Rapid development over recent years in laser technology has enabled much improved speed and accuracy in methane analysis across all measurement platforms. Although fast Tuneable Diode Laser (TDL) methane analyzers for application in eddy covariance have been available for more than a decade, these systems were not readily applicable in remote Arctic environments because of the need for liquid nitrogen cooling, and the high power requirements. The former has improved with the availability of less demanding quantum cascade and cavity ringdown laser systems, while the latter has been addressed by the recent introduction of low-power laser-based open path systems. However, many technological hurdles still remain, relating mainly to the power demand of these systems.

Torsten Sachs

Torsten Sachs
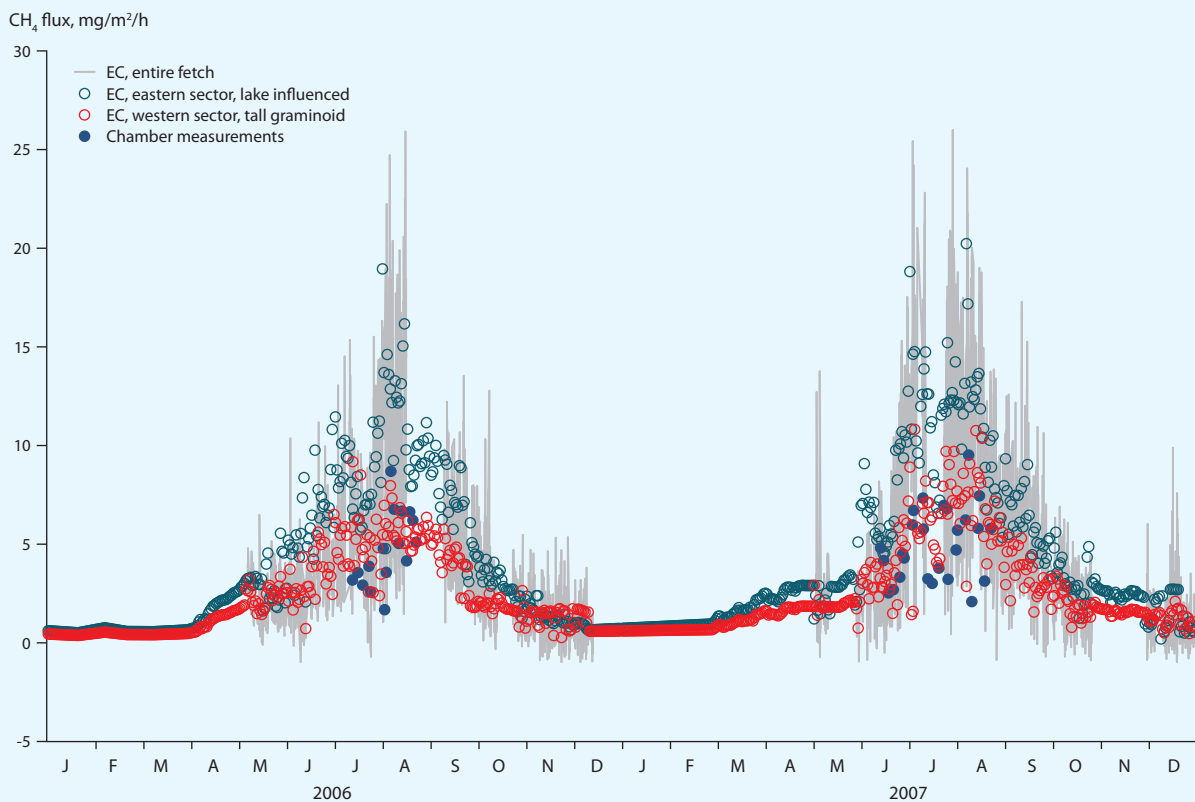
Fig. 3.3 Measuring methane fluxes. Upper right: Eddy covariance (EC) equipment to quantify surface-atmosphere heat, water vapor, carbon dioxide, and methane exchange. The EC method relies on fast (≥10 Hz) measurements of the 3D wind vector, temperatures, and concentrations of the gases of interest to derive their turbulent transport. Lower panel: Typical EC flux data showing two years of growing season emissions from a subarctic permafrost mire (Stordalen, northern Sweden) and a gap in winter due to instrumental and power problems which are typical – even at this site which has sophisticated capabilities for logistics and winter access compared to most other Arctic sites (Jackowicz-Korczyński et al. 2010). Middle right: combined automatic closed chamber (background) and gradient method (yellow tower) set-up to quantify methane flux. Measurement hut with lasers in the foreground. Middle left: flux measurement aircraft carrying EC equipment to quantify fluxes over larger areas.

traps without prior knowledge of seep locations (Walter Anthony and Anthony 2013). Other studies have shown problems with extrapolating lake emissions based on trapped air bubbles (Wik et al. 2011) and in general there is still a large uncertainty associated with lake-based episodic emission as well as emissions outside the growing season, although they undoubtedly represent highly important terms in the general terrestrial/limnic ecosystem–atmosphere interaction (Bastviken et al. 2011).

Indirect and remote methods to infer methane fluxes include tall tower (i.e. for atmospheric studies, as opposed to the flux towers mentioned earlier measuring direct ecosystem–atmosphere exchange) and airborne *in situ* concentration measurements as well as total atmospheric column concentration observations from spaced-based sensors. All of these rely on inverse modelling to derive surface flux estimates, typically on much coarser spatial scales than direct flux measurements. This is covered in Ch. 7.

The limited spatial coverage of existing observational methods can be enhanced by airborne eddy covariance flux measurements. Airborne flux measurements of northern wetland methane emissions were first made in the late 1980s and early 1990s in two large-scale experiments over the Yukon-Kuskokwim Delta (Ritter et al. 1992) and over the Hudson Bay Lowlands and northern boreal forest regions of Canada (Ritter et al. 1994). However, airborne methane flux measurements have not found their way into routine seasonal observations and have gained renewed momentum only recently with large-scale flight campaigns in Alaska, Canada, and first flights in Siberia (Sachs et al. 2012; Serafimovich et al. 2013; Kohnert et al. 2014).

3.4 Quantification of methane emissions from Arctic terrestrial sources

A recent comparison of methane emission estimates from global terrestrial ecosystem models revealed substantial variation (Melton et al. 2013). The suite of models demonstrated extensive disagreement in both their simulations of wetland areal extent and methane emissions, in both space and time. Simple metrics of wetland area, such as the latitudinal gradient, show large variability, principally between models that use inundation dataset information and those that independently determine wetland area. Agreement between the models improves for zonally summed methane emissions, but large variation between the models remains. For annual global methane (CH_4) emissions, the models vary by ±40% of the all-model mean (190 Tg CH_4/y) (Melton et al. 2013).

An international effort to quantify regional carbon fluxes globally was also undertaken recently (the Global Carbon Project – Regional Carbon Cycle Assessment and Processes (RECCAP; Canadell et al. 2011). As part of this effort, McGuire et al. (2012) conducted a thorough review of the data (Fig. 3.4) and modeling work available to date on natural methane emissions from Arctic tundra ecosystems. Much of the following is based on an updated version of this review.

Observational studies (the methods for which are discussed in Sect. 3.3) generally indicate that Arctic tundra is a substantial source of methane to the atmosphere during summer and that there has not been a substantial change in the strength of the
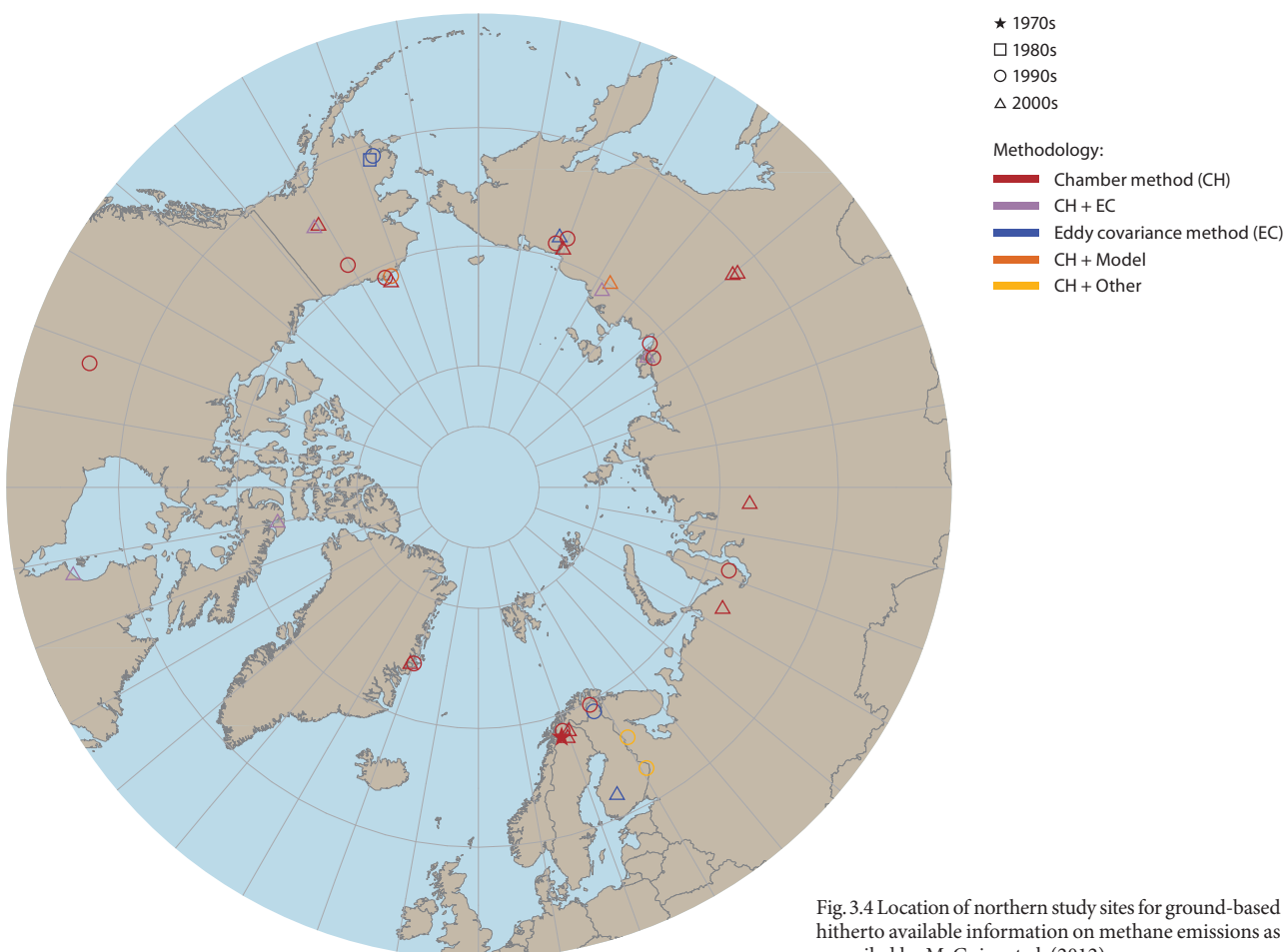
Fig. 3.4 Location of northern study sites for ground-based hitherto available information on methane emissions as compiled by McGuire et al. (2012).

Table 3.1 Summary of average ground-based observational flux estimates (120 published studies) on a per square meter basis (McGuire et al. 2012) from sites shown in Fig. 3.4. Emissions to the atmosphere in g CH_4 m^2 per summer or per year. 'Summer' is defined by the individual studies which cover various lengths. Site year is the total number of measurement years at the collected sites analyzed by McGuire et al. (2012) and used to obtain the mean flux.

Time period	Wet tundra			Dry/mesic tundra		
	Mean	Site year estimates	95% confidence interval	Mean	Site year estimates	95% confidence interval
Summer	12.3	38	7.2–17.3	1.1	25	0.4–1.9
Annual	19.5	22	11.3–27	3.1	24	0.4–5.7

source between the 1990s (4.0–10.4 g CH_4/m^2 per summer, across regions) and 2000s (1.9–18 g CH_4/m^2 per summer across regions; McGuire et al. 2012). (Note that 'summer' is used as the unit because most observational studies are constrained to the growing season. Where full annual studies are available the unit of year is used instead.) The difference in these ranges is most likely to be due to different sites being studied in the two decades and it may, hence, carry more of a spatial than temporal significance. The existing observations suggest that there are differences among different tundra types as mean summer emissions of methane for wet tundra were 12.3 g CH_4/m^2 per summer over the measurement period compared with 1.1 g CH_4/m^2 per summer for dry/mesic tundra, with no overlap in the confidence intervals (Table 3.1; Fig. 3.4; McGuire et al. 2012). Dry tundra and subarctic heath ecosystems act as a very small but significant atmospheric methane sink (Whalen and Reeburgh 1990b; Bartlett et al. 1992; Christensen et al. 1997). There are only a few studies that have estimated the exchange of methane in winter, and these studies indicate that tundra ecosystems are a moderate source of around 4.0 (0.13–8.0) g CH_4/m^2 per winter to the atmosphere (McGuire et al. 2012, supplementary information). The comparison of tundra methane emissions between summer and truly annual estimates (which are rare) suggests that methane emissions in winter support this range, as annual fluxes in wet tundra are 19.5 g CH_4/m^2; that is, 7.2 g CH_4/m^2 higher than summer fluxes and 2 g CH_4/m^2 higher in dry tundra (see Table 3.1) (McGuire et al. 2012).

As part of the RECCAP process, extrapolations of the local-scale flux observations were also made. Based on the mean and range of methane observations for different geographical regions of the Arctic, from sites in Fig. 3.4, McGuire et al. (2012) developed estimates and uncertainty ranges of methane emissions for the whole of the Arctic tundra before and after year 2000. This analysis suggests that tundra emitted 13.3 Tg CH_4/y to the atmosphere in the 1990s, with a range of uncertainty between -1.3 and 29.3 Tg CH_4/y. The analysis suggested that tundra was a stronger emitter of methane during the 2000s (26.7 Tg CH_4/y), but that the uncertainties since 2000 are much larger than in the 1990s (between 0 and 68 Tg CH_4/y). It is suspected that the larger uncertainty in the 2000s is associated with more methane measurements across a greater diversity of tundra vegetation types. Across the two decades, the McGuire et al. (2012) analysis of observations indicates that tundra emitted 14.7 Tg CH_4/y (0–29.3 Tg CH_4/y). The latter estimates are obviously sensitive to the estimated area of tundra used to calculate them. McGuire et al. (2012) followed a tundra area (mask) defined in the RECCAP study. Section 3.6 includes a brief discussion of the uncertainties associated with the areal estimates and their implications for future projections.

Emissions from freshwater systems are often neglected. In addition to the almost entirely terrestrial wetland emissions, Arctic freshwaters also contribute methane to the atmosphere and this input has been estimated to be as high as 13 Tg CH_4/y from all open freshwaters north of 54°N (that is, about 1.8 million km^2) (Bastviken et al. 2011). The freshwaters may also have played an important role in how northern ecosystems have generated feedback effects in the natural climate system during the past thousands of years (Walter Anthony et al. 2014). These lake and freshwater related emissions are influenced by ebullition events to a greater extent than are those from wetlands. As such, they are more difficult to quantify at a regional scale. Recent advances have shown simple relationships with energy input to freshwater systems as a good predictor of emission (Wik et al. 2014).

3.5 Quantification of carbon stocks and spatial extent

3.5.1 Size and characteristics of the Arctic soil carbon reservoir

This section addresses organic carbon stocks in Arctic soils where they matter for potential changes in methane release. For methane to be produced in soils (and then emitted to the atmosphere) there needs to be an organic carbon source. Estimating the amount of carbon stored in Arctic soils is therefore critical to projections of future methane emissions in a warming Arctic. Low temperatures, wet conditions and permafrost (soil or peat that is frozen for at least two consecutive years) are favorable for the accumulation and preservation of organic matter in soils as the decomposition rates are limited. In the northern hemisphere, permafrost soils occur on about 25% of the land area (23 million km^2), either as a continuous cover (continuous permafrost, >90% of the area) or patchy (discontinuous, 50–90% of the surface) and sporadic permafrost (10–50% of the surface) (Brown et al. 2014). Estimates of the amount of global organic carbon in Arctic soils have been revised upward recently, amounting to about 50% of the world's global soil carbon (Tarnocai et al. 2009). Decomposition of this carbon in a rapidly warming Arctic, and the resulting emissions of carbon dioxide or methane, is a potentially important feedback to climate warming. However, the extent to which this carbon is available for decomposition is dependent on its conservation in frozen ground and vulnerability to permafrost degradation, burial depth, and how easily the organic material is decomposed (McGuire et al. 2010; Van Huissteden and Dolman 2013). Cryoturbation (vertical movement of soil resulting from freeze-thaw

Fig. 3.5 Carbon distribution of northern permafrost soils derived from the Northern Circumpolar Soils Database (Hugelius et al. 2013, 2014).

Soil organic carbon content at
0-1 m depth, kg C/m^2

- 0.1 - 10
- 10 - 25
- 25 - 50
- 50 - 100
- > 100
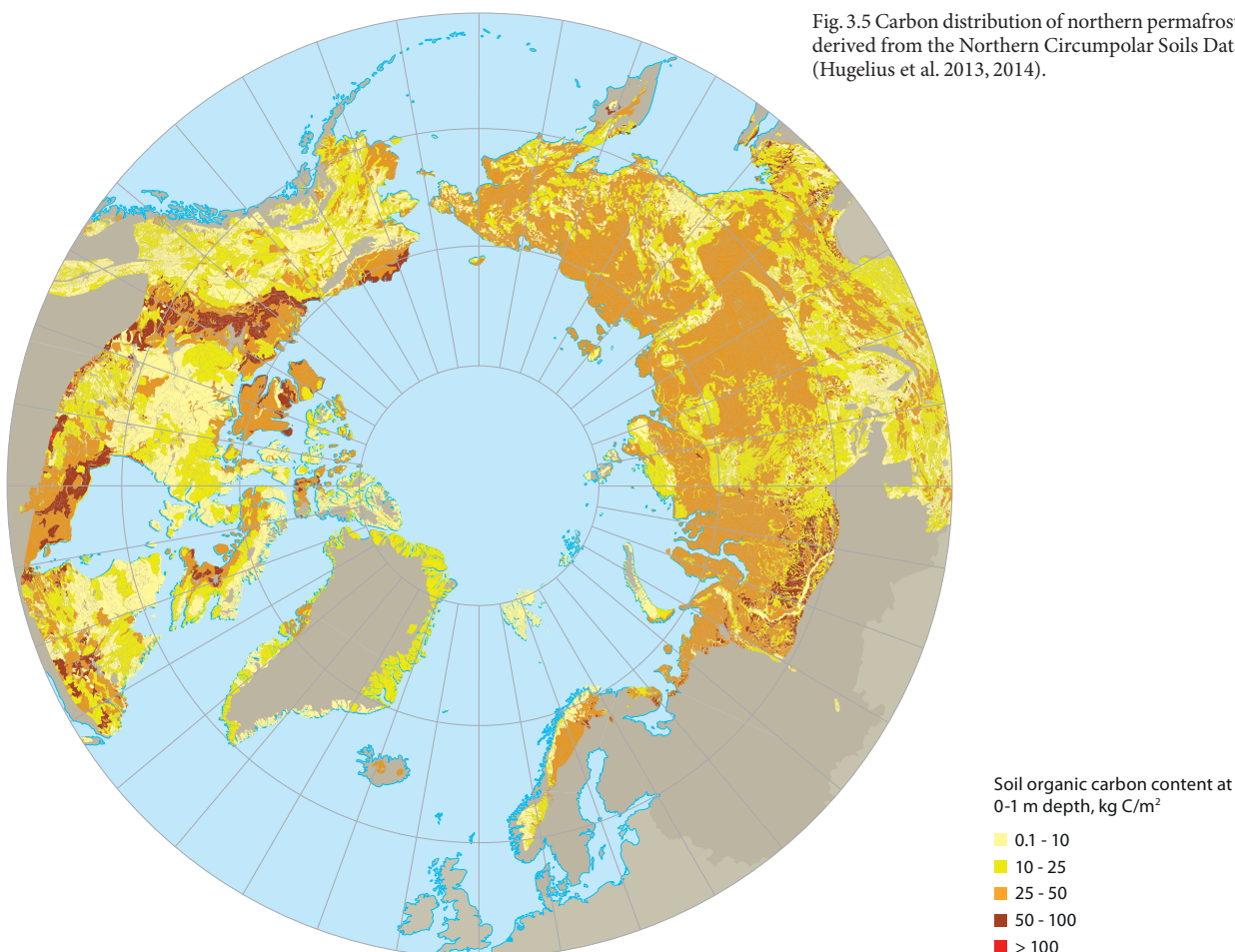
processes) mixes carbon to deeper levels in the soil, thereby potentially removing it from layers of rapid decomposition (Kaiser et al. 2007; Koven et al. 2009). On the other hand, permafrost thaw may cause erosion processes and soil subsidence resulting in lake and pond formation and erosion, processes that can expose soil carbon to either anaerobic decomposition causing methane and carbon dioxide emission, aerobic decomposition resulting in carbon dioxide emission, or transport as dissolved and particulate organic carbon to rivers and streams to lakes and the sea (Van Huissteden and Dolman 2013; Vonk and Gustafsson 2013). The latter processes have been neglected in considerations of Arctic tundra carbon cycling but have attracted increased attention recently (Vonk and Gustafsson 2013; Cory et al. 2014).

Older inventories of Arctic soil carbon included only the top 100 cm of soil; however, as permafrost thaw may affect soil organic matter (SOM) at greater depths, Tarnocai et al. (2009) also included soil layers up to 300 cm depth. Tarnocai et al. (2009) also regionalized soils and organic deposits across the Arctic,

making a subdivision between peatland areas, alluvial deposits, and yedoma. The highest organic carbon contents are found in peat soils and peaty, cryoturbated mineral soils (32.2–69.6 kg/m^2). Although yedoma soils have a low carbon content, due to the vast extent of these deposits, this adds up to a considerable carbon pool (Zimov et al. 2006; Schirrmeister et al. 2010, 2011).

The most recent estimates for Arctic soil carbon stocks converge on a range between 1400 and 1850 Pg C for all northern permafrost soils (750–1024 Pg C for peatlands, 200–450 Pg C for yedoma and 241–250 Pg C for alluvial deposits). However, the uncertainties associated with these estimates are large, in particular for carbon content at depth and thickness of deposits. To reduce the uncertainties, the Northern Circumpolar Soil Database is being developed (Hugelius et al. 2013; Fig. 3.5). Hugelius et al. (2014) arrived at lower estimates in particular for yedoma (178±143 Pg C) and alluvial deposits (31±39 Pg C) (Table 3.2); the yedoma estimate being in line with the sediment analysis data of Strauss et al. (2013).

Table 3.2 Recent estimates of Arctic soil carbon, Pg C.

Source	0–100 cm	0–300 cm	>300 cm	>300 cm (delta/ alluvial)	Total
Tarnocai et al. 2009	496	1024	407	241	1672
Schuur et al. 2008; McGuire et al. 2009	Not determined	750	400	250	1400–1850
Hugelius et al. 2014	472±34	1034±183, 1104±133	178 +140/-146	31±39	1300–1370 (uncertainty range: 930–1690)
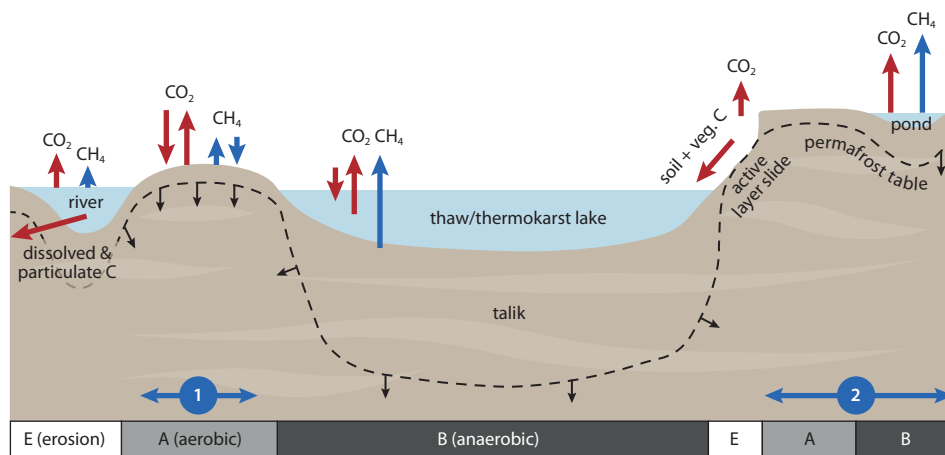
Fig. 3.6 How carbon is lost from Arctic soils with permafrost (fire excluded). The bottom bar indicates various modes of soil carbon transfer. Area 1 represents an area with spatially homogeneous active layer thickness increase and Area 2 represents spatially heterogeneous permafrost thawing driven by differences in soil ice content. After Van Huissteden and Dolman (2013). Terms defined in Box 3.1.

The decomposability (lability) of SOM strongly determines the rate at which carbon stored in soil reservoirs can be transferred to the atmosphere upon thaw and shows considerable variability. Schädel et al. (2014) analyzed the lability of SOM using aerobic incubation experiments on organic and mineral soil cores collected from Alaska and northern Siberia. The fraction of SOM that turns over in less than a year ('fast pool') was less than 5% for all soils. However, the 'slow pool' (defined here by a turnover time of 5–15 years) varied between organic and mineral soils, with organic soils showing the highest values and highest variability. The carbon/nitrogen ratio was a good proxy for the slow pool size. Treat et al. (2015) analyzed a large database of anaerobic incubations. These showed differences in the anaerobic CO_2:CH_4 production ratio (lowest for tundra sites), and overall anaerobic carbon dioxide and methane production (greatest for organic soils and inundated soils, and least for deeper horizons). Methane production was more than four times greater in soil from graminoid (grass) and shrub-dominated sites than in soils from forested sites, indicating that the vegetation community can influence methane fluxes considerably, as also shown by field observations (e.g. Ström et al. 2003; Turetsky et al. 2007). In the absence of any other changes a shift in graminoid species composition may change the CO_2:CH_4 production ratio (Ström et al. 2003). Pedersen et al. (2011) looked across a range of drained thermokarst lake basins of various ages in northern Alaska, and found evidence of substantial decomposable deposits of carbon in even the oldest lake beds (5500 years) and lower soil horizons.

3.5.2 Vulnerability of the Arctic soil carbon reservoir

Vulnerability of the Arctic soil carbon pool to climate change depends on its position with respect to the surface. Deeper (below 1 m) permafrost carbon is less vulnerable to short-term changes in temperature. A distinction can be made between gradual changes (such as changes in active layer thickness, soil wetness, and microbial process rates), and rapid 'pulse disturbances' (such as wildfires and thermal disturbance of permafrost – thermokarst, Fig. 3.6) (Grosse et al. 2011). The latter strongly depend on the distribution of ice in the subsoil (Fig. 3.6) and geomorphological processes resulting from soil subsidence and erosion. The fate of the carbon that is lost from soils is either emitted as carbon dioxide and methane to the atmosphere, or transported as dissolved and particulate organic carbon in rivers. Approximately two-thirds of this river-borne carbon is outgassed to the atmosphere during transport, but a considerable part may be sequestered again in lake, river, and marine sediments (Van Huissteden et al. 2013).

In an 'expert opinion' survey conducted in 2012, experts were asked to provide quantitative estimates of permafrost change in response to four scenarios of warming (Schuur et al. 2013). For the highest warming scenario (RCP8.5), experts hypothesized that carbon release from permafrost zone soils could be 19–45 Pg C by 2040, 162–288 Pg C by 2100, and 381–616 Pg C by 2300 in CO_2 equivalent using 100-year methane global warming potential (GWP). The values become 50% larger using 20-year methane GWP, with a third to a half of expected climate forcing coming from methane even though methane accounted for only 2.3% of the expected carbon release. Experts projected that two-thirds of this release could be avoided under the lowest warming scenario (RCP2.6) (Schuur et al. 2013).

Both temperature and precipitation changes may affect permafrost soils. Ijima et al. (2010) reported increases in soil temperature and soil wetness after four years of high rainfall and snowfall in the central Lena basin in Siberia. These changes resulted locally in taiga forest die-back (Ijima et al. 2014) and decreases in boreal forest carbon sequestration. On the other hand, water-limited plant communities in High Arctic environments may benefit from soil moisture increases (Elberling et al. 2008). Increased active layer thickness enhances decomposition of older soil carbon as shown by climate manipulation experiments (e.g. Natali et al. 2014). For example, Dorrepaal et al. (2009) report that more than 69% of the increase in soil respiration was attributed to SOM near the base of the active layer in a warming experiment in a subarctic peatland.

While expansion of existing lakes may increase in a warmer and wetter climate, it is ultimately limited by fluvial and subsurface drainage of lakes (Jones et al. 2011; Van Huissteden et al. 2011). There is a very limited body of reliable data on lake expansion, and even less so on how this may relate to changes in lake methane emissions, since it requires extensive multi-year high resolution remote sensing studies and has to take into account any non-climatic lake level changes (Plug et al. 2008; Jones et al. 2011). In southern discontinuous permafrost areas, lake area tends to decrease by regrowth (filling in of lakes to become wetlands) and subsurface drainage (Roach et al. 2011). Observation data from the Seward Peninsula (Alaska) indicate a net decrease of lake area resulting from the drainage of

Tg CH$_4$/y
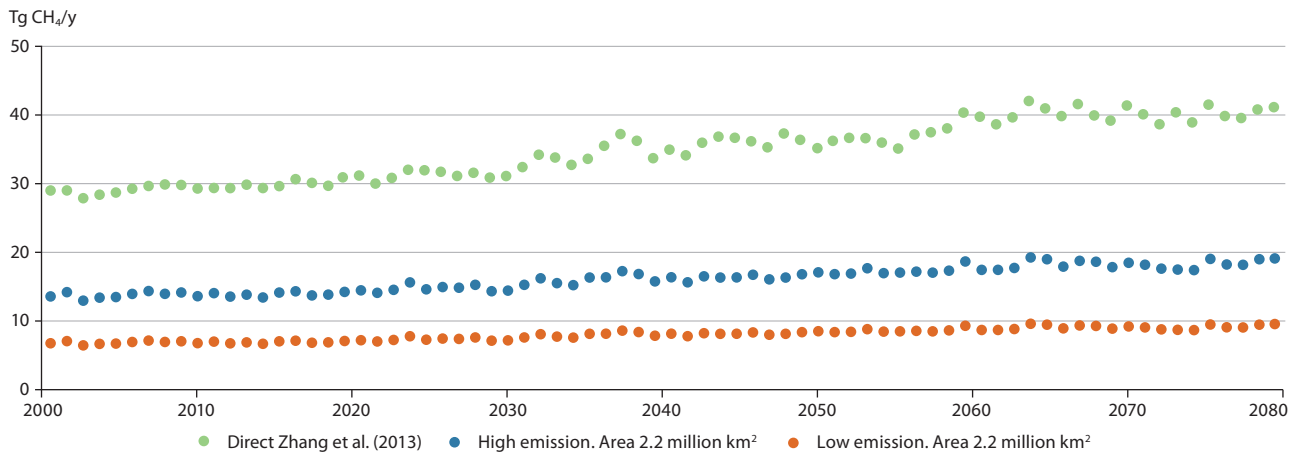
Fig. 3.7 Annual tundra emission started at present day with high and low emission as synthesized from observations by McGuire et al. (2012). Also shown is the direct output from the model as reported by Zhang et al. (2013) as applied to RECCAP domain which covers a larger area.

large lakes, while the number of smaller lakes and ponds is growing rapidly (Jones et al. 2011). In other areas there are also indications of rapidly increasing numbers of smaller lakes and ponds (Jorgenson et al. 2006). In western Siberia, a relationship was established between lake size and lake water carbon dioxide and methane concentration, with the smaller lakes showing the highest gas concentrations (Shirakova et al. 2013). This pattern indicates that small features below the resolution of current lake and wetland databases may be important controls on carbon transfers from permafrost soils to the atmosphere.

3.6 Estimates of future methane emissions from natural terrestrial sources

A variety of simple empirical as well as advanced ecosystem process models have been used to estimate methane emissions from tundra into the future, including: (1) empirically-based regressions of net methane fluxes (Moore and Roulet 1993; Frolking and Crill 1994; Christensen et al. 1996; Bellisario et al. 1999; Kaplan, 2002); (2) daily flux estimates based on either predicted or observed water chemistry, temperature, and respiration (Potter and Klooster 1997); (3) site, regional, and global scale approaches that include vertical structure, aqueous and gaseous transport, competition between processes affecting methane concentrations, and simple representations of water chemistry (Cao et al. 1996; Walter et al. 2001; Zhang et al. 2002; Zhuang et al. 2004; Petrescu et al. 2010; Tian et al. 2010; Wania et al. 2010b; Riley et al. 2011); and (4) models of all the above types that also include details of microbial population dynamics, aqueous chemistry, and soil horizontal heterogeneity (Grant 1998, 1999; Segers and Leffelaar 2001a,b. LPJ-GUESS WHyMe is the updated version of LPJ-GUESS (The Lund-Potsdam-Jena General Ecosystem Simulator, Smith et al. 2001), customized for upland and wetland ecosystems for the northern high latitudes. For upland ecosystems, Arctic-specific plant functional types have been adopted to encompass deciduous and evergreen shrubs and four open-ground tundra species (Wolf et al. 2008). For wetland ecosystems, the model has incorporated recent developments to LPJ-DGVM by Wania and co-workers (LPJ WHyMe v1.3.1 – Wania et al. 2010b) that include soil freezing processes, peatland hydrology, peatland plant functional types (PFTs), and methane dynamics.

McGuire et al. (2012) showed that LPJ GUESS WHyMe agreed with observations, inverse modelling, and three other process-based ecosystem models in predicting that the Arctic land area was a stronger carbon dioxide sink in 2000–2006 than in 1990–1999 and, based on observations as mentioned earlier, there were indications of an increasing source to the atmosphere of methane.

Global wetlands are estimated to emit ~140–280 Tg CH$_4$/y (Kirschke et al. 2013) from a total area of ~5 million km^2, half of which lies north of 50°N (Matthews and Fung 1987). To assess the sensitivity of northern emissions to wetland area, Petrescu et al. (2010) applied a single methane-wetland model to five different wetland distributions. Areas varied by a factor of two (2.2–4.4 million km^2) and reported emissions varied by a factor of four (38–157 Tg CH$_4$/y).

Since these form major sources of uncertainties annual tundra emissions have been calculated based on: (1) estimated spatial area of wetland tundra, i.e. the lower end of the areal range above for all northern wetlands (2.2 million km^2); (2) high and low estimated per square meter emissions as compiled from observational studies by McGuire et al. (2012; Sect. 3.4); and (3) the direct output of the Zhang et al. (2013) study applied to the RECCAP areal domain (McGuire et al. 2012). Taken together, this method provides an envelope of methane emission estimates for the present and a range of scenarios into the future (Fig. 3.7).

It is noted that the estimates by Zhang and co-workers (Fig. 3.7) are somewhat above what the atmospheric observations and associated inverse modelling currently suggest (see Ch. 7). These inverse atmospheric modeling estimates suggest a source of around 20 Tg/y during the first decade of the timeline projected in Fig. 3.7. At the same time, this may indicate that the observational evidence underestimates total emissions (Fig. 3.7).

3.7 Natural terrestrial emissions for AMAP methane climate modeling

Based on the range of outputs shown in Sect. 3.6, the natural emission scenarios span changes between a modest 10 Tg/y to more than 40 Tg/y for natural terrestrial methane emissions through the year 2080. These projections do not consider abrupt changes or accelerating trends, although

such changes are possible during this period. Given the potential for decomposition discussed in Sect. 3.5, changes in decomposition rate could be an important factor in the future. In addition to these aspects of uncertainty, it is also known that many processes are not well represented in current models; including hydrology, lake dynamics, permafrost, thermokarst and thermal erosion. These are all likely to impact future methane emissions. Therefore, for the combined climate scenarios developed in Ch. 8 simple estimates of low, medium and extreme natural terrestrial emissions are utilized rather than output from specific model runs such as the examples discussed in Sect. 3.6.

3.8 Conclusions

3.8.1 Key findings

In relation to the guiding questions outlined at the start of this report, understanding of natural terrestrial methane sources has increased markedly over the past decades. The estimated scale of current emissions varies between measurement and model estimates but in general falls within the range 10–30 Tg CH_4/y. This understanding combined with the large organic carbon reservoirs in the source ecosystems suggests significant potential for increasing emissions in a changing climate but the rate and scale of this potential increase is still very uncertain. The major controls on natural methane emissions are all climatically controlled, either directly (temperature, precipitation/hydrology) or indirectly (vegetation change, permafrost collapse/erosion) and, hence, any change in climate should drive a change in emission from this large natural source. In this study, a range of climate change estimates (Ch. 8) have been applied based on projected scenarios over a 50-year time horizon which spans 25–50 Tg CH_4/y all also including possible changes in the natural marine environments (see Ch. 4). A more extreme scenario for natural emission change of 100 Tg CH_4/y has also been included, acknowledging the uncertainty and possible step-changes or accelerating trends that are not dealt with in current process models.

3.8.2 Recommendations

Uncertainty associated with current estimates of natural terrestrial methane emissions may be reduced through several means:

- Increased ground-based monitoring of natural methane sources. The current capability for methane flux monitoring in the Arctic is very limited and needs increased areal coverage.

- Expanded continuous flux monitoring networks with winter emission measurement capabilities. The great constraint on these is the logistical infrastructure needed for operation at remote sites and in a harsh winter climate. Basic needs such as transport and power supply are restricted in most of the remote Arctic areas in winter. Improvements in site and field station infrastructures are pivotal.

- More and better research site infrastructure and comparability of instrumentation in the Arctic.

- Cross-disciplinary approaches to document source to sink emissions and transport issues that include terrestrial, freshwater and near-coastal environments.

- Airborne observations are needed to enhance spatial coverage, and space-based monitoring should be developed to an operational standard for monitoring ground-based source variations.

- Novel technology, using gas sensing technology as well as drones and satellite-based sensors should be further developed in order to enable improved high resolution understanding of point sources in space and time as well as to help provide better year-round coverage of ecosystem–atmosphere fluxes.

Acknowledgments

4. Natural marine methane sources in the Arctic

Lead authors: Frans-Jan W. Parmentier, Anna Silyakova, Arne Biastoch, Kerstin Kretschmer
Contributing author: Giuliana Panieri

4.1 Introduction

The world's oceans are traditionally viewed as a small contributor to the contemporary global methane budget (Ehhalt 1974; Kirschke et al. 2013). However, the tremendous amount of methane thought to be stored in ocean sediments (Milkov 2003; Hester and Brewer 2009) signifies the vast potential of the marine environment to emit large amounts of this greenhouse gas. The most important reservoir for methane is suggested to be in the form of gas hydrates, which are found at depth along the edge of the continental margin and may be present at shallower depths in subsea permafrost-associated areas. The methane stored within these hydrates originates from deeper in the ocean sediment, from thermogenic or biogenic sources. Other methane sources within the ocean include geological seeps and production of methane in surface waters.

This chapter focuses on the size, controlling processes and factors, and potential future changes in these methane sources within the context of the Arctic Ocean. For the purposes of this report, the area referred to as the Arctic Ocean includes continental shelf areas and its surrounding seas (see Fig. 4.1), unless specified otherwise. These areas vary widely, from deep basins in the central Arctic Ocean to shallow continental shelf regions. Some of these shelf regions – such as the Laptev Sea – contain large areas of subsea permafrost, while others do not. Moreover, most marginal seas in the central Arctic basin are covered by sea ice either throughout the year, or for a large part of the year. Other seas experience large seasonal changes in sea ice cover, and have shown a dramatic decline in sea ice over recent decades. This variety within the seas of the Arctic translates into a diversity of methane sources, and their vulnerability to climate change and accompanying sea-ice decline differ accordingly.

Methane hydrates in the sediments of the Arctic Ocean and its marginal seas are considered more vulnerable to climate change than elsewhere in the world, due to their presence at shallower depths within the Arctic. These hydrates form in ocean sediment under high pressures and low temperatures because these conditions allow for the formation of an ice-like structure that can trap methane within its crystal structure – commonly known as 'gas hydrate'. Since climate warming is occurring rapidly in the Arctic – and this trend is expected to continue (see Ch. 1) – it has been hypothesized that destabilization of gas hydrates could occur in the Arctic. If the methane contained within hydrates were released to the atmosphere over a relatively short period of time, this would amplify global warming (Nisbet 1989). Also, the Arctic Ocean contains large shelf regions with subsea permafrost, and it has been proposed that more methane will be released when these sediments thaw, either from gas hydrates or the decomposition of previously frozen organic matter. Underlining these concerns, recent expeditions have discovered hotspots of methane release from gas hydrates along the west coast of Spitsbergen (Westbrook et al. 2009; Bünz et al.
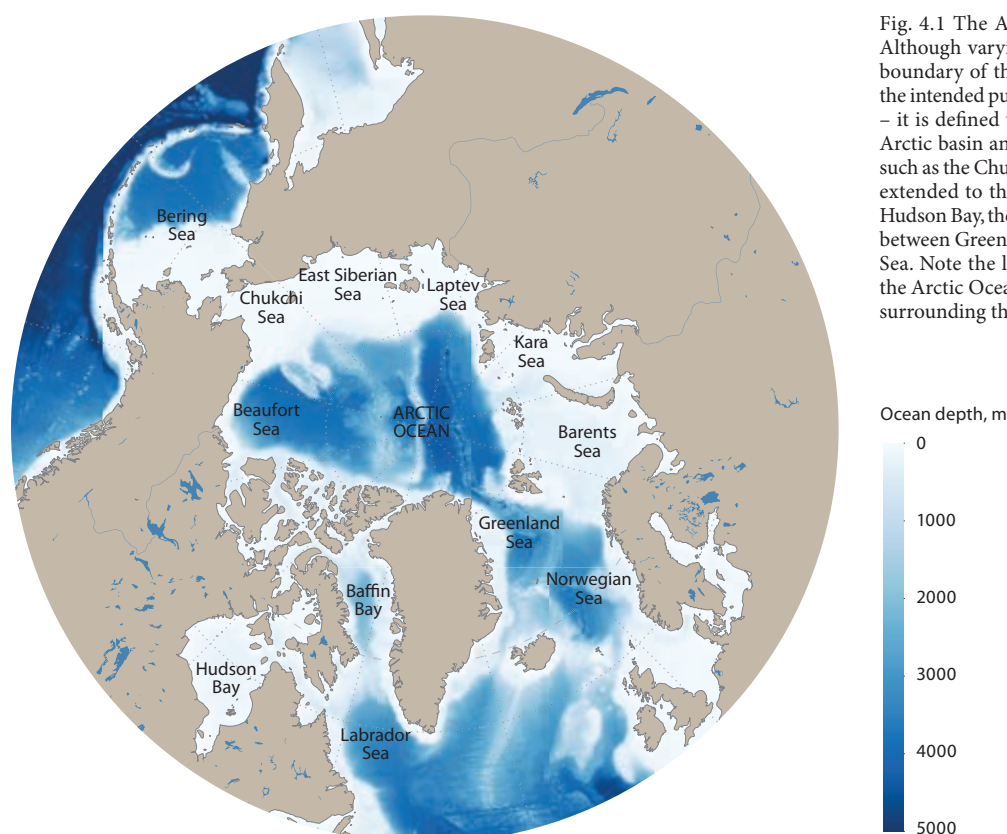
Fig. 4.1 The Arctic Ocean and adjacent seas. Although varying definitions exist of the exact boundary of the Arctic Ocean – depending on the intended purpose of the accompanying study – it is defined within this report as the central Arctic basin and the surrounding shelf regions, such as the Chukchi Sea and the Barents Sea, and extended to the other named seas, namely the Hudson Bay, the Labrador Sea, the Nordic Seas in between Greenland and Norway, and the Bering Sea. Note the large continental shelf region of the Arctic Ocean with relatively shallow depths, surrounding the deep central basin.

Ocean depth, m

0

1000

2000

3000

4000

5000

2012) and from the shallow waters along the East Siberian coast where subsea permafrost is thought to be broadly distributed (Shakhova et al. 2010). This emphasizes the potential of the Arctic Ocean as a source of methane, and stresses the need for a thorough understanding of these sources.

Despite this potential, knowledge of the distribution, functioning and likely future change in these methane sources is much less developed than for methane sources in the terrestrial Arctic. While good progress has been made on determining the methane budget of the terrestrial Arctic (McGuire et al. 2012), the dearth of observations in the Arctic Ocean leaves many questions unanswered. This lack of understanding is not only due to the vast area involved, but also to the logistical challenges of taking measurements in an ocean that is largely covered by sea ice. Despite such complexities, a better understanding of these sources, and their expected future change, is paramount. This chapter, therefore, aims to provide clarity, constrain uncertainties, and assess the vulnerability of methane deposits in the Arctic Ocean to climate change. Specifically, and in parallel with Ch. 3 on natural terrestrial sources, this chapter seeks to address the following questions posed in Ch. 1 (Table 1.1):

What are the current methane emissions from Arctic marine sources?

What are the controlling processes and factors that strongly influence natural emissions?

How may these emissions from natural sources in the Arctic change in the future?

What are the uncertainties or limitations in these estimates?

4.2 Methane sources and reservoirs in the Arctic Ocean

4.2.1 Subsurface methane production

Methane production is common throughout the subsurface of the world's oceans and occurs through microbial, thermogenic or abiogenic processes. The three processes occur at varying depths within the sediment column and under differing conditions (see Box 4.1, Fig. 4.2).

Microbial methane is produced by methanogenic archaea, microorganisms that form methane through carbon dioxide reduction or the conversion of acetate (Garcia et al. 2000) – similar to the terrestrial sources (see Sect. 3.2). Since the activity of methanogens depends on temperature, this process occurs within anoxic and sulfate-depleted zones in ocean sediments at various depths and timescales, with an optimum temperature of around 35–40°C and a maximum of 55–60°C (Judd 2004). Such temperatures are reached at depth due to an increase in temperature according to the local geothermal gradient. Depending on the thermal gradient and according to the temperature constraints, the zone of microbial methanogenesis is mainly limited to the top 1 or 2 km of ocean sediments, in which about 10% of the total organic carbon is typically converted to methane (Judd 2004).

Organic matter in deeper layers (such as coal beds) may be degraded when temperatures increase over 110°C with depth (Milkov 2005), resulting in a concomitant production

Box 4.1 Areas of methane production, oxidation and migration

Deep within the sediment, temperatures are high enough (over ~100°C) for thermogenic formation of methane. Higher in the sediment, temperatures are lower (below ~60°C) and suitable for microbial methane production. The methane generated in these two zones can migrate upwards, and may be sequestered in gas hydrates. While migrating towards the seafloor, methane can be anaerobically oxidized in the sulfate-methane transition zone (orange), or aerobically oxidized in the oxic upper part of the sediment (separated by the dashed line). The position of the oxic/anoxic sediment boundary can vary considerably depending on local conditions. Any methane that survives these oxidation zones may diffuse up into the ocean, but is still subject to further aerobic consumption within the water column (blue). Methane released through bubble plumes dissolves into the seawater, exposing it to aerobic consumption. In contrast, relatively small amounts of methane can be formed under certain specific conditions in the surface mixed layer. Finally, methane may be released into the atmosphere from surface waters. Note that the graphic is not drawn to scale and has an exaggerated proportion of near sea-floor processes. Abiogenic formation of methane is not shown. For a detailed description of these processes see Reeburgh (2007).
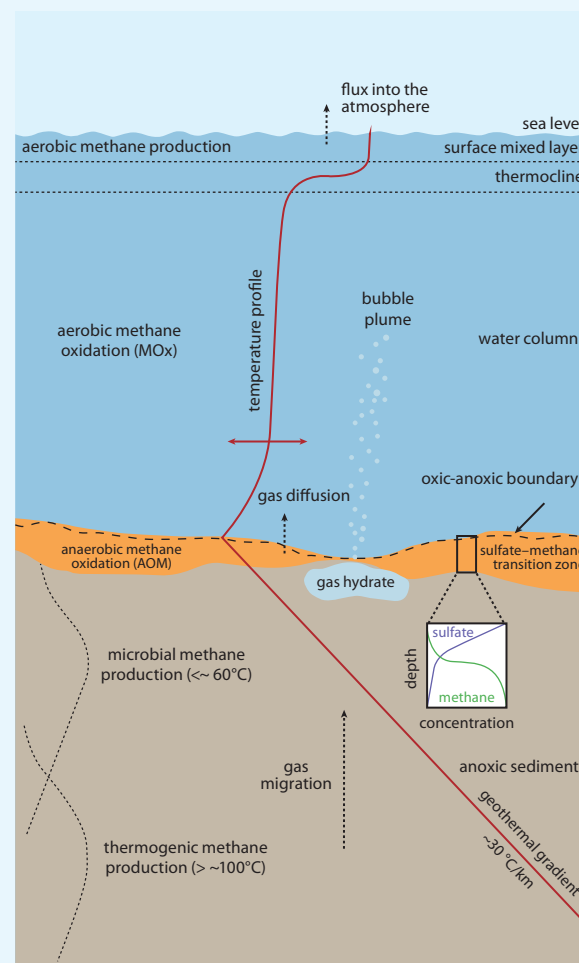
Fig. 4.2 Typical areas of methane production, oxidation and migration within the ocean and its sediments.

of thermogenic methane. Due to the higher temperature requirement, typical depths for thermogenic methane formation are deeper than the zone of microbial methanogenesis, and according to the prevailing geothermal conditions may extend down as far as 4 to 5 km (Judd 2004). Thermogenic methane is often associated with petroleum, coal and other forms of hydrocarbon compounds and fossils (Archer 2007), and may be released through gas seeps. Such seeps are geographically widespread across the sea floor (Judd 2004; Skarke et al. 2014) and are characterized by high methane effluxes to the water column (Niemann et al. 2013).

Abiogenic methane formation does not involve organic matter and is said to occur where methane is derived through metamorphic processes such as serpentinization, where the hydration of minerals leads to the formation of hydrogen. The hydrogen produced in this process can react with carbon-containing gases, leading to the formation of methane. Abiogenic processes are commonly associated with hydrothermal vents and faults in the oceanic crust, degassing of mafic magmas and cooling of mafic igneous rocks (Etiope and Sherwood Lollar 2013). However, it is not yet clear how large the contribution of abiogenic methane formation is to the global carbon cycle (Proskurowski et al. 2008), or the Arctic in particular, because it is difficult to distinguish between abiogenic and biotic sources once the methane from the two sources is mixed. Nonetheless, serpentinization is known to occur at mid-ocean ridges within the Arctic Ocean and the methane produced there can accumulate in gas hydrates (Rajan et al. 2012).

The methane produced via the three pathways is buoyant and, due to pressure gradients, is advected toward the surface of the sea floor. The gas may then be sequestered in gas hydrates, oxidized in the sediment, or released into the water column, as discussed in the following sections.

4.2.2 Gas hydrate formation and occurrence

Gas hydrates are solid crystalline compounds in which gas molecules are lodged within a clathrate crystal lattice (Fig. 4.3). Within this lattice, gas hydrates may hold hydrocarbons, carbon

Fig. 4.3 Structure of a methane hydrate block found during a research cruise with the German research ship FS *SONNE* in the subduction zone off Oregon (Pacific Northwest, USA) at a depth of about 1200 m in the upper meter of the sediment. Source: Wikimedia Commons.

dioxide or hydrogen sulfide, but methane is typically the main gas component (Buffett 2000). Gas hydrates are, therefore, commonly referred to as methane hydrates. Methane contained within gas hydrates usually migrated from deeper sediment layers before it was captured (Reed et al. 1990). Isotopic analyses indicate that the majority of the hydrate deposits on Earth contain biogenic methane (Archer 2007), although hydrate formation may theoretically sequester methane of various origins (Rajan et al. 2013).

In areas of sufficient methane availability, methane hydrates form under low temperature and high pressure (Kvenvolden 1988a). Due to these required conditions, natural methane hydrate deposits occur in those areas where cold bottom water is present, and the pressure of the overlying water and sediment column is sufficient. Commonly, such regions include the outer continental margins, slopes and rises (Kvenvolden 1993), but also areas of permafrost, both onshore and offshore (Kvenvolden 1988a), as shown in Fig. 4.4. The depth over which the required
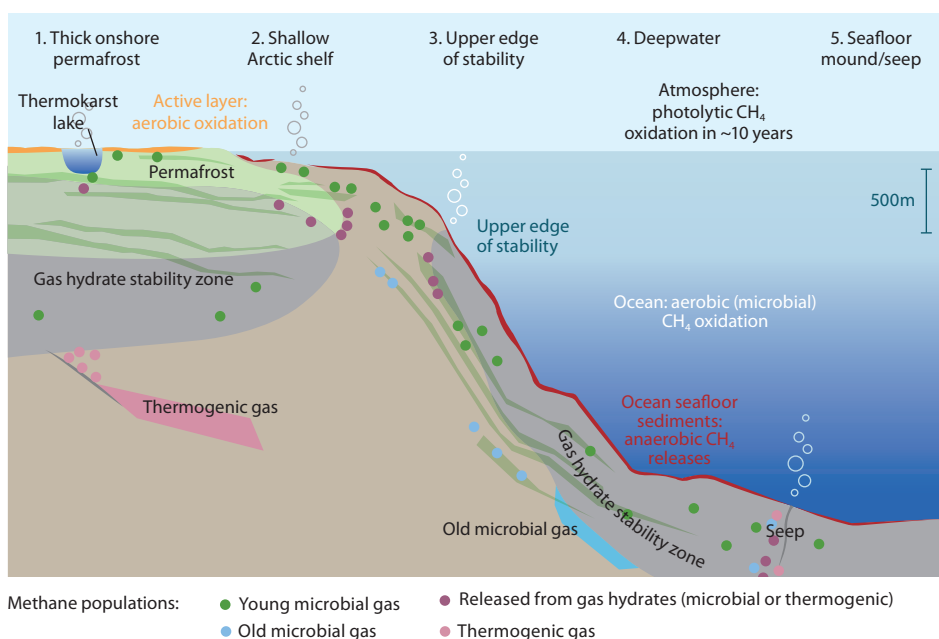
Fig. 4.4 Gas hydrate distribution and methane migration pathways in the Arctic Ocean. In permafrost regions (left of graphic), gas hydrates may occur at shallower depths, due to the lower sediment temperatures. In areas where subsea permafrost has degraded, gas may rise upwards. Outside permafrost regions, active gas hydrates typically occur at the edge of the continental margin, where rising bottom water temperatures may destabilize their upper edge. In the deep ocean, methane may originate from seeps, typically of geologic origin. Meanwhile, anaerobic oxidation of methane occurs at the top of the sediment (red line), while aerobic oxidation occurs within the water column. Redrawn from Ruppel et al. (2011).

conditions prevail is known as the gas hydrate stability zone (GHSZ). Globally, the GHSZ starts at water depths exceeding 300–500 m (Kvenvolden 1988a) up to a depth where sediment temperature increases beyond the stability threshold (Archer et al. 2009). In the Arctic, however, gas hydrates are found at the shallower end of the quoted depth range, since the average bottom water temperature is lower in polar regions, while permafrost-associated methane hydrates may occur at even shallower depths of ~200 m (Ruppel 2014). Even so, the thickness of the GHSZ in the Arctic region still varies, and depends on changes in heat flow (geothermal gradient), amount of higher-order hydrocarbon gas (Rajan et al. 2013), ocean bottom temperature, and seawater salinity (Giustiniani et al. 2013).

Many researchers have used information concerning areas where the required pressure and temperature conditions for methane production are known to occur, together with data obtained from drilling campaigns such as hydrate pore filling, to estimate the total global amount of methane contained within hydrates. Recent estimates range from 455 to ~2500 Pg C (Milkov 2003; Archer 2007; Burwicz et al. 2011; Denisov et al. 2011; Wallmann et al. 2012), although much higher estimates of 10,000 Pg C or even 64,000 Pg C have previously been suggested (Klauda and Sandler 2005; Kvenvolden 1988a). Specific estimates for the Arctic Ocean have a large uncertainty, ranging from 116 to 900 Pg C (Kvenvolden 1988b; Biastoch et al. 2011; Kretschmer et al. 2015). Of these large potential deposits, the amount of permafrost-associated gas hydrates – both onshore and offshore – may represent only a very small fraction of about 1%, and a recent conservative estimate sets these deposits at ~20 Pg C (Ruppel 2014).

4.2.3 Surface water sources of methane

Methane production in the ocean is not limited exclusively to the sediment, since production is also possible in surface waters (Grossart et al. 2011). This helps to explain the long known fact that the oxygenated mixed layer at the ocean surface is oversaturated in methane compared to the atmosphere (Lamontagne et al. 1973; Rhee et al. 2009). This phenomenon of methane production in oxic environments is also referred to as the 'Ocean Methane Paradox' (Kiene 1991), since oxic environments normally favor the consumption – not formation – of methane. Above geological seeps, oversaturation of the surface mixed layer could be due to a higher influx of methane rather than methane production (Solomon et al. 2009), but this would not explain oversaturation in other parts of the ocean.

There are several mechanisms of methane production possible in oxygenated surface waters, and most involve microbes and non-competitive substrates. Under phosphate limitation, for example, methane can be produced as a by-product of the decomposition of phosphonates (Karl et al. 2008; Carini et al. 2014). These organic compounds are characterized by a carbon-phosphorus (C-P) bond and act as a source of phosphate during aerobic growth, releasing methane in the process. When nitrate is limiting, it has been suggested that methane can be produced as a by-product of dimethylsulfoniopropionate (DMSP) degradation (Damm et al. 2010). DMSP is produced by a variety of phytoplankton species (Stefels 2000) and utilized by bacteria as a source of energy and carbon (Kiene et al. 2000). Finally, methane can also be produced within the digestive tracts of herbivorous zooplankton (through

conversion of trimethylamine, see De Angelis and Lee 1994), fish guts (e.g. Oremland 1979), and anoxic microenvironments in ocean particles, such as fecal pellets (Scranton and Brewer 1977; Marty 1993). Due to the close proximity to the surface of many of these processes, a connection has been suggested with observed methane fluxes above the Arctic Ocean (Kort et al. 2012). Although the relative contribution of these processes to the methane budget of the Arctic Ocean remains unclear, it is likely to be a small – but possibly significant – source.

4.3 Controls on methane sources

4.3.1 Anaerobic and aerobic consumption of methane

About 90% of all methane produced in marine sediments, of biotic and abiotic origin, is consumed by anaerobic oxidation (Reeburgh 2007), which occurs in the upper sediments from millimeters to more than 200 m below the sea floor (Knittel and Boetius 2009) (see Fig. 4.2). Anaerobic oxidation of methane is mediated by a microbial consortium of archaea and sulfate-reducing bacteria (Knittel and Boetius 2009) and generates high concentrations of hydrogen sulfide, which supports chemosynthetic communities that gain energy from sulfide oxidation (Treude et al. 2003), as well as bicarbonate, which precipitates as authigenic carbonates (Boetius et al. 2000). This process contributes to the dynamic biogeochemistry found at the very top of the sediment column, and its general reaction is as follows:

$$CH_4 + SO_4^{2-} \longrightarrow HCO_3^- + HS^- + H_2O \qquad \text{Eq. 4.1}$$
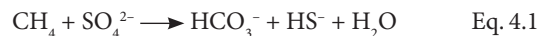
Because this reaction requires both methane and sulfate, the process occurs where these overlap, and the highest anaerobic oxidation of methane and sulfate reduction rates are therefore found in this sulfate-methane transition zone (Iversen and Jørgensen 1985) (see Fig. 4.2). The necessary sulfate for this reaction is transported from the overlying seawater, and the peak concentration of sulfate is usually found at the sediment-water interface (D'Hondt et al. 2002). As both sulfate and methane are reduced in this area, due to microbial activity in the sediment and anaerobic methane oxidation, it is possible that methanogenesis can start to dominate once sulfate is depleted (Archer 2007). However, even when methane bypasses the anaerobic microbial filter, it can be subsequently oxidized by aerobic bacteria in aerated surface sediments (Boetius and Wenzhöfer 2013 and references therein) or, once it is released from the ocean sediment, in the oxic water column (Hanson and Hanson 1996; Murrell 2010) according to the following chemical reaction:

$$CH_4 + 2O_2 \longrightarrow CO_2 + 2H_2O \qquad \text{Eq. 4.2}$$
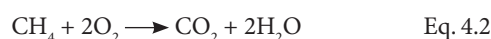
Rates of methane oxidation are dependent on the microbial community and the amount of available methane (Murrell 2010), indicating that aerobic methane oxidation is a dynamic process, and can change depending on the availability of methane or changes in hydrography (Valentine et al. 2001). Although aerobic methane oxidation lowers the potential of methane to reach the atmosphere, the process also leads to a diminished oxygen concentration, an enhanced partial pressure of carbon dioxide, and a lower pH (Biastoch et al. 2011).

4.3.2 Fate of rising methane bubbles

While the oxidation processes described in the previous section act on dissolved methane, the solubility of methane in water is low. This can, therefore, lead to the formation of bubbles in areas of high methane production, after which ebullition allows the gas to bypass oxidation layers and release from the seabed. Because bubble streams rise quickly through the water column, ebullition is an important transport pathway for methane. At the moment of escape from the seabed, methane bubbles have a high methane concentration, typically more than 90% (Leifer and Patro 2002). During the rise towards the surface, however, bubbles are subject to dissolution (McGinnis et al. 2006), which reduces the methane concentration inside the bubble, and allows for some – if not all – of the methane released through ebullition to be dissolved and subsequently oxidized in seawater.

Methane bubble dissolution in the water column is due to many factors (Rehder et al. 2009). For example, the large difference between the high methane concentration inside the bubble and the low concentration of the outside seawater is a strong driver of dissolution. The transfer of gas from the bubble is affected by gas solubility and diffusivity, which both depend on pressure and seawater temperature. Furthermore, seawater density and viscosity, bubble density, and the mobile or immobile surface of the bubble interface affect the flow field around the bubble. However, one of the most important factors affecting the behavior of bubbles following their release from the seabed is water depth. As bubbles rise higher in the water column, pressure drops, and bubbles may expand. Following the escape of methane into the seawater, however, the bubble shrinks and can dissolve. Although, bubbles that escape the seabed within the GHSZ shrink and dissolve much more slowly than those released above this zone. This is related to the formation of a methane hydrate rim around the bubble, leading to a 'frozen bubble' (McGinnis et al. 2006), which depends on depth, temperature, the partial pressure of methane within the bubble and the methane concentration outside. Once formed, a hydrate rim surrounding a bubble may allow it to rise much further than otherwise expected.

The size of the bubble also strongly affects its behavior (Schneider von Deimling et al. 2011). For example, bubbles with an initial diameter ≤4 mm shrink and dissolve steadily before reaching the thermocline, while bubbles with an initial diameter >10 mm are expected to increase in size during their ascent towards the surface. Furthermore, upwelling flows and surfactants may reduce the dissolution of bubbles and allow them to survive for much longer (Solomon et al. 2009).

Nonetheless, even when a bubble has been able to reach the surface, dissolution is expected to have led to a significant lowering of the methane concentration within the bubble, such that most of the methane has been stripped from the bubble by that time. While examples are known of bubbles with an oily coating that survive transport to the surface from much greater depths (Solomon et al. 2009), most bubble plumes are not expected to reach the atmosphere in waters deeper than 100 m (McGinnis et al. 2006). In the Arctic, this has been shown to be true for bubble plumes off the west coast of Spitsbergen, which failed to reach the surface from depths ranging from 150 to 400 m (Westbrook et al. 2009; Berndt et al. 2014). In shallower waters of the marginal seas (for example tens of meters) methane bubbles have a better chance of surviving their ascent through the water column, and releasing methane to the atmosphere (Shakhova et al. 2014).

4.4 Emission to the atmosphere

4.4.1 Measurement techniques

Measurements of the amount of methane released from the Arctic Ocean into the atmosphere are essential to assess its contribution to the greenhouse-gas budget of the Arctic. Diffusive methane emissions from the ocean to the atmosphere are dependent on the difference in the partial pressure of methane within the ocean water and the atmosphere. Hence, accurate concentration measurements of both are required to achieve a reliable flux estimate. The concentration of methane in water is, in most cases, determined from headspace equilibration (e.g. Reeburgh 2007); bottles are filled and flushed with seawater, after which a headspace gas (typically nitrogen or helium) is injected in sufficient volume to allow most of the methane to equilibrate into it, while excess seawater is drained out. After vigorous shaking of the samples – to allow for sufficient equilibration – the concentration of methane within the headspace is measured with the use of a gas chromatograph, while the remaining methane within the seawater can be estimated with the use of known solubility values. The methane concentration in the air above the sea surface can either be determined by gas chromatography on air samples, or with the use of a gas analyzer. Once the two concentrations are known, the diffusive flux to the atmosphere can be determined following Wanninkhof (1992) with the use of two equations:

$$\text{Flux} = k(C_w - C_{eq}) \qquad \text{Eq. 4.3}$$

Here, k is the gas transfer coefficient, C_w is the gas concentration in seawater, and C_{eq} is the expected methane concentration in seawater when in equilibrium with the measured atmospheric concentration above the sea surface (determined with a solubility coefficient). The gas transfer coefficient, k, depends on the wind speed, and is often defined as:

$$k = 0.31u^2 \, (\text{Sc}/660)^{-1/2} \qquad \text{Eq. 4.4}$$

where u is the average wind speed at a fixed height above the sea surface (typically 10 m), Sc is the Schmidt number, which depends on seawater temperature and salinity, and 0.31 and 660 are experimentally derived coefficients (for details see Wanninkhof 1992). It is worth noting, however, that alternative methods for determining k have been proposed in recent years, by studying the gas exchange of lakes, which may work better in the case of low wind speeds (Cole and Caraco 1998; Crusius and Wanninkhof 2003) or when a system is cooling or warming (MacIntyre et al. 2010). In addition, the above-cited relationship to determine the sea-to-air flux has received a proposed update through the incorporation of progressing insight (Wanninkhof 2014). Despite these progressions, however, much of the understanding of sea-to-air fluxes is developed in temperate areas, and may not be translatable directly to the Arctic due to the presence of sea ice, more frequent high winds, and low winter temperatures (Bourassa

et al. 2013). Keeping these uncertainties and complications in mind, such equations do retain usefulness because they allow for a simple first-order calculation of the sea–air flux while requiring only a few basic parameters such as wind speed and the concentrations of methane within seawater and the air above it. For a more thorough discussion on sea–air gas transfer equations than presented here, see Wanninkhof et al. (2009).

A potentially large uncertainty in gas transfer equations, however, arises from the fact that bubbles are not captured – while this has been suggested to be a major part of the total emission to the atmosphere in certain areas (Shakhova et al. 2014). In recent years, therefore, other methods have been explored to derive more accurate flux estimates. Eddy covariance, for example, is a technique that is typically used for terrestrial flux measurements (see Ch. 3 for details), but can be used on ships as well, when adjusted for the motion of the vessel, and has been applied with varying success (e.g. Miller et al. 2010). Alternatively, methane fluxes can be measured from airborne platforms (Kort et al. 2012) but direct flux measurements from moving platforms are not always straightforward, and the most commonly used method remains the use of gas transfer coefficients.

4.4.2 Arctic Ocean emission estimates

Even though understanding of sources and sinks has grown significantly in the past four decades, estimates of the oceanic contribution to the global atmospheric budget of methane have varied relatively little over that period (Ehhalt 1974; Rhee et al. 2009; Kirschke et al. 2013). One of the reasons for this low variation is that the open ocean – away from the continental shelves – has been shown to be a low emitter of methane, despite an oversaturation in methane and a vast surface area (Conrad and Seiler 1988; Bates et al. 1996; Rhee et al. 2009). As shown in Sect. 4.3, a large part of the methane released into the oceanic water column is ordinarily consumed before it reaches the surface, limiting the potential of methane to reach the atmosphere from the ocean floor. For example, the amount of methane that escapes into the atmosphere from bubble plumes emanating from slope hydrates along the west coast of Spitsbergen is probably limited (Marín-Moreno et al. 2013).

The most likely area, therefore, from which methane released from the ocean floor could reach the atmosphere, is the continental shelf region. Here, the water column is shallower, for example of the order of tens of meters, and dissolution and oxidation thus lower. Since the earliest global estimates, such areas were expected to be responsible for the majority of marine methane emissions (Ehhalt 1974). This underlines the role of the Arctic Ocean: continental shelves make up about half of the surface area of this region (Jakobsson 2002) – or about 20% of the world's total shelf area. Extrapolating from global emission estimates for continental shelf areas, it is estimated that Arctic shelf regions emit 1–12 Tg CH$_4$/y into the atmosphere (McGuire et al. 2009).

The notion of the Arctic Ocean's continental shelves as an important source of methane has been supported in recent decades by observations from several expeditions in various parts of the Arctic, such as the largest and shallowest shelf region – the East Siberian Arctic Shelf (ESAS). Surface waters in this area, underlain by subsea permafrost, are heavily supersaturated

toward the atmosphere and bubble plumes have been detected in numerous locations (Shakhova et al. 2010). Using data from subsequent expeditions in this area, the original flux estimate of 8 Tg CH$_4$/y was raised to 17 Tg CH$_4$/y after including a best-guess estimate for bubble size and methane content of bubble plumes in the region (Shakhova et al. 2014). It should be noted, however, that this is the largest flux estimate in the literature for any region of the Arctic Ocean, and – within the constraints of the atmospheric budget as presented in Ch. 7 – there is little room for such a large source next to current estimates of tundra and freshwater emissions. This stresses the high uncertainty involved with such flux estimates, and the challenges involved in providing accurate upscaling from bottom-up measurements. Exemplifying the poor understanding of the total size of methane emissions from shallow ocean waters, gas release from the seabed has also been observed in waters above other Arctic continental shelf regions, such as the Beaufort and Kara Seas (Paull et al. 2007b; Portnov et al. 2013). It is unclear how much of the methane from these sources reaches the atmosphere, but it suggests that methane release in shallow waters is relatively common.

Accordingly, bottom-up measurements remain inconclusive on how much methane escapes the Arctic Ocean as a whole due to the large variety of sources, each with their own uncertainties and spatial heterogeneity. Measurements of the concentration of methane and its carbon isotope ratio ($\delta^{13}C_{CH_4}$) in air samples taken within the Arctic may help to clarify whether a large source of methane is being released from the ocean. Hydrates and other sources, such as wetlands, have different $\delta^{13}C_{CH_4}$ values (Fisher et al. 2011), and this can be used as a tool to show which source is more dominant in the Arctic. Such measurements in the late summer of 2008 and 2009 at the Zeppelin monitoring station in Spitsbergen revealed $\delta^{13}C_{CH_4}$ values that were indicative of wetlands as the predominant natural source of methane within the Arctic, and not hydrates (Fisher et al. 2011; see also Ch. 6). Then again, considerable variation in the $\delta^{13}C_{CH_4}$ values of a particular source can exist and the presence of a significant marine source cannot be excluded, although it does indicate that it is unlikely that a large release of methane – for example more than tundra emissions – is currently coming from the Arctic Ocean. Further measurements like these, closer to hotspots such as the ESAS and in combination with inverse modeling, could help to constrain the size of methane emissions from the Arctic Ocean into the atmosphere, of which current estimates range from as low as 1 Tg CH$_4$/y to as high as 17 Tg CH$_4$/y. This large range illustrates that estimates of the methane flux from the Arctic Ocean are highly uncertain.

4.5 Evidence of methane release in the geologic past

The Arctic Ocean Region is believed to be a significant source of methane, albeit small in comparison to the global atmospheric budget (Kirschke et al. 2013). The concern is, however, that large increases in the methane release from the Arctic Ocean, for example through the destabilization of gas hydrates stored in sediments along the continental margin and in areas of subsea permafrost, could occur due to global warming. To gauge this risk, warm periods in the geologic past can be considered as potential analogues for future releases of methane from

the Arctic Ocean. Due to its predominantly biogenic origin, methane released from hydrates has a low $\delta^{13}C$ ratio, with typical $\delta^{13}C$ values of -60‰ (Kvenvolden 1993). Carbon isotope excursions (CIE) in the geologic past – represented by large changes within paleo records of $\delta^{13}C$ – are therefore of interest when clues are sought within the paleo record of methane release from gas hydrates.

Although several CIEs have been proposed to be due to massive releases of methane (Hesselbo et al. 2000; Krull and Retallack 2000), one CIE of particular interest occurred ~56 million years ago during a period of intense global warming; a hyperthermal known as the Paleocene-Eocene thermal maximum (PETM). This period is characterized by a massive global temperature rise of 5–8°C, over a relatively short period of a few thousand years (Kennett and Stott 1991; Zachos et al. 2001; Tripati and Elderfield 2005). The large CIE associated with this period occurs as a shift of more than 3‰ in marine and terrestrial records of $\delta^{13}C$, which implies that several thousand Pg of ^{13}C-depleted carbon entered the oceans and atmosphere (Zachos et al. 2005). As the size of this carbon pulse is comparable to what could be released – in the absence of mitigation activities – from anthropogenic sources (Dickens 1999), the PETM is often used as an analogue of what future climate change could bring. Nonetheless, there are significant differences between the PETM and current climatic conditions. For example, the prevailing climate prior to the PETM was warmer than present day, with no ice caps present at the poles. Consequently, an amplification of high latitude temperatures through an ice-albedo feedback was absent, and the difference between polar and tropical temperatures was much smaller (Sluijs et al. 2006). The response of the current climate to a similar carbon pulse would, therefore, differ on those fronts.

It has been suggested that the large input of ^{13}C-depleted carbon into the ocean and atmosphere during the PETM was due to a pulse of ~1000 to ~2000 Pg of methane released from gas hydrates (Dickens et al. 1995); similar in size to what is thought to be stored in present-day ocean sediments (Milkov 2003). This hypothesis has since been heavily debated (e.g. Archer 2007; Dickens 2011). Alternatively, the CIE has been attributed to a range of other sources, such as wildfires, thermogenic methane, and carbon release from thawing permafrost on land (McInerney and Wing 2011). Of these, the latter has received the most interest, as it accounts for the size and timing of the PETM – and smaller hyperthermals that followed it – relative to changes in orbital forcing. These warm periods are thought to have led to permafrost thaw in the terrestrial Arctic and the deglaciated Antarctic region, causing massive amounts of carbon to be released into the atmosphere (DeConto et al. 2012). This hypothesis does not exclude a large contribution of methane from gas hydrate dissociation, and it is conceivable that both gas hydrates and permafrost thaw were responsible for the conditions of the PETM, resulting in the observed CIE.

While the PETM represents an extreme case of global warming, other strong negative shifts in $\delta^{13}C$ have been seen in paleo records of the last 60 thousand years (kyr), when the climate was much colder. During interstadials (relatively brief warm intervals in this period), large methane increases are evident in ice core records that have been attributed to gas release from hydrates (Kennett et al. 2000, 2003; Nisbet 2002). A possible trigger for

such releases could be sediment disturbance from slope failures or pockmark explosions (Hovland and Judd 1988). The 'clathrate gun hypothesis' suggests that a moderate warming of bottom waters by 2–3.5°C led to a vast destabilization of methane hydrates, signifying the possibility of a future positive feedback in response to global warming. Indeed, a single large event such as the 8.2 kyr Storegga landslide has been suggested to have released as much as 1–5 Pg C into the ocean (Archer 2007), while pockmarks provide more evidence of sudden past releases of methane from the seabed (Hovland and Judd 1988). If these methane pulses were sufficient to break through the filtering capacity of the water column, an emission to the atmosphere may have occurred.

However, methane hydrates carry a distinct deuterium/ hydrogen (D/H) isotope ratio and a release from such deposits via the ocean into the atmosphere would show an increase in this ratio in the ice core records. However, analyses from ice core data reveal that the D/H ratio was either stable or decreased (Sowers 2006), suggesting dominance of a non-oceanic source. In the case of the Storegga slide, this may be explained by the suggestion that much less methane than previously assumed was present in the sediment before the slide occurred (Paull et al. 2007a), reducing the possibility of a massive emission. But even if other large abrupt releases of methane did take place, the D/H isotope ratio indicates that not much of it left the ocean. Consequently, methane increases during interstadials and the warming at the end of the last glacial period were probably related to freshwater sources, such as wetlands and lakes (Chappellaz et al. 1993b; MacDonald et al. 2006; Walter et al. 2007), rather than marine sources such as gas hydrates.

Since the release of methane from destabilized gas hydrates is more likely to have played a role in the extreme warm conditions of the PETM, rather than during the brief – and much less warm – interstadials of the predominantly cool Quaternary, it is implied that quite extreme global warming is required for a quick release of methane from gas hydrates into the atmosphere. This does not mean, however, that no methane has been released from gas hydrates. A continuous sedimentary record from 23.5 kyr to the Holocene in the Vastnesa Ridge contains $\delta^{13}C$ anomalies interpreted to represent methane emission events (Panieri et al. 2014). Instead of isolated pulse emissions, other recent evidence shows that methane has been released from gas hydrates off the coast of West Spitsbergen for thousands of years (Berndt et al. 2014). This fits within the narrative of gas hydrates in general feeding carbon slowly, rather than abruptly, into the ocean system over the duration of millennia (Archer et al. 2009).

4.6 Hydrate modeling

4.6.1 Modeling rationale

While direct measurements and paleoclimatological research are both valuable tools to provide insight into present-day emissions and past source variability, modeling can identify locations of possible gas hydrate deposits, explore future climate change scenarios, and assess the vulnerability of deposits to projected global warming. The models can be applied from the local (Thatcher et al. 2013) to the pan-Arctic scale (Biastoch et al. 2011). Local-scale models can be used to assess the development in time of known deposits, while pan-Arctic models can give

additional information such as the expected size of deposits, and in which areas most warming is expected to occur. Models are, therefore, a useful tool to assess the risk of gas hydrate destabilization following temperature rise, and may help to reduce the uncertainty surrounding possible future scenarios.

As such, Sect. 4.6 provides an evaluation of model projections at the pan-Arctic scale, the locations where gas hydrates are expected to occur, and their vulnerability to warming associated with a rise in atmospheric carbon dioxide concentration within the 21st century.

The modeling approach presented here (Kretschmer et al. 2015) is a continuation of previous modeling work, as demonstrated by Biastoch et al. (2011), which described the processes involved with a release of methane into the Arctic Ocean from dissociating gas hydrates. Notably, the model does not explicitly represent gas hydrates found in subsea permafrost. However, those deposits are located further down from the seabed than the slope gas hydrates modeled here, and may be considered less vulnerable to rising bottom water temperatures in comparison (see Sect. 4.7.2). Furthermore, due to the vast uncertainties involving methane consumption and production in the water column, the model results are not a prediction of how much this release would contribute to higher atmospheric concentrations. Rather, the results help to constrain the outer bounds of estimates of future methane release from gas hydrates along the continental margin. If the expected amount of methane entering the ocean from gas hydrate dissociation is considered to be small compared to emissions from high-latitude terrestrial ecosystems, for example, it is likely that the future impact of gas hydrates on the atmosphere will be small in comparison, too.

4.6.2 Model setup

The general approach described here, although differing in details of the calculation, was previously performed to quantify the impact of global warming on the fate of methane hydrates for a regional study of the Arctic Ocean (Biastoch et al. 2011). The model combines data from an ocean general circulation model (OGCM) under present-day conditions, an ensemble of atmosphere/ocean model experiments under increasing carbon dioxide concentrations, and a geophysical model to estimate the hydrate inventory. The OGCM configuration, as specified in Box 4.2, has been applied in a range of scientific analyses and has been demonstrated to provide a realistic state of the global oceanic circulation and its interannual to decadal variability (Behrens et al. 2013; Fischer et al. 2013; Rühs et al. 2013). To apply this model setup to the future development of gas hydrate deposits, an atmosphere/ocean coupled climate model is necessary to prescribe future atmospheric forcings, and here the Kiel Climate Model (KCM) is used (Park et al. 2010). KCM is a combination of the atmosphere model ECHAM (Roeckner 2003) and an ocean configuration similar to the one described above, but with lower horizontal (2°) and vertical (31 levels) resolutions.

Two global warming experiments were used here: a control experiment under present-day climate conditions and a series of twenty-two 100-year-long global warming simulations. First, the control simulation was forced with constant greenhouse gas concentrations representative of late 20th century conditions (CO_2 = 348 ppm) and integrated over 1100 years in total. This

Box 4.2 Ocean general circulation model configurations

The configuration of the ocean general circulation model used here is based on the 'Nucleus for European Modelling of the Ocean' – or NEMO (Madec 2008) – and consists of an ocean/sea-ice model at 1/4° nominal resolution (Barnier et al. 2006). Bottom slopes and the resulting ocean circulation are adequately represented through 46 geopotential levels in the vertical (ranging from 10 m at the surface to 250 m at deepest levels), and a partial bottom cell formulation (Barnier et al. 2006). The model is initialized with temperatures and salinities from the World Ocean Database (Levitus et al. 1998) for mid- and low latitudes and from the Polar Science Center Hydrographic Climatology (PHC 2.1) for high latitudes (Steele et al. 2001). Spin-up occurs over a period of 30 years (using atmospheric forcing of the years 1978–2007), and this is then integrated over a 60-year long hindcast period (1948–2007). Atmospheric forcing at the sea surface is provided at 6-hourly (wind speed, temperature, humidity), daily (short and long wave radiation) to monthly (precipitation) resolutions (Large and Yeager 2008) and implemented through bulk formulae according to the CORE-II protocol (Griffies et al. 2009).

simulation was subsequently used as the basis for the global warming experiments. The experiments were started at different points in time of the control simulation with an increase in carbon dioxide concentration of 1% per year, until a doubling was reached in about 70 years, after which concentrations were stabilized for another 30 years at the doubled level of just under 700 ppm. This transient climate response is different from a classical doubling of carbon dioxide levels since ocean heat uptake delays warming (Flato et al. 2013), although the higher initial concentration (348 ppm rather than the pre-industrial level of 280 ppm) does result in a more extreme warming scenario eventually.

The resulting future climate scenarios were used together with hindcast data for 1948–2007 (see Box 4.1) in a geophysical model to calculate the current and future gas hydrate inventory (see Box 4.3). Changes in the gas hydrate inventory due to global warming were defined as the differences between the individual members of the global warming ensemble and the corresponding periods in the control experiment. Finally, the results were three-dimensionally interpolated onto the ocean model grid to benefit from its higher resolution. After performing the same procedure as for the present-day fields, ensemble averages of methane and carbon flux changes were built from the resulting inventories.

4.6.3 Hydrate abundance and vulnerability to warming

While the modeling approach described in Sect. 4.6.2 is similar in many ways to that of Biastoch et al. (2011), there are some notable differences which can help explain deviations from previously attained results. The differences include a higher model resolution (1/4° vs. 1/2°), more ensemble members (i.e. 22 instead of 8), and a linear rise in atmospheric carbon dioxide and associated temperature increase instead of an instantaneous warming of the sediments through a step-function. However, the most significant difference is the

Box 4.3 Calculation of the gas hydrate inventory

The present-day methane hydrate inventory was estimated using the following procedure. Global water temperatures and salinities, averaged over the last 20 years (1988–2007), were extracted from the OGCM hindcast (see Box 4.1). By combining these data with global fields for sediment thickness (Laske and Masters 1997; Divins 2003) and heat flow (Hamza et al. 2007), and applying a modified Pitzer approach (Tishchenko et al. 2005), the current GHSZ was determined. The GHSZ was defined as that part of the sediment column where the hydrostatic pressure of pore fluids exceeds the dissociation pressure of methane hydrates (for calculation details see Burwicz et al. 2011). The methane hydrate inventory within the GHSZ was estimated following the transfer function of Wallmann et al. (2012), using global particulate organic carbon concentrations (Seiter et al. 2004; Romankevich et al. 2009) because this is one of the controls on gas hydrate formation (Wallmann et al. 2012). In the future scenarios, only the effects of changing temperature and salinity were considered, as it was assumed that in the coming 100 years sea level rise, and associated pressure changes, will not significantly influence the stability of gas hydrates.

implementation of the transfer function of Wallmann et al. (2012) to estimate the gas hydrate inventory instead of using a constant of mean hydrate pore filling. In reality, typical values of gas hydrate pore filling can vary by an order of magnitude (Archer et al. 2009).

The new approach has led to a regionally estimated gas hydrate inventory north of 60°N of about 116 Pg C. This is a much lower estimate than that derived using the previous version of this model (Biastoch et al. 2011) and the difference can be explained by the use of dynamically calculated, rather than constant, hydrate pore filling. The global estimate of the gas hydrate inventory based on this revised approach – 1146 Pg C – sits comfortably within the range of other global estimates (see Sect. 4.2.2). The lower gas hydrate inventory estimate, compared to the previous study, translates into a lower potential for a large release of methane. Figure 4.5 shows where and how much gas hydrate is likely to destabilize following a doubling of carbon dioxide in the atmosphere to ~700 ppm, once steady-state conditions have been reached. The decreases in the gas hydrate inventory are in the same general regions as found by Biastoch et al. (2011). Although steady-state conditions can be useful to indicate where deposits are most vulnerable, this situation is not reached
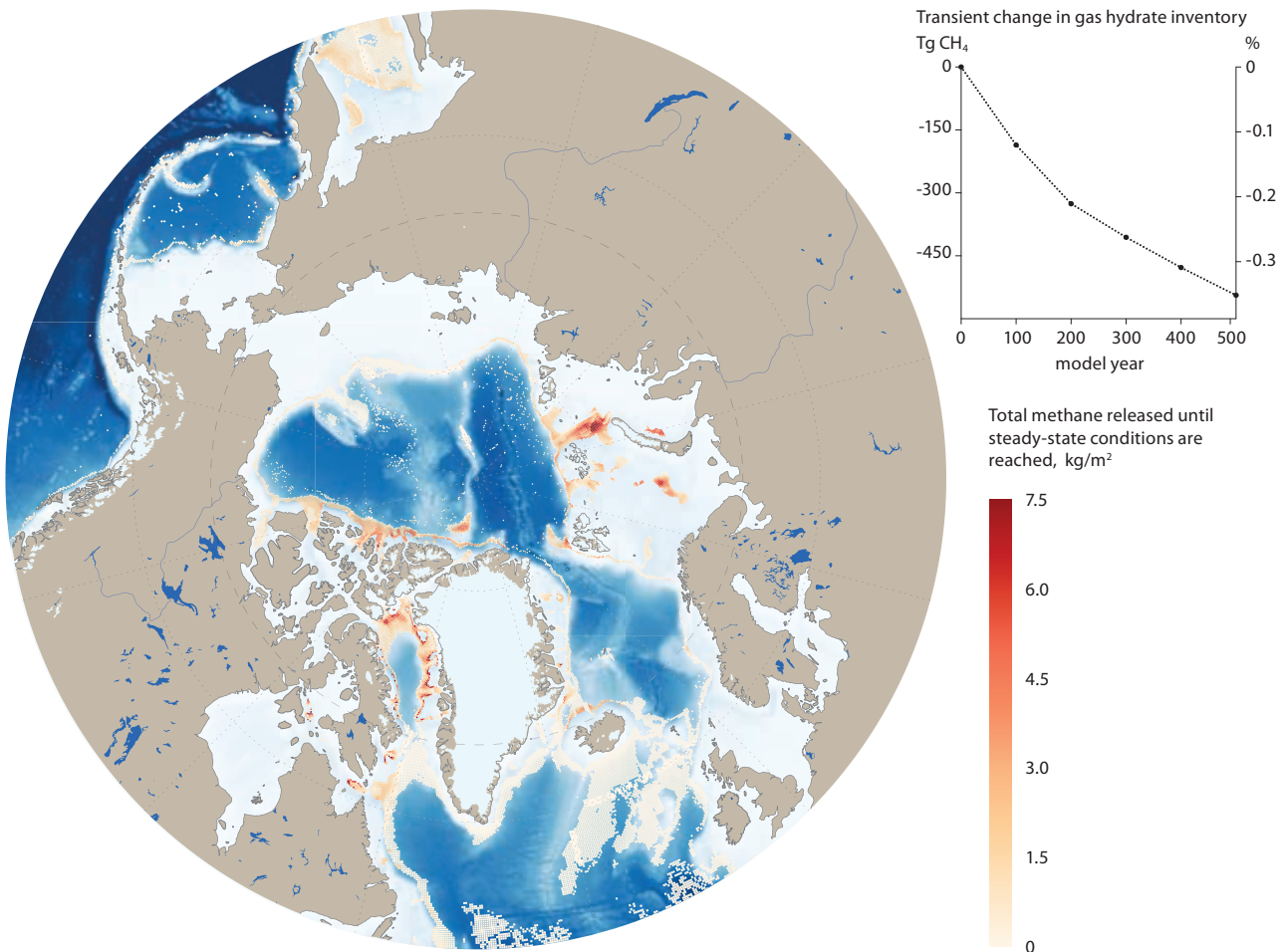
Fig. 4.5 Amount of methane released from dissociating gas hydrate up until steady-state conditions are reached, following a doubling of carbon dioxide in the atmosphere. Due to the slow penetration of heat into ocean sediments, however, this release will take place over many centuries. To illustrate this point, the inset shows the transient reduction in methane inventory, which represents the cumulative amount of methane released from gas hydrates over time, as well as the percentage of the total gas hydrate inventory this represents. The largest reductions are seen north of Novaya Zemlya, and along the coasts of West Greenland and the Canadian archipelago. Note that gas hydrate deposits in subsea permafrost are not modeled, due to the greater unknowns, and therefore methane release from these regions is not displayed.

within the next 100 years due to the slow transfer of heat into ocean sediments. Therefore, as is clear from the inset in Fig. 4.5, the total amount of methane released this century is much lower. For the region north of 60°N, the ensemble mean of the model results indicates that in total ~0.1% of the gas hydrate inventory will dissociate over the next 100 years, which would amount to an additional 0.19 Pg of methane released into the ocean. On average, this equates to a release of 1.9 Tg CH_4/y from the seabed into the ocean over the next 100 years, on top of present-day emissions. This flux is two orders of magnitude lower than the result obtained with the previous version of the model (Biastoch et al. 2011), mainly due to the much lower estimate used in this study for the inventory of gas hydrates.

As current estimates of the release of methane from various sources in the Arctic Ocean to the atmosphere range from 1 to 17 Tg CH_4/y (see Sect. 4.4.2), an increase of 1.9 Tg CH_4/y into the ocean seems small in comparison. An important source of uncertainty in that number, however, lies in the estimated size of the underlying gas hydrate inventory, since previously published estimates have been known to differ by orders of magnitude (Hester and Brewer 2009). But even when the gas hydrate inventory is underestimated by as much as an order of magnitude, this does not mean that the flux of methane to the atmosphere changes by a similar amount. Methane released into the ocean from dissociating gas hydrate is still subject to dissolution and oxidation processes within the water column, and so only a proportion will enter the atmosphere.

It is important to note that the modeling work presented here has some deliberate omissions. It does not include the role of submarine landslides or pockmarks, nor does it represent potential changes to methane production in the surface mixed layer, and it does not include emissions from subsea permafrost areas in the Arctic. Although there may be potential for changes in these sources, considerable uncertainty about the nature of these emissions exists (see next section), and inclusion in models is therefore – at present – problematic. Furthermore, the amount of gas hydrate associated with subsea permafrost may be much lower than in the rest of the Arctic Ocean (Ruppel 2014), and less susceptible to modern climate change (Dmitrenko et al. 2011). While large uncertainties on the future development of the Arctic Ocean as a methane source remain, the risk of large contributions from gas hydrates along the continental margin appears to be low based on model calculations presented here.

4.7 Estimates of future Arctic Ocean emissions

4.7.1 Deep water gas hydrate deposits

One of the best-studied gas hydrate reservoirs in the Arctic is located along the edge of the continental margin off the coast of West Spitsbergen, where methane is presently being released into the ocean (Westbrook et al. 2009). Bottom water temperatures in this region have shown an upward tendency over the past thirty years, and this has led to concern that this has intensified or initiated gas hydrate release by lowering

the top of the GHSZ (Westbrook et al. 2009). Modeling work on these hydrates has indicated, however, that even under an extreme warming scenario (RCP8.5), this region would show a limited gas release into the Arctic Ocean of 0.03 Tg CH_4/y (Marín-Moreno et al. 2013). Although hydrates in the rest of the Arctic Ocean may respond differently to climate change, a simple extrapolation of these results along the continental margin suggests that methane release from gas hydrates into the ocean may increase by as little as ~6.1–33 Tg CH_4/y over the next three centuries (Marín-Moreno et al. 2013). Surprisingly, despite the basic upscaling from a single region, this range – at least at the lower end – is close to that of the model results presented in Sect. 4.6.3 (1.9 Tg CH_4/y released into the ocean), adding confidence to the numbers obtained there.

It is important to remember that the numbers quoted above represent a methane flux into the Arctic Ocean, not the atmosphere. Most of the gas hydrates discussed here are located hundreds of meters below the sea surface, allowing for significant dissolution and oxidation of methane while it migrates through the water column to the sea surface (McGinnis et al. 2006). Methane emissions from the surface of the Arctic Ocean are, therefore, expected to be significantly lower than from the seabed, underscoring the relatively small impact on the atmosphere from gas hydrates located along the continental margin.

The model results do not include sudden methane release from catastrophic events such as submarine landslides or pockmark explosions, even though it has been suggested that such occurrences can release large amounts of methane in a single event. However, there is no indication from ice-core records of any large contribution from such incidents in at least the past 20 kyr, despite a huge event such as the Storegga slide (see Sect. 4.5) and the knowledge that submarine slides are common (Hampton et al. 1996). Moreover, many slides occur outside the GHSZ and are often triggered by earthquakes, which does not imply an increase due to climate change (Talling et al. 2014). Barring extremely rare events, a large increase in methane emissions from submarine landslides does not appear likely, but significant uncertainty remains. However, submarine slides do present a much more acute and clear danger when they trigger deadly tsunamis (Talling et al. 2014).

4.7.2 Subsea permafrost

The shallow parts of the continental margin have received significant interest in recent years, particularly those parts that are underlain by subsea permafrost – such as the East Siberian Arctic Shelf (Romanovskii et al. 2005; Shakhova et al. 2010; Dmitrenko et al. 2011). The subsea permafrost located in the ESAS – as in the Beaufort Sea and Kara Sea – is a remnant from the last glacial period, when this area was exposed to the cold atmosphere due to the much lower sea level and the absence of a large ice cap in the region. The area flooded some 8000 years ago, following sea level rise, and this raised temperatures at the top of the sediment by 12–17 °C to near-zero temperatures (Shakhova et al. 2010; Dmitrenko et al. 2011). The permafrost has since slowly degraded under these raised temperatures to its present day condition, and this is suggested to have led to a perforation of the permafrost 'lid' (Shakhova et al. 2010).

Indeed, gas release from the sediment has been recorded in this area and others with subsea permafrost (Paull et al. 2007b; Shakhova et al. 2010; Portnov et al. 2013), although it is not yet clear whether the gas originates from dissociating gas hydrates rather than other processes of methane formation or migration (Ruppel 2011). For example, thermogenic methane originating from deep within the earth has been associated with releases along faults and regions of terrestrial permafrost thaw (Walter Anthony et al. 2012). Since geological seeps are common in the ocean (Judd 2004), a process analogue to this terrestrial example may also occur in the marine environment. Alternatively, pingo-like features, or small mounds on the ocean floor, are widespread in areas of subsea permafrost and have been hypothesized to act as conduits for methane to bypass the impermeable frozen sediment altogether (Paull et al. 2007b; Portnov et al. 2013). Modeling studies have suggested that open taliks, formed over millennia below paleo-river channels or submerged thaw lakes, may also allow methane to reach the surface (Nicolsky et al. 2012; Frederick and Buffett 2014) – although this needs to be validated by field studies. Finally, the decomposition of organic matter in the sediment of these areas may represent another source of methane.

Regardless of the origin of the methane emanating from the seabed, the penetration of heat into the permafrost is a very slow process, and contemporary climate change is, therefore, not expected to affect the stability of subsea permafrost for centuries (Dmitrenko et al. 2011). Consequently, it seems unlikely that a sudden and large release of methane will occur in the near future, and that the development of these emissions will be much more gradual (Notz et al. 2013; Parmentier and Christensen 2013). Nonetheless, large uncertainties surround emissions from this region: knowledge of the thermal state of the subsea permafrost is poor, and the quantity – or depth – of hydrate deposits is uncertain (Ruppel 2014). Furthermore, measurements suggest that subsea permafrost areas are a significant source of methane when placed in an Arctic context. Continued monitoring of these regions and increased efforts to understand the processes associated with the release and consumption of methane in these waters is, therefore, advisable to reduce uncertainties and better assess potential risks.

4.7.3 Ocean surface

While net emissions from the ocean floor to the atmosphere may not change radically, a major change has already taken place in recent decades at the ocean surface. During this period, a rapid decline in sea-ice extent has occurred, resulting in a wide range of consequences for the Arctic Ocean and beyond (Parmentier et al. 2013; Bhatt et al. 2014). Sea ice acts as a barrier for emissions from the ocean to the atmosphere, and previously it was hypothesized that the seasonal release of methane from the ocean may be related to the presence of ice, since much higher methane concentrations were measured under sea ice than in open water (Kvenvolden et al. 1993). Recent airborne observations also show a connection to sea ice, with fluxes observed over leads – large open fractures within the ice (Kort et al. 2012). The source of the methane, however, is not certain, although formation of methane in oxic surface waters has been suggested to play a role (Damm et al. 2010).

At the moment it is still unclear how sea ice-related processes may influence the methane flux from the Arctic Ocean to the atmosphere, but a change following sea ice decline is conceivable. For example, more open water, and for longer periods of the year, allows methane that would previously have been trapped under the sea ice – and perhaps oxidized – to be readily released to the atmosphere. More open water might also allow storms to ventilate surface waters (Shakhova et al. 2014), although much uncertainty about trends in the size and frequency of storms large enough to ventilate the surface mixed layer remains. Finally, recent evidence points towards processes within the sea ice as significant controls on the atmospheric flux (Crabeck et al. 2014; Zhou et al. 2014), adding to the likelihood that the declining sea ice cover will affect methane emissions, although the magnitude and direction of this change are unclear due to the many and large unknowns.

4.8 Conclusions

4.8.1 Key findings

Current estimates of the size of methane emissions from marine sources vary widely, from 1 to 17 Tg CH_4/y. Due to the difficulty of measuring fluxes from the Arctic Ocean, these numbers are accompanied by high uncertainty – much more so than for the terrestrial domain. Notably, the highest estimate of 17 Tg CH_4/y is difficult to reconcile with the atmospheric budget, because it does not leave much room for tundra and freshwater emissions (see Ch. 7), which indicates that this range more than adequately represents the probable size of present-day Arctic Ocean methane emissions.

The factors influencing methane emissions from the Arctic Ocean are many and diverse. Methane is produced throughout ocean sediments from biogenic, thermogenic and abiogenic sources. While migrating upwards, methane can be stored in gas hydrates, or released from the ocean floor. Before reaching the ocean, however, methane can be oxidized anaerobically in the sulfate-reduction zone, and aerobically in the water column. If the water column is deep enough, these oxidation processes can severely reduce the atmospheric impact of oceanic methane sources. However, processes have been suggested that provide possibilities for methane production in aerobic surface waters as well, complicating the picture further.

Emissions from marine sources may change in the future, as large alterations in the Arctic Ocean – such as sea-ice decline – are already occurring. Their precise impact on methane emissions is uncertain, however, due to the limited number of observations and current limitations in models. Excluding areas with shallow subsea permafrost, due to model limitations, this report projects that any future increase in methane emissions from gas hydrates to the ocean is likely to be relatively small. But the possibility of submarine landslides to release large pulses of methane from the ocean floor, and the ability of such releases to reach the atmosphere, cannot be discounted. Translating a methane flux from the seabed into the ocean to a flux from the ocean into the atmosphere remains very difficult because significant methane consumption occurs within the water column. Therefore, methane reaches the atmosphere more readily from shallow areas, possibly with

subsea permafrost, where water column consumption is lower. However, the impact of contemporary climate change in these areas will probably be damped by the slow penetration of heat into the sediment (Dmitrenko et al. 2011). This reduces the likelihood that gas hydrate deposits in subsea permafrost will be strongly affected in the near future, and it is still uncertain whether dissociating gas hydrates contribute to the release of methane in these areas at all, whether other sources are in play, or a combination of the two. Methane sources in areas with subsea permafrost are poorly understood and associated with significant uncertainty, as is also the case for methane production in the surface mixed layer, and the effects of sea-ice decline on methane fluxes to the atmosphere. In a global context, however, current expectations are that the Arctic Ocean is, and will remain, a relatively small source (Kirschke et al. 2013). To explore further the potential future climate impact of an increase in methane emissions from the Arctic, Ch. 8 assesses a range of scenarios featuring conceivable responses from the marine and terrestrial environments combined.

4.8.2 **Recommendations**

Continued monitoring of Arctic marine methane sources remains of high importance, due to the large uncertainties involved. Although gas hydrates located in deep waters appear to be at low risk to release large amounts of methane into the atmosphere, there is still low confidence surrounding estimates of the size of the gas hydrate reservoir, which vary by orders of magnitude. Gas hydrates, therefore, remain an important area of interest, and a better assessment of how much is present, and their vulnerability, would help greatly to constrain emission estimates. Furthermore, the potential for emissions and the role of gas hydrates within the climate system would be more easily identified with an improved knowledge of past methane emissions through the evaluation of high-resolution records (e.g. from ice cores, marine sediment cores, or carbonate crusts).

Moreover, the amount and condition of permafrost-associated gas hydrates is still largely unknown, and deserves more thorough understanding. This includes an improved mapping of the thermal state of subsea permafrost as well as more and improved measurements of the emission to the atmosphere from this region. Such measurements could benefit from the development and implementation of new techniques to determine the sea-to-air flux of methane. To understand this flux, an enhanced understanding is also needed on the production of methane within the surface mixed layer, where the various contributions to the observed methane supersaturation require improved comprehension.

In addition to improved characterization and quantification of methane sources, expanding knowledge of the processes that control consumption of methane within the sediment and the water column would help to improve flux estimates. The latter, for example, involves many unknowns, as knowledge of the microorganisms involved, and the processes controlling their activity, is often lacking. While bubble plumes from the deep seabed are unlikely to reach the atmosphere, considerable uncertainty remains on how much of the methane dissolved in the water column bypasses oxidation and reaches the atmosphere, and what happens to larger outbursts of methane, such as from submarine landslides. Additionally, the impact of sea-ice decline on the oceanic methane budget is still poorly understood, as are the physical and biological processes in sea ice itself. How this affects methane emissions needs to be investigated further.

Because most of the processes mentioned here are currently poorly represented within models, any newly obtained knowledge following from these recommendations will need to be incorporated into models and validated, to expand capability to predict the future development of the Arctic Ocean as a methane source. Although current knowledge may seem to indicate that large changes within the oceanic methane budget are not expected to occur in the near future, the huge uncertainties and unknowns, combined with the large quantities of methane stored and generated within the seabed, warrants ongoing study and regular monitoring of emissions and processes to better assess the present and future impact of marine sources on the Arctic methane budget.

Acknowledgments

5. Anthropogenic methane sources, emissions and future projections

Authors: Lena Höglund-Isaksson, Allison Thomson, Kaarle Kupiainen, Shilpa Rao, Greet Janssens-Maenhout

5.1 Introduction

Many human activities result in methane emissions to the atmosphere. The origin of these emissions is either biological or fossil. Biological anthropogenic sources include anaerobic decomposition of organic waste material and incomplete combustion of biomass. Methane of fossil origin is released during extraction, transmission and processing of coal, oil and natural gas or during incomplete combustion of fossil fuels. This chapter reviews existing inventories and projections of future anthropogenic methane emissions at a global level as well as for the Arctic nations in order to address the following questions.

What are current global anthropogenic methane emissions, and those of Arctic nations?

How will the magnitude of emissions change in the future under different policy assumptions?

What percentage of global methane mitigation potential is controlled by Arctic Council nations?

What are the principal sources of uncertainty in these estimates of current and future anthropogenic emissions?

Anthropogenic methane emissions can be inferred from inverse modelling (see Ch. 7); however, because methane mixes rapidly in the atmosphere, identifying the contribution from individual sources with inverse models can be challenging. Separating sources is useful for mitigation planning purposes, for example, in evaluating which human activities to target with mitigation effort. Emission inventories were developed to generate bottom-up estimates of sector-specific emissions by compiling data on human activity levels and combining them with the associated emission factors.

While the focus of natural methane sources in Ch. 3 (terrestrial) and 4 (marine) is on emissions released in the Arctic region, this chapter addresses anthropogenic emissions and abatement potential globally as well as for the eight Arctic nations, and all within the timeframe to 2050. Since methane is well mixed in the global atmosphere, it is important to assess the potential to reduce warming in the Arctic region through reductions in methane emissions globally as well as by the Arctic nations themselves. It is estimated that more than half of the anthropogenic methane emissions from Arctic nations come from the fossil fuel sector and that these contribute about a third of global methane emissions from fossil fuel sources. Managing future methane emissions from these activities is therefore of particular importance in Arctic nations. Methane emissions from fossil fuel sources have thus received special attention in this chapter.

In preparing this chapter, the authors had full access to recent emission scenarios from the Greenhouse gas and Air pollutant Interactions and Synergies (GAINS) model developed by the International Institute for Applied Systems Analysis (IIASA

2013). The model results were therefore used to assess sector emissions and future reduction potentials in the individual Arctic nations. Future emissions scenarios from the GAINS model also served as input for the climate impact analyses presented in Ch. 8. In addition, the GAINS model was used to analyze the impacts of black carbon on Arctic climate in an earlier AMAP assessment (AMAP 2011b) and in an assessment by the AMAP Expert Group on Black Carbon and Ozone to be published later in 2015 (see Ch. 1 for details).

5.2 Global anthropogenic methane emissions in past years

5.2.1 Emission inventory approach

Detailed knowledge about sector-specific contributions to global anthropogenic methane emissions in past years rests primarily on the results of emission inventories. These are compiled bottom-up from regional estimates of sector-specific emissions. Emissions are usually estimated as the product of an activity level and an appropriate emission factor with adjustments made for effects of regulations implemented to control emissions (e.g. IPCC 2006; Amann et al. 2011), such that, global emissions in year t are estimated as:

$$E_t = \sum_{is} [A_{its} \times ef_{is} \times control_{its}] \qquad \text{Eq. 5.1}$$

where A_{its} is the activity level in sector s in country/region i and year t, ef_{is} is the unabated emission factor, that is, the average amount of emissions released per unit of activity from sector s in country/region i when no measures are adopted to control emissions, and $control_{its}$ is a factor between 0 and 1 adjusting for the effects on emissions from emission control measures in place in sector s in country/region i and year t. Hence, emissions estimation requires the compilation of source-specific activity levels, emission rates and related emission control factors. When this information is not readily available, the data are derived by applying consistent methodological approaches which make use of the available relevant information.

5.2.2 Sources of uncertainty in methane emissions estimates

Generating a bottom-up inventory of global anthropogenic methane emissions involves three main steps: identifying the sources of emissions, collecting the activity data and associated emission factors, and estimating emissions. Table 5.1 lists some of the influential sources of uncertainty in estimates of current and future emissions of anthropogenic methane.

Information about activity levels is frequently available from statistical databases. Although the general quality of internationally recognized statistical databases is high, the

Table 5.1 Potential sources of uncertainty in global methane inventories of past anthropogenic emissions and emission projections.

Parameter	Emission inventories of past emissions	Projections of future emissions
Activity data	• Factors in identification of emission source sectors • Factors in activity data reported to statistical databases • Handling of missing activity data and strategies chosen to bridge information gaps • Factors in the geospatial allocation of activities and emissions to grids • Factors in the representativeness of the proxy used for gridding	• Factors in the expected future development of key activity drivers, for example, affected by future economic growth, technological progress and structural changes in energy systems • Factors in the spatial movement of point sources • Factors in the change of spatial pattern of the proxy data used
Emission factors	• Factors affecting the representativeness of a limited number of on-site emission measurements to emission characteristics for whole countries/regions • Choice of methodology to derive emission factors based on information availability (i.e. Tier 1 to Tier 3 in IPCC's terminology, see Sect. 5.2.2) • Lack of information about country-specific factors affecting emissions • Strategies chosen to bridge information gaps • Use of default emission factors • Uncertainty inherent in implied emission factors reported by countries to the UNFCCC	• All sources of uncertainty present in the derivation of historical emission factors will also be present in emission projections
Emission control	• Factors in identification and effectiveness of existing control technology • Representation of the effects on emissions of the implementation of existing emission regulations, determined, for example, by assumptions about removal efficiencies and applicability of technologies	• Factors in the future development of control technology • Factors in the future penetration (uptake) of control technology • Factors in the adoption and stringency of future climate policies • Factors in the effectiveness of future policies in stimulating adoption of mitigation technology and strategies

underlying collection of data will vary in quality, particularly when the coverage is global. Inventory developers need to apply a consistent strategy for handling missing activity data. Although uncertainty in activity data may be high in some sectors and regions, finding the appropriate emission factors is likely to be a more important source of uncertainty. At best, direct on-site emission measurements are available and have been collected in a way which makes them representative for a larger geographical area, such as a country or a province of a country. This is rarely the case, however. Instead, to extend emission assessments to global coverage, country/region and sector-specific emission factors must often be derived from available information about how emissions are affected by different country and sector-specific factors for which data are available. For example, on-site or atmospheric measurements of fugitive methane emissions from oil and gas extraction are only available from a limited number of fields typically situated in Canada and the USA (see Sect. 5.2.4). Without direct measurements from the rest of the world, it is necessary to derive country-specific estimates of emission factors based on available country-specific information (for example, the type of hydrocarbons extracted and the amounts of associated gas generated, recovered and flared).

The Intergovernmental Panel on Climate Change (IPCC 2006) provides recommended methodological approaches to derive emission factors under different levels of information availability. These range from the use of global or world region default factors (Tier 1) to extensive use of country-specific

information in the derivation of emission factors (Tier 2), and to making use of site-specific measurements and information (Tier 3). Although the IPCC emission reporting guidelines are usually followed closely, there are still a range of choices in the methodological approach which means that some uncertainty remains and will affect the consistency in emission estimates between inventories.

To a varying extent, emission inventories also make use of implied emission factors reported by Annex-1 countries (countries obliged to submit annual emission inventories in the common reporting format) to the United Nations Framework Convention on Climate Change (UNFCCC 2013). Implied emission factors are derived by dividing the reported sector-specific emissions by the reported activity data. In their reporting, countries are required to follow the IPCC guidelines; however, here also, the level of sophistication in the chosen methodological approach can vary.

5.2.3 Recent inventories of global anthropogenic methane emissions

Independent bottom-up inventories have been produced by the United States Environmental Protection Agency (USEPA 2006, 2012), the IIASA GAINS model (UNEP 2011a; ECLIPSE 2012, 2014; Höglund-Isaksson 2012) and the Emissions Database for Global Atmospheric Research (EDGAR 2010, 2013), which is an inventory compiled by the European Commission Joint Research Centre (EC-JRC) and Netherland's Environmental

Assessment Agency (PBL). A comparison is also made with the global emission inventory used as starting point for the future emission scenarios generated by the family of Integrated Assessment Models (IAMs) that contributed to the Representative Concentration Pathways (RCPs) feeding into scenarios used for the IPCC Fifth Assessment Report (Lamarque et al. 2010; IPCC 2014). These models are the Global Change Assessment Model (GCAM) of the Joint Global Change Research Institute, the Model of Energy Supply Systems and the General Environmental Impacts (MESSAGE) of IIASA, the Asia-Pacific Integrated Model (AIM), and the PBL Integrated Model to Assess the Greenhouse Effect (IMAGE), hereafter referred to as the 'RCP models'. The RCP models were calibrated to global anthropogenic methane emissions in base year 2000 based on Lamarque et al. (2010), who combined the EDGAR v4.1 (2010) inventory with that of the UNFCCC and other sources for a comprehensive consistent global data set (van Vuuren et al. 2011a).

Table 5.2 provides an overview of the referenced inventories with indications of their level of aggregation, specification of source sectors and geographical regions, and their base year and timeframe. All inventories cover the major methane emission sources: fossil fuel production, transmission and distribution; livestock (enteric fermentation and manure management); rice cultivation; solid waste and wastewater. The USEPA and EDGAR inventories provide country-specific estimates of methane emissions for all countries of the world. The GAINS model produces country-specific estimates for Europe, North America, Asia, Australia and New Zealand, provincial estimates for 32 Chinese and 23 Indian provinces, and estimates for Latin America and Africa each aggregated to four regions. The RCP data archive (IIASA 2009) contains methane emissions with the world split by nine major regions, although the resolution of the individual RCP models is higher (see Table 5.2). Methane emissions are reported for 13 source sectors by the USEPA and 25 source sectors by EDGAR. The GAINS estimates of methane emissions can be aggregated to about 80 different sources for which emission factors are identified separately. (It should be

noted that the sector aggregation level for the reporting of emissions is different from the level of aggregation used in the estimation of emissions. For example, when counting the total number of individual source sectors identified and used in common for the estimation of emissions of a large number of air- and waterborne substances, the number of source sectors amount to over 4000 in the EDGAR inventory and over 2000 in the GAINS model. Only a subset of these source sectors has direct relevance for methane, and in the reporting of emissions they are further aggregated.) GCAM covers 54 separate source sectors for methane.

For past years, the USEPA (2012) adopts the emissions reported by countries to the UNFCCC. The GAINS model and the EDGAR inventory recognize that countries have used different methodological approaches to derive reported emissions. Instead of adopting reported emissions as they are, GAINS and EDGAR produce independent estimates of historical emissions using a consistent approach for all countries (for example, when deriving country-specific emission factors). Usually, this means making extensive use of country-specific information, and adopting IPCC default factors or implied emission factors reported to UNFCCC when sufficient country-specific information is unavailable (Höglund-Isaksson 2012; Olivier et al. 2012). The USEPA, the GAINS model and the EDGAR inventory all take into account the effects on past emissions of abatement technology adopted in response to already implemented emission control policies.

Figure 5.1 shows global anthropogenic methane emissions in years 2000, 2005 and 2010 as estimated by the USEPA (2012), the GAINS model (ECLIPSE 2014), and EDGAR (2013). For the year 2000, there is close agreement between inventories that about 300 Tg CH_4 was released globally from anthropogenic sources. Between years 2000 and 2010 total emissions are estimated to have increased by 13% and 14% in the USEPA and GAINS inventories, respectively, and by 21% in the EDGAR inventory. The largest increases in emissions are estimated from coal mining and oil and natural gas systems. In the EDGAR

Table 5.2 Inventory databases and models of global anthropogenic methane emissions.

Source	Approach	No. of methane source sectors	No. of geographical regions	Period covered	Home institute	References to methane data and assessments
USEPA	Integrated emission model	13 (in reporting format)	200	2000–2030 (10-yr interval)	USEPA, USA	USEPA 2006, 2012; UNEP 2011a
GAINS	Integrated emission model	~80 with direct relevance for methane	162	1990–2050 (5-yr interval)	IIASA, Austria	ECLIPSE 2012, 2014; Höglund-Isaksson 2012; Shindell et al. 2012
EDGAR v4.1	Emission inventory	25 (in reporting format)	234	1970–2005 (annual)	JRC, EC; PBL	EDGAR 2010
EDGAR v4.2FT2010	Emission inventory	25 (in reporting format)	234	2000–2010 (annual)	JRC, EC; PBL	EDGAR 2013; Olivier et al. 2012
MESSAGE (RCP8.5)	Integrated assessment model	9	11	1990–2100 (10-yr interval)	IIASA, Austria	IIASA 2009; Riahi et al. 2011
GCAM (RCP4.5)	Integrated assessment model	54	14	1990–2100 (15-yr interval)	Pacific Northwest National Laboratory and the University of Maryland, USA	IIASA 2009; Thomson et al. 2011; Smith and Mizrahi 2013
AIM (RCP6.0)	Integrated assessment model	21	24	1990–2100 (10-yr interval)	National Institute for Environmental Studies, Japan	IIASA 2009; Masui et al. 2011
IMAGE (RCP2.6)	Integrated assessment model	n.a.	26	1990–2100 (10-yr interval)	PBL, Netherlands	IIASA 2009; van Vuuren et al. 2011b

Tg CH$_4$
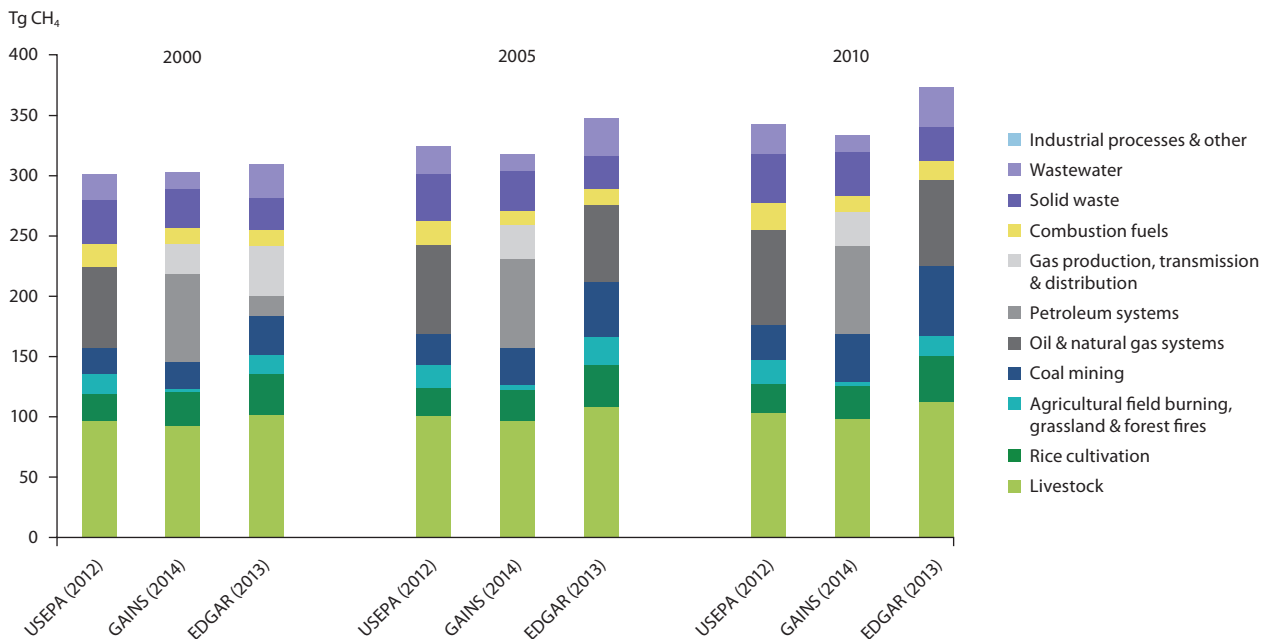
Fig. 5.1 Estimates of global anthropogenic methane emissions 2000 to 2010. Sources: USEPA (2012), GAINS (ECLIPSE 2014), EDGAR (2013).

inventory, emissions from these sources increase more rapidly than in the other two inventories. As statistics on fossil fuel production and consumption are relatively good and not likely to differ much between inventories, the differences can probably be attributed to variations in region-specific emission factors.

Despite relatively good agreement between the inventories on total emissions from year 2000 onwards, differences remain at the sector level. This points at high uncertainty in emission inventory estimates, as also discussed by the IPCC (2014).

To better understand the sector differences, Table 5.3 presents a detailed sector comparison of global anthropogenic methane emissions estimated in 2005, which is a common year for which several recently published inventories have detailed, sector-specific data available. The most recent estimates for year 2005 by the USEPA (2012), GAINS (ECLIPSE 2014) and EDGAR (2013) range from 321 to 349 Tg CH$_4$ emitted globally from anthropogenic sources. Agricultural emissions from livestock and rice cultivation account for about 40% of global emissions in all inventories, with the exception of the 2006 version from the USEPA (USEPA 2006), where it accounts for 56%. Fossil fuel production and use account for between 24% and 31% of emissions in the older estimates by the USEPA (2006) and the RCP models (IIASA 2009), while the more recent assessments from the USEPA (2012), GAINS (ECLIPSE 2014) and EDGAR (2013) suggest these sources to contribute between 34% and 43%. The upward revision of fossil fuel emissions appears to be the result of more measurements becoming available, in particular for fugitive emissions from oil and gas extraction. This is discussed in more detail in Sect. 5.2.4. Waste and wastewater sectors account for about 20% of global methane emissions in all reviewed inventories, while the contribution from incomplete combustion of biomass varies between 3% and 13%. The latter difference appears to derive from variations in sector inclusion. While the GAINS model (UNEP 2011a; ECLIPSE 2012, 2014; Höglund-Isaksson 2012) only accounts for methane from open burning of agricultural field residues, USEPA (2012), EDGAR (2013)

and GCAM (2009) also include emissions from large-scale biomass burning (forest, savannah, grassland and peat fires). The reason for the exclusion of these sources in the GAINS model is the difficulty of distinguishing the origin of forest and grassland fires as anthropogenic or natural (Höglund-Isaksson 2012).

Kirschke et al. (2013) published a review of estimates of global methane emissions in the period 1980 to 2009 (see also Sect. 2.2) using results from both top-down inverse models and bottom-up emission inventories. The results shown for the estimates of anthropogenic emissions, indicate that global estimates of bottom-up inventories tend to be lower than the estimates following from top-down inverse model results based on direct measurements of methane concentration in the atmosphere. This is particularly true for the period 1980-2000, when top-down estimates of global anethropogenic methane emissions are 13% to 19% higher than bottom-up estimates. Agreement between top-down and bottom-up estimates improves for the years after 2000, which is displayed in the far right columns of Table 5.3. The inventories referenced by Kirschke et al. (2013) are a draft inventory by USEPA (2011) and EDGAR version 4.2 (EDGAR 2012). These versions are very similar to the inventories for 2005 presented in the final version of the inventory by the USEPA (USEPA 2012) and in the updated EDGAR version 4.2FT2010 (EDGAR 2013). The estimates of global anthropogenic methane emissions from 2012 or later by the USEPA, GAINS and EDGAR, fall within the ranges given by Kirschke et al. (2013), however, the mean contribution of 96 Tg CH$_4$ or 29% from the fossil fuel sector presented for 2000 to 2009 by Kirschke et al. (2013) appears on the low side compared to the range of 34% to 43% estimated for year 2005 in the more recent inventories.

In a recent article by Nisbet et al. (2014), the trend in year-to-year variation for methane concentration in the atmosphere shows a relatively steep increase from about 1630 ppb in 1985 to about 1775 ppb in 2000, then remaining relatively constant at around 1775 ppb until 2008, when the methane

Table 5.3 Inventories of global anthropogenic methane emissions estimated for year 2005. Data in Tg CH_4 in year 2005.

Sector	USEPA (2006)	USEPA (2012)	GAINS (UNEP 2011a)	GAINS (Höglund-Isaksson 2012; ECLIPSE v.4A – ECLIPSE 2012)	GAINS (ECLIPSE v.5 – ECLIPSE 2014)	EDGAR v4.1 (EDGAR 2010)	EDGAR v4.2 FT2010 (EDGAR 2013)	GCAM RCP4.5 (2009)	GCAM (Smith and Mizrahi 2013)	IMAGE (IIASA 2009)	AIM (IIASA 2009)	MESSAGE (IIASA 2009)	Kirschke et al. (2013) Review top-down 2000–2009	Kirschke et al. (2013) Review bottom-up 2000–2009
Livestock	114	101	96	96	96	108	108	89	94					
Rice cultivation	61	24	27	27	27	34	34	37	42					
Solid waste	36	39	41	44	35	28	28	63	25					
Wastewater	27	23	9	13	13	30	30		40					
Coal mining	18	25	40	31	31	42	46	23	35	Not available in more detail				
Natural gas production	52	73	72	10	10	19	19	27	29					
Gas trans. & dist.				17	18	28	28	9	8					
Oil production & refinery	3			72	77	26	17	10	11					
Combustion fossil fuels	0	11		2	3	13	13	4	19					
Combustion biofuels	0	9	0	8	9			13						
Agricultural waste burning	0	20	3	3	3	1	1	2	25					
Forest & grassland burning	0		0	0	0	19	22	25						
Industrial processes	0	0	0	0	0	0	0	1	0					
Agriculture	174	124	123	123	123	142	143	126	136	133	136	134	209 (180–241)	200 (187–224)
Waste & wastewater	62	61	50	57	48	58	58	63	65	55	62	73		
Fossil fuels	74	109	112	131	138	128	122	73	102	92	87	104	96 (77–123)	96 (85–105)
Biomass burning (including biofuels)	0	30	3	11	12	20	24	40	25	27	27	26	30 (24–45)	35 (32–39)
Other	0	0	0	0	0	0	0	1	0	2	1	1	0	0
Total	310	325	288	323	321	349	347	301	330	309	314	339	335 (273–409)	331 (304–368)

concentration again increases reaching almost 1825 ppb in 2013. This variation in atmospheric methane concentration over the past few decades is not explained by inverse model results using existing inventories of anthropogenic and natural methane emissions. Nisbet et al. (2014) concluded that more data and measurements are needed to improve existing emission inventories in order to resolve the current divergence between top-down and bottom-up estimates of global methane emissions.

5.2.4 Global methane emissions from oil and natural gas systems

Methane emissions from oil and natural gas systems include fugitive emissions released during extraction at the well, leakage from gas transmission pipelines, storage facilities and gas distribution networks, and from incomplete combustion of gas flares. Together these sources are important contributors to global methane emissions and, in relative terms, more important sources for Arctic nations. Oil and natural gas systems are also emission sources with a particularly large

Table 5.4 Global estimates of methane emissions from oil and natural gas systems at a sub-sector level in 2005. Data in Tg CH$_4$ in year 2005.

Activity (production)	Emission source	Using IPCC (2006) default emission factors	GAINS (Höglund-Isaksson 2012)	USEPA (2006)	USEPA (2012)	EDGAR v4.2 FT2010 (EDGAR 2013)	GCAM (2009)
Crude oil	Vented associated gas	9.4–65.6	55.9				
	Flared associated gas	0.02–0.16	1.9	3.1		16.3	9.8
	Unintended leakage	0–19	13.4				
	Oil refinery	0.10–0.25	0.2			0.6	0.2
Natural gas	Vented associated gas	n.a.	1.8		73.5		
	Flared associated gas	0.0005–0.005	0.055			19.2	27.2
	Unintended leakage	1.1–70.8	8.1	52.4			
	Gas transmission and storage	0.4–14.0	7.7			17.4	8.6
	Gas distribution networks	2.6–32.5	9.2			10.2	
Total		14–202	98	56	74	64	46

spread in estimated magnitudes between different global inventories (see Table 5.3). Table 5.4 presents estimates by the different global emission inventories of methane emissions from oil and natural gas systems in year 2005 in as much detail as allowed by available data. Note that in 2005, shale gas extraction through hydraulic fracturing was less than it is currently, and emissions estimated from gas production refer almost exclusively to extraction of conventional natural gas. As shown in Table 5.4, the default ranges suggested in the IPCC guidelines (2006: vol.2, Ch.4, Tables 4.2.4 and 4.2.5) are wide and would, if applied globally, correspond to between 14 and 202 Tg CH$_4$ released from oil and natural gas systems in 2005. In the existing global emission inventories, the corresponding global estimate ranges between 46 and 98 Tg CH$_4$. The inventories use similar sources and magnitudes of activity data, and accordingly the differences in emission estimates derive primarily from differences in the methodology used to derive the emission factors.

Here, discussion is focused on uncertainty in the estimates of fugitive emissions released at the level of the well during extraction of oil and gas, as this is one of the larger sources in oil and natural gas systems emissions. Emissions from gas transmission and distribution are also substantial contributors to global methane emissions (e.g. Lelieveld et al. 2005). There are several reasons for the relatively high uncertainties in the estimates of fugitive methane emissions from oil and gas extraction. There are a limited number of published direct emission measurements, and those that do exist are often specific to certain fields in the USA or Canada (e.g. Kirchgessner et al. 1997; Harrison et al. 2011; Howarth et al. 2011; Johnson and Coderre 2011; Pétron et al. 2012; Allen et al. 2013; Karion et al. 2013). Methane is released from different stages of the extraction process and affected by the rate of recovery of 'associated gas' (the term for waste gas released from the oil well during extraction, which can be recovered and utilized as natural gas, reinjected to enhance the pressure of the well, or flared or vented to the atmosphere), the fraction of unrecovered associated gas being flared or vented, how well unintended leakage from equipment and wells is controlled, whether production is on- or off-shore, the type or nature of the hydrocarbons being extracted, and the extraction method – for example unconventional or conventional sources

(IPCC 2006: vol.2, Ch.4; Howarth et al. 2011; Johnson and Coderre 2011). As these parameters are typically country- or even site-specific, without more systematic measurements their magnitudes remain largely unknown for most major oil and gas producing countries. Another challenge is that some atmospheric field measurements have been made over combined oil and gas fields, which makes source attribution difficult as both oil and gas production release methane (Brandt et al. 2014).

Table 5.5 provides an overview of the magnitudes of implied methane emission factors for oil and gas production in 2005 published from direct measurements in the USA and Canada and in comparison to implied emission factors used in various national or global emission inventories. Note that unless indicated, the emission factors do not account for gas losses during refining, transmission or distribution and do not account for emissions from shale gas extraction through hydraulic fracturing. As shown, there is a wide spread in implied emission factors, which illustrates the high uncertainty in the emission estimates and identifies a need for more direct measurements. Despite the wide range and with the exception of the very low emission factors reported by Denmark and Norway, the emission factors in Table 5.5 fall within the default ranges specified in the IPCC (2006) guidelines.

Further investigation into the discrepancies shown in Table 5.5 between implied emission factors used to estimate emissions from oil extraction, show that EDGAR (2013) and the USEPA (2012) apply emission factors, which, when derived from global estimates of emissions, would correspond to about the amount of methane released per barrel of oil produced in the USA and Canada (e.g. Kirchgessner et al. 1997; Johnson and Coderre 2011). The GAINS model used a different approach, which is described in detail by Höglund-Isaksson (2012: supplement). The USA and Canadian measurements are used as starting points for the derivation of emission factors taking into account information about country-specific amounts of associated gas generated, recovered, flared or vented (PFC Energy 2007; EIA 2011a; Johnson and Coderre 2011). It is recognized that associated gas generated during oil extraction must be either recovered (to be reinjected or utilized as an energy source) or not recovered and then flared or vented

Table 5.5 Implied emission factors for methane emissions from oil and gas extraction as estimated from direct USA and Canadian measurements and in comparison with emission factors used in national and global emission inventories.

Country/ Region	Reference	Geographic area and year	Oil production, g CH$_4$/ barrel crude oil	Gas production, g CH$_4$/ m^3 dry gas
Canada	National inventory to UNFCCC 2013	Whole country 2005	1250	2.9
	Johnson and Coderre 2011	Alberta province, Canada in 2008, direct measurements	390[a] (conventional); 820[a] (heavy oil)	0.11[a]
USA	National inventory to UNFCCC 2013	Whole country 2005	720	8.4
	Brandt et al. 2014	Review of 20 years of published direct US measurements	Concludes that measured emissions suggest national emissions from oil and gas production ~1.5 times national inventory (but source attribution is uncertain)	
Russia	National inventory to UNFCCC 2013	Whole country 2005	510	3.9
Denmark	National inventory to UNFCCC 2013	Whole country 2005	29	0.0096
Norway	National inventory to UNFCCC 2013	Whole country 2005	17	0.0067
Global[c]	EDGAR 2013	Global in 2005	685	3.2
	USEPA 2006	Global in 2005	120	19[b]
	USEPA 2012	Global in 2005	Not attributed to oil or gas. Total oil and gas systems 1.3 times the estimate of USEPA (2006)	
	GCAM 2009	Global in 2005	360	9.8
	GAINS (Höglund-Isaksson 2012)	Global in 2005	2600	3.6
	IPCC (2006) default range	Global in 2005	360–3100	0.39–25

[a] Refers only to intended venting of associated gas and does not include fugitive emissions from unintended leakage; [b] includes emissions from transmission and distribution losses; [c] implied global emission factors when assuming global production in 2005 is 27 million barrels of oil and 2800 billion cubic meters of dry natural gas (EIA 2013).

to the atmosphere for safety reasons. While recovery rates exceeding 90% of the associated gas generated are typical for the USA, Canada and Europe (EIA 2011a), rates are often lower in other parts of the world. This is particularly the case for oil fields that are far from exhaustion and so do not recover extensive amounts of associated gas for reinjection to enhance well pressure, or when there is a lack of gas infrastructure near the oil fields to facilitate the utilization of recovered gas (Hulbak Røland 2010; Johnson and Coderre 2012; Ite and Ibok 2013).

In comparison to the use of emission factors, which at a global scale are comparable to emission factors measured for the USA and Canada, Höglund-Isaksson (2012) found that by adjusting for country-specific rates of generation and recovery of associated gas, global amounts of unrecovered associated gas from oil production become about four times higher. The derived weighted average global recovery rate of associated gas from oil production is then about 70%, which means that about 30% of associated gas generated globally would remain unrecovered and must be flared or vented. Hence, the amount of associated gas not recovered is three to six times higher under this assumption than if it is assumed that 5–10% remain unrecovered as would be the case if recovery rates of 90–95% were assumed globally – see Höglund-Isaksson (2012: table 7 in the supplementary material) for details. Once country-specific amounts of unrecovered associated gas have been derived, the problem is then to establish how much of this gas is being vented as opposed to flared. There is an almost complete lack of published measurements on this and Höglund-Isaksson (2012) resorted to using the only measurements available, which were published by Johnson and Coderre (2011) and representative for oil and

gas wells active in the Canadian province of Alberta in 2008. The measurements show that the fraction of unrecovered associated gas vented (instead of flared) is 29% for conventional oil wells and 88% for heavy oil wells (and not including measurements from shale oil extraction). The considerable share of unrecovered associated gas vented as opposed to flared from heavy oil wells is explained by CAPP (2002) by heavy oil wells being relatively shallow and characterized by a low reservoir pressure. To achieve a reasonable flow of oil from the well, the gas pressure must be controlled which is often done through a gas vent with gas typically vented directly to the atmosphere. Note that despite a higher venting to flaring fraction for heavy oil wells, the overall amount of unrecovered associated gas generated is usually lower than for conventional oil wells. The amount of associated gas vented per unit of oil produced may therefore still be comparable to conventional oil wells (Johnson and Coderre 2011). By applying the Canadian fractions for venting as opposed to flaring to the country-specific amounts of unrecovered associated gas, Höglund-Isaksson (2012) derived country-specific amounts of associated gas vented from conventional and heavy oil wells, respectively. Simultaneously, country-specific amounts of unrecovered gas flared were derived, which can be verified against country-specific estimates of gas flared measured from satellite images (NOAA 2010). At a global level, the match is found to be close, although there remain unexplained discrepancies at the country level. The result of this difference in the methodological approach is visible in Tables 5.4 and 5.5 as the estimate of global methane emissions from oil production in GAINS (ECLIPSE 2012, 2014; Höglund-Isaksson 2012a) being a few times higher than for the EDGAR (2013) and USEPA (2012) assessments.

For natural gas extraction, the uncertainty in emissions is also high and the upper bound value for the range of IPCC (2006) default factors is more than 60 times the lower bound value (see Table 5.4). In the GAINS model, Höglund-Isaksson (2012) found lower global estimates for methane emissions from conventional natural gas production in 2005 than reported by EDGAR (2013) and the USEPA (2012). The measurements presented by Johnson and Coderre (2011) for Canada and by PFC Energy (2007) for Russia and used in the global assessment by Höglund-Isaksson (2012), indicate very small amounts of associated gas vented from conventional gas production compared with oil production. Primarily, emissions from gas production appear to derive from unintended leakage, which tends to vary from site to site. Brandt et al. (2014) found in a survey of natural gas emission measurements published for the USA over the past 20 years, that the national inventory compiled by the USEPA probably underestimates methane emissions from oil and natural gas systems, with actual emissions being about 1.5 times higher. They also found that when adding up site-specific measurements, total emissions are often dominated by a few 'super-emitters'. Another finding was that source attribution to oil or natural gas production is highly uncertain.

Advancements after 2005 in hydraulic fracturing technology have instigated a rapid increase in shale gas production in the USA to the extent that in 2009 the USA overtook Russia as the world's largest gas producer (EIA 2013). Explorations for potential future extraction using this technology are underway in other parts of the world (EIA 2011b). There is a small but growing body of emission measurements from extraction of unconventional gas sources, which apart from shale gas (gas from shale deposits) also include extraction of limited amounts of coal bed methane (gas extracted from coal beds) and tight gas (gas trapped underground in impermeable rock formations). In general, these emission measurements suggest higher methane emission factors for unconventional than for conventional gas extraction (Howarth et al. 2011; Pétron et al. 2012; Allen et al. 2013; Karion et al. 2013; Caulton et al. 2014), but the uncertainty range is wide with measurements ranging from 0.4% of gas produced found from selected on-site measurements (Allen et al. 2013) to 6–12% from atmospheric measurements over specific gas fields (Karion et al. 2013).

In the most recent ECLIPSE scenario (ECLIPSE 2014), the GAINS model adopts an emission factor for unconventional gas extraction of 4.3% of gas produced with current technology, and assumes that it is technically possible with existing technology to control leakage to 0.3% of gas extracted – a level comparable to carefully managed conventional gas wells (Cathles et al. 2012).

Hence, to reduce the high uncertainty in global estimates of fugitive methane emissions from oil and gas extraction, more published studies based on direct measurements are needed. The measurements should preferably be derived in a systematic manner to provide source attributed emission factors that are representative for extraction of different types of hydrocarbons (including unconventional sources) in different world regions.

5.3 Global projections of future anthropogenic methane emissions

5.3.1 Use of integrated assessment models in climate policy

Integrated Assessment Models (IAMs) are used in climate policy to evaluate potential strategies and costs for transformation in the energy and land sectors of the economy under different socio-economic, technological and policy futures. Scenarios of future anthropogenic greenhouse gas emissions are driven by internally consistent sets of assumptions about future development in socio-economic factors, such as population and economic growth, technological factors such as availability and cost of energy technologies, and different ambition levels of a future climate policy (e.g. Kelly and Kolstad 1999). The global warming effect of the resulting future emission scenarios is evaluated in IAMs using climate response models. One application of IAMs with specific relevance for this assessment is to analyze possible future pathways to pre-determined targets for emissions (or radiative forcing). Examples of this type of policy target include the commitment of the G8 countries to keep the global average temperature in 2050 within 2°C of pre-industrial levels (G8 2009). This approach to emission target-setting can be informed by current scientific understanding of the risks and consequences of climate change, as assessed, for example, by the IPCC (2013b, 2014). The IAMs that produced the RCPs project future emissions and land-use change, with (RCP2.6, RCP4.5 and RCP6.0) or without (RCP8.5) additional climate policies, in order to meet pre-determined radiative forcing targets in 2100 (IPCC 2014). Closely related and sometimes referred to as IAMs, but here referred to as integrated emission models, are the USEPA (2012) and IIASA's GAINS models. These do not contain the full suite of estimations contained in the IAMs, but produce emission scenarios for the next few decades starting from detailed source-specific emission inventories and with a high resolution in sources, technical abatement potentials, and costs. Their primary purpose is to provide information to policymakers on concrete ways to meet a near-term emission reduction target through adoption of existing technology. Examples of adopted policy targets based on projections by integrated emission models are the commitments by the European Union to reduce greenhouse gas emissions by 20% in 2020 and by 40% in 2030 below the 1990 emission level (EC 2014). These targets were set after analyses of future emissions and reduction potentials for carbon dioxide (CO_2) using the PRIMES model and for non-CO_2 greenhouse gases, including methane, using the GAINS model (Höglund-Isaksson et al. 2012; Capros et al. 2013).

Uncertainty in future emissions is closely linked to the sources of uncertainty in the emission inventory used as the starting point and in the future development of the parameters listed in Table 5.1.

5.3.2 Global baseline and mitigation scenarios for anthropogenic methane emissions

An overview of recent projections of global anthropogenic methane emissions by the USEPA, GAINS and the family of RCP models is provided in Table 5.6.

The USEPA (2012, 2014) adopts externally produced global energy scenarios from the International Energy Agency and the US Energy Information Administration (EIA 2009; IEA 2009). They present a baseline and a mitigation scenario defined for the timeframe 2000–2030 with 2010 as base year for projections and

Table 5.6 Overview of recent projections of future global anthropogenic methane emissions.

Model	Scenario; completion date	Scenario period (base year for projections)	Energy drivers	Agricultural drivers	Baseline/ mitigation scenario	Implied carbon price, EUR/tonne CO$_2$eq		References to data or scenario applications
						In 2030	In 2050	
USEPA	Baseline; 2012	2000–2030 (2010)	EIA (2009); IEA (2009)	FAPRI 2010	Baseline	0	0	USEPA 2012
	Mitigation; 2014	2010–2030 (2010)			Mitigation	-37 to >200		USEPA 2014
GAINS	CLE; 2011	2005–2030 (2005)	IEA-WEO2009 (IEA 2009)	FAO 2003	Baseline	0	0	UNEP 2011a; Shindell et al. 2012
	MFR; 2011	2005–2030 (2005)			Mitigation	-200 to >200		
	CLE; 2012i	2005–2030 (2005)	IEA-WEO2009 (IEA 2009)	FAO 2003	Baseline	0	0	Höglund-Isaksson 2012
	MFR; 2012i	2005–2030 (2005)			Mitigation	-200 to >200		
	CLE; 2012ii	2005–2050 (2010)	IEA-WEO2011 (IEA 2011a) until 2035; POLES model (Russ et al. 2009) for 2040–2050	Alexandratos and Bruinsma 2012	Baseline	0	0	ECLIPSE 2012
	MFR; 2012ii	2005–2050 (2010)			Mitigation	-200 to >200		
	CLE; 2014	1990–2050 (2010)	IEA-ETP (IEA 2012) with split of conventional and unconventional gas extraction from IEA (2011b)	Alexandratos and Bruinsma 2012	Baseline	0	0	ECLIPSE 2014
	MFR; 2014	1990–2050 (2010)			Mitigation	-200 to >200		
GCAM	Reference; 2009	2000–2100 (2000)	In the RCP models, activity drivers are developed within each model in consistency with certain population and income growth assumptions and not exceeding predetermined pathways of radiative forcing until 2100 of 2.6, 4.5, 6.0 or 8.5 W/m^2 (Moss et al. 2008, 2010).		Baseline	0	0	IIASA 2009; Thomson et al. 2011
	GCAM 6.0; 2009	2000–2100 (2000)			Mitigation	1.1[a]	2.8	
	RCP4.5; 2009	2000–2100 (2000)			Mitigation	7.1[a]	17.8	
	GCAM2.6; 2009	2000–2100 (2000)			Mitigation	30.9[a]	77.7	
	GCAM Counterfactual; 2013	2005–2030 (2000)			Baseline	0	0	Smith and Mizrahi 2013
	GCAM Reference; 2013	2005–2030 (2000)			Baseline	0	0	
MESSAGE	RCP8.5; 2009	2000–2100 (2000)			Baseline	0	0	IIASA 2009; Riahi et al. 2011
	MESSAGE 6.0; 2009	2000–2100 (2000)			Mitigation	11.5	30.6	
	MESSAGE 4.5; 2009	2000–2100 (2000)			Mitigation	28.4	75.5	
	MESSAGE 2.6; 2009	2000–2100 (2000)			Mitigation	232	615	
AIM	RCP6.0; 2009	2000–2100 (2000)			Mitigation[b]	0[b]	0[b]	IIASA 2009; Masui et al. 2011
IMAGE	RCP2.6; 2009	2000–2100 (2000)			Mitigation	65	130	IIASA 2009; van Vuuren et al. 2011b

[a] Linear interpolation between 2020 and 2035; [b] carbon price starts rising only after 2050, that is, scenario could be regarded as Baseline in the 2000–2050 timeframe.

Box 5.1 The technical possibility range for future emissions in the GAINS model

The GAINS model identifies a technical possibility range for future emissions between a baseline scenario, assuming no further climate policy implemented beyond that already prescribed in current legislation (CLE), and a maximum technically feasible reduction (MFR) scenario, which assumes maximum adoption of existing abatement technologies from 2020 onwards and without consideration of costs or further advances in technological development. Note that the technical possibility range between CLE and MFR refers strictly to technical solutions to reduce emissions, while at least in a longer time-frame, there are also non-technical possibilities to reduce emissions (see Box 5.2). Once the technical possibility range for future emissions has been estimated, a marginal cost curve is developed to describe the additional cost of each emission unit reduced when moving from the CLE to the MFR emission level (see Sect. 5.3.5 for further discussion on costs).

To determine the extent of control implementation that can be deemed 'feasible', technical applicability rates are identified for each technology and region (usually a country) based on region-specific circumstances. For example, the adoption of feed changes to reduce methane emissions from ruminant cattle is only assumed feasible for the fraction of animals in intensive systems and when animals are fed indoor. Another example is the installation of ventilation air methane (VAM) oxidizers on coal mine shafts, which is assumed feasible only for the fraction of coal mined underground in regions where the average VAM concentration rate is high enough to keep up a self-sustained oxidation process. The assumption of no future technological development in methane control technology in the MFR scenario is deliberately conservative. It recognizes that without further policy incentives to reduce emissions, and unless there is a strong increase in the future price of (recovered) gas, there are few endogenous drivers for the adoption of methane control technology, which in turn is the principal driver for technological development. Note that this is in contrast to what can be expected for technological development in carbon dioxide control technologies that enhance energy efficiency. Development to reduce costs and improve the efficiency of this type of technology will primarily be driven by incentives to cut energy costs, with carbon dioxide reductions as co-benefits. The role of climate policy is then to speed up rather than, as is often the case for methane control technology, to be the sole instigator of technology adoption and technological development.

assuming in the baseline that no further climate policy is being implemented in the future. In a similar manner, the GAINS model adopts externally produced global energy scenarios from the International Energy Agency (IEA 2009, 2011a, 2012) as drivers for baseline and mitigation scenarios. Global methane emission scenarios have been defined for 2005 to 2030 with 2005 as base year for projections (UNEP 2011a; Höglund-Isaksson 2012; Shindell et al. 2012) as well as to 2050 with 2010 as base year for projections (ECLIPSE 2012, 2014). The GAINS model identifies a technically possible range for future emissions between a baseline scenario under current legislation (CLE) and a maximum technically feasible reduction (MFR) scenario (see Box 5.1 for further details).

The RCP models GCAM, MESSAGE, AIM and IMAGE produce their own scenarios of energy system change in response to projections of future population, income and climate mitigation strategies (van Vuuren et al. 2011a). The four RCP pathways are defined for the entire century 2000 to 2100 and each pathway represents a specific final climate target defined as the radiative forcing from all gas species in the year 2100. The RCP2.6 forcing pathway assumes a peak and decline in radiative forcing in response to stringent climate mitigation policy, with year 2100 forcing at 2.6 W/m^2. The RCP4.5 and RCP6.0 forcing pathways stabilize radiative forcing in 2100 at 4.5 or 6.0 W/m^2, respectively, in response to climate policy, while the RCP8.5 forcing pathway represents a high population growth scenario with no further climate policy introduced and with radiative forcing rising to 8.5 W/m^2 in 2100 (and continuing to rise beyond that). With the exception of RCP8.5, which is a baseline scenario with a global carbon price of zero, the other RCP scenarios reflect different levels of future global carbon prices and herewith associated mitigation targets (see Table 5.6). Although the RCP scenarios are defined in terms of single radiative forcing pathways, the model groups producing the RCPs can, for the assumed levels of economic and population growth, estimate alternative future emission scenarios for the full range of forcing targets (i.e. from 2.6 to 8.5 W/m^2 in 2100). As shown in Table 5.6, for this review the chapter authors had access to the full range of baseline and mitigation scenarios produced by the MESSAGE (2009) and GCAM (2009) models, but not for the AIM and IMAGE models for which data availability was limited to the information stored in the RCP database version 2.0 (IIASA 2009).

Figure 5.2 displays the expected future growth in global methane emissions as projected in the baseline and mitigation scenarios listed in Table 5.6. All models start from a global methane release of about 300 Tg in year 2000. The baseline scenarios project emissions assuming no further policies are introduced to mitigate climate change. The high population growth scenario by MESSAGE 'RCP8.5; 2009' projects a strong increase in emissions to almost 700 Tg CH$_4$ in 2050. The GCAM 'Reference; 2009' scenario projects a more moderate increase to 430 Tg CH$_4$ in 2050. The two revised GCAM baseline scenarios to 2030 presented by Smith and Mizrahi (2013) represent a 'Counterfactual; 2013' baseline, where no additional mitigation is adopted after 2005 and a 'Reference; 2013' baseline, where additional emission reductions happen at no additional cost because of an uptake of options assumed to be profitable because they involve potentials to recover and utilize gas. The recently produced projections 'Baseline; 2012' by the USEPA (2012) and 'CLE; 2012ii' (ECLIPSE 2012) and 'CLE; 2014' (ECLIPSE 2014) by the GAINS model are based on reported statistics until year 2010 and reflect future emission reductions only to the extent prescribed in current legislation. By definition it should be expected that the GAINS CLE scenario falls somewhere in between the Counterfactual and Reference scenarios defined by Smith and Mizrahi (2013) to 2030. While the Counterfactual scenario assumes fixed emission factors and future emissions driven only by changes
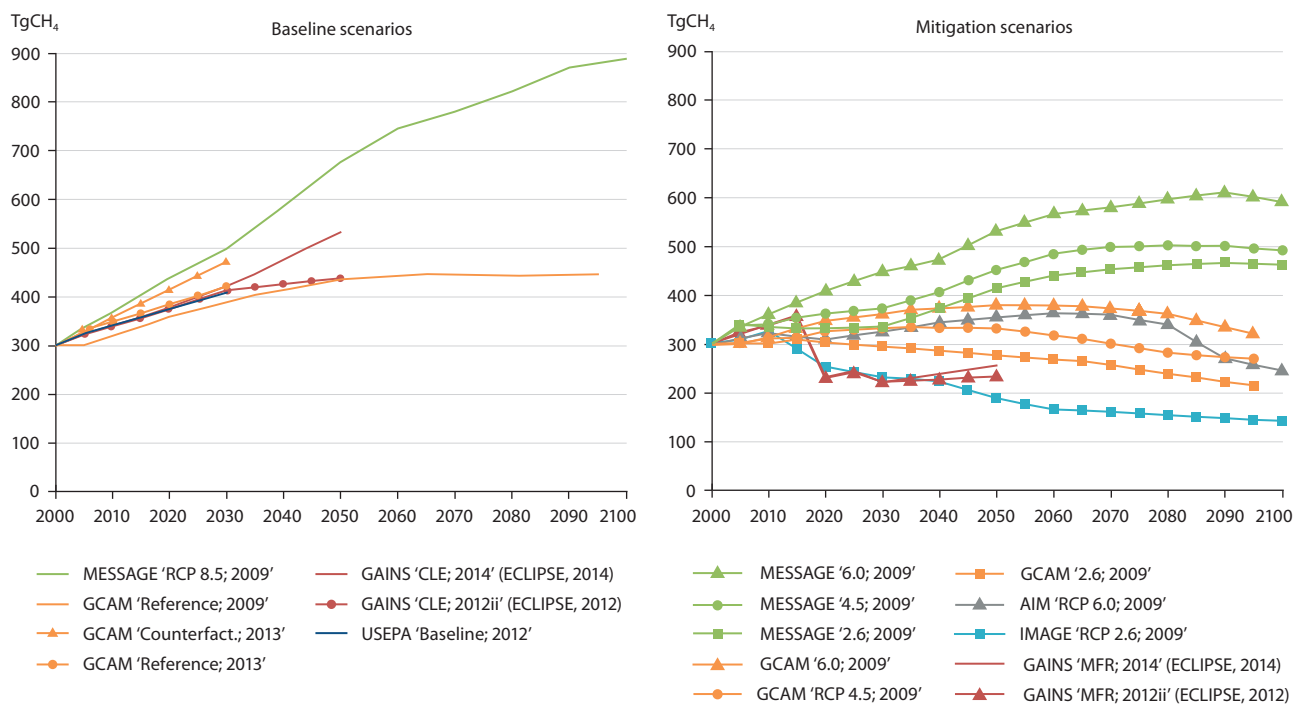
Fig. 5.2 Scenarios of future global anthropogenic methane emissions by different integrated assessment models (IAMs). Baseline scenarios with no further policy incentives implemented to reduce emissions (left) and mitigation type scenarios with policy-driven emission reductions (right).

in activity data, the GAINS CLE scenario in addition reflects effects on implied emission factors from continuous uptake of control technology to the extent prescribed by current legislation. The Reference scenario reflects effects on emissions from all control options that are estimated as available at a net profit, which with the cost assumptions made by Smith and Mizrahi (2013), seems to include more options than those adopted in direct response to current legislation and reflected in GAINS CLE.

The reviewed baseline scenarios agree closely on the emission pathway to 2030, rising to 414 Tg CH_4 in the USEPA scenario and 423 Tg CH_4 in the GAINS CLE scenarios. The GAINS model presents two different projections between 2035 and 2050, where the 'CLE; 2012ii' combines a global energy scenario to 2030 from IEA-WEO (IEA 2011a) with a global energy scenario to 2050 from the POLES model (Russ et al. 2009). The 'CLE; 2014' scenario uses an energy scenario to 2050 from the IEA-ETP group (IEA 2012) and distinguishes between production of conventional and unconventional gas by attributing shares of the types of gas produced using country-specific trends from IEA (2011a). Global methane emissions increase more rapidly in the latter scenario due to a stronger increase in global gas consumption, to a large extent driven by higher future extraction of shale gas, and the introduction in GAINS of higher emission factors for unconventional than for conventional gas extraction.

The mitigation scenarios displayed in Fig. 5.2 show the development of global methane emissions in the mitigation scenarios listed in Table 5.6. All the scenarios assume implementation of climate policy which has effects on future methane emissions. Except for the scenarios projected by the MESSAGE model, where emissions are driven by high population growth, all models project mitigation scenarios with less than 400 Tg CH_4 released in 2050. In the timeframe

to 2050, the MFR scenario defined in the GAINS model is close to the most optimistic (2.6 W/m² in 2100) mitigation scenarios generated by the IMAGE and GCAM models. This means that the emission possibility range defined in the GAINS model between the CLE and MFR scenarios, corresponds well to the range of possible future methane emission scenarios defined by the RCPs until 2050 (IIASA 2009). The mitigation scenario from USEPA (2014) estimates a technical reduction potential in global methane emissions of 35% below baseline in 2030, which is less optimistic than the 48% estimated by the GAINS model and the most stringent RCP scenario (RCP2.6) from the IMAGE model. The reasons for the differences are discussed in Sect. 5.3.3.

5.3.3 Global technical abatement potential for methane by technology

The global maximum feasible reduction for methane in 2030 as estimated by the GAINS model (ECLIPSE 2014) is specified by sector and control technology in Table 5.7. It is estimated that global methane emissions can be reduced by 201 Tg CH_4, which is 48% below CLE emissions in 2030. The largest abatement potentials are found from reduced venting of associated gas released during oil production; reduced leakage from natural gas production, transmission and distribution; source separation and treatment of biodegradable waste to replace landfill disposal; and control of coal mine methane emissions through extended pre-mining degasification and installation of ventilation air oxidizers during mining. The technical abatement potential in the agricultural sector is found to be relatively limited. Options include changes in management practices to control methane emissions from continuously flooded rice fields and some limited reduction potentials from control of methane from enteric fermentation through changes in animal diets for ruminant livestock and anaerobic digestion of manure

Table 5.7 Global anthropogenic baseline (CLE) methane emissions and maximum technically feasible reduction potentials (MFR) by sector as estimated in the GAINS model (ECLIPSE 2014). See Höglund-Isaksson (2012) for a further description of measures.

Sector	Control measure	GAINS model (ECLIPSE 2014)					UNEP 2011a	USEPA 2014
		2005	2030 CLE	2030 MFR	2030 MFR	2030 MFR	2030 MFR	2030 MFR
		Tg CH$_4$	Tg CH$_4$	Tg CH$_4$	Change in Tg CH$_4$	Percentage change in CLE in 2030		
Livestock	Enteric fermentation: diet changes	96.3	113.2	109.3	-3.9	-3	-4	-9
	Manure management: anaerobic digestion							
Rice cultivation	Mixed: aeration, alternative hybrids, sulfate amendments	26.8	29.1	20.0	-9.1	-31	-31	-26
Agricultural waste burning	Ban	3.1	3.7	1.7	-2.0	-53	0	0
Solid waste	Maximum separation and treatment, no landfill of biodegradable waste	34.7	44.7	7.4	-37.3	-83	-84	-61
Wastewater	Extended treatment with gas recovery and utilization	13.2	17.9	9.1	-8.8	-49	-53	-35
Coal mining	Pre-mining degasification	30.8	56.4	24.7	-31.7	-56	-56	-60
	Ventilation air oxidizer with improved ventilation systems							
Conventional natural gas production	Recovery and utilization of vented associated gas	9.9	13.6	6.8	-6.8	-50	-75	
	Good practice: reduced unintended leakage							
Unconventional gas production	Good practice: reduced unintended leakage	0	22.1	3.8	-18.3	-83	0	
Long-distance gas transmission	Leakage control	8.1	7.8	3.7	-4.1	-53	-60	-58 (all oil and gas sources)
Gas distribution networks	Leakage control and replacement of grey cast iron networks	9.8	12.7	1.4	-11.3	-89	0	
Oil production and refinery	Recovery and utilization of vented associated gas	76.6	90.9	22.0	-68.9	-76	-75	
	Good practice: reduced unintended leakage							
Other sources	No control options identified	11.4	10.9	10.9	0	0	0	0
Total		321	423	221	-202	-48	-38	-35

(Hristov et al. 2013). More extensive emission reductions in the agricultural sector would involve non-technical options, such as broader structural changes in production and consumption systems (see Box 5.2). The two far right columns of Table 5.7 compare the most recent global methane abatement potential in 2030 from the GAINS model with that of other comparable estimates available for 2030. The GAINS model was used for an analysis of the global methane reduction potential in 2030 presented in a report for UNEP (2011a) and further analyzed by Shindell et al. (2012) on the benefits of near-term reductions in methane and black carbon emissions. The more limited global reduction potential of 38% below CLE emissions in 2030 used in these analyses is due to a selection of measures which for the UNEP report were identified as relatively inexpensive. Expensive options such as replacement of grey cast iron pipes for gas distribution were excluded. In addition, there is also an effect from later GAINS scenarios accounting for higher emissions and reduction potentials from shale gas compared to conventional natural gas extraction. The more limited technical reduction potential of 35% for global methane emissions in 2030 estimated by the USEPA (2014) in comparison to the

48% in the GAINS model, is primarily the result of a higher baseline and reduction potential from oil and gas production in the GAINS model and a larger reduction potential from solid waste in GAINS due to differences in the choice of abatement approach for this sector. The GAINS model assumes methane emissions from landfills can most effectively be removed by preventing the biodegradable waste being landfilled in the first place (through the use of waste separation, recycling and treatment), while the USEPA approach is primarily based on removing methane from landfills through landfill gas recovery and incineration of mixed waste.

5.3.4 Future emissions and technical reduction potentials by world region

Estimates of methane emissions in 2030 by world region from the GAINS 'CLE; 2014' and 'MFR; 2014' scenarios (ECLIPSE 2014) are shown in Fig. 5.3. There are large variations between world regions in the contribution from different sectors to total methane emissions and reduction potentials. Both emissions and reduction potentials tend to be greater in regions with

Box 5.2 Methane abatement potentials from technical vs non-technical options

The MFR abatement potential considered in the GAINS model (see Box 5.1) refers strictly to technical abatement options, implicitly assuming no major changes in production and consumption structures; that is, no changes in consumer preferences, institutional patterns or land use. Such changes are typically slow and difficult to implement in isolation from other structural changes in society. The focus of the GAINS model is on abatement potentials in the next few decades and in this timeframe it is not considered feasible to expect large emission reductions from non-technical measures that involve major structural changes.

At a global level the technical reduction potential of methane emissions from agricultural sources is limited. In particular, controlling enteric fermentation emissions from ruminant livestock – the largest agricultural methane source – is difficult without changing current production and consumption structures for food (Hristov et al. 2013). For example, in developing countries where production systems are often extensive with large animal herds grazing outdoor, there are practical limits to the applicability of controlled changes in the feed of cattle or the installation of anaerobic digesters to treat manure. Intensified production can curb emissions by reducing animal stocks while preserving output levels; however, it requires major transformations of current production structures including increased demand for land

to grow animal feed (FAO 2006). This risks interfering with the use of land for other purposes including food production (FAO 2006; Garnett 2009; Hristov et al. 2013). Another complication is that many smallholder farmers keep large livestock herds not primarily for production of milk or meat, but as a way of storing assets in the absence of functioning credit institutions (Udo et al. 2011). As more productive breeds are often less robust than indigenous breeds, intensification of production may not be in the interest of the farmers unless institutions for long-term asset storage are put in place. An option that is expected to be effective in controlling methane, as well as other greenhouse gases, from livestock rearing, is a change in consumer preference towards lower consumption of meat and milk products (Hedenus et al. 2014). Major changes in consumption patterns in response to targeted policies are typically slow.

Hence, in the timeframe to 2050 the global abatement potential for methane is likely to rely primarily on technical solutions that are readily available. In sectors other than agriculture, technical abatement options exist with extensive reduction potentials, in particular in fossil fuel production and waste and wastewater sectors. With functioning infrastructure for utilization of recovered gas or separation and recycling of waste, methane abatement in these sectors often comes at a relatively low cost or even at a profit (Höglund-Isaksson 2012).
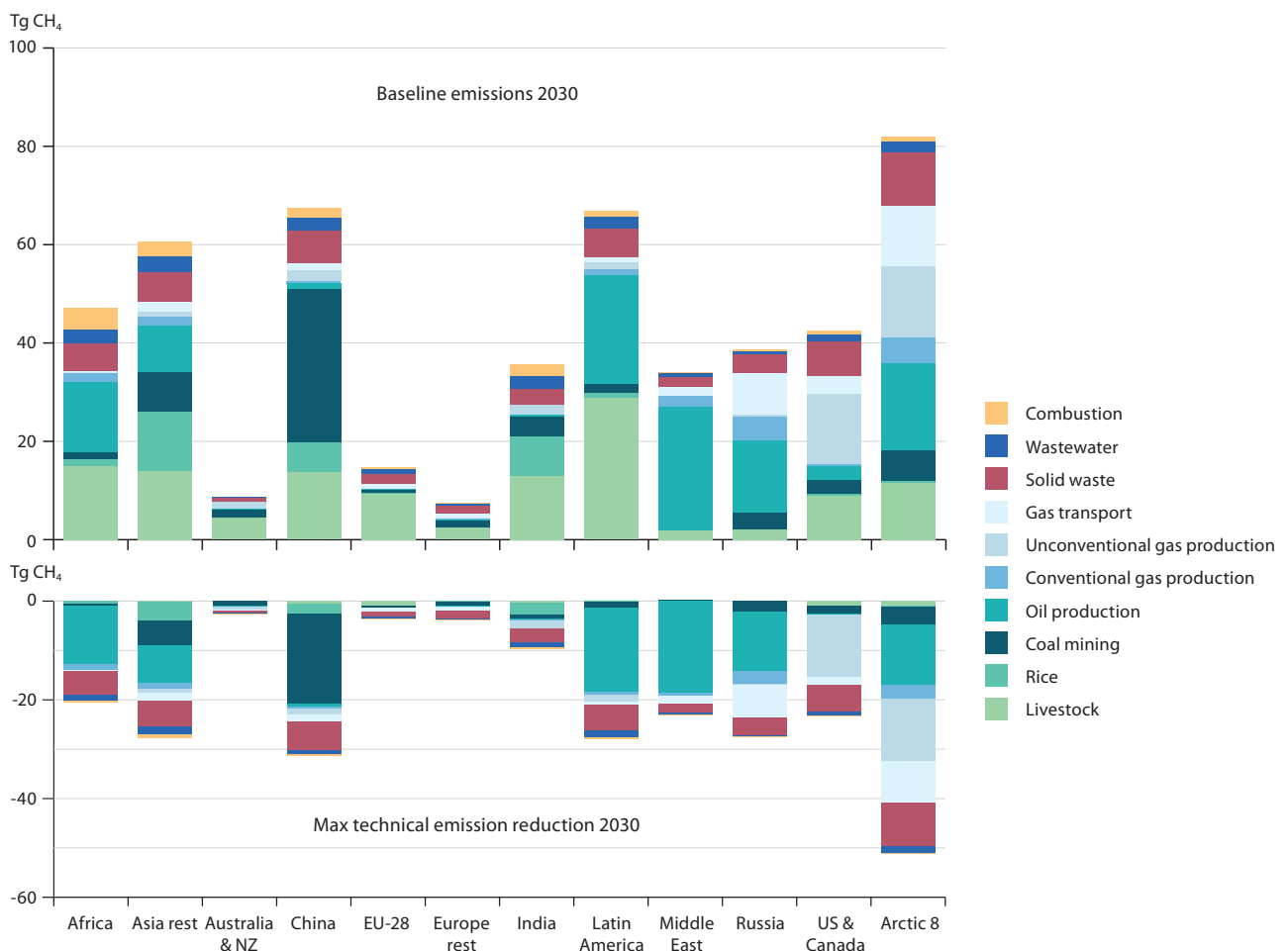
Fig. 5.3 Estimates of methane emissions in 2030 by world region from the GAINS model (ECLIPSE 2014): current control legislation ('CLE; 2014'; upper) and maximum technically feasible reduction of methane emissions in 2030 ('MFR; 2014') relative the CLE emissions in 2030 (lower).

extensive extraction of fossil fuels. For comparison, Fig. 5.3 also shows the collective contribution to global methane emissions from the eight Arctic nations. When considered as a single world region, the Arctic nations' contribution to global anthropogenic methane emissions and their reduction potential is substantial in comparison to other major world regions.

5.3.5 Cost of future reductions in global anthropogenic methane emissions

As explained in Box 5.1, the MFR scenario in the GAINS model refers to a global emission level of anthropogenic methane when existing technology is implemented to the greatest technically feasible extent. That a technology is considered *technically* feasible to implement, however, does not always mean that it is *socially* feasible to implement, because the latter will also take into consideration the cost of implementing the technology. Therefore, abatement cost information is of interest to policymakers. The USEPA (2014) and the GAINS model (Höglund-Isaksson 2012) provide estimates of the marginal abatement cost curve (MACC) for reducing emissions from the baseline emission level to the MFR emission level in year 2030. These cost curves are illustrated in Fig. 5.4 and reflect the direct marginal cost of purchasing, implementing and operating the identified methane abatement measures at the global scale. Note that the indirect cost to society caused by methane's contribution to climate change is not part of the marginal abatement cost curve. Such effects would be part of a marginal damage curve, which would move in the opposite direction to the marginal abatement cost curve, that is, the marginal damage curve would decline as the marginal abatement cost curve increases with reduced emissions. As shown by the marginal abatement cost curves in Fig. 5.4, apart from being more limited in its maximum technical reduction potential in 2030 (as discussed in Table 5.7), the USEPA MACC curve falls within the range of the low and high MACCs defined

by the GAINS model. It should be noted that although the global MACC curves defined for methane abatement in 2030 by the USEPA and GAINS are of similar magnitudes in total, differences exist at the sector level between the estimates of the two models.

The purpose of defining a range for the GAINS MACC is to indicate how different developments in the future gas price and investor perspectives could be expected to affect the future cost of methane abatement. Many methane abatement options involve reduced leakage or the opportunity to utilize recovered natural gas or biogas as sources of energy. Depending on the increase in the future gas price, some of the options are likely to become profitable in 2030. This is illustrated in the MACC curves in Fig. 5.4 as options falling below the zero cost line. The GAINS low MACC reflects the assumptions that the average global gas price increases to 20 EUR/GJ in 2030 and that investors consider the entire lifetime of equipment in investment decisions. This means that about two-thirds of the entire technical reduction potential in 2030 falls below the zero cost line and would be adopted without additional costs or the need for additional policy incentives to be put in place. The GAINS high MACC reflects the assumption of an average global gas price remaining at a low level of 5 EUR/GJ in 2030 and that investors have the perspective of a maximum ten years irrespective of whether the lifetime of the equipment is longer. This means that only 13% of the entire technical reduction potential in 2030 is expected to be realized at a net profit to investors and without additional policy incentives. Hence, external factors, in particular the development of the future price of gas, have significant effects on the future cost of reducing methane emissions and the need for further policies to stimulate such reductions.

Euro/tonne CH$_4$ Euro/tonne CO$_2$eq (GWP$_{100}$=25)

Change in global anthropogenic methane emissions in 2030, Tg CH$_4$

GAINS low MACC 2030   GAINS high MACC 2030   USEPA MACC 2030
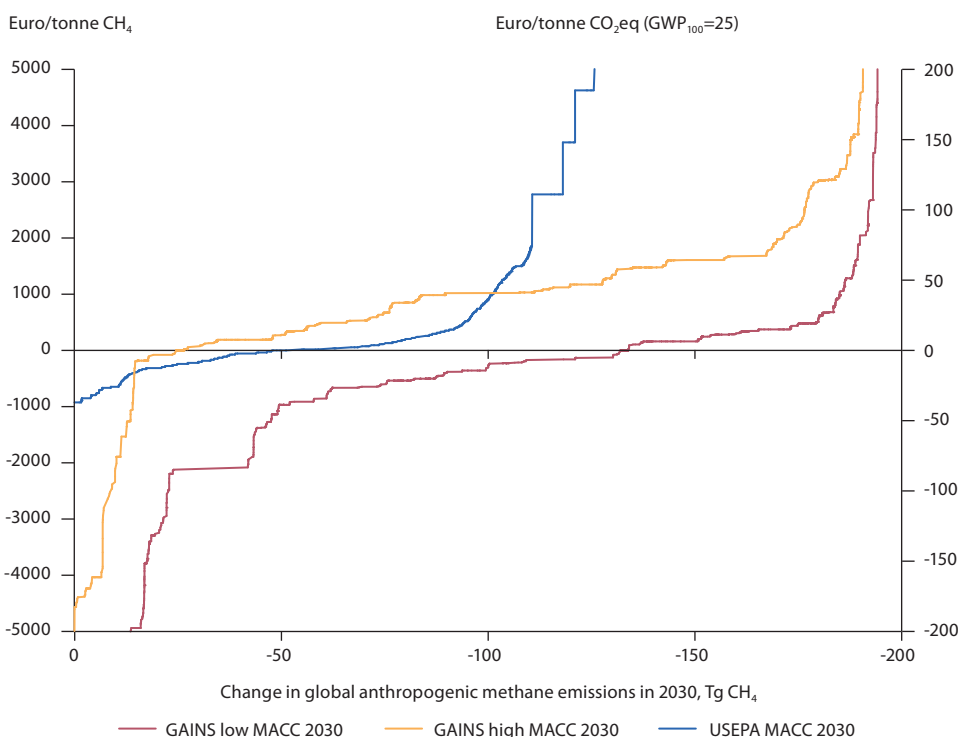
Fig. 5.4 Marginal abatement cost curves (MACC) for the technical abatement of global anthropogenic methane emissions in year 2030 as estimated by the USEPA (2014) and the GAINS model (Höglund-Isaksson 2012). The GAINS low MACC assumes a global average gas price of 20 EUR/GJ in 2030 and the GAINS high MACC assumes a global average gas price of 5 EUR/GJ in 2030 and a time-perspective for the investors limited to a maximum of ten years.

5.4 Anthropogenic methane emissions in Arctic nations

5.4.1 Contribution of Arctic nations to current and future anthropogenic methane emissions

The 'Baseline; 2012' scenario by the USEPA (USEPA 2012) and the 'CLE; 2014' and 'MFR; 2014' scenarios by the GAINS model (ECLIPSE 2014) allow for separation of future emissions by sector for the eight Arctic nations. Estimates by both model groups agree well in that the Arctic nations release about a fifth of global anthropogenic methane emissions (see Fig. 5.5). The USA and Russia contribute over 90% of these emissions, Canada about 6%, and the five Nordic countries less than 2%. The growth in future anthropogenic methane emissions is expected to be slightly more pronounced in non-Arctic than Arctic nations, driven largely by an expected strong increase in emissions from coal and gas extraction in non-Arctic nations.

5.4.2 Sources and abatement potentials for anthropogenic methane emissions in Arctic nations

Emission estimates for anthropogenic methane reported by the Arctic nations to the UNFCCC (UNFCCC 2013) for year 2005 are displayed in total and by sector in Fig. 5.6. The Arctic nations report releases of 56 Tg CH_4 in 2005 of which 55% was from fossil fuel production, transmission and distribution, 23% from agriculture and 19% from waste and wastewater sectors. This is slightly less than the 59 Tg CH_4 estimated by the USEPA (2012) for the same countries and year and clearly less than the 67 Tg CH_4 estimated by the GAINS model (ECLIPSE 2014). Figure 5.6 shows that in 2030 the USEPA estimates that baseline emissions from the Arctic nations will amount to 72 Tg CH_4, while the corresponding estimate in the GAINS CLE scenario is 82 Tg CH_4 in 2030 and 103 Tg CH_4 in 2050. The reason for the higher emission estimate throughout the analyzed period in the GAINS model can be referred to the higher estimates of venting of unrecovered associated gas from oil production following from the methodological differences explained in Sect. 5.2.3. The GAINS MFR scenario is displayed as a red dashed line in Fig. 5.6a and shows that with existing technology implemented to a maximum technically feasible extent, Arctic nations could reduce anthropogenic methane emissions to 31 Tg in 2030 and keep emissions at a low level throughout 2050 despite increasing levels of activity. The two-step reduction in the MFR curve in 2020 and 2030 is a feature of the model structure and reflects different assumed time-lags in the decomposition of biodegradable waste in landfills. The effect of diverting this type of waste away from landfills is reflected as emission reductions that are delayed 10 or 20 years depending on how fast different types of waste decompose (Höglund-Isaksson 2012).

Table 5.8 lists estimated methane emissions and abatement potentials in Arctic nations in 2005 and 2030 by sector and control measure. Emissions and abatement potentials are displayed both in absolute amounts and as fractions of global
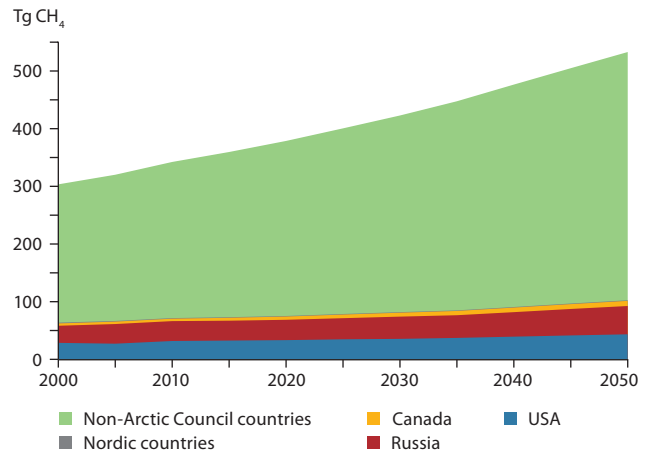
Fig. 5.5 The contribution of Arctic nations to global anthropogenic methane emissions between 2000 and 2050. Source: GAINS 'CLE; 2014' scenario (ECLIPSE 2014).
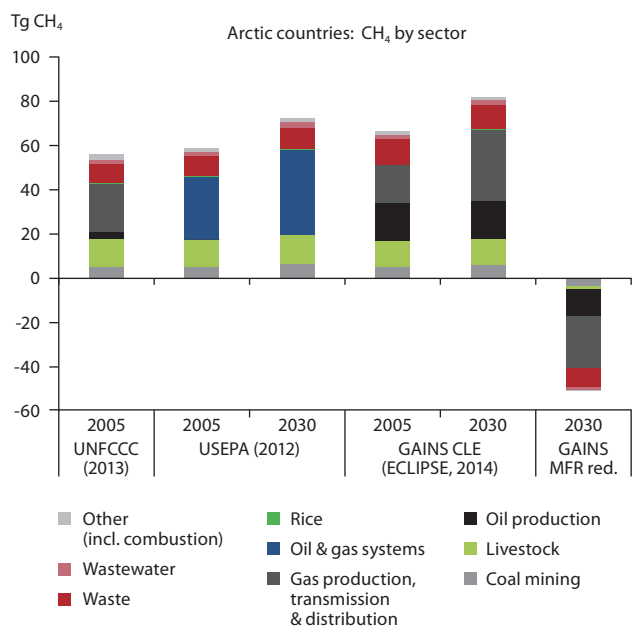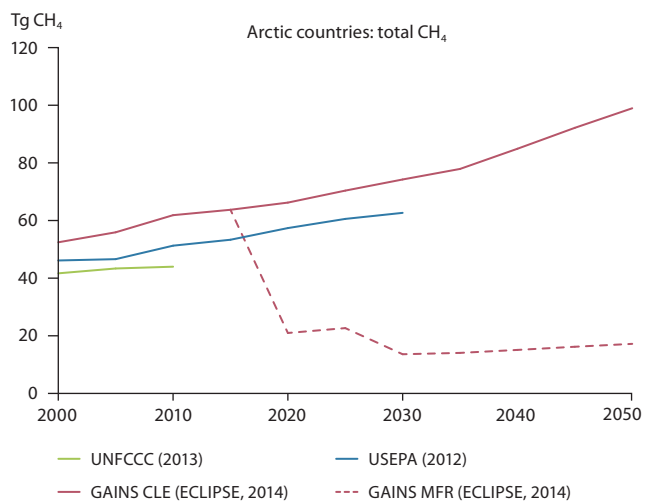
Fig. 5.6 Anthropogenic methane emissions in the Arctic nations as estimated by the USEPA (2012) for 2000–2030, by the GAINS model (ECLIPSE 2014) for 2000–2050 and as reported by countries to the UNFCCC (2013) for years 2000–2010 (upper). Anthropogenic methane emissions in the Arctic nations by sector in 2005 and 2030 as estimated by the respective inventories (lower). The GAINS MFR reduction potential in 2030 is relative to the CLE emission level in 2030.

Table 5.8 Baseline (CLE) methane emissions and maximum technically feasible reduction potentials (MFR) in Arctic Council nations by sector as estimated in the GAINS model (ECLIPSE 2014). See Höglund-Isaksson (2012a) for a further description of measures.

Sector	Control measure	2005	2030 CLE	2030 MFR	2030 MFR reduction	2005	2030 CLE	2030 MFR reduction
		Tg CH_4	Tg CH_4	Tg CH_4	Change in Tg CH_4	Percentage of global		
Livestock	Enteric fermentation: diet changes	11.8	11.6	10.4	-1.2	12	10	30
	Manure management: anaerobic digestion							
Rice cultivation	Mixed: aeration, alternative hybrids, sulfate amendments	0.4	0.4	0.2	-0.1	1	1	1
Agricultural waste burning	Ban	0.3	0.3	0.2	-0.2	10	9	8
Solid waste	Max separation and treatment, no landfill of biodegradable waste	11.4	11.0	2.1	-9.0	33	25	24
Wastewater	Extended treatment with gas recovery and utilization	1.9	2.1	0.8	-1.3	15	12	14
Coal mining	Pre-mining degasification	5.1	6.2	2.6	-3.6	16	11	11
	Ventilation air oxidizer with improved ventilation systems							
Conventional natural gas production	Recovery and utilization of vented associated gas	5.1	5.3	2.5	-2.7	51	39	40
	Good practice: reduced unintended leakage							
Unconventional gas production	Good practice: reduced unintended leakage	0	14.5	1.9	-12.6	0	65	69
Long-distance gas transmission	Leakage control	7.2	6.8	3.0	-3.8	90	87	91
Gas distribution networks	Leakage control and replacement of grey cast iron networks	4.7	5.4	0.8	-4.6	48	43	40
Oil production and refinery	Recovery and utilization of vented associated gas	17.9	17.7	5.4	-12.3	23	19	18
	Good practice: reduced unintended leakage							
Other sources (including combustion)	No control options identified	0.9	0.7	0.7	0.0	7	6	n.a.
Total		67	82	31	-51	21	19	25
Relative abatement potential					-63%			

emissions and abatement potentials. The overall technical abatement potential of methane in Arctic nations is estimated at 51 Tg CH_4 in 2030 or 63% below CLE emissions (ECLIPSE 2014). This makes up a quarter of the entire global technical reduction potential estimated for anthropogenic methane in 2030. The greatest technical abatement potentials are found from reduced venting of associated gas and better control of unintended leakage during oil and gas production.

5.4.3 Sources and abatement potentials for anthropogenic methane emissions by country

A number of policies which directly or indirectly affect methane emissions have already been adopted in the eight Arctic nations. These include both legally binding regulations and voluntary agreements and are listed in Table 5.9. With current policies, both the baseline scenario by the USEPA (2012) and the GAINS CLE scenario (ECLIPSE 2014) estimate

a 23% increase in emissions between 2005 and 2030. Figure 5.7 shows this expected increase in emissions between 2005 and 2030 by country and sector. Baseline emissions are expected to increase in the USA and Canada, primarily due to continued expansion of shale gas production, and in Russia, due to an increase in the production of conventional natural gas. Methane emissions from solid waste disposal are expected to increase in Canada and Russia, driven by increased generation of waste as a result of economic growth and continued extensive reliance on landfill disposal of biodegradable waste with only limited recovery of landfill gas.

The bar to the far right in the country graphs in Fig. 5.7 (denoted 'MFRred 2030') illustrates the maximum technically feasible abatement potential in 2030 by sector and country as estimated by the GAINS model (ECLIPSE 2014). The technical abatement potential in 2030 is estimated at 4 Tg CH_4 for Canada and 20 Tg CH_4 for the USA, which is 46% below baseline emissions in both countries. The technical abatement potential for Russia is estimated at 27 Tg CH_4 or 70% below baseline emissions
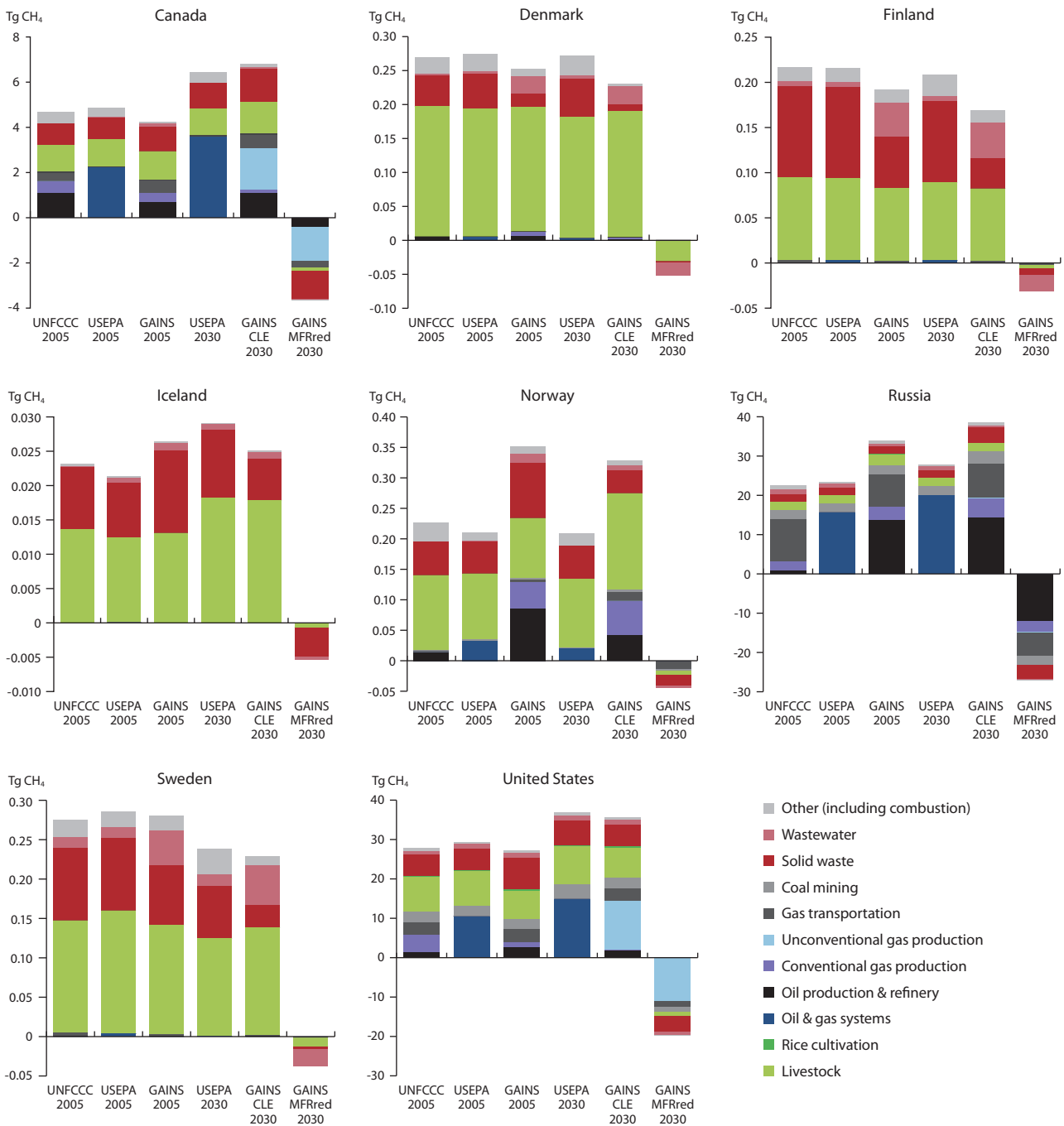
Fig. 5.7 Anthropogenic methane emissions by Arctic nations in 2005 and 2030 as reported to UNFCCC (2013) and as estimated by the USEPA (2012) and the GAINS model (ECLIPSE 2014), the latter including emission reduction in MFR in 2030. Note the large differences in scale along the Y-axes between countries. The GAINS MFR reduction potential in 2030 is relative to the CLE emission level in 2030.

in 2030. For the five Nordic countries the entire technical abatement potential in 2030 is estimated at 0.17 Tg CH$_4$, or 13% to 23% below baseline emissions in the respective country.

The largest abatement potentials for Canada and the USA are found by controlling emissions from unconventional gas extraction and by diverting biodegradable solid waste away from landfills by extending existing separation, recycling and treatment schemes. The greatest potentials for methane abatement in Russia are expected from extended recovery and utilization of associated gas from oil production and reduced leakage from gas pipelines and networks. Both the USA and Russia are estimated to have potentials to reduce methane emissions from coal mines through extended pre-

mining degasification and implementation of ventilation air oxidizers on shafts from underground mines. The technical abatement potentials from livestock rearing are expected to be limited with existing technology in all countries. Enteric fermentation emissions from cattle can be controlled through changing the animal diets, but this is typically restricted to regions and periods when animals are fed concentrates while indoor. Manure management emissions can be reduced through the use of well managed anaerobic digesters, which also generate valuable biogas. With expected increases in future energy prices (IEA 2012), the GAINS model estimates that farm-scale anaerobic digestion for treatment of pig manure from large pig farms would become profitable in the USA, Canada and Western Europe (Höglund-Isaksson 2012). Further

Table 5.9 Existing policies and voluntary initiatives affecting methane emissions in Arctic nations.

Country	Sector	Policy or voluntary initiative	Source
Canada	Oil and gas systems	Requirements for oil and gas producers in the provinces of Alberta, British Columbia, and Newfoundland to limit flaring and venting resulting in, for example, a 40% reduction in venting and a 60% reduction in flaring of solution gas in Alberta. Recently implemented requirements in Saskatchewan and New Brunswick are expected to achieve similar reductions.	Alberta Energy Regulator (2013, 2014); BC Oil and Gas Commission (2013); Canadian Minister of Justice (2009); Saskatchewan Ministry for Energy and Resources (2011); New Brunswick Department of Energy and Mines (2013)
	Solid waste	Provincial regulations in British Columbia, Manitoba, Ontario, Quebec and Prince Edward Island require the collection and utilization and/or flaring of landfill gas (although requirements may depend upon facility size, age, etc.). Under the Provincial regulations in Alberta, facilities can reduce their emissions physically, use offsets or contribute to the Climate Change and Emissions Management Fund.	BC Ministry of Environment (2008); Manitoba Ministry of Conservation and Water Stewardship (2009); Ontario Ministry of Environment (2007); Québec MDDELCC (2011); PEI Ministry of Environment, Labour and Justice (2009); Alberta Energy Regulator (1998); Ontario Ministry of Energy (2009)
		Province of Ontario has feed-in tariff in support of landfill gas electricity generation.	
	Livestock	Voluntary provincial greenhouse gas offset protocols in Alberta and Quebec address methane emissions from the anaerobic decomposition of agricultural materials (Alberta) and covered manure storage facilities (Quebec).	Alberta Environment (2007); Québec MDDELCC (2009)
Denmark	Oil and gas systems	EU Fuel Quality Directive: Reduce life-cycle greenhouse gas emissions of fossil fuels by 10% between 2010 and 2020 including reductions of flaring and venting at production sites.	EU Directive 2009/30/EC
		Gas flaring only allowed with specific permission of the government and venting only permitted in the case of emergency.	GMI and EC (2013)
	Solid waste	EU Landfill Directive: Until 2016 reduce landfill disposal of biodegradable waste by 65% from the 1995 level and implement compulsory recovery of landfill gas from 2009.	EU Directive 1999/31/EC
		EU Waste Management Framework Directive: The waste hierarchy must be respected, that is, recycling and composting preferred to incineration/energy recovery, which in turn is preferred to landfill disposal.	EU Directive 2008/98/EC
		National ban on landfill of untreated biodegradable waste in effect since 1997.	BEK nr. 1473 af 21/12/2009
	Wastewater	EU Urban Wastewater treatment Directive: "Appropriate treatment" of wastewater from urban households and food industry must be in place by 2005 and receiving waters must meet quality objectives.	EU Directive 1991/271/EEC
	Livestock	National law on the promotion of renewable energy, which includes subsidy on biogas generated, for example, from manure.	Lov 1392, 2008
Finland	Solid waste	EU Landfill Directive: Until 2016 reduce landfill disposal of biodegradable waste by 65% from the 1995 level and implement compulsory recovery of landfill gas from 2009.	EU Directive 1999/31/EC
		EU Waste Management Framework Directive: The waste hierarchy must be respected, that is, recycling and composting preferred to incineration/energy recovery, which in turn is preferred to landfill disposal.	EU Directive 2008/98/EC
	Wastewater	EU Urban Wastewater treatment Directive: "Appropriate treatment" of wastewater from urban households and food industry must be in place by 2005 and receiving waters must meet quality objectives.	EU Directive 1991/271/EEC
Iceland	All sources	No policies specifically addressing methane. Emissions probably small because of small population and cold climate.	Jonsson (2014)
Norway	Oil and gas systems	Gas flaring only allowed with specific permission of the government and venting only permitted in the case of emergency.	GMI and EC (2013)
	Solid waste	National ban on deposition of biodegradable waste in covered landfills from 2004.	FOR-2004-06-01-930
Russia	Oil and gas systems	In the April 2007 State of the Union address, president Putin announced an intent to make better utilization of associated gas a national priority.	Carbon Limits (2013)
		"Estimation of fines for release of polluting compounds from gas flares and venting of associated gas from oil production." (Translation from Russian by A. Kiselev, 2014).	Decree No.1148, Nov 8, 2012 of the Russian Federal Government
		As of 2012, all flared associated gas must be metered or the methane fine increases by a factor of 120.	Evans and Roshchanka (2014)
	Other sources	"About greenhouse gases emission reduction." General policy addressing greenhouse gases, but unclear how methane is specifically addressed.	Decree No.75, Sep 30, 2013 of the Russian Federal Government
Sweden	Solid waste	EU Landfill Directive: Until 2016 reduce landfill disposal of biodegradable waste by 65% from the 1995 level and implement compulsory recovery of landfill gas from 2009.	EU Directive 1999/31/EC
		EU Waste Management Framework Directive: The waste hierarchy must be respected, that is, recycling and composting preferred to incineration/energy recovery, which in turn is preferred to landfill disposal.	EU Directive 2008/98/EC

Country	Sector	Policy or voluntary initiative	Source
Sweden	Solid waste	National ban on landfill of untreated biodegradable waste from 2001.	SFS 2001:512
	Wastewater	EU Urban Wastewater treatment Directive: "Appropriate treatment" of wastewater from urban households and food industry must be in place by 2005 and receiving waters must meet quality objectives.	EU Directive 1991/271/EEC
United States	Oil and gas systems	EPA's Natural Gas STAR Program: voluntary partnership that encourages oil and natural gas companies to adopt cost-effective technologies and practices that improve operational efficiency and reduce emissions of methane.	USEPA (2014)
	Coal mining	EPA's Coalbed Methane Outreach Program: voluntary program whose goal is to reduce methane emissions from coal mining activities.	USEPA (2014)
	Solid waste	EPA's Landfill Methane Outreach Program: voluntary assistance program that helps to reduce methane emissions from landfills by encouraging the recovery and beneficial use of landfill gas as an energy resource.	USEPA (2014)
	Livestock	EPA's AgSTAR Program: voluntary outreach and educational program that promotes the recovery and use of methane from animal manure.	USEPA (2014)

methane emission reduction potentials in the solid waste sector are limited in the Nordic countries, because bans on landfill disposal of untreated biodegradable waste have already been fully or close to fully implemented in Denmark, Finland, Norway and Sweden (see Table 5.9).

5.4.4 Uncertainty in oil and gas systems emissions in Arctic nations

A major source of uncertainty in the estimates of anthropogenic methane emissions and reduction potentials in the Arctic nations relates to emissions from oil and gas production, transmission and distribution. Five Arctic nations – Canada, Denmark, Norway, Russia and the USA – currently produce about a quarter of the oil and about half of the natural gas in the world (IEA 2012). The five countries reported to the UNFCCC (2013) to have emitted 10 Tg CH_4 from oil and gas production (excluding pipeline transmission, refining and distribution) in 2005. The corresponding estimate in the GAINS model (ECLIPSE 2014) is 23 Tg CH_4 in 2005, of which 18 Tg was from oil and gas

production in Russia. The reported emission factors for oil and gas production presented in Table 5.5 and reproduced in Fig. 5.8, show a wide range in magnitude between countries. It is notable that Canada, which has recent systematic on-site measurements (Johnson and Coderre 2011), reported 72% higher emissions per energy unit of oil produced than the USA, 167% higher than Russia, and a few thousand percent higher than what was reported for Norway and Denmark. Comparisons to Denmark and Norway are difficult because all oil and gas production takes place offshore, which means that any unintended leakage of methane from equipment at the seabed is likely to oxidize before it reaches the sea surface (see Ch. 4). With respect to the magnitude of methane emissions released intentionally through flaring and venting of associated gas during oil production, results from satellite images of gas flares from NOAA (2010) presented in Fig. 5.8 suggest that the energy content of gas flared, expressed as percent of PJ oil produced, are indeed low in Norway and Denmark, but still close to or of about the same magnitude (between 0.2% and 2% of the energy content of oil produced) as in Canada and the USA. Russian flaring rates are
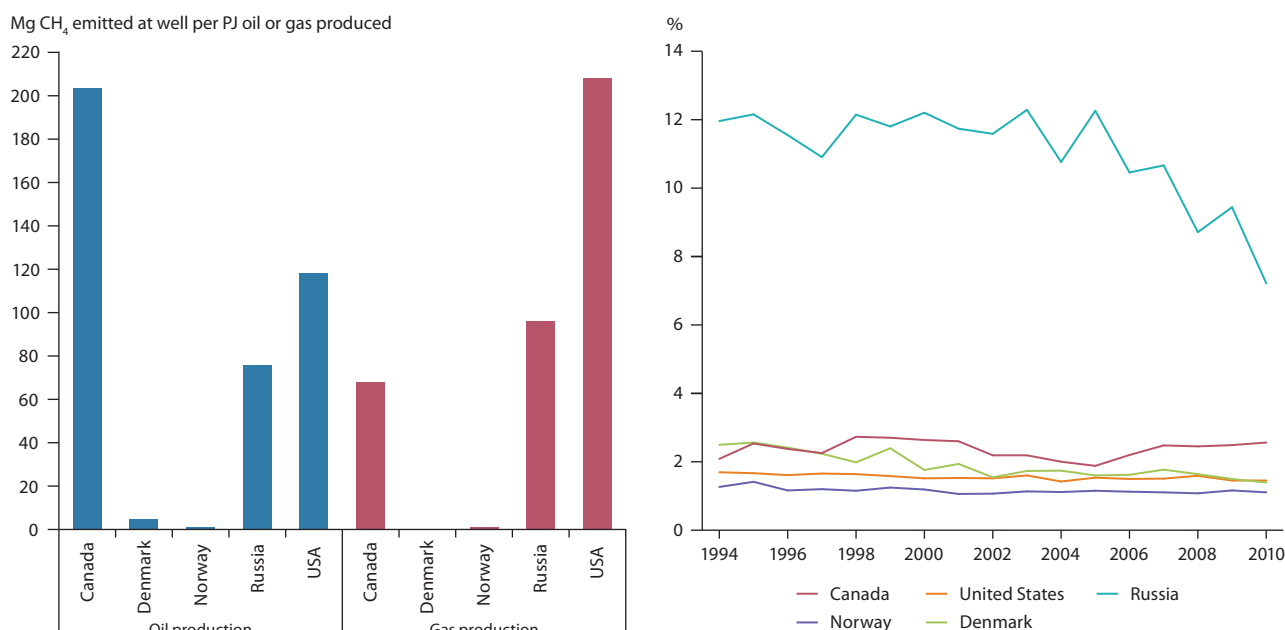
Fig. 5.8 Implied methane emission factors for oil and gas production reported to UNFCCC (2013) (left) and energy content of flared gas as fraction of crude oil produced based on data from satellite images (NOAA 2010) (right).

considerably higher at about 12% per PJ oil produced until 2005, however falling rapidly to about 7% per PJ oil produced in 2010. If the Canadian measurements of Johnson and Coderre (2011) are taken as evidence that whenever flaring takes place, there is also likely to be some venting, then venting per unit of oil produced would be expected to be of about the same magnitude for Denmark as for the USA, with Norway at about half that, and with considerably higher magnitudes for Russia. However, this is not what is seen in the implied emission factors reported to the UNFCCC (2013) (see also Fig. 5.8a). This large and mainly unexplained discrepancy in reported emission factors points to the high uncertainty in reported emissions and indicates a need for more systematic measurements.

5.5 Use of anthropogenic methane emission scenarios in climate models

Chapter 8 presents the results of two climate modeling experiments to assess the effects on surface air temperature of the maximum technically feasible implementation of existing methane control technology, either globally or in the eight Arctic nations only. For these exercises, the GAINS scenario ECLIPSE v4a (ECLIPSE 2012) was used. The scenario ECLIPSE v5 (ECLIPSE 2014) only became available in April 2014, which was too late for it to be included in the climate modelling experiments for the present assessment. For comparison, the results of both scenarios are displayed in Fig. 5.9. The ECLIPSE (2012) scenario combines a global energy scenario to 2030 from IEA World Energy Outlook 2011 (IEA 2011a) with a global energy scenario to 2050 from the POLES model (Russ et al. 2009). The ECLIPSE (2014) scenario uses a consistent energy scenario to 2050 from IEA
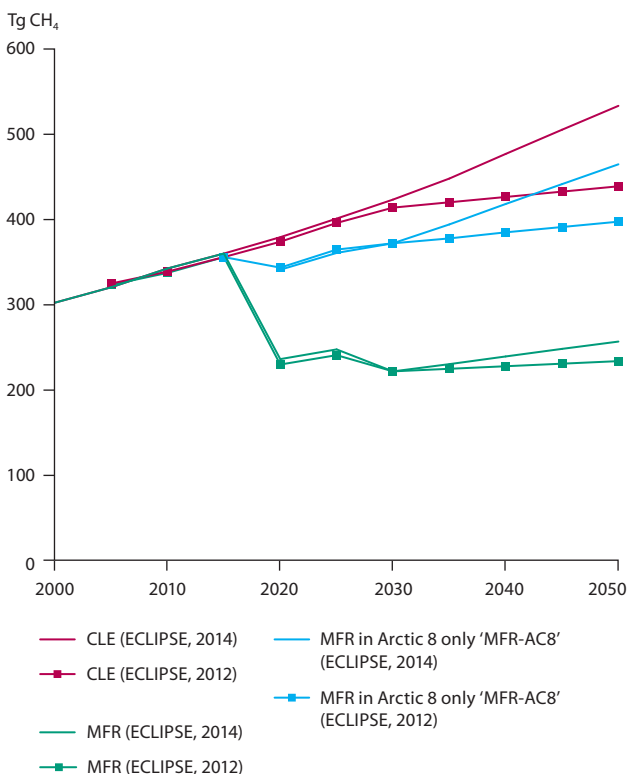
Energy Strategies Perspectives 2012 (IEA 2012) and attributes shares of gas produced to conventional or unconventional gas using country-specific trends from the IEA (2011b). Global methane emissions increase more rapidly in the ECLIPSE (2014) scenario than the ECLIPSE (2012) scenario due to a stronger increase in global gas consumption (partly driven by increased extraction of shale gas in the USA and Canada), and the introduction in the GAINS model of higher emission factors for unconventional than for conventional gas extraction. The MFR scenarios (ECLIPSE 2012, 2014) assume uptake of technical control options, which almost exclusively address methane emissions, without affecting emissions of other species contributing to radiative forcing. The only option included which affects emissions of other species, is a ban on the burning of agricultural waste residuals. This source contributes, however, to less than 1% of global methane emissions in the CLE scenarios (ECLIPSE 2012, 2014).

5.6 Conclusions

5.6.1 Key findings

This chapter reviews recent global assessments of anthropogenic methane emissions, their expected future development and estimated reduction potentials. Because methane is a gas which mixes rapidly in the global atmosphere, it is of interest to review emissions at the global scale as well as for the area covered by the eight Arctic nations. The following key findings have been identified:

- Bottom-up emission inventories agree fairly well in terms of the overall magnitude of global anthropogenic methane emissions in recent years, that is, about 300 Tg CH_4 in 2000 and between 320 and 346 Tg CH_4 in 2005. However, the relative contributions from the different source sectors differ markedly between inventories, which can be taken as an indication of high uncertainty within existing emission inventories despite the relatively close agreement between them in terms of total emissions.

- Without further implementation of control policies addressing methane than currently adopted, global anthropogenic methane emissions are estimated to increase to between 400 and 500 Tg CH_4 in 2030 and between 430 and 680 Tg CH_4 in 2050. Primary drivers for the expected emission increase are increased coal production in China and extended shale gas extraction in the USA and Canada, activities which are known to release fugitive methane emissions.

- With maximum technically feasible implementation of existing control technology, the estimated reduction potential for global anthropogenic methane emissions amounts to about 200 Tg CH_4 in 2030, which is almost 50% below baseline emissions. The control technologies assessed to have the greatest reduction potentials are extended recovery of associated gas from oil production, control of fugitive leakages from gas production, transmission and distribution, extended separation, recycling and treatment of biodegradable waste instead of landfill disposal, extended pre-mining degasification of coal mines, and the implementation of ventilation air oxidizers on shafts from underground coal mines.

Tg CH_4

Fig. 5.9 Scenarios for global anthropogenic methane emissions from the GAINS model (ECLIPSE 2012, 2014). The three ECLIPSE (2012) scenarios were used in the model experiments presented in Ch. 8.

Legend:
- CLE (ECLIPSE, 2014)
- CLE (ECLIPSE, 2012)
- MFR (ECLIPSE, 2014)
- MFR (ECLIPSE, 2012)
- MFR in Arctic 8 only 'MFR-AC8' (ECLIPSE, 2014)
- MFR in Arctic 8 only 'MFR-AC8' (ECLIPSE, 2012)

- External factors, in particular the development of the future price of gas, could have significant effects on the future cost of reducing methane emissions and on the need for further policies to stimulate such reductions. The reason is that many measures to reduce methane emissions involve gas recovery or reduced gas leakage, which means potential opportunities to utilize the recovered gas as a source of energy.

- With current policies addressing methane emissions, the eight Arctic nations are estimated to contribute about a fifth of global anthropogenic methane emissions.

- As a single world region, the eight Arctic nations emit more anthropogenic methane and have a larger technical abatement potential than any other major world region (e.g. Latin America, Middle East, Africa or China).

- The maximum technically feasible reduction of anthropogenic methane in Arctic nations in 2030 is estimated at 63% below baseline emissions or about a quarter of the entire global reduction potential. Within this reduction potential, measures related to fugitive methane emissions from shale gas extraction in the USA and Canada, reduced venting of associated gas from oil production in Russia, and reduced leakage from gas pipelines and distribution networks in all three countries, have the greatest potential to contribute to reduced methane emissions in Arctic nations.

5.6.2 Recommendations

As a major contributor to global anthropogenic methane emissions and with a considerable potential to reduce methane emissions by employing existing technology, the eight Arctic nations are in a good position to contribute significantly to emission reductions in global methane emissions. For the same reason, the Arctic nations could also make important contributions towards reducing uncertainty in emission estimates and abatement potentials by supporting improvements in existing methane measurement networks.

- **Increase the number and type of systematic on-site measurements and make results publically available to help reduce the large uncertainty in global methane emission estimates.** This would be particularly important for the potentially substantial fugitive methane emissions from oil and gas systems for which very few direct measurements exist that are source attributed and representative for different types of hydrocarbons in different world regions.

- **Support a continuous dialogue between developers of top-down and bottom-up emission estimates in order to resolve the current unexplained divergence in global methane estimates.** Currently, the observed year-to-year variation in methane concentration in the atmosphere over the past few decades cannot be explained by global anthropogenic (and natural) emission inventories. This is a problem because historical emission inventories are the basis for future projections.

6. Long-term monitoring of atmospheric methane

Lead authors: Douglas Worthy, Carrie Taylor, Ed Dlugokencky, Elton Chan, Euan G. Nisbet, Tuomas Laurila
Contributing authors: Rebecca E. Fisher, James France, David Lowry, Anna Karion, John Miller, Colm Sweeney, James W.C. White

6.1 Introduction

Long-term, systematic measurements of atmospheric methane abundance from a well-calibrated network of air sampling sites are essential to support an assessment of long-term trends, as well as changes in shorter term variability. Measurements are made using sampling strategies that provide information about atmospheric levels over different temporal and spatial scales. Low frequency (i.e. weekly) air samples collected in flasks at remote background sites sample well-mixed air that yields large-scale information about the Arctic region. Continuous measurements are also made at some sites, with the data subsequently averaged to generate a high-frequency (e.g. hourly) time series. Such measurements provide information about the variability in atmospheric methane concentrations, from which information about processes affecting levels at local to regional scales can be determined. When combined with models of atmospheric chemistry and transport, measurements of atmospheric abundance can provide information about methane emissions at larger spatial scales than flux measurements with micrometeorological techniques (see Ch. 3 and 7). Atmospheric methane data provide an important, large-scale perspective to understanding global and regional carbon sources and sinks. As a result of atmospheric transport and mixing, the observed changes in atmospheric concentration reflect large-scale balance or imbalance between emissions and losses (or sinks). Given this relationship, and with sufficient measurement precision and surface coverage (e.g. measurement sites), source region signatures can be inferred.

Further information about emission source type can be obtained from measurements of stable isotopic composition, because methane originating from different sources can have different isotopic signatures.

This chapter summarizes the most recent observations of atmospheric methane from Arctic and sub-Arctic monitoring sites. The objectives of this chapter are to present analysis of available ambient methane observations from a suite of Arctic locations and to highlight how long-term observational data can be used to gain an improved understanding of regional-scale processes and sources affecting methane.

The objectives are targeted in order to answer the science questions posed to the Methane Expert Group, including:

What are the trends and variability in Arctic methane concentrations and what are the primary drivers of this variability?

How much of a trend in atmospheric methane abundance can be detected with the current monitoring network?

Is there evidence of increasing Arctic methane emissions in the atmospheric observations?

This chapter focuses on the long-term systematic measurements of atmospheric methane, and does not address short-term field campaign measurements targeted towards improved understanding of atmospheric processes, nor does it include an analysis of column measurements that provide information on the vertical distribution of methane.

6.2 Surface observations of atmospheric methane

Atmospheric methane monitoring in the Arctic began in the mid-1980s. Analytical instruments used to measure atmospheric methane are calibrated against a common standard scale – the World Meteorological Organization's Global Atmosphere Watch (WMO GAW) methane mole fraction scale – and measurements are reported as dry air mole fractions. Atmospheric methane is measured in nanomoles (billionths of a mole) per mole of dry air and reported as parts per billion (10^9; ppb). (For simplicity, throughout this chapter – and consistent with the rest of this report – methane mole fractions are referred to as methane concentrations or abundances.) Gas chromatography with flame ionization detection has typically been used for analysis of methane in weekly discrete air samples collected in flasks. In addition to gas chromatography, recent technological advances have allowed for higher resolution continuous (hourly) observations, primarily through the incorporation of new multi-species analyzers, including carbon dioxide (CO_2), methane (CH_4) and carbon monoxide (CO), using cavity enhanced absorption spectroscopy techniques such as Cavity Ring Spectroscopy (Crosson 2008) and Off-Axis Integrated Cavity Output Spectroscopy (O'Keefe et al. 1999).

Data compatibility and accuracy are ensured primarily through participation in the WMO GAW program. Three main factors contribute to the uncertainty of a single methane measurement: the reproducibility of the calibration values assigned on the standard gas cylinders used to determine the ambient methane mixing ratios; the time-dependent analytical uncertainty for each measurement; and the standard deviation of each hourly averaged or single flask air sample measurement. These uncertainties are generally quantified by independent laboratories (Andrews et al. 2013). However, the most relevant metrics to assess relative uncertainty among individual laboratories are results reported from ongoing standard gas and real air comparisons (Masarie et al. 2001). Inter-laboratory and methodological comparison exercises provide a mechanism to link many individual network data sets in order to provide a measure of network comparability, and to characterize measurement uncertainty (Masarie et al. 2001; Andrews et al. 2013). The WMO has set a global network comparability target goal for methane of ±2 ppb (WMO 2005). Previously reported results of international laboratory intercomparison activities showed consistent average agreement between participating laboratories to be better than 2 ppb (Worthy et al. 2005).

Fig. 6.1 Long-term methane atmospheric monitoring sites in the Arctic and sub-Arctic region (Arctic Circle shown by gray dashed circle at 66.56°N). Remote background sites are shown by green circles; regionally influenced sites are shown by red circles. Air sampling for methane at Mould Bay and Station-M (shown in yellow) stopped in April 1997 and June 2009, respectively.

While the number of sites monitoring atmospheric methane abundance has increased over the past five years, particularly in the Arctic and sub-Arctic regions, the long-term observational network likely remains inadequate to quantitatively characterize polar methane fluxes, given the importance and variety of the potential sources and the vast area of the Arctic. Figure 6.1 shows the sites where multi-year, surface-based discrete (i.e. flask sampled) measurements, continuous measurements, or a combination of both are readily available. The length and continuity of the data record varies from site to site (see Table 6.1). Figure 6.1 and Table 6.1 do not represent the full list of observations potentially available for the Arctic, but rather

those stations for which data were available, tied to a common standard and of known quality. Based on these data only, this assessment provides the most comprehensive overview of long-term Arctic atmospheric methane observations currently possible, given the limited number of observing stations in the Arctic.

For the purposes of this study, monitoring sites were characterized as either remote background or regionally influenced. This distinction is for comparative purposes only, and relates primarily to the location of the site relative to source regions. It is also normal that measurements taken at many of

Table 6.1 Summary of available observations of methane in the Arctic.

Station name (Country)	Latitude / Longitude	Height, m above sea level	Sampling History
Alert (Canada)	82.5°N / 62.5°W	210	
Behchoko (Canada)	62.8°N / 116.1°W	179	
Cambridge Bay (Canada)	69.1°N / 105.1°W	38	
Churchill (Canada)	58.7°N / 93.8°W	29	
Inuvik (Canada)	68.3°N / 133.5°W	100	
Mould Bay (Canada)	76.3°N / 119.4°W	30	
Pallas (Finland)	68°N / 24.1°E	560	
Summit (Greenland)	72.6°N / 38.4°W	3238	
Storhofdi (Iceland)	63.4°N / 20.3°W	118	
Ny-Ålesund (Norway)	78.9°N / 11.9°E	474	
Station M (Norway)	66°N / 2°E	0	
Cherskii (Russia)	68.5°N / 161.5°E	30	
Teriberka (Russia)	69.2°N / 35.1°E	40	
Tiksi (Russia)	71.6°N / 128.9°E	8	
Barrow (USA)	71.3°N / 156.6°W	11	
CARVE Tower (USA)	65°N / 147.6°W	611	
Cold Bay (USA)	55.2°N / 162.7°W	21	
Shemya (USA)	52.7°N / 174.1°W	40	

Sampling History axis: 1985   1990   1995   2000   2005   2010   2015

Legend: ■ Flask   ■ Hourly   ■ Monthly

CH$_4$, ppb

CH$_4$, ppb

Change in CH$_4$, ppb/y

Fig. 6.2 Historical time series of methane concentration at several remote background sites in the Arctic. Smoothed data curves were generated by passing monthly mean methane data through a smoothing function (Nakazawa et al. 1997) for sites starting prior to 1994, with weekly flask samples from NOAA's Cooperative Global Air Sampling Network. For illustrative purposes, the trend, generated using the same smoothing function routine, is shown in black for Alert, Canada.

Fig. 6.3 Change in methane abundance at remote background sites within the Arctic. The upper plot shows zonally-averaged (60°–90°N) atmospheric methane concentrations together with the deseasonalized trend, while the lower plot shows the instantaneous methane growth rate determined as the time-derivative of the trend in the upper plot. Zonal means are determined from weekly samples at background sites representing large volumes of well-mixed atmosphere collected as part of the NOAA Cooperative Global Air Sampling Network. Curve-fitting methods are as described by Dlugokencky et al. (2009).

the weekly flask sampling sites reflect background information, because sampling protocols dictate sampling to occur when winds originate from 'clean air' sectors.

Measurements in Arctic locations have been conducted for many decades at remote background sites. These sites are generally coastal, high elevation and relatively far removed from major source regions. An example of extended time series plots for the remote background baseline observatories at Alert (Canada), Cold Bay (USA), Summit (Greenland), Ny-Ålesund (Norway), Storhofdi (Iceland), Barrow (USA) and Shemya (USA) is shown in Fig. 6.2. The smoothed seasonal cycles of methane were derived from the digital filter technique of Nakazawa et al. (1997), using weekly flask samples from NOAA's Cooperative Global Air Sampling Network (Dlugokencky at al. 1994). The near 30-year Arctic record shows an overall increase in methane abundance, consistent with evidence from Arctic and Antarctic ice cores that show a near 300% increase in atmospheric methane concentration since the late 1800s (Etheridge et al. 1992; Blunier et al. 1993). The rate of increase in the atmosphere changed from around 14 ppb/y in the 1980s to near zero over the period from 1999 to 2007. From 2008 to 2013, the observed abundance of methane in the atmosphere has increased annually at around 6 ppb/y (see Sect. 6.3).

6.3 Large-scale trends in Arctic atmospheric methane

Methane emissions mix through the troposphere on time scales that are much shorter than the globally-averaged atmospheric lifetime for methane (9.1±0.9 y; Prather et al. 2012). So, to first order, trends in atmospheric concentration are about the same everywhere on Earth. It is only because of the high quality and inter-laboratory consistency of measurements made by national laboratories that subtle features in zonal

averages from smaller regions such as the Arctic can be used to assess temporal changes in emissions. Zonally-averaged dry-air methane abundance at the Earth's surface for the area 60°–90°N determined from remote background sites in NOAA's Cooperative Global Air Sampling Network is shown in Fig. 6.3. The seasonality observed in the graphic has three components: seasonality in methane emissions at a regional scale, seasonality in photochemical methane destruction at the hemispheric scale, and seasonality in the height of the Arctic boundary layer. The trend in methane abundance results from the imbalance between emissions and sinks.

Figure 6.3 also illustrates changes in the atmospheric growth rate over time, showing the instantaneous rate of methane increase, calculated as the time-derivative of the deseasonalized trend. From the start of measurements through to 2006, the atmospheric growth rate decreased from about 14 ppb/y in 1983 to near-zero in 1999/2000, after which a period of interannual variability is evident, with no strong trend observed.

Residuals from a function that approximates the long-term trend and seasonal cycle (2nd-order polynomial and 4 annual harmonics; Thoning et al. 1989) fitted to the methane zonal averages in Fig. 6.3 are plotted in Fig. 6.4. The residuals represent deviations (anomalies) from the long-term behavior. Carbon monoxide is included as it provides additional context on potential sources (i.e. biomass burning) that may affect the long-term trend in atmospheric methane. Changes in the sign of the trend of the residuals in 1992 and 2007 indicate changes in the global methane budget that have affected the trajectory of its future atmospheric burden.

The change observed in 1992 is most likely to have been related to a reduction in anthropogenic emissions from the former Soviet Union (Dlugokencky et al. 1994, 2011; Worthy et al. 2009), and has implications for what may be said about the potential impacts of a warming Arctic on natural emissions.
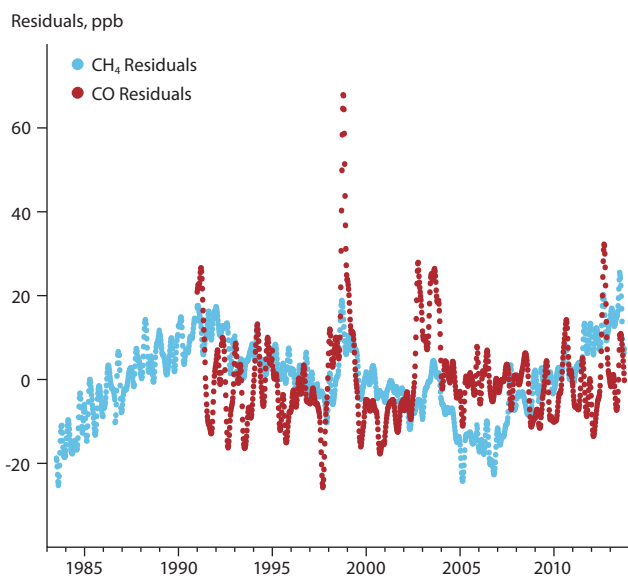
Residuals, ppb

Fig. 6.4 Difference (residuals) between zonal means (53° to 90°N) and function fitted to them that captures mean quadratic trend and seasonal cycle for methane (CH₄) and carbon monoxide (CO) measured in the same samples.

Superimposed on the long-term pattern of atmospheric methane abundance is interannual variability. The main drivers of interannual variability are related to emissions from wetlands and biomass burning (Bousquet et al. 2006), which are affected by large-scale multi-year changes in weather patterns such as the El Niño-Southern Oscillation (ENSO) (Dlugokencky et al. 2009). Specific drivers affecting Arctic methane emissions are surface air and soil temperatures, because the rate of methane production by methanogens is very temperature dependent, with emissions generally increasing with increasing temperature (see Ch. 3). Precipitation amounts can affect the areas and relative wetness of wetlands (wetter conditions generally result in greater emissions, all other parameters the same; see Ch. 3), but they also affect the rate of methane emission from biomass burning, as more burning tends to occur in dry years. The molar ratio of CO to CH₄ for biomass burning is in the range 10 to 20 (Christian et al. 2003), so observations of carbon monoxide are very sensitive to biomass burning. Strong signals from biomass burning at high northern latitudes in 1998, 2002, and 2003 are evident in the CO residuals and are consistent with bottom-up estimates of biomass burning emissions (van der Werf et al. 2006). There may also be contributions to methane anomalies from wetlands.

An anomaly in the Arctic methane time series occurred in 2007 (Fig. 6.4). Atmospheric methane at polar northern latitudes (53°–90°N) increased 13.1±1.3 ppb in 2007, which is greater than the global average increase of 7.9±1.6 ppb (Dlugokencky et al. 2009). Since 2007, Arctic atmospheric methane has been increasing at about the global rate, ~6 ppb/y (2008–2013). The higher annual increase in 2007 in the Arctic, in comparison to the global value, suggests a contribution from Arctic sources, but the magnitude of changes in emissions and attribution to the Arctic region must be understood in the context of atmospheric transport, using a chemical transport model. Arctic emissions mix into a much shallower atmospheric boundary layer than tropical emissions, for example, so relatively large annual increases in Arctic atmospheric methane abundance do not necessarily mean the presence of correspondingly large

anomalies in Arctic source emissions (Bousquet et al. 2011). Bergamaschi et al. (2013) found that total methane emissions in the latitude zone 60°–90°N were ~2 Tg CH₄/y greater in 2007 than the average for 2000–2011, but slightly below the average for 2008–2011. Several other studies also found a small increase in Arctic emissions in 2007, consistent with the atmospheric observations (Bousquet et al. 2011; Bruhwiler et al. 2014b).

The Arctic is warming at about twice the global mean rate (see Ch. 1). It is also known that methane emissions from boreal wetlands were a major driver of increased atmospheric methane concentrations in the past (Ch. 3). Therefore, the potential for increased methane emissions from natural sources in the Arctic is an important consideration in evaluating recent changes in methane abundance. Based on measurements of carbon monoxide in the same samples that were measured for methane (Fig. 6.4), the increase in 2007 is not likely to have resulted from biomass burning. Other evidence suggests that changes in the rate of methane loss by reaction with hydroxyl radical (OH) are also not the cause (Dlugokencky et al. 2009). The most likely source contributing to the Arctic increase in 2007 is increased wetland emissions resulting from warmer and wetter than average conditions (Dlugokencky et al. 2009; see also Ch. 3). This scenario is consistent with isotopic measurements (see Sect. 6.6), which show a decrease in $^{13}C_{CH4}$ of methane consistent with wetland emissions. The continued increase since 2007 is likely to have resulted from methane-enriched air transported from lower latitudes, rather than increasing emissions in the Arctic.

Further evidence from the atmospheric observations, which indicates that methane emissions are not detectably increasing at the Arctic scale, is shown in Fig. 6.5, which shows the differences in annual mean methane abundance between northern polar (53°–90°N) and southern polar (53°–90°S) latitudes. From 1984 to 1991, the difference was increasing at 0.4±0.3 ppb/y. Beginning in 1992, a decrease in anthropogenic methane emissions from the former Soviet Union, estimated at 10.6 Tg CH₄/y (Dlugokencky et al. 2003), had a profound effect

Interpolar difference, ppb
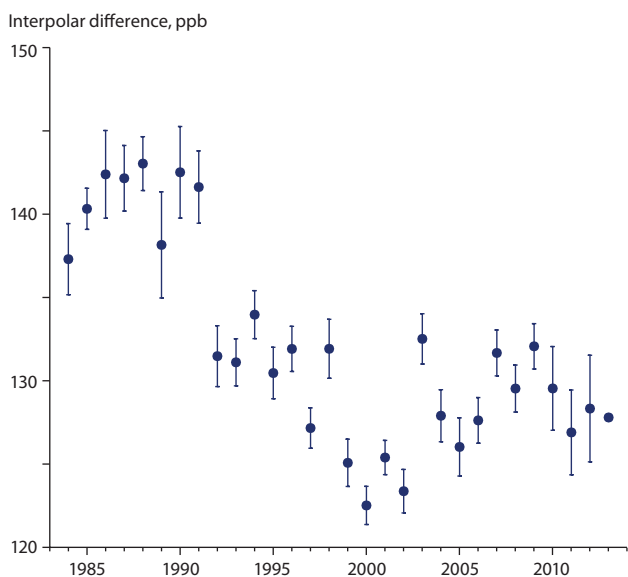
Fig. 6.5 Differences between observed northern polar (53°–90°N) and southern polar (53°–90°S) annual mean methane (CH₄) mole fractions as a function of time. Uncertainties on annual mean differences through 2012 are estimated with a Monte Carlo technique. All uncertainties are 68% confidence intervals.

on the interpolar difference (IPD). Starting in 1992, the trend in IPD reversed sign and was -0.1±0.1 ppb CH_4/y through to 2013. While the IPD varies interannually, it has not returned to the values observed in the late 1980s. Changes in the IPD can potentially provide a sensitive indicator of changes in Arctic methane emissions such as those that may result from changing anthropogenic activity, thawing permafrost, and destabilization of shallow methane hydrates in the marine environment.

6.4 Continuous methane measurements at Arctic locations

This section focusses on data from continuous hourly atmospheric methane measurements at Arctic observation sites to characterize the daily, seasonal and interannual variability in methane concentration. All measurements are directly traceable to the WMO Global Atmosphere Watch X2004 international scale maintained by the Central Calibration Laboratory at NOAA/ESRL in Boulder, Colorado (Dlugokencky et al. 2005).

6.4.1 Diurnal and day-to-day variability

Hourly measurements of methane abundance for 2012 at Inuvik (Canada), Tiksi (Russia) and Cherskii (Russia) – three regionally influenced sites – were chosen to illustrate the observed short-term variability at sites located in the proximity of extensive wetland regions (Fig. 6.6). Also plotted, for reference, are smoothed curves fitted to the methane weekly flask data from the remote background stations at Alert (Canada), Cold Bay (USA), Summit (Greenland) and Ny Ålesund (Norway). The smoothed seasonal cycles were obtained by applying the curve-fitting procedure of Nakazawa et al. (1997) and are included for qualitative comparison with the hourly measurements. Figure 6.6 also includes a magnified view for August 2012, further illustrating the large diurnal and day-to-day variability at regionally influenced sites.

In winter, the observed variability is linked primarily to atmospheric transport from anthropogenic source regions at lower latitudes because natural wetland emissions are lower during winter. Even at sites such as Alert (Canada), located thousands of kilometers from major source regions, the methane time series is frequently highly correlated with other anthropogenic source indicators such as carbon monoxide and black carbon (Worthy et al. 1994). This is particularly the case during well-defined winter episodes that last ~2 to 5 days in duration, and that result from synoptic meteorology, weak vertical mixing and rapid airmass transport originating from Siberian and/or European source regions (Worthy et al. 1994). The episodic events for Inuvik, Tiksi and Cherskii are particularly pronounced relative to events observed at Alert (not shown) due to their closer proximity to anthropogenic source regions. The magnitude of this variability is driven by regional emission strength, local vertical mixing and synoptic conditions.

In summer, short-term variability is much more apparent (relative to winter) and is dominated by diurnal variations. For diurnal variability to occur two conditions must be met: a local flux in methane and physical mixing of the boundary layer that is diurnal. Under strong solar heating during the
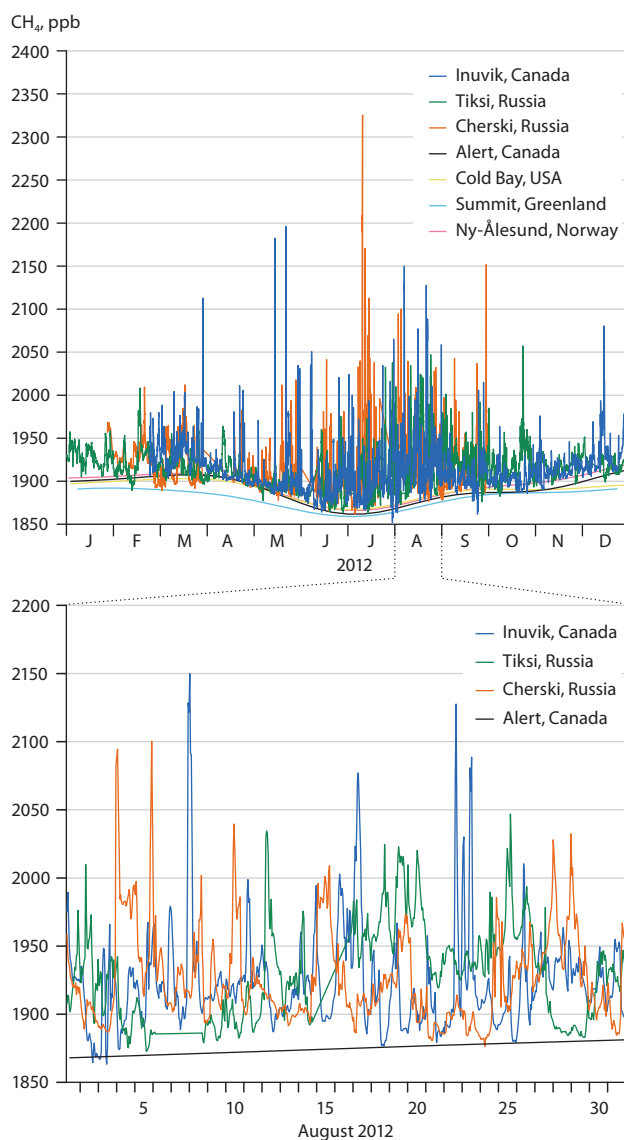
Fig. 6.6 Example of short-term variability in methane abundance at three regionally-influenced sites in the proximity of extensive wetland regions within the Arctic through 2012: Inuvik (Canada), Tiksi (Russia) and Cherski (Russia). Also shown are smooth curves fitted to the methane weekly flask data from four remote background sites: Alert (Canada), Cold Bay (USA), Summit (Greenland) and Ny-Ålesund (Norway). The lower plot shows a magnified window of hourly abundance for August, 2012.

day, the near-surface mixed layer is unstable and generally well mixed throughout the boundary layer. At night, the radiation loss at ground level leads to a cooling of the atmosphere at the surface giving rise to a shallow, stable layer, also known as an inversion. The increase in atmospheric methane during the night is a result of suppressed vertical mixing under this inversion. The magnitude of the nocturnal increase is variable and depends on the depth of the nocturnal inversion and on the regional methane source strength. Owing to enhanced vertical mixing during the day, methane is diluted through the rise of the boundary layer height up to a hundreds of meters or more. In addition, there are also underlying large-scale influences including the regional transport of air masses carrying both anthropogenic and wetland emissions. For example, the hourly data record for Cherskii (Russia) in Fig. 6.6, shows atmospheric methane levels of around 1875 ppb for a three-day period (20–23 August), followed by concentrations greater than 1900 ppb from 24–29 August. Variability of a similar magnitude is evident throughout the monthly time series.
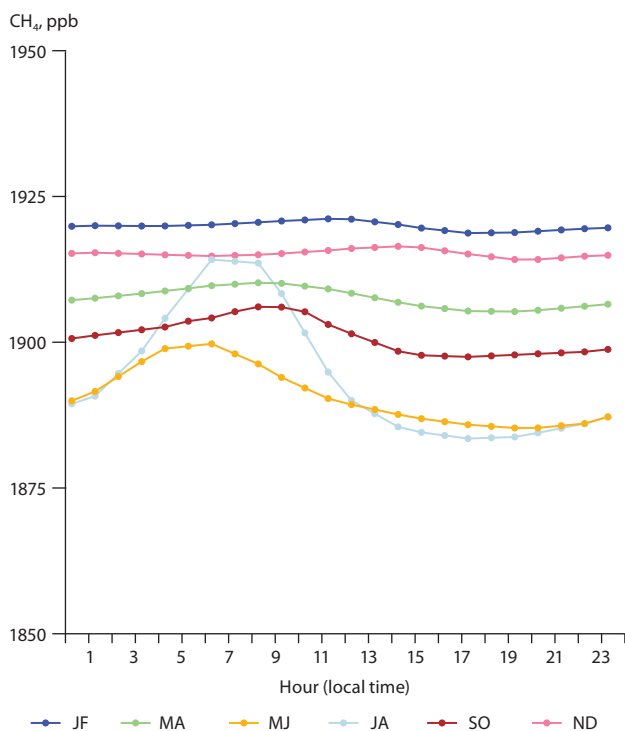
Fig. 6.7 Average diurnal methane cycle at Behchoko (Canada; 62°48'N, 116°93'W) for January/February (JF), March/April (MA), May/June (MJ), July/August (JA), September/October (SO) and November/December (ND), determined from hourly-averaged data from 2011 to 2013.

Fig. 6.8 Mean monthly amplitude of the diurnal signal (daily hourly maximum minus same-day hourly minimum), determined from hourly averaged data from 2011 to 2013.

Average diurnal variability throughout the year at Behchoko (Canada) on the northwest tip of Great Slave Lake (see Fig. 6.1) and approximately 80 km northwest of Yellowknife in Canada's Northwest Territories, is shown in Fig. 6.7. The region surrounding Behchoko comprises steep, wooded hills interspersed with numerous lakes and ponds. The mean diurnal methane cycle is shown for two-month average intervals, determined from hourly average data from 2011 to 2013. The average diurnal cycle at Behchoko is strongly seasonally dependent: hardly apparent during winter, beginning to develop in late spring (May/June), reaching a maximum in August when wetland emissions are expected to be elevated, and weakening again in autumn. In summer, methane abundance peaks at around 0600 to 0800 local standard time (LST), owing to methane build-up during the nighttime inversion and then decreases rapidly to reach a minimum at around 1600 to 1800 LST as the boundary layer expands and mixes. As shown in Fig. 6.6, there can be substantial variability in the diurnal cycle from day-to-day. The patterns observed at Behchoko (Canada) are very similar to the diurnal cycle observed at other regionally influenced sites (see Fig. 6.8).

Figure 6.8 shows the amplitude of the diurnal cycle using all available hourly data between 2011 and 2013 for sites listed in Table 6.1, which includes remote background and regionally influenced sites. Also shown, for contrast, are the amplitudes of the diurnal cycle for two lower latitude Canadian sites (Fraserdale and East Trout Lake) located near major natural sources. Fraserdale (49°53'N, 81°34'W) is located on the southern perimeter of the Hudson Bay Lowland (HBL) region, and on the northern edge of the boreal forest. The HBL comprises about 10% of the total area of northern wetlands, and recent studies have estimated the average methane release from the HBL to be ~2 Tg CH_4/y (Pickett-Heaps et al. 2011; Miller
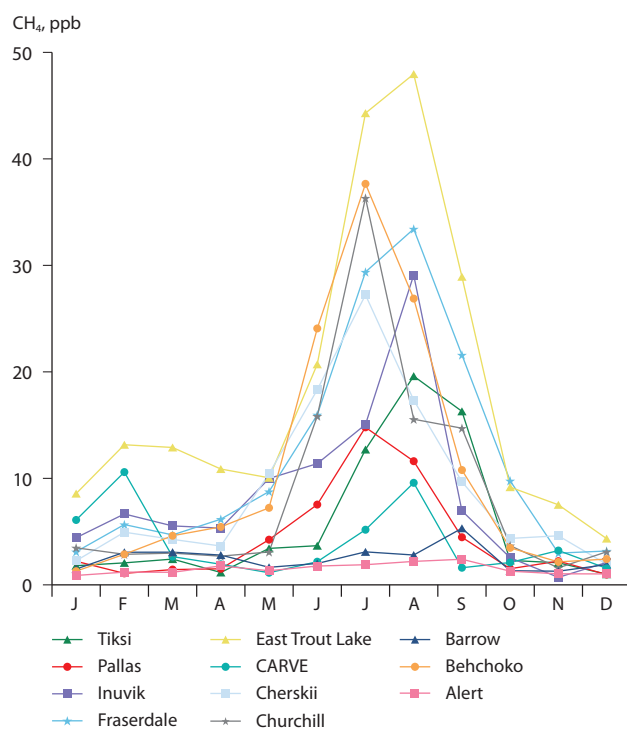
et al. 2014). East Trout Lake (54.3°N, 105.0°W) is located in a boreal forest region in western Canada. The terrain contains extensive areas of impeded drainage. Average methane release in summer from wetland regions in western and eastern Canada is similar in magnitude, with estimated fluxes ranging from 20 to 30 mg/m²/day in July and August (Miller et al. 2014).

From November to April, there is very little diurnal variability observed at any site, although there is detectable daily variability (see winter periods in Fig. 6.6). As already noted, much of the daily variability in methane concentration in winter is likely to be due to transport to these sites from anthropogenic source regions at lower latitudes. Diurnal signals are not apparent at any time of the year at the remote background sites of Barrow (USA) and Alert (Canada), strongly indicating either a lack of nearby wetland sources or weak diurnal physical mixing of the boundary layer. In spring and probably soon after the snow melts, nighttime increases in atmospheric methane concentration increase noticeably due to the thawing of the surface soil layer and the subsequent start of wetland activity. Diurnal signals at the regionally influenced sites are greatest in July/August, owing to the probable maximum of wetland methane fluxes at this time of year and the accumulation of methane into a shallower inversion layer at night. The CARVE, Alaska site (64.99°N, 147.60°W) shows the smallest diurnal amplitude, at around 10 ppb. This may be due to relatively low wetland emissions for this region in 2012, but only one year of atmospheric data is currently available. A complicating factor is that the CARVE tower is located on a ridge, several hundred meters higher than its surrounding, and as a result will be less sensitive to local-scale emissions and likely weaker diurnal physical mixing of the boundary layer. For the Arctic located sites, Pallas (Finland) and Behchoko (Canada) show the largest mean diurnal amplitudes, at around 30 ppb.

The diurnal signals start to decrease significantly in September/October, which may be a result of decreased wetland activity, coupled in timing with declining air temperature and thus weaker diurnal physical mixing of the boundary layer and the freezing of the surface soil layer. In High Arctic areas this time of year has been shown, in some years, to coincide with an outburst of methane from wetlands (Mastepanov et al. 2008, 2013), but this phenomenon has not been observed at lower latitudes. At the more southerly sites of Fraserdale and East Trout Lake (Canada), the diurnal signals extend further into autumn, possibly owing to a slightly longer influence from wetland sources (Kuhlmann et al. 1998).

Generally, atmospheric methane measurements at the regionally influenced sites reflect a complex mix of air mass transport from natural and anthropogenic sources, as well as an interaction between the daily cycling of the wetland flux and the vertical mixing dynamics in the atmospheric boundary layer. This is particularly evident during summer when atmospheric methane levels are highly influenced by local and regional wetland emissions and when diurnal cycles are strongest.

6.4.2 Seasonal and interannual variability

From the preceding discussion, it is clear that nighttime methane measurements at sites that observe diurnal signals are not representative of a large, well-mixed volume of the lower troposphere. As a result, nighttime measurements should not be included in the calculation of mean seasonal cycles and trends in methane concentration at regionally influenced sites. Excluding nighttime data is even more important when comparing the mean annual methane cycle at these sites with that at remote background sites. Thus, at the regionally influenced sites, measurements made during the late afternoon (1600 to 1800 LST) – when convective mixing is well developed – are most representative of large spatial scales.

Figure 6.9 compares annual methane cycles at six remote background sites with annual methane cycles at six regionally influenced sites. The characteristics observed during the two-year period are relatively consistent at each of the remote background sites, showing an annual methane cycle with an amplitude of about 55 ppb from the minimum observed in July/August to the maximum observed in February. This is likely to have been driven by the seasonality of methane emissions and sinks in combination with a seasonally variable meridional atmospheric circulation pattern. The high methane levels observed at the remote background sites in winter are due to a negligible OH sink and contributions from long-range transport of polluted air containing methane from anthropogenic emissions at lower latitudes. During spring, methane levels begin to fall due to an increasing OH sink and dilution of northern air masses with air from lower latitudes and aloft containing lower methane concentrations. During summer, the global tropospheric OH sink is strongest, resulting in a minimum in the annual methane cycle in July. By late mid-summer, methane levels begin to increase as the effectiveness of the OH sink decreases and air masses arrive from lower latitudes containing methane from both wetland and anthropogenic emissions. The timing of the annual minimum at the remote background sites can vary from year to year by as much as six weeks, probably due to interannual variability in methane emissions from northern wetlands (Mastepanov et al. 2013).
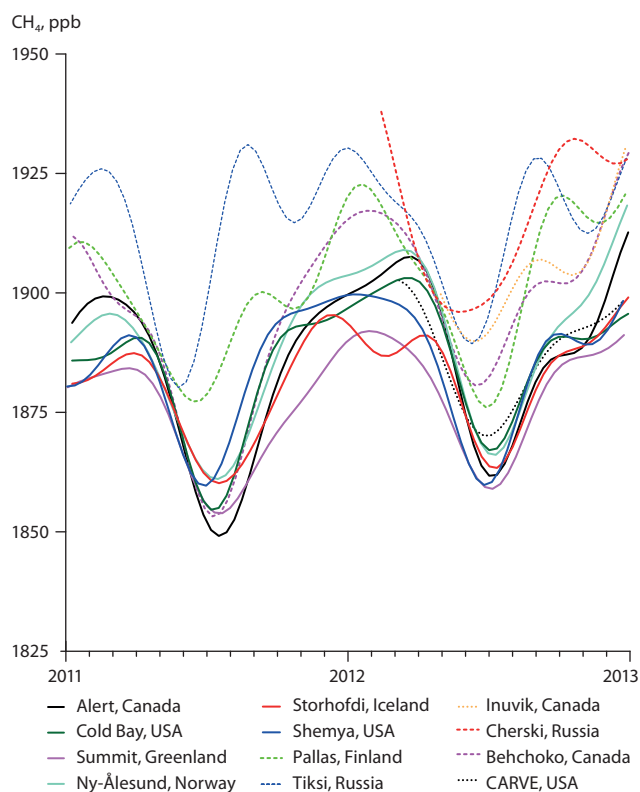
Fig. 6.9 Smoothed seasonal cycles of atmospheric methane concentration for six remote background sites (solid curves) and six regionally influenced sites (dashed curves) through 2011 and 2012. The smoothed seasonal cycles were derived from the digital filter technique of Nakazawa et al. (1997) using weekly discrete air samples for the remote background sites and afternoon hourly-averaged data (1600, 1700 and 1800 LST) for the regionally influenced sites.

The annual methane cycle at the six regionally influenced sites also shows a maximum during winter, but slightly elevated (except for the CARVE site, Alaska) relative to the remote sites, probably due to their closer proximity to anthropogenic source regions. An additional feature in the annual methane cycle of the regionally influenced sites (except for the CARVE site, Alaska), is the presence of a distinct secondary peak in late summer. The magnitude of this secondary peak at these sites relative to the suite of remote background sites varies from site to site and from year to year. Data from the more southerly site at Fraserdale (Ontario, Canada; Worthy et al. 1998) also show a similar secondary peak in summer. This has been shown to be the result of advection of air with enhanced methane levels due to emissions from the extensive wetlands north of Fraserdale, in the Hudson Bay Lowland region, which is a well-documented source of methane (Roulet et al. 1994). It is reasonable to conclude, considering the timing of the summer divergence that the secondary peak observed in mid-summer is predominantly due to the regional influence of wetland emissions. Year-to-year variability in the offset of the regionally influenced sites relative to the remote background sites is probably due to the seasonality in regional wetland methane emissions, atmospheric transport and boundary layer depth.

6.4.3 Trajectory cluster analysis

The observed rise and fall of methane concentrations in the lower atmosphere reflects the transport of methane over long distances, resulting from winds and mixing that take place in the atmosphere. It is possible to infer the magnitude of
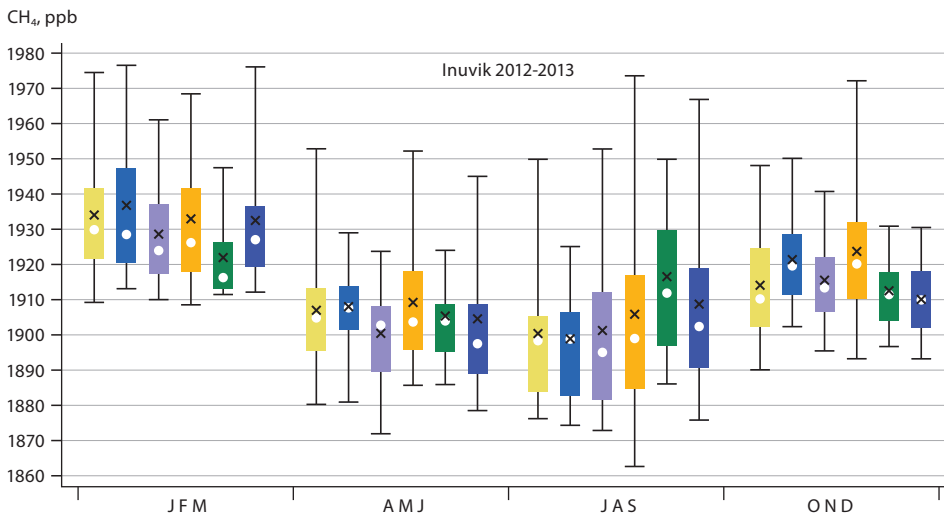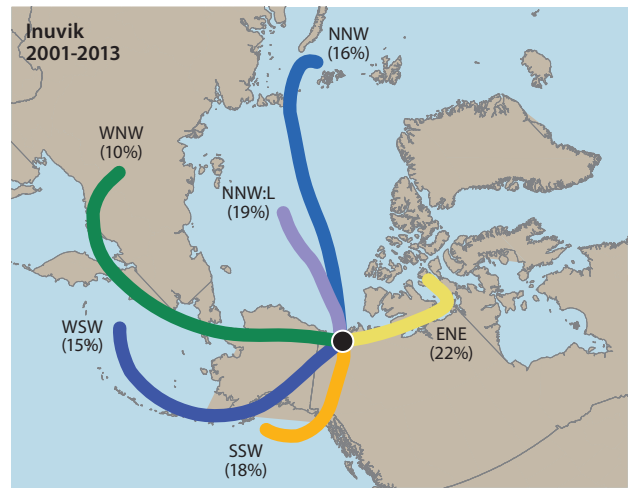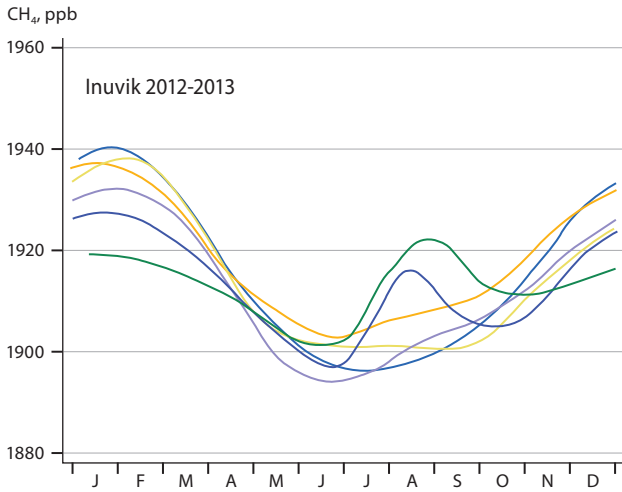
Fig. 6.10 Trajectory analysis and the associated variability in methane concentrations by cluster for Inuvik, Canada. The graphic shows the six cluster means (upper right), trajectory probability density maps (lower plots), the associated annual variations (upper left), and seasonal box-and-whisker methane plots by trajectory clusters (left). Seasonal breakdowns: January/February/March (JFM), April/May/June (AMJ), July/August/September (JAS) and October/November/December (OND).
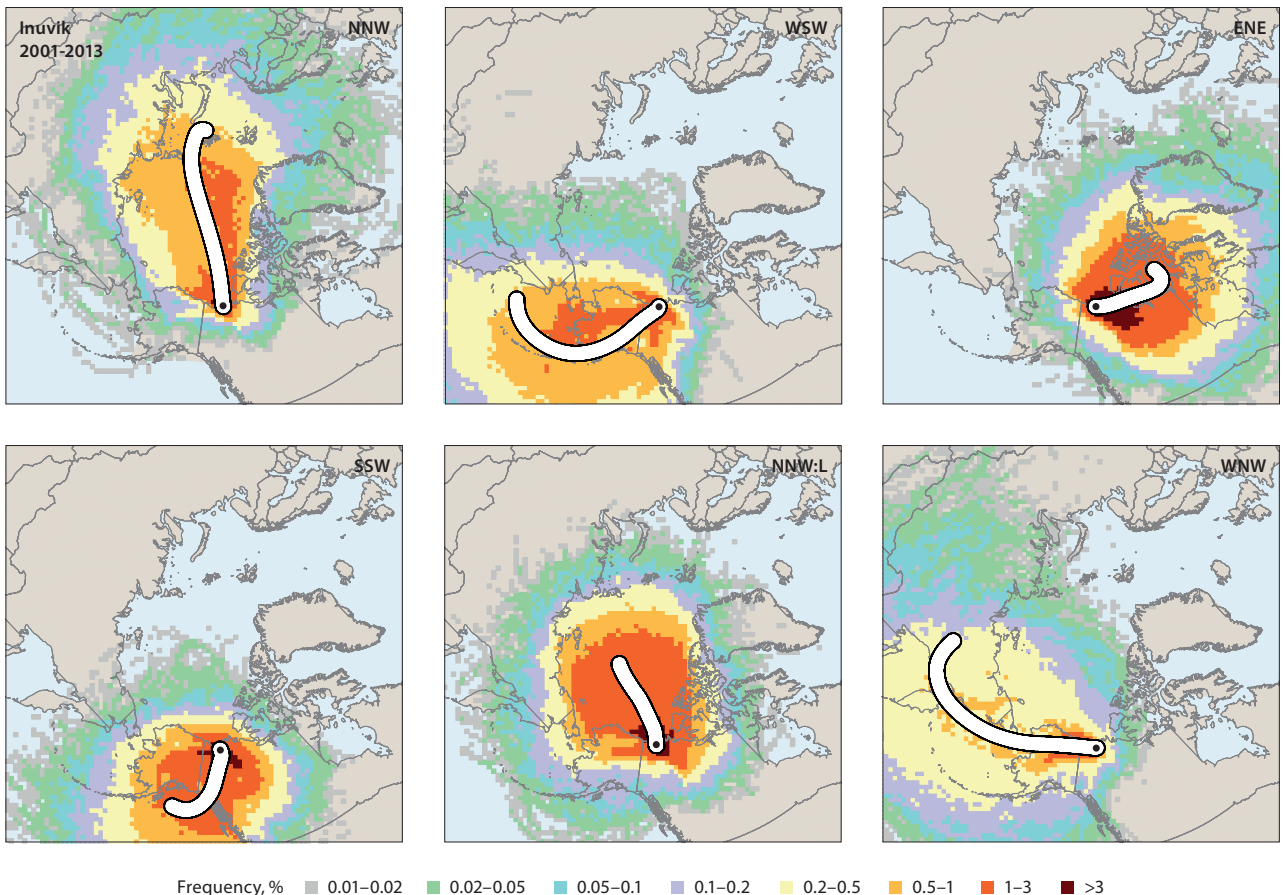
sources from observed atmospheric concentrations using atmospheric transport models, if the monitoring network is sufficiently dense. With the increase in Arctic monitoring of methane over the past few years, it is possible to start to identify the regions which contribute most strongly to atmospheric concentrations observed at these sites. The next step is to scale up this information to estimate source strength for a given spatial area, however, that requires a full atmospheric transport modelling approach and is explored in more detail in Ch. 7. The analysis presented here provides the context for that investigation.

Temporal variability in synoptic weather patterns leads to specific regional-scale transport pathways that can significantly affect concentrations over downwind locations. The magnitude of this effect depends upon the magnitude of upwind emissions and the rate of transport of the air mass. Several techniques have been used to study how atmospheric concentrations differ with transport path, but the majority of approaches tend to utilize back-trajectories to characterize the transport. Overall, more meaningful conclusions can be drawn when atmospheric concentrations are examined in relation to ensembles or large groupings of trajectories, as opposed to individual trajectories. Here, a trajectory cluster analysis has been applied to nine Arctic monitoring sites with continuous hourly-averaged data, to determine which upwind areas tend to lead to higher and/or lower observed methane concentrations. These regions can then be examined for their correspondence to known natural or anthropogenic methane sources present in these regions.

The type of trajectory cluster analysis used here has also been used in other studies to create ensembles of trajectories or 'trajectory clusters' with common transport pathways (Dorling and Davies 1992; Dorling et al. 1992; Chan and Vet 2010). The ensembles or clusters determined through this approach reflect typical meteorological patterns in the area around the receptor sites. Six different clusters were determined to be sufficient to differentiate the main transport patterns.

A detailed example of the trajectory cluster analysis for Inuvik (Canada), a regionally-influenced site in the proximity of extensive wetland regions, is shown in Fig. 6.10. The annual methane cycles at Inuvik were examined according to the six main transport pathways (see upper left plot of Figure 6.10). The methane observations at Inuvik are linked with source regions covering air flow up to ten days back in time (the six upper right panels). Clear evidence of a secondary summer peak is observed from the western (WNW and WSW) clusters where transport over known wetland regions has occurred. In contrast, for the clusters originating from the Arctic Ocean to the north and north-east (NNW and ENE), secondary peaks in the annual methane cycle are much less obvious, clearly showing the impact of methane emissions from wetlands in the region. The centre panel of Fig. 6.10 shows the four seasonal box-and-whisker methane plots for the Inuvik site. This provides a measure of the variability observed by cluster and by season.

Figure 6.11 shows the mean annual methane cycle according to transport pathways for the other eight sites included in the analysis. The method used is to establish climatologically, the synoptic flow patterns associated with these sites. The

endpoint for the vectors shown represents the mean upwind distance ten days back in time. Shorter vectors thus indicate slower travel speed and possible stagnation along the path while longer vectors are related to stronger wind speeds. The percentage of trajectories for a given cluster is shown on the endpoint of the mean vector. The direction labelled with 'L' represents a lighter (slower) transport speed relative to the other cluster from the same direction. Similar to Inuvik (Canada), the sites exhibit various magnitudes in the summer secondary peak, contingent on transport direction. Barrow (Alaska, USA) shows a small enhancement in summer methane concentration for air masses originating from the SSW and SSE sectors, relative to the ocean clusters to the north. At Behchoko (Canada), enhancements are found from the two western clusters while at Churchill (Canada) more obvious enhancements in summer methane concentration are associated when air masses originate from the WNW, WNW:L and WNW:L2 clusters. Slightly further south in central Alaska, the CARVE site shows some evidence of a summer peak from the WNW and WNW:L clusters, but these are not nearly as pronounced as those observed at the other high latitude North American sites (such as Churchill).

On the other side of the Arctic landmass, the clustered annual methane concentrations at Tiksi and Cherskii (Russia) also show distinctly different annual cycles associated with the transport of air masses originating from land clusters relative to ocean clusters. The amplitude of the summer peak for land clusters is more pronounced at these two sites than that observed at any of the North American sites, possibly suggesting a closer proximity to more extensive wetland emission sources. In contrast, sites located far from wetland sources (i.e. Alert, Canada) do not appear to show secondary summer peaks associated with any transport direction.

At Pallas (Finland), methane concentrations originating from the south are significantly enhanced throughout the year compared to other transport directions. This is likely to be due to the transport of methane from both anthropogenic and wetland emission sources in the mid-latitudes.

6.5 Methane measurements at Tiksi on the coast of the Laptev Sea

Observations of methane concentration at Tiksi (Russia) were initiated in July 2010 to aid in understanding terrestrial emissions from the Siberian tundra and marine emissions from the shallow Laptev and East Siberian Seas, which are known for methane hydrate deposits in the seabed and oversaturated seawater methane concentrations (Shakhova et al. 2010). The Tiksi monitoring station is operated by the Yakutian hydrometeorological service, and measurements are conducted through co-operation between the Finnish Meteorological Institute, the US National Oceanic and Atmospheric Administration, the Arctic and Antarctic Research Institute and the Voeikov Main Geophysical Observatory (St. Petersburg). The city of Tiksi (about 5000 inhabitants) is located on the coast of the Laptev Sea and within several hundred kilometers of both the Lena River and an extensive wetland area (~300,000 km^2). The city is approximately 5 km north of the measurement location.
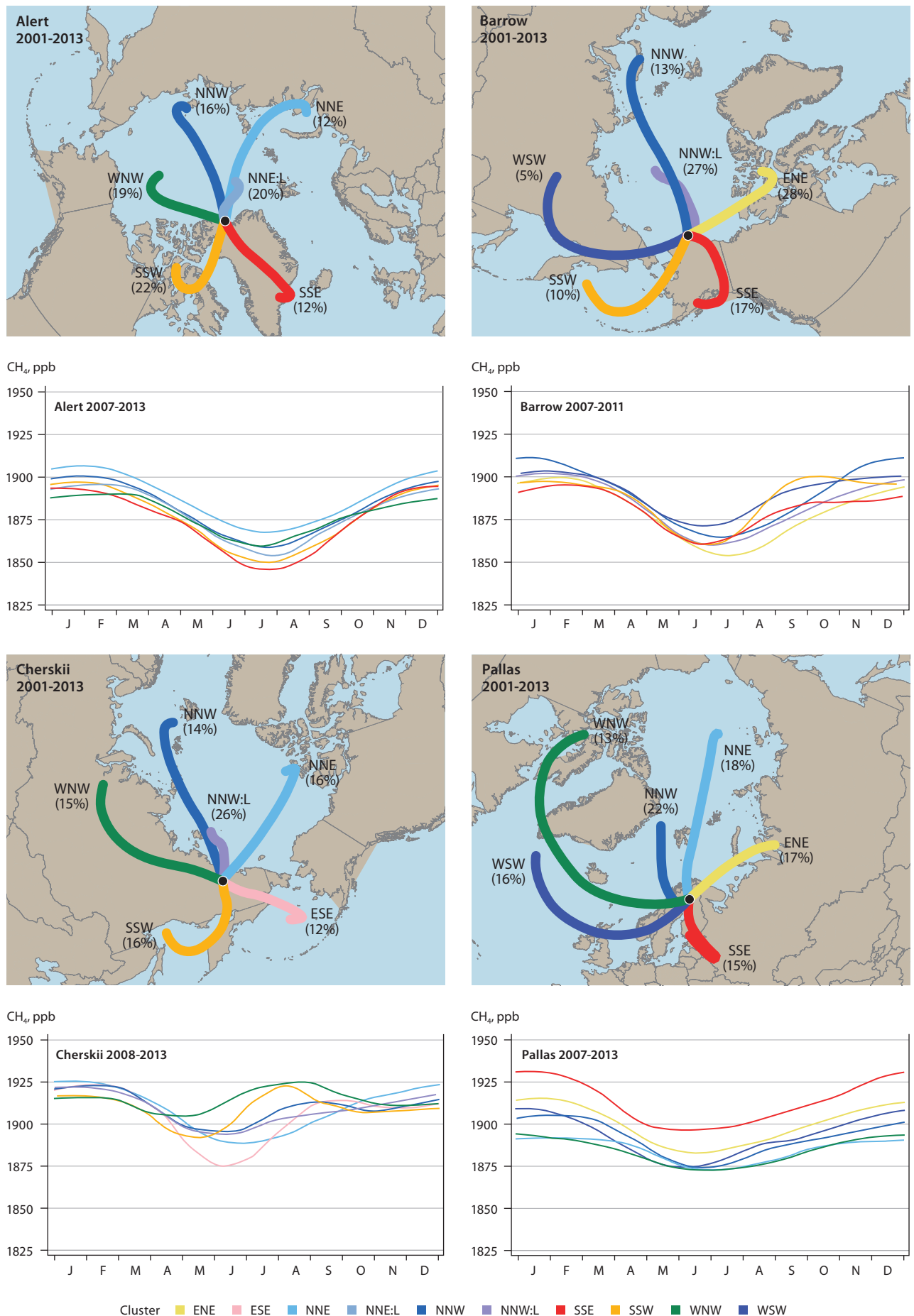
Fig. 6.11 Trajectory cluster mean vectors at eight high-latitude sites with continuous methane measurements. Six trajectory clusters were sorted by the k-means clustering technique similar to that of Chan and Vet (2010) using Euclidean distance as the dissimilarity metric on 10-day air parcel backward trajectories from 2001 through 2013 for all sites.

CH$_4$, ppb   Top soil, °C

Tiksi 2012

CH$_4$, ppb   **Tiksi July–September 2012**
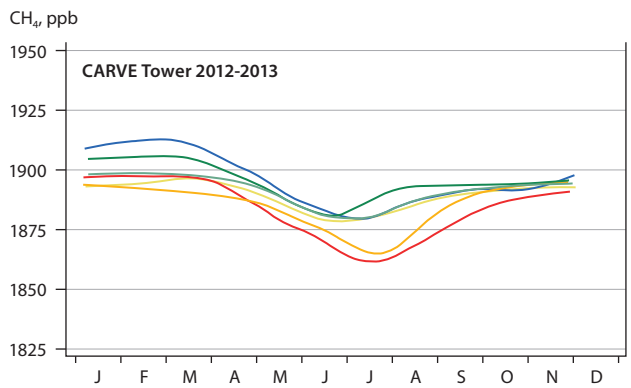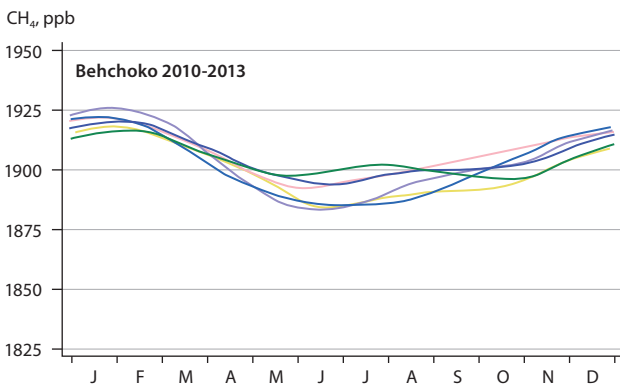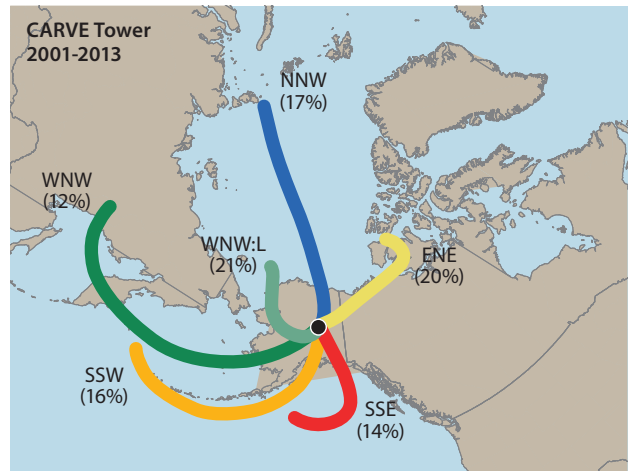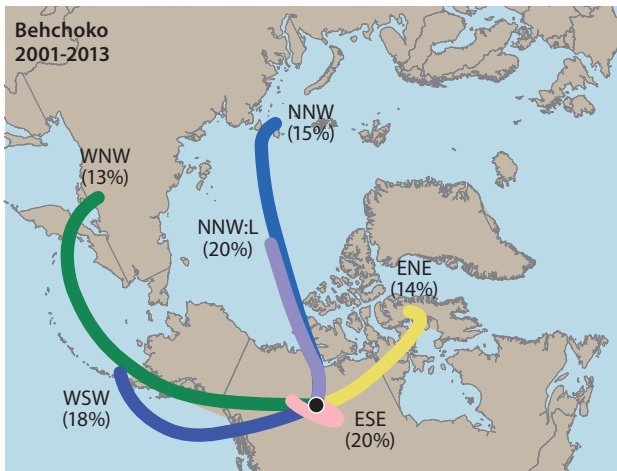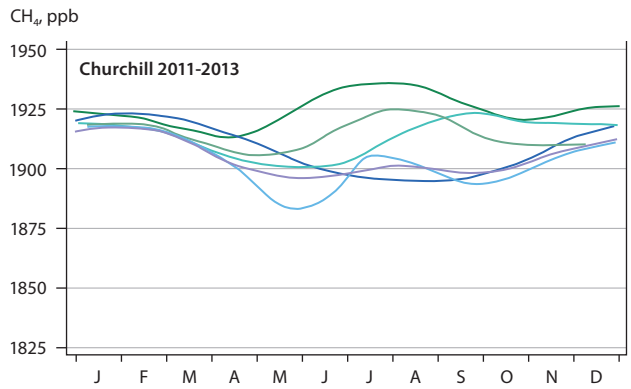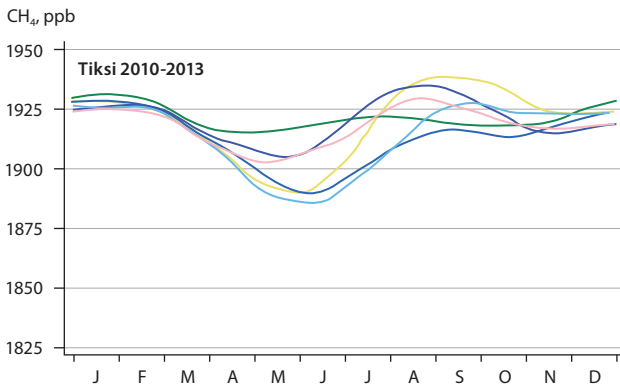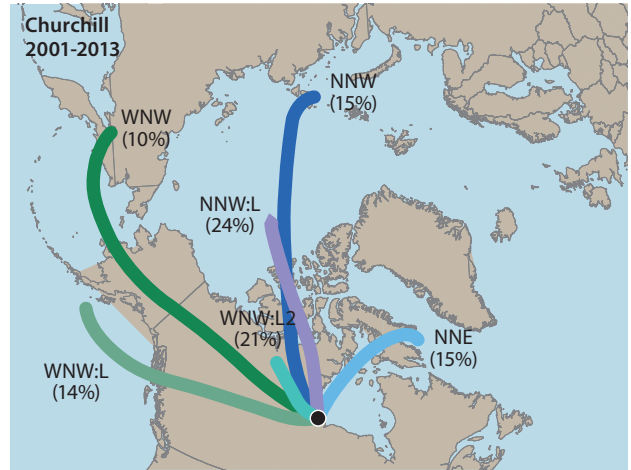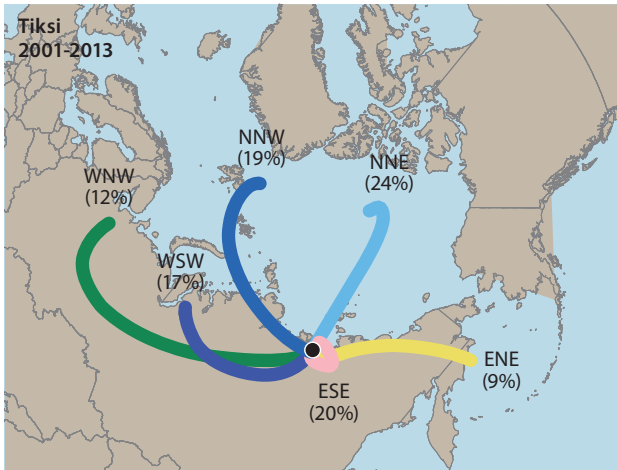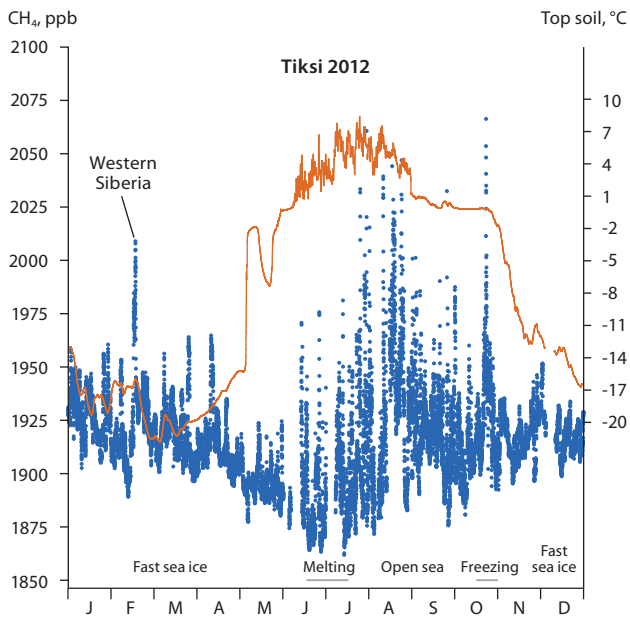
Fig. 6.12 Half-hourly averaged methane concentrations at the Tiksi monitoring station (Russia) on the Laptev Sea coast through 2012. Surface soil (5cm) temperature and sea-ice conditions for the Laptev Sea ice are also shown.

Fig. 6.13 Half-hourly averaged methane concentrations (July–September 2012) relative to wind direction at the Tiksi monitoring station (Russia) on the Laptev Sea coast. Observations are only included if wind speed is greater than 3 m/s, because wind direction is not well developed when wind speed is low.

The annual cycle of atmospheric methane (see also Sect. 6.4.2) reflects winter emissions from industrial sources in the western and southern parts of Siberia. In summer, the Laptev Sea is ice-free from early July to mid-October, indicating the potential presence of marine methane emissions. This is roughly the same period as when the terrestrial surface active layer in the tundra has thawed and methane production takes place. Elevated methane concentrations during this period are apparent (Fig. 6.12). Methane increased during calm nights, indicative of local tundra emissions (and this was confirmed by the micrometeorological method – not shown). On average, ambient methane levels at Tiksi are higher than at other High Arctic sites because of extensive Siberian wetland emissions and often limited vertical mixing in the stable shallow atmospheric boundary layer.

To evaluate the potential emission intensity around the Tiksi site, half-hourly average methane concentrations were plotted relative to wind direction during the main open water period for the Laptev Sea and the terrestrial active season (Fig. 6.13). Methane concentrations (when low wind speed cases are excluded) were between 1870 ppb (background level) and 2050 ppb (the highest concentration). As a generalization, methane concentrations did not appear to reflect wind direction. The lack of elevated concentrations when winds are from the south and southwest sectors may be because uplands and the Verhoyansk Mountains are in that direction. The highest concentrations observed when the wind direction was from the Laptev Sea sector were relatively modest, which does not indicate extensive emissions in that area. Concentrations were slightly elevated when winds were from the eastern sector, where widespread coastal wetlands occur. Trajectory analysis (see Sect. 6.4.3; Fig. 6.11) also confirms elevated concentrations when air masses originate from the east.
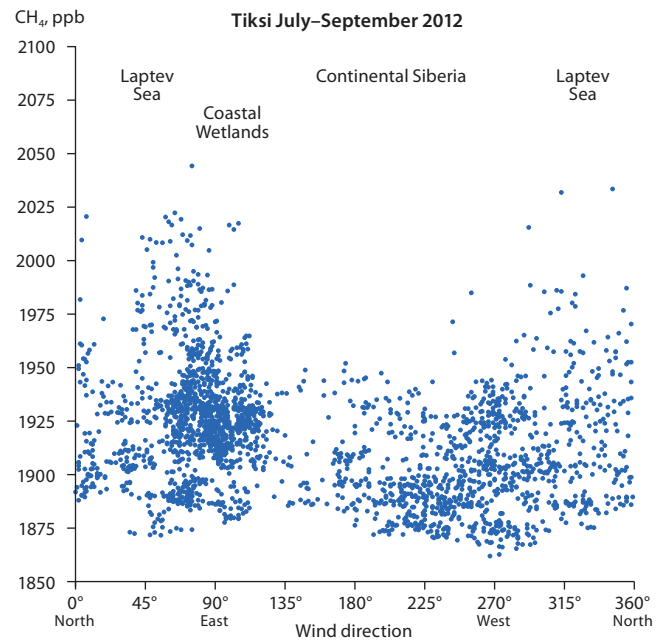
6.6 Isotopic measurements

Atmospheric monitoring of methane isotopes – primarily $\delta^{13}C_{CH4}$ – in ambient air, coupled with trajectory analysis, can help distinguish the contribution of specific source types to atmospheric methane concentrations. For reference, background ambient air has a $\delta^{13}C_{CH4}$ value of around -47.3‰ in the northern hemisphere and -46.9‰ south of the Inter-Tropical Convergence Zone. Deviations from the background level can be used to identify sources of methane present in Arctic air, which can be either enriched or depleted in ^{13}C depending on the formation process. Different sources of carbon have different signatures of ^{13}C, which are often referred to as isotopic fingerprints (Table 6.2). Biogenic sources are relatively depleted in ^{13}C (also referred to as 'light'), and thermogenic sources are relatively enriched in ^{13}C (also referred to as 'heavy'), in comparison to background air. For example, wetlands emit methane with $\delta^{13}C_{CH4}$ around -70±5‰, depending on location, meteorology and local species composition in the wetlands (e.g. dominance of *Eriophorum* cottongrass or *Sphagnum* mosses), while methane from gas exploration emits methane with $\delta^{13}C_{CH4}$ from -35±10‰ to -55±10‰ depending on the reservoir. Methane from biomass burning can also have a large impact as this source is quite 'heavy', $\delta^{13}C_{CH4}$ about -28‰, relative to other sources.

6.6.1 Available data

Routine monitoring of $\delta^{13}C_{CH4}$ to high precision (around 0.04–0.07‰) is taking place at Cold Bay (Alaska; 55.2°N, 162.7°W), Barrow (Alaska; 71.3°N, 156.6°W), Alert (Nunavut, Canada; 82.4°N, 62.5°W), Ny Ålesund (Svalbard, Norway; 78.9°N, 11.9°E), Pallas (Finland; 68.0°N, 24.1°E) and Kjolnes (Norway; 70.5°N, 29.1°E). Measurements at these stations sample the marine boundary layer except for Pallas, where the samples are inland from central northern Scandinavia. Samples are collected

Table 6.2 $^{13}C_{CH4}$ Isotopic ratios for Arctic methane sources. Based on Dlugokencky et al. (2011), Fisher at el. (2011), Sriskantharajah et al. (2012), Nisbet (2001), Walter et al. (2006), Kirschke et al. (2013) and unpublished data supplied by Royal Holloway, University of London (RHUL) and Environment Canada.

Source	$\delta^{13}C_{CH4}$ ‰
Coal and industry, Europe	-35 ± 10
Natural gas, UK North Sea	-35 ± 5
Natural gas, Siberia (exported to EU)	-50 ± 5
Natural gas, Alberta/BC	-55 ± 10
Ruminants, C4 diet	-50 ± 5
Ruminants, C3 diet	-70 ± 5
Arctic wetlands, Finland	-70 ± 5
Boreal wetlands, Canada	-65 ± 5
Biomass burning, boreal vegetation	-28 ± 2
Landfills, Europe	-57 ± 4
Thermokarst lakes	-58 to -83
Hydrates, Arctic	-55 ± 10

weekly or twice weekly at Cold Bay, Barrow, Alert, Ny Ålesund and Pallas, and are analyzed at the University of Colorado by INSTAAR (Institute of Arctic and Alpine Research) for NOAA.

Royal Holloway, University of London (RHUL) also analyzes samples from Ny Ålesund (daily Mon-Fri); Alert (weekly), Pallas (weekly) and Kjolnes (weekly). Results for Alert and Ny Ålesund (unpublished) analyzed by RHUL are closely comparable to the INSTAAR data and show the same amplitude of the seasonal cycle, which provides confidence that observations from different sites and laboratories can be combined to investigate pan-Arctic characteristics.

In addition to the in situ data, aircraft data are also available. The UK MAMM project (Methane and other greenhouse gases in the Arctic – measurements, process studies and modelling)

supports flights from Sweden to Spitzbergen, collecting air at various altitudes along the flight path. In particular, the aircraft searches for air masses that have come from northern European Russia and northern Siberia, as well as occasionally sampling air that in part has come from the east Siberian Arctic shelf. Trajectory analysis is used prospectively and retrospectively to identify source regions for the sampled air. Other aircraft data include those from the NOAA/ESRL Cooperative Network sites, as well as survey flights undertaken as part of the NASA Carbon in Arctic Reservoirs Vulnerability Experiment (CARVE) http://science.nasa.gov/missions/carve/.

6.6.2 Annual cycle

There is clear seasonality in $\delta^{13}C_{CH4}$ in the Arctic, and this is apparent in Figs. 6.14 and 6.15 which show the NOAA/INSTAAR high precision $\delta^{13}C_{CH4}$ measurements for 2000–2012 at four Arctic monitoring stations. An additional non-Arctic measurement site (Mace Head, Ireland) is included for reference. Isotopic measurements become 'heavier' (less negative) in winter, peaking around the time of the spring melt, and then, after melting, shifting to become significantly 'lighter' (more negative) in summer, to reach a minimum $\delta^{13}C_{CH4}$ in autumn. The amplitude of the seasonal $\delta^{13}C_{CH4}$ cycle appears to have increased over time, and in recent years is of the order of 1‰ or more. Globally, the seasonality in $\delta^{13}C_{CH4}$ increases with latitude and is most pronounced in the Arctic, where the OH sink is limited, especially in winter.

The seasonality of $\delta^{13}C_{CH4}$ is systematically offset (i.e. out of sync) from the seasonality in methane concentration, which peaks in late autumn or early winter, some months before the isotopic peak. Concentration minima typically occur in June or July. This offset between atmospheric methane concentration and the isotopic cycle suggests that there is a major 'light' (i.e. biogenic) source that inputs methane to Arctic air from July to October. Another factor that influences the cyclicity, both in methane concentration and isotope fractions, is atmospheric mixing
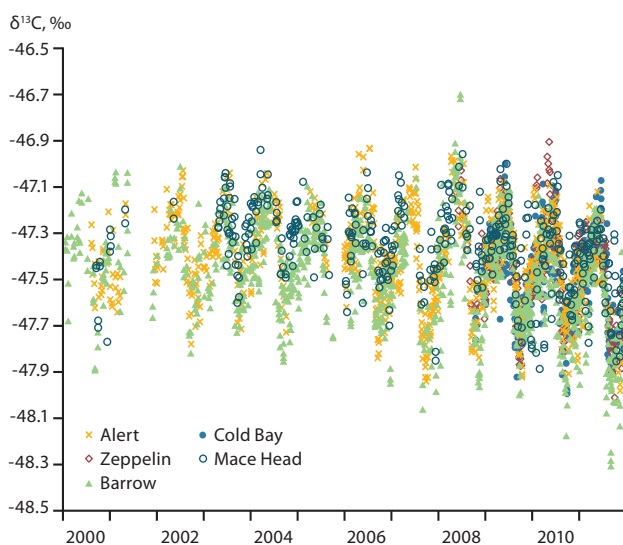
Fig. 6.14 Multi-site NOAA/INSTAAR high precision $\delta^{13}C_{CH4}$ measurements for 2000 through 2012 at the following monitoring stations: Cold Bay (USA), Barrow (USA), Alert (Canada), Ny Ålesund/ Zeppelin (Norway) and Mace Head (Ireland).
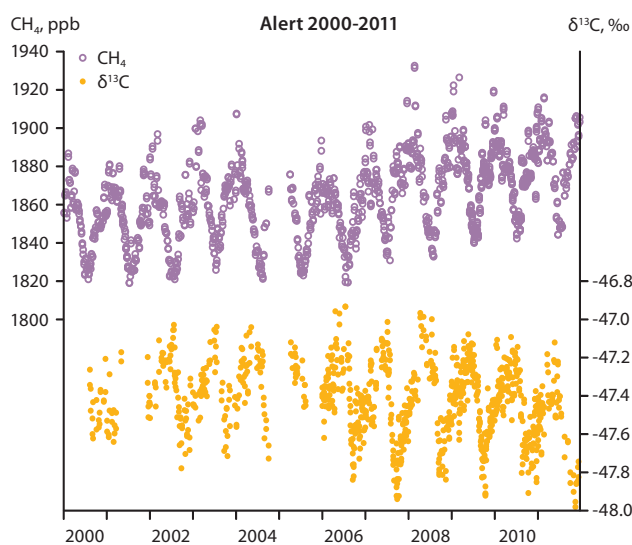
Fig. 6.15 Detail of Arctic NOAA/INSTAAR results from Alert (Canada): (upper) methane concentrations and (lower) methane isotope ($\delta^{13}C_{CH4}$) record.

with background Atlantic and Pacific air from lower latitudes. This may contribute to the concentration decline in spring, OH destruction, which in May-July will reduce concentrations and drive $\delta^{13}C_{CH4}$ 'heavier'. Also stratospheric inputs via episodes of polar vortices, may similarly reduce methane concentration and drive an increase in $\delta^{13}C_{CH4}$, especially in winter.

6.6.3 Identification of Arctic methane sources

Fisher et al. (2011) found that the bulk Arctic methane source signature for air arriving at Spitzbergen in late summer 2008 and 2009 was about $\delta^{13}C_{CH4}$ -68‰. The source signature of methane in these samples had $\delta^{13}C_{CH4}$ -68.6±4.5‰ in July 2009 and $\delta^{13}C_{CH4}$ -68.7±4.4‰ in October 2010. Air sampled daily at Ny Ålesund in September–October 2009 had a source signature of $\delta^{13}C_{CH4}$ -67.4±3.1‰. Recent unpublished work by RHUL in collaboration with the Norwegian Institute for Atmospheric Research and with the MAMM project showed very similar results, which clearly reflect an Arctic wetland source (see Table 6.2). In contrast, also at the Ny Ålesund station, Fisher et al. (2011) found that in March to May 2009 (when wetlands are frozen), the small Arctic springtime source, calculated from measurements in air samples collected daily, was $\delta^{13}C_{CH4}$ -52.6±6.4‰. Although the precision of this determination is poor, this bulk Arctic source signature closely matches Russian Arctic gas supplies (Dlugokencky et al. 2011) (see Table 6.2). Stratospheric air measured over Finland (RHUL, unpubl.) may also contribute to the decline in mixing ratios during spring while $\delta^{13}C_{CH4}$ increases. More recent studies by RHUL, including airplane transects, have confirmed both the spring and high summer findings of Fisher et al. (2011).

The isotopic results to date, imply that methane emitted in the Arctic, over and above the seasonal background in maritime air entering from further south, is dominated by wetland emissions in summer and a much smaller fossil fuel source in winter. It is possible that the amplitude of the isotopic seasonality may be increasing, which perhaps suggests that wetland emissions are increasing. This is consistent with Arctic warming if emissions of methane from wetlands (methanogenic flux) increase exponentially with temperature, although methane consumption (methanotrophy) would also be expected to increase (see Ch. 3 and 4).

There has been much debate about the possibility of significant methane release from methane hydrates in the Arctic Ocean as temperatures rise (Nisbet 1989; Archer et al. 2009). In particular, large fluxes have been estimated by upscaling emissions measured from the eastern Siberian Arctic Shelf (Shakhova et al. 2010) and there is clear evidence for submarine bubble plumes (Westbrook et al. 2009), although these methane bubbles do not necessarily reach the sea surface (see Ch. 4). The isotopic results of Fisher et al. (2011) and unpublished data from the MAMM campaign suggest that methane hydrates are not currently a major source of atmospheric methane. Although isotopic values in hydrates can vary greatly, most Arctic hydrates have a $\delta^{13}C_{CH4}$ of around -55±10‰ (Milkov et al. 2005; Fisher et al. 2011) (see Table 6.2). If such comparatively 'heavy' hydrate-sourced fluxes contributed substantially to the approximately -53‰ late winter/spring Arctic methane increment reported by Fisher et al. (2011), then that same signal would be expected, at least to some extent, to affect summer Arctic methane observations.

However, this has not yet been observed. To determine source contributions with certainty, additional measurements are required, as well as transport modelling.

6.7 Conclusions

6.7.1 Key findings

The recent expansion of Arctic methane measurements has enabled improved characterization of daily, seasonal and interannual variations in atmospheric methane levels at the local and regional scale. Overall, there has been an increase in atmospheric methane abundance since measurements began, despite some interannual variability. Since 2008, the mean Arctic atmospheric methane concentration has been increasing at about the global rate, ~6 ppb/y (2008–2013). From these measurements, it is evident that in winter, regionally influenced sites are impacted by transport from mid-latitude source regions while in summer, there is considerable variability due to strong diurnal cycles. Before calculating seasonal cycles and long-term trends, it is important to separate out the impacts of localized diurnal variability so that any subsequent analysis is performed on data that are more representative of large, well-mixed volumes of the troposphere. The annual cycle at remote background sites shows a minimum in methane concentration in July/August and a maximum in February. The annual cycle at regionally and locally influenced sites also show a maximum in February as well as a secondary peak in methane concentration in late summer. This secondary peak is likely to be due to the advection of air with enhanced methane levels due to emissions from wetland areas.

Methane isotopic data from Arctic measurement sites provide additional evidence that summer atmospheric concentrations are dominated by contributions from wetlands sources, and in winter by local and regional fossil fuel sources.

There is general concern that Arctic ecosystems may undergo significant changes if Arctic warming trends continue. This is especially true for methane since existing and potential natural Arctic methane sources are large and widespread (i.e. wetlands and marine methane hydrates). The climate feedback from such changes could potentially be very large although, to date, no definitive changes in Arctic methane emissions have been detected by the existing observational network.

An important goal of international observational programs is to provide high quality data to support the characterization of regional-scale information on greenhouse gases. One capability of such programs is the ability to infer emissions from anthropogenic source sectors. With the improved availability of long-term, high time resolution methane observations and coincident improvements in modelling capability (see Ch. 7 and 8), it will eventually become possible to track regional emissions of methane, including those from fossil fuel use, agriculture and waste over long periods. Equally important will be the ability to utilize long-term observations to evaluate observational constraints on large-scale emissions and sinks, and to improve understanding of the carbon cycle for large ecosystems such as tundra and high boreal forest regions, an approach which is detailed in Ch. 7.

6.7.2 Recommendations

The data presented in this chapter have the potential to identify and locate major sources of Arctic methane by type and seasonality. However, continuity in long-term data records for both weekly and hourly measurements is essential to support this work. Integration of the long-term observational data (including isotopic measurements) with short-term airborne measurements and data from ground-based remote sensing platforms would provide a more accurate representation of the true spatial and temporal gaps in the observing system. This analysis should be completed as a next step. Subsequently, and as modelling capabilities continue to evolve, a detailed assessment of the adequacy of the observational network to detect future atmospheric change and to support the characterization of sources may be warranted. Ensuring the timely availability of both short- and long-term observational data to support future analyses is critical to ensuring a full understanding of the limitations of the current observing system. Common data archiving and quality control/assurance practices would also improve data inter-comparability.

Finally, maintaining the existing long-term data records, as well as continuing to evaluate the spatial and temporal coverage of Arctic atmospheric methane measurements is an essential component in improving the ability to assess the overall impact of regional and global methane sources, as well as to assess the response of the Arctic to climate change.

Acknowledgments

7. Modeling of atmospheric methane using inverse (and forward) approaches

Authors: Lori Bruhwiler, Philippe Bousquet, Sander Houweling, Joe Melton

7.1 Introduction

The abundance of methane in the Arctic atmosphere arises from a balance between the transport of methane into the Arctic from sources outside the Arctic and local sources and sinks, with a small contribution from chemical loss during summer. This chapter focuses on the application of modeling techniques for understanding the Arctic methane budget. Inverse models provide a means to systematically incorporate bottom-up information about methane emissions (bottom-up approaches include direct flux measurements, process models of emissions, or economic data – see Ch. 3, 4 and 5) with atmospheric observations and simulated atmospheric transport. This framework allows estimation of emissions that are optimally consistent with both bottom-up and top-down information (i.e. the observations). The chapter also shows how atmospheric observations along with atmospheric transport modeling can provide useful information for evaluating process-based emission models. This ultimately leads to improvements in prognostic modeling, for example models that project future changes in the climate system based on scenarios of changes in anthropogenic emissions, or feedbacks between the climate system and trace gas emissions. Simulating the observed atmospheric trace gas concentration record over past decades is an important test for coupled climate models. Prognostic climate modeling is the topic of Ch. 8.

This work addresses several of the policy-relevant science questions in Table 1.1 (Ch. 1). It also explores whether the current distribution of atmospheric observations is adequate for determining potential trends in Arctic emissions. The consistency between Arctic methane emission estimates from top-down approaches (using information from atmospheric observations) and bottom-up approaches (using flux measurements and emission inventories) is also considered in order to establish whether emission estimates from the two approaches can be reconciled. The chapter concludes by assessing how well variability in Arctic atmospheric methane concentration can be understood using current observations and modeling tools.

7.2 Inverse modeling approaches for understanding Arctic methane emissions

7.2.1 Introduction to atmospheric inverse modeling

Atmospheric inverse modeling techniques are potentially powerful data analysis tools because they combine information from atmospheric observations with best available information about emissions, sinks and transport of atmospheric species.

Atmospheric inverse models produce three-dimensional distributions of atmospheric trace species (e.g. greenhouse gases and air pollutants) that are optimally consistent with spatially distributed observations. As such, they provide spatio-temporal distributions that are useful for studies of atmospheric chemistry and pollution as well as evaluation of column retrievals from surface or space-based platforms. Inverse models go one step further than optimal interpolation because they also result in estimated emissions and sinks of atmospheric trace species. In this sense they extract information from observed concentrations and use it to infer distributions of emissions and sinks. The numerical techniques used to accomplish this are very similar to those used for numerical weather prediction. The atmospheric inverse models are also known as assimilations because observations are incorporated into a model that simulates the behavior of an atmospheric species, and they are systematically used to refine estimates of its distribution and emissions (Box 7.1).

The numerical optimization techniques used in atmospheric inverse modeling processes to estimate emissions range from mass-balance approaches to assimilation methods that are similar to those used in weather forecasting. Atmospheric transport models used in inverse models include 1-D diffusion models (Bolin and Keeling 1963), zonal average models (e.g. Enting and Mansbridge 1989; Tans et al. 1990; Brown 1993, 1995) and detailed 3-D atmospheric models, sometimes with simple chemistry to calculate chemical loss. Early application of inverse techniques to atmospheric trace gas source/sink estimation explored the atmospheric budgets of carbon dioxide (Enting and Mansbridge 1989; Tans et al. 1990) and chlorofluorocarbons (Hartley and Prinn 1993; using a 3-D transport model). The first attempt to deduce emissions of methane using a 2-D approach appears to be the studies of Brown (1993, 1995).

The studies of Hein and Heimann (1994) and Hein et al. (1997) used a full 3-D atmospheric transport model to estimate global emissions of methane from the dominant natural and anthropogenic emissions. They also used global atmospheric observations of methyl chloroform (CH_3CCl_3, MCL) to adjust their photochemical simulations of the hydroxyl radical (OH). The inverse model of Hein et al. (1997) solved adjustments to global total emissions for each and therefore did not recover spatial information about emissions. Later studies attempted to retrieve information about the spatial and temporal variability of methane emissions, generally by dividing the globe into source regions. The sizes of the source regions have ranged from global (Hein et al. 1997) to continental (e.g. Bousquet et al. 2006; Bergamaschi et al. 2007; Bruhwiler et al. 2014a) to the size of transport model grid boxes (Houweling et al. 1999). Some studies estimated total emissions, while others estimate emissions from individual anthropogenic and natural source categories.

Box 7.1 Inverse techniques for estimating source strengths of atmospheric trace species

There are three distinct components to inverse modeling techniques for estimating source strengths (i.e. emissions): (1) the best available bottom-up information about emissions and losses; (2) observations of atmospheric concentrations, and (3) models of atmospheric transport. The best available prior estimates of emissions (sources) and removals (sinks) (hereafter referred to as 'priors') are first used to simulate the abundance of the atmospheric species sampled at observation sites. Priors can come from reported inventories of natural and anthropogenic emissions, and from ecosystem-based process models. The atmospheric observations may come from surface network sites, profiles measured from aircraft, and retrievals from satellite observations or upward-looking ground-based spectrometers. Atmospheric transport models use bottom-up emissions to compute atmospheric concentrations, referred

to as forward simulations since they effectively translate emissions to atmospheric concentrations.

The next step is to use a numerical optimization procedure to adjust estimated parameters (emissions, for example) to achieve optimal agreement of modelled atmospheric concentrations with the observed atmospheric concentrations given uncertainty in prior emissions and sinks. This is the inverse (backward) step in the sense that it uses atmospheric concentrations to infer emissions. The resulting emission estimates at a particular time step may be used as the starting point (or first guess) for the next time step, with the background atmospheric abundance being adjusted to the new estimated distribution. A schematic representing the inverse modeling process is shown in Fig. 7.1.
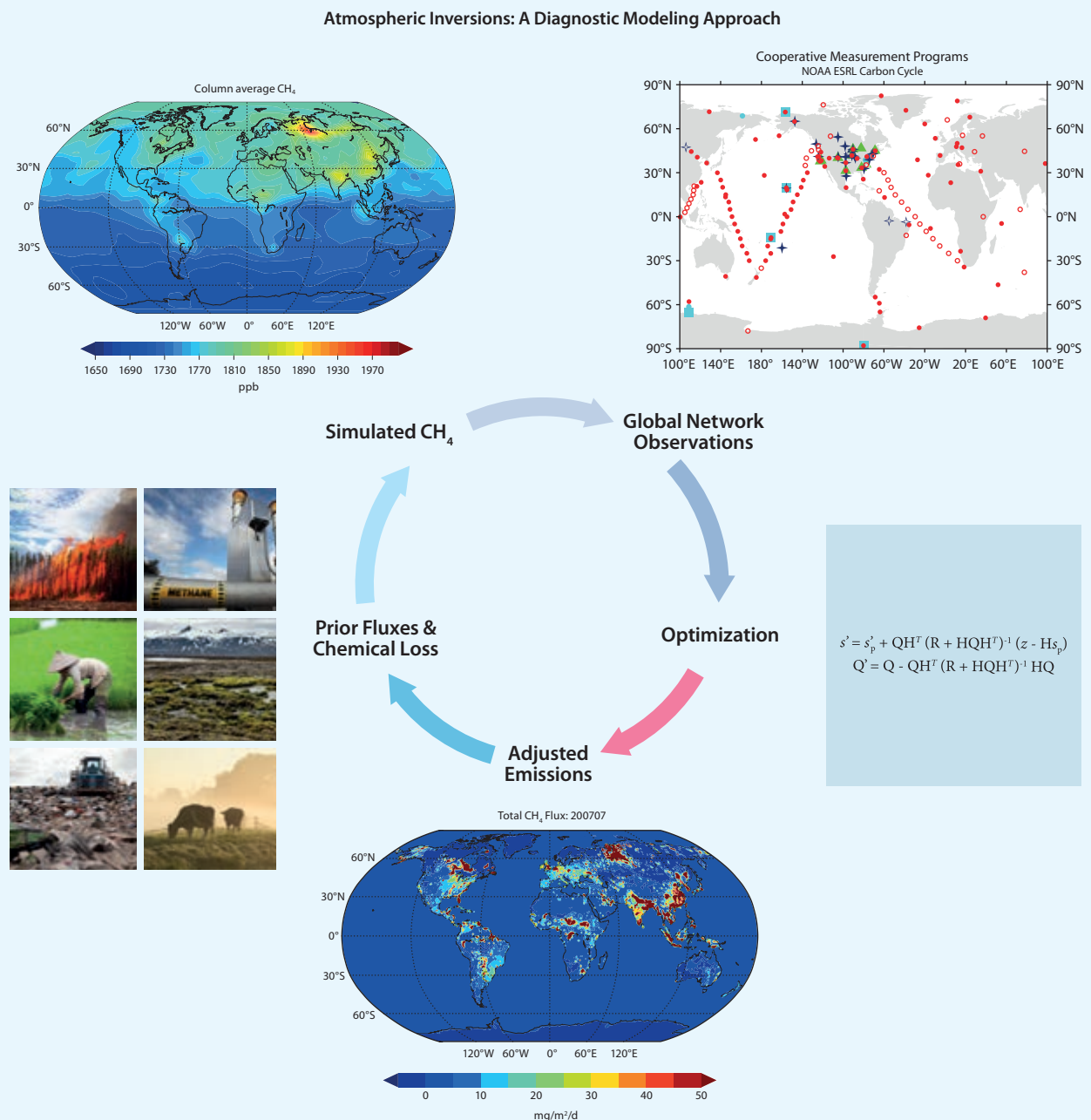
Fig. 7.1 Schematic illustrating the atmospheric inverse modeling process.

The first study to use global surface data to explore the spatial distribution of methane emissions was that of Houweling et al. (1999) who concluded that, while their estimated emissions reproduced large-scale features such as the inter-hemispheric methane gradient reasonably well, their approach could not resolve small-scale variability of emissions. They also noted that successfully reproducing the meridional (north-south) gradient is dependent on accurate representation of inter-hemispheric exchange in the transport model as well as accurate distribution of the chemical sink. Another important finding of Houweling et al. (1999) was that compared to the *a priori* distributions of emissions, the *a posteriori* emissions tended to be reduced at high northern latitudes and increased at tropical and southern latitudes, a result since found by many other studies (e.g. Mikaloff Fletcher et al. 2004a,b; Bousquet et al. 2006; Chen and Prinn 2006; Bergamaschi et al. 2009; Bruhwiler et al. 2014a). Possible reasons for this include overestimated bottom-up emissions at high northern latitudes and underestimated bottom-up emissions at low and southern latitudes, and possible overly-stable atmospheric transport leading to accumulation of methane at lower levels, and consequently underestimated emissions. In addition, underestimation of chemical loss could result in higher compensating emissions in the tropics where the tropospheric chemical loss is fastest.

The inverse model results of Bousquet et al. (2006, 2011), Bergamaschi et al. (2013), Bruhwiler et al. (2014a) and Houweling et al. (2014) indicate that year-to-year variability in wetland emissions is largely responsible for interannual variability in methane growth rate, with biomass burning responsible for a smaller contribution. Bruhwiler et al. (2014a) and Bergamaschi et al. (2013) concluded that over the past decade there has been no detectable increase in emissions of methane from the Arctic although in 2007, emissions from the Arctic were 2–4 Tg higher than normal due to the unusually warm and wet growing season that year.

7.2.2 Role of uncertainty in inverse modeling

Measurements at many surface network sites are carefully calibrated, and have small uncertainties (see Ch. 6) compared to the larger uncertainties associated with transport and mixing at spatial scales reflected by the surface measurements. It is currently difficult to quantify the uncertainty related to transport models except at very large scales (Patra et al. 2011); however, advances in computing have made it possible to run such models at ever higher spatial resolution while allowing for ensemble approaches to evaluating transport uncertainty. Global observations constraining important processes, such as planetary boundary mixing and cloud formation, can lead to improvements in transport simulations.

The study of Patra et al. (2011) evaluated and compared a suite of atmospheric transport models that used prescribed emission scenarios over the period 1990 to 2007 and observations of methane, radon, sulfur hexafluoride (SF6) and methyl chloroform at a limited number of background sites as well as satellite retrievals of methane in the upper troposphere and stratosphere. Their analysis indicated a considerable range in inter-hemispheric exchange time among the models (1.2 to 1.8 years). They also found differences between the models in regions that feature deep cumulus convection, and their analysis provided evidence that differences between the model simulations occurred due to differences in vertical mixing and stratosphere-troposphere exchange. A related study by Locatelli et al. (2013) used synthetic observations constructed using the transport models included in the study by Patra et al. (2011) and a common inversion framework. They found that transport errors alone could cause a spread in the total estimated global emissions of 27 Tg/y; 5% of the global total emissions. Priorities for future research include devising strategies for measurements that can help evaluate transport models, and improving transport models especially parameterization of convection and planetary boundary mixing processes not currently resolved at grid-scale.

For the prior emission and sink estimates, some processes are believed to be relatively well known, and so are given low or even zero uncertainties in atmospheric inverse models. A zero uncertainty means that the emission is not adjusted by the inverse procedure. For example, carbon dioxide emissions from fossil fuel combustion are considered sufficiently well-known and so are not estimated by most inverse model systems. For methane the emissions from production of oil, gas and coal are much more uncertain particularly in relation to fugitive emissions (see Ch. 5 for discussion of uncertainties related to anthropogenic emissions). Natural methane emission estimates are also uncertain (see Ch. 3 and 4). With wetlands being the largest natural source of methane, estimating their emissions is a particularly important aspect in applying atmospheric inverse modeling techniques. Even when there is agreement between process-model based natural emissions and measured methane emissions (e.g. local estimates made at flux towers located near wetlands), considerable uncertainty is introduced in extrapolating the data to larger spatial scales. This issue is addressed in more detail in Sect. 7.3 by evaluating a suite of current wetland emission models against multi-decadal surface observations, an exercise that allows an assessment of how well wetland emission models are able to represent the regional and global scale.

Overestimated chemical loss due to OH at tropical and southern latitudes could lead to overestimation of methane emissions. Understanding possible trends and variability in OH abundance is an important issue for estimating the budget of atmospheric methane since it is the largest term in the methane budget, approximately balancing sources (see Ch. 2). Characterizing OH variability and long-term trends remains a challenge (see Ch. 2 for a more detailed discussion of OH and its variability).

7.2.3 Importance of adequate observational coverage

Adequate observational coverage in space and time is required to fully constrain inverse models at national or regional scales (Box 7.1). Only about 100 surface sites globally provide measurements of atmospheric methane and many only measure weekly. A small number of sites provide continuous measurements. Of these, sites that represent the background atmosphere remote from strong local sources are most commonly selected for use in global inverse models (see Ch. 6) due to the difficulty of simulating continental sites using atmospheric models that have relatively coarse spatial resolution. The limited number of these sites means that some regions are inadequately

Box 7.2 The potential for satellite data to constrain atmospheric inverse models

Surface observations maintained consistently for decades provide the best means of detecting atmospheric methane trends and characterizing its global-scale distribution. They are also necessary for developing and evaluating remotely-sensed retrievals, such as those from satellites or ground-based, open path spectrometers such as TCCON. Space-based retrievals, on the other hand, have the advantage of frequent global coverage. Using surface observations and satellite data together offers a reasonable approach to improving the ability of inverse models to reduce uncertainties in the budget of atmospheric trace gases.

The calibration and validation of current satellite observations for methane is an ongoing endeavor, particularly in linking them to the ground surface measurements and calibration of the WMO-GAW (Global Atmosphere Watch program of the World Meteorological Organization) greenhouse gases program which is essential to ensure global consistency across horizontal and vertical dimensions. A particular concern is possible drift over time, and consistency between satellite data records. Current satellite instruments have been shown to have persistent biases in space and time (e.g. Bergamaschi et al. 2013; Houweling et al. 2014) that must be accounted for

if satellite data are to be assimilated into atmospheric inverse models. Remotely-sensed observations of column methane using ground-based upward looking Fourier spectrometry have been used to detect biases in the satellite data and this has resulted in bias correction schemes that have been somewhat successful (Houweling 2014).

The current satellite instruments provide only limited information for Arctic regions. Instruments operating in the visible and short-wave infrared spectrum, such as SCIAMACHY and GOSAT, rely on sunlight, which is absent during the Arctic winter. In other months of the year, the low angle of the sun complicates the retrieval of information from satellite radiance data. Infrared sounders, such as AIRS and IASI, are mostly sensitive to the upper troposphere, where signals of surface emissions are small. At higher latitudes, their sensitivity is further reduced by the lack of thermal contrast between the surface and the atmosphere as well as uncertainties in surface emissivity related to variations in snow and ice cover. Mission plans are emerging that will improve polar region coverage and the measurement instrumentation for methane, but are some years from implementation.

resolved by global inverse models, including the tropics and some regions of the Arctic, both of which have emissions from wetlands (natural wetlands and, in the case of the tropics, rice paddies) that are likely to be significant. It is important to recognize that in regions not constrained by observations, the estimated emissions are likely to be relatively close to the prior estimates. This means that in these regions it will be difficult for inverse models to detect emission changes.

Other potential data sources that could help constrain inverse models include aerial surveys and observations made from towers. Methane column abundance from satellite platforms may eventually significantly increase the spatial and temporal coverage of observational constraints; however, the measurement techniques are still under development and the current generation of passive satellite instruments is not able to retrieve much useful information from the Arctic (see Box 7.2).

7.2.4 Results from inverse model studies

As part of the present assessment, ten atmospheric inverse models were reviewed and robust features in the results that are common among them were identified. Results from six of the models were compiled by Kirschke et al. (2013) in a synthesis study of the global methane budget over recent decades. The present study has built on this work by obtaining more recent results from the studies of Bergamaschi et al. (2013) and Houweling et al. (2014). The inverse model approaches are summarized in the Appendix.

The various inverse model results span a range of possible configurations and assimilation techniques. Several different transport models and driving meteorological data products are used, thus allowing for evaluation of possible transport biases. The spatial resolutions of the transport models range from 3.75°×2.5° to 6°×4°, with the number of vertical levels ranging from 19 to 47. Multiple optimization techniques are used and fall into the categories of variational and ensemble

approaches. Some of the inverse models use only surface observations while others use a combination of space-based and surface observations. The spatial resolutions of the emissions estimated by the inverse models span the transport model grid scale (i.e. 6×4 grid boxes) up to continental-scale source regions. In practice, this means that some inverse models will solve for emissions coming from each Arctic transport model grid box while others will solve for the net emissions spread over regions the size of Siberia or the North American Arctic. The frequency at which emissions are estimated by the inverse models considered here is either monthly or weekly.

As previously noted, inverse model results are dependent on prior emission estimates. All of the inverse models compiled here use the widely available anthropogenic emissions inventories EDGARv3.2 or EDGARv4.1 (Emission Database for Global Atmospheric Research; European Commission 2009) for prior anthropogenic emissions estimates. These products cover the past few decades. Prior estimates of biomass burning emissions come from either GFEDv2 or GFEDv3 (Global Fire Emissions Database; Giglio et al. 2006; van der Werf et al. 2006). For wetland emissions, the models used either Matthews (1989) or the Kaplan (2002) wetland distribution and parameterization based on soil carbon, moisture and temperature. None of the inverse approaches included in this study used detailed bottom-up wetland process models to provide prior estimates of wetland emissions.

The inverse models considered also vary in their approach to data selection. Observations from background atmospheric sites are universally used, however in some cases only sites with long data records were used. Other inverse models used harder-to-model continental sites in addition to background sites, or retrievals derived from radiances observed from satellites. It is beyond the scope of this study to review in detail the sites used in each inverse model exercise, or the amount of weighting applied to the various observations used.

7.2.4.1 **Inverse model estimates of source magnitude**

As shown in Table 7.1, the atmospheric inverse model results surveyed agree to within ~40% for total Arctic methane emissions for the years 2000 to 2010 (the period over which the maximum number of model results is available). The average annual total emission across ten inverse models is 25 Tg CH_4/y with a wide range spanning 18.5 to 28.8 Tg/y. The largest contribution to Arctic emissions is from wetlands, followed by anthropogenic emissions. There is a small but interannually variable contribution from biomass burning.

While the inverse model studies show relatively good agreement among them, all tend to reduce estimates of high latitude emissions relative to priors, implying that the prior emissions are too large and inconsistent with observed methane levels in the atmosphere. The estimates of McGuire et al. (2012) for 2000–2010 based on pan-Arctic terrestrial flux measurements suggest a source of 25.0 Tg CH_4/y from Arctic tundra wetlands with uncertainty ranging from 10.7 to 38.7 Tg CH_4/y. Atmospheric inverse models suggest a lower source of 15.5 Tg CH_4/y on average from the region 60–90°N over the period 2000–2010 (see Table 7.1). Estimates from field studies may be biased towards larger emissions if measurement sites tend to be located near large sources and do not represent the Arctic over large scales. This could at least partially account for the lower estimates based on atmospheric observations. On the other hand, the inverse models may not be able to accurately distinguish between anthropogenic and natural emissions. If the anthropogenic emissions are overestimated, then the estimated emissions from wetlands could be larger resulting in better agreement with the bottom-up estimates. Furthermore, as discussed in Sect. 7.2.2, if the models are biased towards stability then emissions could be underestimated. However, it is very encouraging that the bottom-up and top-down approaches are reasonably consistent.

In addition to wetlands, other significant natural methane emissions have recently been proposed for the high northern latitudes. Walter Anthony et al. (2007) estimated that ebullition (i.e. direct release of methane bubbles) from Arctic lakes could add an additional 24±10 Tg CH_4/y, an estimate on a par with bottom-up estimates of wetland emissions. Relatively shallow lake waters enable bubbles to transport methane directly and rapidly to the atmosphere from sources such as buried methane hydrates and organic-rich, anoxic sediments. Shakhova et al. (2014) estimated a methane hydrate source of ~17 Tg CH_4/y for the shallow continental shelf waters of the Eastern Siberian Arctic Shelf (see Ch. 4). Walter Anthony et al. (2012) proposed that seepage of methane from geologic sources may also occur on land as permafrost thaws and glaciers recede even though hydrates require high pressure and low temperature to exist (meaning they must lie far below the surface). Total natural emissions including all of these processes would be over 70 Tg CH_4/y, an amount that significantly exceeds the total Arctic emissions (i.e. including anthropogenic emissions) as estimated by the inverse model studies constrained by atmospheric observations (Table 7.1). Note that many of the bottom-up studies rely on a small number of observations that are extrapolated to pan-Arctic annual total emissions.

A number of factors may be contributing to the discrepancy between the bottom-up estimates and top-down atmospheric

Table 7.1 Average annual emissions for the period 2000–2010 from multiple inverse model studies for the Arctic region (60° to 90°N). Three inverse model studies calculated total emissions only, so the total emissions were averaged across ten studies. Seven inverse model studies were used to compute the averages for each source category. See the Appendix for details about the inverse model studies. Source: Bergamaschi et al. (2013), Kirschke et al. (2013), Houweling et al. (2014).

Source	Tg CH_4/y
Wetlands	15.5 (11.1–27.4)
Biomass burning	0.6 (0.4–1.0)
Anthropogenic	9.3 (7.2–10.5)
Total emissions	25.0 (18.5–28.8)

inverse model results. It is possible that the polar atmosphere in atmospheric transport models is too stable, leading to a simulated accumulation of methane near the surface (rather than mixing and diluting methane throughout the atmospheric column). The inverse model will therefore reduce emissions in order to match observations. Recent studies have addressed the potential for transport errors to be aliased into estimated emissions (Patra et al. 2011; Locatelli et al. 2013). There could also be some double counting of emissions in bottom-up estimates between natural wetlands and other inland water areas, as well as incorrect extrapolation of local emissions to pan-Arctic scales. However, the spatial and temporal information coming from the observations ultimately places strong constraints on the amount of methane that can be emitted in the Arctic and elsewhere according to inverse models. It is clear that the total amount of all the proposed emissions from wetlands, lakes, possible geologic sources and the shallow Eastern Siberian Arctic Ocean, together with the Arctic anthropogenic emissions, is significantly larger than the total emissions implied by atmospheric observations. This suggests that either some bottom-up emissions are overestimated, or that the loss processes that remove methane from the atmosphere are not yet well understood. Note, however, that quantifying and correcting possible model transport biases may result in higher emissions estimates.

7.2.4.2 **Inverse model estimates of spatial variability in methane emissions**

The global latitudinal distribution of total methane emissions estimated by the inverse models is shown in Fig. 7.2. From this graphic, it is evident that the tropics and populated sub-tropical latitudes dominate the global methane budget. The spread between the results is considerable, although all models show large tropical and northern sub-tropical emissions. There do not appear to be systematic differences between those approaches that use space-based observations and those that do not. Likewise, properties such as which transport model or assimilation technique is used do not appear to stand out (see Appendix).

Figure 7.2 also shows the zonal distribution of estimated emissions for Arctic latitudes. With the exception of one inverse model that appears too high relative to the others, the models agree to within about 40% for each 1° latitude zone. All models except one show a steep decline in emissions with increasing latitude.

Tg CH$_4$/y

Tg CH$_4$/y
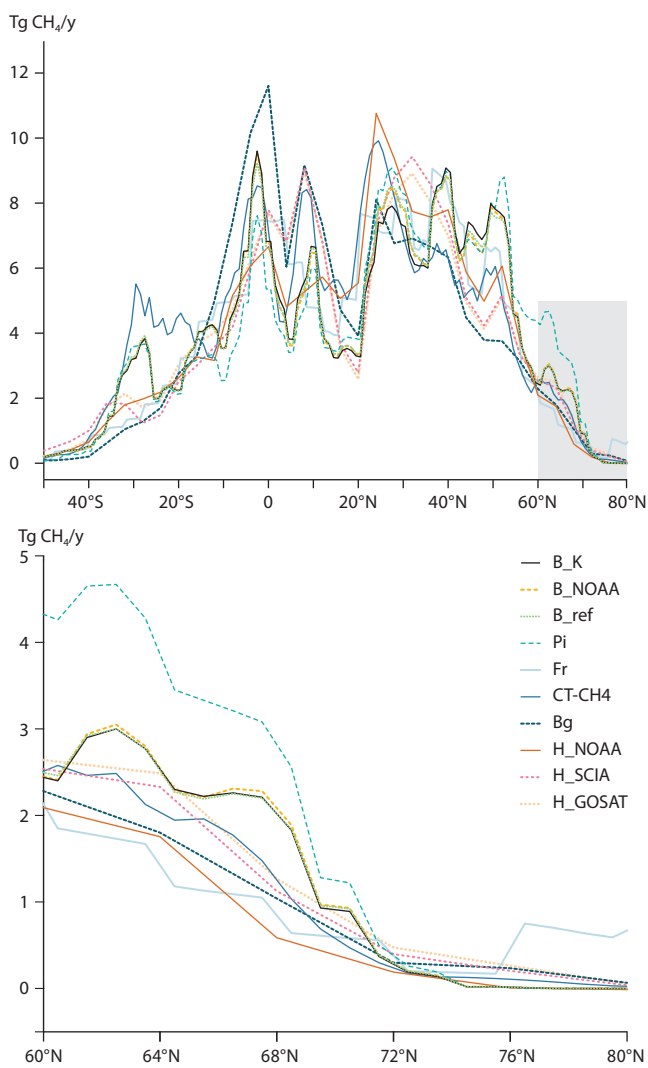
Fig. 7.2 Annual average latitudinal (upper) and Arctic zonal (lower) distribution of methane emissions for ten atmospheric inverse model studies for the period 2000 to 2010. See Appendix for details of the individual approaches.

7.2.4.3 Inverse model estimates of temporal variability in methane emissions

Monthly total methane Arctic emission estimates from the inverse model studies over the past decade are shown in Fig. 7.3. The past decade was chosen because although some of the studies cover shorter periods (see Table 7.1) they all give results for at least some part of the period 2000–2010. Note the large seasonal cycle of total emissions, with a peak during summer when microbial methane production occurs most rapidly due to seasonally warmer surface soils as well as an abundance of soil moisture. The winter minimum mostly reflects anthropogenic emissions (because natural emissions are low in the cold season). Many of the inverse models do not provide error estimates; however, those for the CT-CH4 inverse model (light blue shaded area) have been included to show at least one estimated uncertainty range. The differences between the model results are often greater than the estimated error for the CT-CH4 data.

The lower panel of Fig. 7.3 shows the mean estimated Arctic emissions across the models, together with the model spread (i.e. the area between the highest and lowest model estimates, shaded area). The model spread can be large during summer,

sometimes up to 40 Tg CH$_4$/y. During winter the spread is smaller; 20 Tg CH$_4$/y or less. The mean for peak summer emissions is steady at about 55–60 Tg CH$_4$/y.

Although the mean exhibits little interannual variability, some of the model results vary significantly from year to year. For example, the CT-CH4, H_SCIA and H_GOSAT models show peak emissions of about 80 Tg CH$_4$/y for 2007, although the Pi and Fr models show little difference in 2007. Results for 2008 are more variable with some models generating higher than average results and some lower.

None of the models show evidence of a trend over the period 2000–2010 towards increasing summer Arctic emissions. This may indicate no trend, or that the inverse models are not sensitive enough to detect changes that have occurred. Increasing observational coverage and ensuring the continuation of long records is essential for increasing the sensitivity of atmospheric inverse models to changes in emissions. It is also useful to develop, evaluate and improve bottom-up models of emissions so that sparsely observed regions are represented as well as possible, because biases and errors in the prior emissions coming from bottom-up models can end up biasing large-scale emission estimates produced by atmospheric inversion modeling approaches.

Tg CH$_4$/y
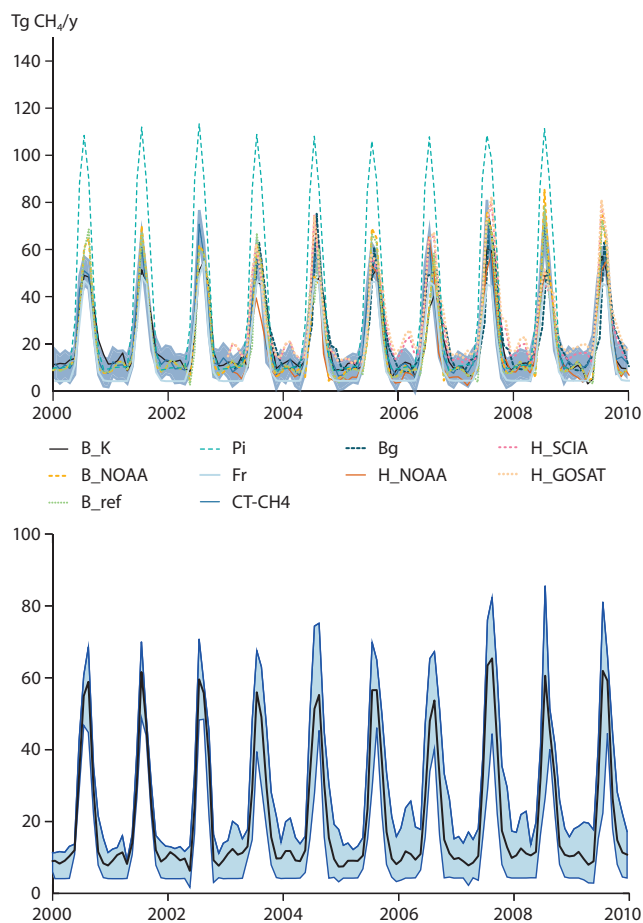
Fig. 7.3 Distribution of monthly Arctic methane emissions for ten inverse models for the period 2000 to 2010 (upper panel). See Appendix for details of the individual approaches. The light blue shading represents the estimated 1 standard deviation confidence interval (estimated error) for the CT-CH4 model. The mean (black line) and model spread (shaded blue) of the suite of model results is shown in the lower panel. Note that the model spread does not include the Pi model, which appears to be an outlier. Also note the difference in scale for the upper and lower panels.
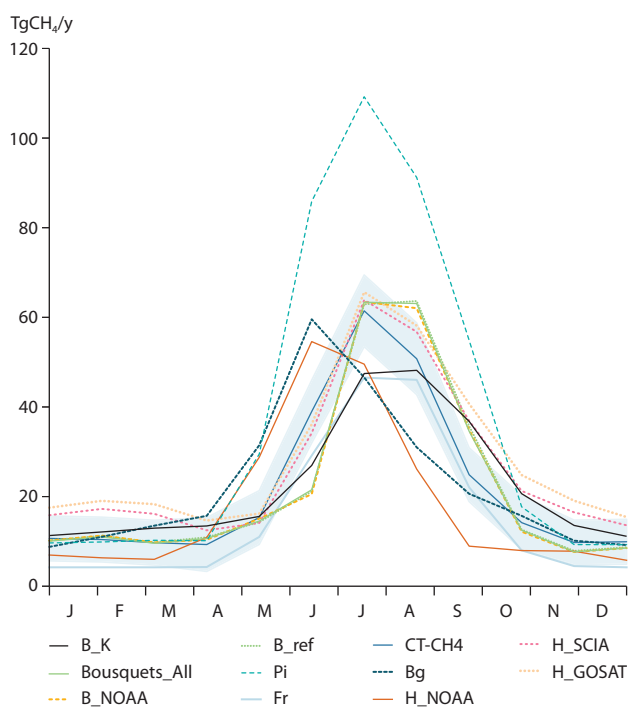
Fig. 7.4 Average seasonal cycle of Arctic methane emissions for eleven inverse model studies for the period 2000 to 2010. See Appendix for details of the individual approaches. The shaded area is the estimated uncertainty for the CT-CH4 model.

The average annual cycle of Arctic methane emissions estimated by the suite of models is shown in Fig. 7.4. Most inverse models show emissions below 20 Tg CH$_4$/y during the cold season rising to values of 50–60 Tg CH$_4$/y during the warm season when methane production in Arctic wetlands is highest. It is interesting that the models vary in the timing of their summer maxima. Two models have maximum summer emissions during June, while others have maxima in July or August. There is no clear correlation between the timing of maximum emissions and whether satellite or surface observations are used to constrain the model. Note that the observed annual cycle in Arctic methane concentrations shows a minimum at mid-summer, when wetland emissions are highest (see Fig. 6.9), and a maximum during winter. The chemical loss of methane (due mostly to reaction with OH) is greatest during summer, when solar irradiance is highest and temperatures are warm, and the methane annual cycle results from this. A small secondary peak in Arctic methane concentrations can often be seen in observations during late summer and early autumn, and this is probably because wetland emissions are highest towards the end of the growing season when wetland soils are warmest, while at the same time chemical loss is slowing as the days grow shorter (see Ch. 6). This suggests that inverse models that show the greatest emissions after the summer solstice may be more realistic than those that do not.

Interannual variability in estimated emissions is further explored in Fig. 7.5. Interannual variability was computed by subtracting an average seasonal cycle (shown in Fig. 7.4) from the results of each model. The lower panel of Fig. 7.5 shows the mean and model spread of the interannual variability from the suite of inverse models. The spread is relatively high indicating that the models do not agree on the timing of emission anomalies (i.e. when higher/lower than average seasonal emissions occur).

On the other hand, most models do agree that 2007 was a year with higher than average emissions, and this makes it possible to assess both the sensitivity of the models to variability in emissions and their ability to detect emission trends, since the climatic conditions for 2007 were exceptionally warm and wet (Dlugokencky et al. 2009). The models on average estimate that 2.2 Tg CH$_4$ more than average (15.5 Tg/y, Table 7.1) were emitted across the Arctic during the warm season of 2007, with a spread of -0.4 to 5.2 Tg CH$_4$.

Attribution of interannual variability in observed methane concentration to individual sources and regions is an important analysis contribution of the top-down approach. Based on zonal average analysis of atmospheric network observations, Dlugokencky et al. (2009) pointed out that in 2007 the global increase in methane was equal to about a 23 Tg imbalance between sources and sinks and that the largest increases in atmospheric methane concentration growth occurred in the Arctic (>15 ppb/y). This does not necessarily imply that the largest surface flux anomalies occurred at high northern latitudes. Bousquet et al. (2011) noted that the relatively weak vertical mixing characteristic of polar latitudes results in a greater response in atmospheric methane concentrations to anomalous surface emissions than at tropical latitudes where strong vertical mixing rapidly lofts methane emitted at the surface through a deep atmospheric column. Transport models used as a component of inverse models are in theory able to simulate the more stable polar atmosphere, and can therefore play an important role in helping to resolve surface flux signals from variability in atmospheric transport processes, although care must always be taken to consider possible biases in modeled transport.
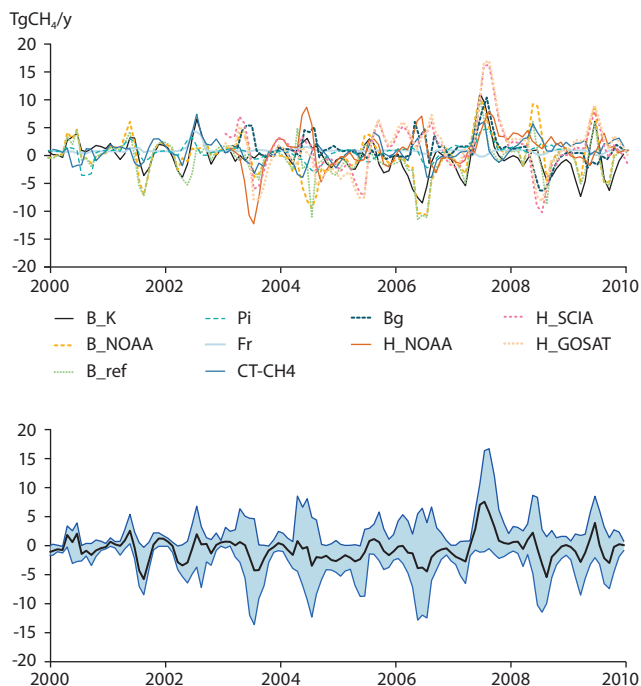
Fig. 7.6 Interannual variability of Arctic methane emissions for ten inverse model studies computed by subtracting an average seasonal cycle for each inverse model (upper panel). See Appendix for details of the individual approaches. The mean (black line) and range (shaded blue) of the interannual variability for the suite of inverse model results is shown in the lower panel. The range is defined by the maximum and minimum of the inverse model ensemble.

7.3 Evaluating global wetland models using forward modeling and atmospheric observations

Chapter 3 assessed the potential for increased methane emissions from Arctic wetlands in response to a changing climate, reviewing processes that control methane emissions and evaluating how these may change in the future using a terrestrial ecosystem model. This section shows how global atmospheric observations can be used to evaluate terrestrial ecosystem models that predict wetland methane emissions (hereafter referred to as wetland models) by assessing how well they reproduce the observed record of atmospheric methane. This is relevant to inverse modeling because simulated emissions from wetland models may be used as prior flux estimates, in addition to their potential use in coupled biosphere-climate models. The approach used here to evaluate the wetland emission models is to use a forward modeling approach to simulate atmospheric methane concentrations for each wetland model using an atmospheric transport model given constant non-wetland natural emissions, anthropogenic emissions and chemical sinks (Box 7.3).

Modeling emissions from wetlands is challenging because processes that vary significantly over scales as small as meters must be represented at the model grid scale (typically 100–500 km) which represents a significant scaling challenge in part due to how well the global distribution of wetlands is characterized in time and space, which in turn depends on information about soil hydrology and water table depth in many remote parts of the world. Space-based observations can be useful for mapping/estimating wetland distribution and area, but translating this information to emissions data requires information on standing water depth, which influences the amount of methane released at the land surface. In addition, the remote sensing datasets are not able to capture water just below the ground surface (i.e. when soils are saturated but not inundated), and which may be relevant in methane production zones.

A number of models have been developed to simulate methane emissions from wetlands. A recent model comparison project (Wetland and Wetland CH4 Inter-comparison of Models Project – WETCHIMP– Melton et al. 2013) was established to systematically compare wetland methane models for simulations of large-scale wetland characteristics and corresponding methane emissions. Models participating in the model inter-comparison ran a series of experiments to evaluate the response of wetland models to changes in temperature, precipitation and atmospheric carbon dioxide levels. They found that wetland models vary significantly both in simulated wetland distribution and simulated methane emissions. Modeled wetland emissions appeared to be most responsive to projected increases in atmospheric carbon dioxide levels and less sensitive to projected changes in temperature and precipitation throughout this century. Melton et al. (2013) pointed out that there are large uncertainties in modeled responses and potential nonlinearities and feedbacks between temperature and precipitation that are not currently accounted for in the wetland models. In addition, there is a lack of agreement among the models. Furthermore, Melton et al. (2013) argued that adequate data do not currently exist to constrain the models at atmospheric scales (i.e. to upscale the

Box 7.3 Methodology for testing wetland models

The TM5 atmospheric transport model driven by meteorology from the European Centre for Medium-Range Weather Forecasts (ECMWF) ERA-Interim project (Krol et al. 2005) was used for the simulations described here. The simulations were initialized with interpolated zonal average surface observations for 1989 scaled vertically using a previous model run. Wetland methane emissions were held constant for the first three years, then varied with time starting in 1992. Results for the period 1992 through 2004 were used for the analysis shown here (consistent with the comparison period used by Melton et al. 2013).

This study adopted the same set of anthropogenic and natural non-wetland emissions used as prior emission estimates for the CarbonTracker-CH4 assimilation system (Bruhwiler et al. 2014a and references below). Although emissions from wetlands dominate natural emissions of methane, smaller natural sources include enteric fermentation in insects (mainly termites; Sanderson 1996) and wild ruminants (Houweling et al. 1999). Fires represent a relatively small part of the atmospheric methane budget; however, they are an important contribution to interannual variability in methane concentration. The fire emissions used for this study are based on the GFEDv3 dataset (Giglio et al. 2006; van der Werf et al. 2006). Pre-calculated OH fields from a global chemical model constrained to match global observations of methyl chloroform were used for the chemical sink. Loss by reaction of methane with atomic chlorine (Cl) and excited state oxygen (O^1D) are also included and these processes are mainly important in the stratosphere. The total chemical loss fields consist of a single repeating seasonal cycle that varies spatially in latitude, longitude and altitude. The resulting methane lifetime is about 9.5 years. Details of the chemical loss fields are as reported by Bergamaschi et al. (2005). Oxidation of methane in dry soils (~40 Tg CH_4/y; Ridgwell et al. 1999) is also included.

Anthropogenic emissions used in this study are the 1°×1° gridded emissions from the EDGAR 3.2FT2000 database (European Commission 2009). Total anthropogenic emissions range from 310 to 350 Tg CH_4/y over the past two decades. This data set is based on emission inventories by country and sector for the years 1990 and 1995 extrapolated to 2000 using production and consumption statistics. The present study did not extrapolate these data over the period covered by these simulations, but instead kept anthropogenic emission estimates constant at 2000 levels. Simulations using different estimates for anthropogenic emissions (e.g. Schwietzke et al. 2014) suggest that differences in the anthropogenic part of the methane budget results in concentrations differences of within 20 ppb.

models from local to regional and global scales), although as discussed here observed gradients and temporal variability can provide valuable insights into whether the wetland models can represent emissions at large scales. As discussed in Sect. 7.2.2, potential biases and errors in the prior emissions lead to biases in inverse model estimates of methane emissions. It is therefore useful to identify the wetland models that are most realistic so that the best possible prior emission estimates can be used in the inverse model studies. In turn, use of simulated wetland

Table 7.2 WETCHIMP models used in the present study. Note that the LPJ-WHyMe model covers only northern peatlands so the wetland emissions of Matthews (1989) were used to fill in regions not covered by LPJ-WHyMe in the atmospheric transport simulations.

Model	Resolution	Wetland description	Source
LPJ-Bern	Global, 0.5°×0.5°	Prescribed peatlands and monthly inundation, dynamic wet mineral soils	Spahni et al. 2011
CLM4Me	Global, 2.5°×1.9°	Modeled run-off and water table depth	Riley et al. 2011
DLEM	Global, 0.5°×0.5°	Maximum wetland area from inundation data set with simulated intra-annual variation	Tian et al. 2011
LPJ-WHyMe	Peatlands >35°N 0.5°×0.5°	Prescribed peatlands with simulated soil saturation	Wania 2010a
Orchidee	Global, 1°×1°	Mean inundation with simulated intra- and interannual variability	Ringeval 2011
SDGVM	Global, 0.5°×0.5°	Simulated wetlands	Hopcroft 2011
LPJ-WSL	Global, 0.5°×0.5°	Prescribed monthly inundation	Hodson et al. 2011

emissions in inverse studies may also lead to improvements in the wetland models themselves because adjustments to the prior emissions to match observations will identify times and regions where the bottom-up wetland emissions models are inconsistent with atmospheric data. Finally, improved wetland models will lead to improved confidence in predictions of how wetland emissions may respond to changes in future climate.

Atmospheric observations provide a means of evaluating bottom-up global wetland models because the atmosphere effectively integrates small-scale processes to regional and global scales. Multi-decadal time series of atmospheric methane observations and observed interannual variability provide the data with which to test for the sensitivity of wetland models' methane emissions to variability in temperature and precipitation, and atmospheric carbon dioxide (which can increase productivity in terrestrial ecosystems). The spatial distribution of atmospheric observations can help to evaluate whether the wetland models represent spatial distributions of methane emissions realistically.

7.3.1 Evaluation of wetland models – methods

This section evaluates the ability of the wetland models used by WETCHIMP to reproduce features of global atmospheric surface network observations such as the annual cycle, trends, spatial gradients and interannual variability in methane concentration. In order to do this, it is necessary to specify non-wetland natural and anthropogenic methane emissions (Box 7.3). The annual cycle in atmospheric methane concentration is dominated by atmospheric chemical destruction of methane by OH (Sect. 6.4.2), which is at a maximum around the summer solstice. However, the effect of wetland emissions, especially at high latitudes, adds asymmetry to the annual cycle because wetland emissions are thought to be greatest late in the growing season (around September in the northern hemisphere). Changes in anthropogenic emissions can lead to long-term trends in atmospheric methane concentration, but year-to-year variability in concentration is most likely to be linked primarily to changes in natural emissions as these show a strong response to climatic variability. Spatial gradients are useful for identifying where emissions may be over- or under-estimated.

Table 7.2 lists the WETCHIMP models used in this study (see Wania et al. 2013 and Melton et al. 2013 for more details). The model results vary significantly in terms of both global wetland extent and global wetland emissions. Average annual global total

emissions among the models range from 141 to 264 Tg CH_4 with an average of 190 Tg CH_4, while simulated global wetland areas range from about 7 to 82 million km². The huge range in wetland area is due to differences among the models in the methods used to characterize and identify wetlands from satellite datasets of inundated area, model simulations, distributions of wet mineral soils, or a combination of these. Indeed, the upper bound is due to the LPJ-Bern model, which includes wet mineral soils which greatly increases wetland area. Excluding this model would result in an upper bound of 27 million km². Given the large ranges in global annual methane emissions and wetland area, the atmospheric surface data will provide some indication of which models may be most realistic.

Figure 7.6 shows global total wetland emissions from the WETCHIMP models, global anthropogenic emissions, and
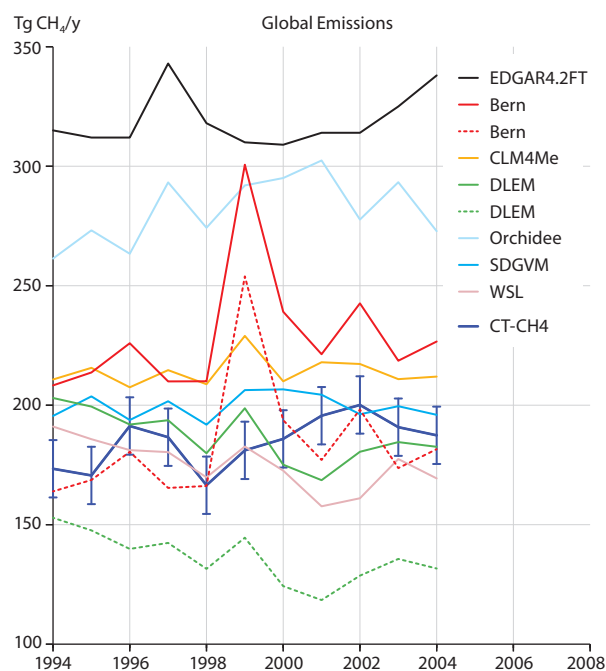
Fig. 7.6 Global wetland emissions from the WETCHIMP models and global anthropogenic emissions from the EDGAR4.2 database. Note that the DLEM model includes emissions from rice agriculture and uptake in dry soils and the Bern model includes rice agriculture. The dashed lines for the DLEM and Bern models show the global emissions from wetlands only. The dark blue line shows estimated global wetland emissions from the CarbonTracker-CH4 inverse model (Bruhwiler et al. 2014a) that is constrained by global observations. Note that the LPJ-WHyMe model is missing from this graphic because it is not a global model and covers only high northern latitudes.

estimates from the CarbonTracker-CH4 global assimilation in which emissions were optimized using atmospheric network observations. Note that many of the models predict global emissions that are significantly higher than those implied by the observation network (as shown by the CarbonTracker-CH4 results).

Atmospheric observations and knowledge of the chemical lifetime of methane provide a cap on total emissions, but as discussed by Bruhwiler et al. (2014a) and Bergamaschi et al. (2013), the spatial distribution of the observation sites is generally not dense enough to distinguish between anthropogenic and wetland emissions at either the global or Arctic scale, although total emissions are well constrained. Sites located near areas with large anthropogenic or natural emissions would help to improve resolution of emission processes.

7.3.2 Evaluation of wetland models – results

The meridional (north-south) gradient of atmospheric methane concentration is a useful diagnostic of the distribution of methane emissions with latitude. A comparison of the observed and simulated meridional concentration gradient normalized to 90°S is shown in Fig. 7.7. Some of the models appear to overestimate wetland emissions, especially at high latitudes. In the northern mid-latitudes (20°–50°N), the models tend to exhibit a slower rise with latitude than observed, implying a low bias in anthropogenic emissions or an underestimate of wetland emissions or a combination of both at these latitudes. Transport that is biased towards atmospheric stability may also lead to higher atmospheric concentrations at lower levels making emissions appear to be overestimated. It should also be noted that the distribution of emissions from source regions to other latitudes is an important component of the atmospheric methane budget. Fig. 7.7 illustrates the importance of having global observations since ultimately the Arctic methane budget cannot be understood without knowing the potential contributions via transport from lower latitudes.

The observed and simulated average annual methane cycle at high northern latitudes (53°–90°N) is shown in Fig. 7.8.
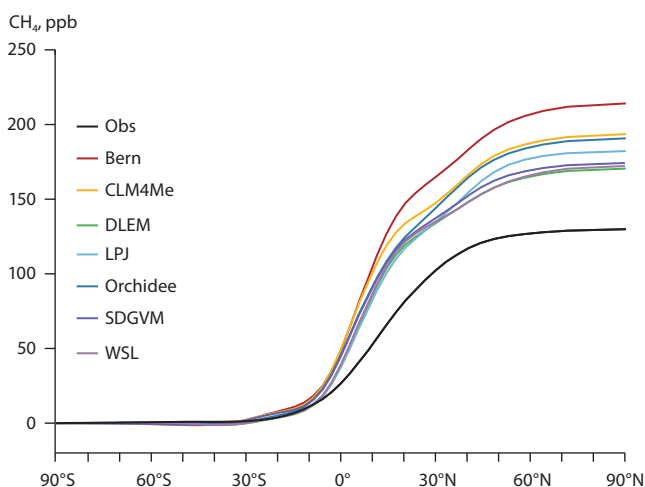
Fig. 7.7 Observed north-south CH_4 gradient normalized to 90°S from surface observations and simulations. Simulated concentrations were sampled at observation sites and averaged, smoothed and filtered identically to the observations. The graphic shows an average over the final year of the simulations, 2004.
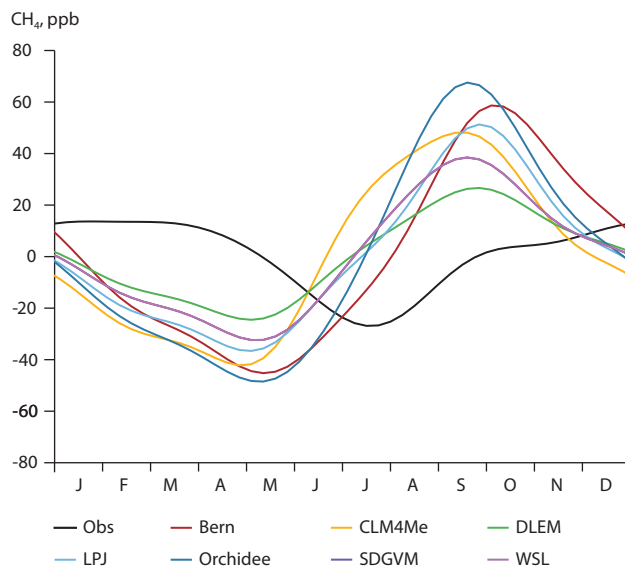
Fig. 7.8 Observed average annual cycle derived from surface methane observations (sites as per Fig. 6.5 for 53°–90°N) and wetland model simulations. Simulated concentrations were sampled at observation sites and averaged, smoothed and filtered identically to the observations.

Comparing the amplitude and phase of the seasonal variation provides an opportunity to assess whether the models capture the timing of the onset of wetland emissions during the warm season as well as the intensity of the emissions. The observations show a July minimum in atmospheric methane concentration due to chemical loss by reaction with OH that occurs most rapidly with the annual maximum in northern hemisphere incident solar radiation. The northern hemisphere summer is also when peak production of methane from wetlands occurs, and the fact that the chemical sink decreases rapidly after the solstice, while the wetland emissions are probably still strong and increasing, often results in a late summer plateau before the winter maximum (see Sect. 6.4.2). The maximum methane concentration occurs during the boreal winter when long-range transport brings methane emitted from anthropogenic and natural sources at lower latitudes into the Arctic, and chemical loss in the Arctic is effectively zero while being at an annual minimum at lower latitudes. In combination with this, local anthropogenic emissions and a very stable polar atmosphere that traps them within the region lead to a buildup of atmospheric methane within the Arctic.

The timing of the summer minimum concentration produced by the forward modeling provides clues about whether the wetland models have emissions too soon or too late in the growing season. As described in Sect. 7.2, the minimum in methane concentration occurs during summer because photochemical loss is greatest during the boreal summer throughout the northern hemisphere (see Ch. 2 and 6). The black line in Fig. 7.8 shows that the observed summer minimum occurs in mid-summer. Note that the seasonal cycle is not symmetric about the summer solstice as would be expected from solar irradiance-driven chemistry. Instead the data show a slight plateau late in the growing season. The models, on the other hand, show a spring concentration minimum followed by a distinct peak late in the growing season. The simulated annual cycles are consistent with overestimated wetland emissions because the annual minimum occurs too early, while methane concentration late in the growing season is too high relative

to the observations. Biases in simulated transport must also be mentioned, because a model that produces an overly-stable atmosphere can result in methane accumulation near the surface, making the apparent overestimation of emissions by the wetland models appear even worse. Overestimation of atmospheric stability is expected to be more of a problem during winter, and this would mean that methane emitted from anthropogenic sources would accumulate at lower levels of the atmosphere. This would tend to result in simulated winter methane concentrations that are higher than observed. However, Fig. 7.8 shows that simulated winter methane concentrations are lower than the annual average, unlike the observations that suggest winter concentrations that are greater than the annual average. This reinforces the idea that the differences in the observed and simulated seasonal cycles are dominated by excessive wetland emissions during the warm season.

Observed interannual variability in atmospheric methane provides an important test of the ability of wetland models to correctly simulate sensitivity to interannual variability in climate forcing parameters such as temperature and precipitation. As shown in Fig. 7.9, the observed Arctic region interannual variability in methane concentration after detrending and removing an average annual cycle suggests that variability is on the order of 20 ppb, a relatively small amount compared to a global average concentration of about 1750 ppb. This variability is thought to primarily reflect small changes in wetland and biomass burning emissions since anthropogenic emissions probably vary at longer timescales. Figure 7.9 suggests that with some exceptions, most models are able to reproduce the observed variability, indicating reasonably good representation of sensitivity of wetlands models to precipitation and temperature variability. Note that the trend towards slower simulated methane growth is due to equilibration of atmospheric methane concentration with the input emissions from each model. This is true for models that use different strategies for locating wetlands. The DLEM, CLM and WSL models use wetland distributions derived from satellite observations, while the SDGVM model predicts wetland distribution internally. Comparisons of longer time series that capture more events would provide greater confidence in the representation of interannual variability by wetland models.

7.4 **Conclusions**

7.4.1 **Key findings**

Inverse atmospheric modeling approaches provide the ability to optimally interpolate sparse observations and to estimate emissions. The estimates may be used to evaluate bottom-up emission models. Long time-series of estimated emissions may also be used to reflect how emissions are changing over time. The two major limitations to applying inverse techniques are sparseness of observations and inadequate representation of atmospheric transport. The lack of observations in inverse models, results in larger uncertainties in estimated emissions over policy-relevant spatial scales. In sparsely observed regions, the emissions will stay close to prior estimates that may have significant errors and biases (see Sect. 7.3). Errors in atmospheric transport also introduce concomitant errors in emission estimates

CH$_4$, ppb/y
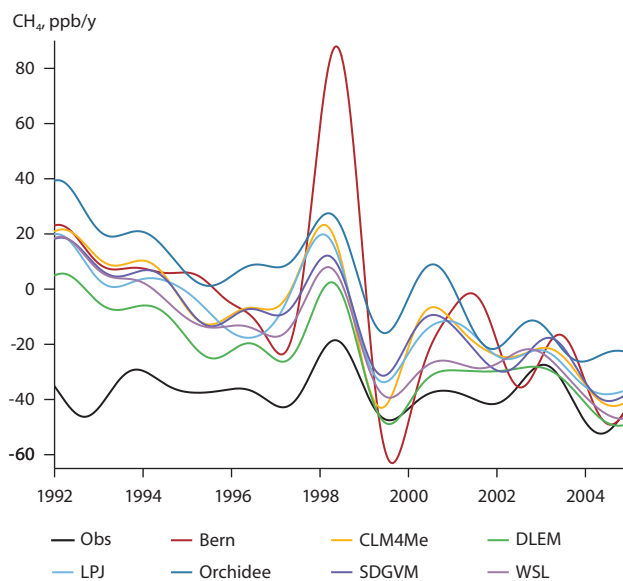
Fig. 7.9 Interannual variability in methane growth rate derived from surface observations and wetland model simulations (sites as per Fig. 6.5 for 53°–90°N). Simulated concentrations were sampled at observation sites and averaged, smoothed and filtered identically to the observations. An average seasonal cycle was removed from the time series to calculate the interannual variability.

that may be difficult to quantify. Inverse models can be improved if observational coverage is expanded, especially over currently sparsely observed regions. Improvements in bottom-up emission models will also help to reduce uncertainty of inverse models by providing more accurate prior emission information. Increasing the resolution of atmospheric transport models and improving the parameterizations of planetary boundary layers and convection will help to further reduce uncertainties in inverse models.

Arctic region natural and anthropogenic emission estimates from the ten atmospheric inverse model studies surveyed in the present study agree reasonably well (within ~40%) over the period 2000 to 2010 and total ~25 Tg CH$_4$/y. None of the inverse models show trends towards increasing emissions over this period; however, most do estimate increased emissions during the exceptionally warm and wet summer of 2007. This increase averages 2 Tg CH$_4$/y above the average over the period 2000 to 2010. The inverse model-derived methane emissions vary significantly in their interannual variability. Inverse models that put more weight on the 'priors' (i.e. the original emissions information used as input) which vary little from year to year will estimate emissions that consequently vary little from year to year. On the other hand, models that put more weight on observations will produce more temporal variability in flux estimates, some of which may be unrealistic. Improving observational coverage in the Arctic will reduce uncertainties and improve the reliability of inverse models. Improved observational coverage may also lead to earlier detection of changing emissions.

Atmospheric inverse models produce emission estimates that are significantly lower than those from bottom-up methods. Bottom-up methods suggest that Arctic wetland emissions alone are about 25 Tg CH$_4$/y, according to the study of McGuire et al. (2012). This is similar to the amount simulated by inverse studies for total Arctic emissions. The inverse models considered in this study estimate only 15.5 Tg CH$_4$/y for wetland emissions.

Indeed if all proposed Arctic sources are considered (such as emissions from lakes, the East Siberian Arctic Shelf and hydrates under permafrost), they significantly exceed the Arctic methane budget as understood from atmospheric methane concentration observations.

Given the importance of wetlands as a source of methane to the atmosphere, the ability to correctly model these natural emissions is important. This is key to integrating wetland processes within the earth system models to accommodate the carbon cycle - climate feedbacks that are required for studies of long-term responses to climate change. Bottom-up models of methane emissions from wetlands were used together with reasonable assumptions for non-wetland emissions and an atmospheric transport model to evaluate model performance against atmospheric observations. This forward modeling approach makes it possible to compare the results of process-based wetland models with atmospheric observations, providing the means to assess how small-scale, process-level information about emissions incorporated into process-based models is applied to regional and global scales.

In this review, the results of the atmospheric inverse model studies indicate that bottom-up models may overestimate emissions both globally and in the Arctic. In addition, although most models are able to reproduce the timing of observed variability, they tend to overestimate sensitivity to year-to-year variability in climate parameters (mainly temperature and precipitation).

None of the atmospheric inverse model results demonstrated an upward trend in emissions for the Arctic region over the period 2000 to 2010, as may be anticipated in response to steadily rising Arctic temperatures. Note however, that the period covered by the inverse models is only about a decade and this may be too short for detecting what may well be currently a small trend in emissions. The possibility that the atmospheric network observations are too sparse to allow detection of trends should also be considered, as well as limitations of atmospheric inverse models arising from representation of atmospheric transport processes, and/or initial estimates of the magnitude of natural and anthropogenic sources within the Arctic region.

7.4.2 Recommendations

The atmospheric inverse modeling technique is a powerful analytical tool that can increase understanding of the global and regional methane budget. Inverse techniques allow a look backwards in time to understand trends in atmospheric concentrations as a function of changing anthropogenic emissions and in response to a warming Arctic (i.e. increased release of methane from natural terrestrial and marine sources). They also serve as a useful diagnostic tool to evaluate the ecosystem process-based models, and thereby improve earth system models for climate projections (see Ch. 8). Recognizing the challenges in estimating the magnitudes of both the natural and anthropogenic sources identified in previous chapters, the inverse technique based on atmospheric observations provides an independent approach to verifying these process- or activity-based (bottom-up) estimates. The atmospheric observations define the maximum limits and temporal variability that serve as validation of the bottom-up estimates, indicating

where sources are over- or under-estimated. They also have the potential to identify missing sources or new sources in the characterization of emissions, such as those related to a warming Arctic or human activities.

Currently, atmospheric inverse models suffer from a lack of accessible high quality, multi-decadal atmospheric methane observations, both surface- and space-based. In addition, integration and collaboration related to improving atmospheric transport processes whether in terms of air quality, or climate or numerical weather prediction will lead to significant improvements in the overall representation of atmospheric transport. Novel approaches to measuring important diagnostic quantities (such as planetary boundary layer depth) can aid in this regard. Recognizing the aggregation of uncertainties and limitations inherent in the application of inverse methodology, recommendations to improve methane emission estimates based on their applications include:

- Increasing spatial coverage of surface observations, deployment of regular aircraft campaigns to characterize specific regions and seasons, and atmospheric column observations for vertical characterization of concentrations.

- Maintaining surface observation sites over multiple decades in order to detect changes in atmospheric concentration as a result of changing anthropogenic emissions, and the response of natural sources to changing climate.

- Further development and evaluation of ecosystem process-based models for estimating wetland sources.

- Continuing improvements to atmospheric transport simulations to better represent convection and planetary boundary mixing processes at smaller spatial scales.

Acknowledgments

Appendix: Global atmospheric inverse model studies reviewed for the comparison discussed in Section 7.2.4.

	B-K	B-NOAA	B-ref	Bg	CT-CH4	Fr	H-NOAA	H-SCIA	H-GOSAT	Pison
Reference	Bousquet et al. 2011; Kaplan 2002	Bousquet et al. 2011	Bousquet et al. 2011; Kirschke et al. 2013	Bergamaschi et al. 2013	Bruhwiler et al. 2014a	Fraser et al. 2013	Houweling et al. 2014	Houweling et al. 2014	Houweling et al. 2014	Pison et al. 2009
Observations	Surface network sites and IMAPv5.5 SCIAMACHY retrievals	Surface network sites	Surface network sites and IMAPv5.5 SCIAMACHY retrievals	Background surface network sites and IMAPv5.5 SCIAMACHY retrievals	Surface network sites	Surface network sites	Surface network sites	Background surface network sites and IMAPv5.5 SCIAMACHY retrievals	Background surface network sites and GOSAT retrievals	Surface network sites
Prior Emissions	EDGARv3.2, GFEDv2, Matthews (1989)	EDGARv3.2, GFEDv2, Matthews (1989)	EDGARv3.2, GFEDv2, Matthews (1989)	EDGARv4.1, GFEDv3.1, Kaplan (2002)	EDGARv3.2 (for 2000), GFEDv3, Matthews (1989)	EDGARv3.2, GFEDv2, Houweling et al. (1999)				
Chemical Sink	OH from atmospheric chemistry model	OH from atmospheric chemistry model	OH from atmospheric chemistry model	Computed by TM5 with full chemistry	Computed by TM5 with full chemistry	OH from atmospheric chemistry model	Computed by TM5 with full chemistry	Computed by TM5 with full chemistry	Computed by TM5 with full chemistry	OH from atmospheric chemistry model
Transport Model	LMDZ	LMDZ	LMDZ	TM5	TM5	GEOS-CHEM	TM5	TM5	TM5	LMPDZ
Meteorology	LMDZ online nudged to ERA40	LMDZ online nudged to ERA40	LMDZ online nudged to ERA40	ECMWF ERA-I	ECMWF Forecast	GEOS-5	ECMWF ERA-I	ECMWF ERA-I	ECMWF ERA-I	LMDZ online nudged to ERA40
Transport Model Resolution	3.75°×2.5°, 19 levels	3.75°×2.5°, 19 levels	3.75°×2.5°, 19 levels	6°×4°, 25 levels	6°×4°, 25 - 34 levels	5°×4°, 47 levels	6°×4°, 25 levels	6°×4°, 25 levels	6°×4°, 25 levels	3.75°×2.5°, 19 levels
Time Resolution of Emission Estimates	Monthly	Monthly	Monthly	Monthly	Weekly	8 Days	Monthly	Monthly	Monthly	Weekly
Spatial Resolution of Emission Estimates	Grid cell	Grid cell	Grid cell	Grid cell	120 land regions and 1 global ocean region	99 land regions and 11 ocean regions	Grid cell	Grid cell	Grid cell	Grid cell
Optimization Technique	Variational	Variational	Variational	m1qn3	Ensemble Kalman Smoother	Ensemble Kalman Filter	m1qn3	m1qn3	m1qn3	m1qn3
Time Window	1983–2010	1983–2010	1983–2010	2003–2010	2000–2010	2000–2010	2003–2010	2003–2010	2003–2010	1990–2008

8. Modeling the climate response to methane

Lead authors: Michael Gauss, Vivek K. Arora

Contributing authors: Charles D. Koven, Dirk J.L. Olivié, O. Amund Søvde, Lena Höglund-Isaksson, Torben R. Christensen, Frans-Jan W. Parmentier, David A. Plummer

8.1 Introduction

Computer models of the atmosphere and other components of the Earth System have been widely used for decades in the scientific community to gain insight into air pollution and climate change beyond what can be learned from measurements and paleo data. Such models allow an understanding of the processes behind observed distributions of chemical species in the atmosphere, and make it possible to assess the effects of past and potential future trends in anthropogenic and natural emissions of various trace gases on atmospheric composition and climate.

This chapter addresses the effect of changes in methane emissions, both from anthropogenic and natural sources, on concentrations of atmospheric methane (in this chapter referred to just as 'methane') and climate. A broad overview of projected climate change in the Arctic, and all associated impacts, was beyond the more narrowly focused mandate of this study. Readers are referred to earlier Arctic Monitoring and Assessment Programme (AMAP) reports for such information (e.g. ACIA 2004, 2005; AMAP 2011a). There was also no attempt to model changes in natural emissions of methane; estimates were based on Ch. 3 and 4 of this report.

The work for this chapter was undertaken in support of the Arctic Council's considerations of the contributions of short-lived climate forcers (SLCFs) to Arctic warming (see Ch. 1). This chapter presents results regarding the climate response, at both global and Arctic scales, to changes in methane concentration for the past and future. The results are obtained through applying different types of model.

The atmospheric lifetime of methane of about 9 years (Ch. 2) is short compared to many other greenhouse gases (carbon dioxide, nitrous oxide, sulfur hexafluoride, halocarbons), but relatively long compared to traditional air pollutants such as nitrogen oxides, particulate matter, etc. Since the lifetime of methane is long enough for it to be well mixed in the troposphere (spatial variability within ±3%) and since measurements of historic methane concentrations are available from ice cores, it has been common practice to *prescribe* methane concentrations in atmospheric composition and climate models rather than calculating them. Methane concentrations for the past and present-day can be derived, to good approximation, from measurements either as global-mean or zonal-mean values with an estimated latitude distribution. The values are then used as input to atmospheric chemistry models which calculate the distribution of chemical species other than methane, and to radiation schemes which calculate the radiative forcing of climate.

Among other objectives, the Methane Expert Group was tasked with quantifying the importance of past and potential future changes in methane emissions and concentrations on Arctic climate. Benefits of possible mitigation measures for methane emissions, globally and in the Arctic nations, were to be estimated.

The use of simple globally-averaged metrics such as Global Warming Potential (GWP) or Global Temperature change Potential (GTP) (see Box 8.1 for definitions) is not sufficient if the objective is to understand, for example, the meridional variation of the climate system response over time to a change in atmospheric composition and forcing. While regional metrics such as the Absolute Regional Temperature Potentials (ARTP; Shindell 2012) do provide the ability to estimate the surface air temperature change in a specific area (e.g. the Arctic) within a chosen time horizon in response to emissions in another region (e.g. the entire globe), there is still a large gap between the spatial scales of information available from the ARTP and that needed for impact assessments (Shindell 2012). Hence, for this study

---

Box 8.1 Key terminology

Global warming potential (GWP)	The radiative forcing due to a pulse emission of a unit mass of a given greenhouse gas in the present-day atmosphere, integrated over a chosen time horizon, relative to that of carbon dioxide (Houghton et al. 1990; Myhre et al. 2013).
Global temperature change potential (GTP)	The change in global-mean surface air temperature at a chosen point in time in response to an emission pulse – relative to that of carbon dioxide. Whereas GWP is integrated over time, GTP is an end-point metric based on temperature change for a selected year (Shine et al. 2005; Myhre et al. 2013).
Methane concentration	In referring to methane abundance, the term *concentration* is used throughout the report, although in using this term what is being expressed is technically a *mole fraction* (given in units of *parts per billion*, ppb).
Model ensemble	Model predictions or projections of climate are often performed as *ensembles*, that is, a number of model simulations of the same period using different initial conditions (if one model is used) or different model formulations (when several models are used). Differences between the modelled climate evolutions across the members of the ensemble may give information on uncertainty associated with model error, errors in initial conditions, or internally generated climate variability.
Prognostic variable	The term 'prognostic' in the context of the present study means that the spatial distribution and temporal variation of the species in question (in this case methane) are calculated explicitly in the model rather than being prescribed from observations. To this end, the model must include detailed emission data and loss terms, and calculate transport and transformation of the species in the atmosphere.

a number of dedicated model experiments were performed to calculate future methane concentration changes in response to changes in methane emissions, and to estimate the resulting climate change in the Arctic in terms of changes in annual-averaged near-surface air temperatures. Emission data for natural and anthropogenic sources are based on Ch. 3, 4, and 5.

The questions addressed in this chapter are:

What is the contribution of historical changes in global atmospheric methane to Arctic climate warming?

What impact will increasing atmospheric concentrations of methane have on climate and will Arctic nations have the ability to influence that impact through mitigation of anthropogenic methane emissions?

How will atmospheric methane concentrations change in response to potential changes in natural methane emissions and how do these changes compare to those that might result from mitigation of anthropogenic methane emissions?

Does the location of anthropogenic methane emissions matter?

8.2 Climate effects of historical changes in methane concentration

To calculate the effects of historical changes in methane concentration on climate until present-day, the Canadian Earth System Model (CanESM2; Arora et al. 2011) was run with and without time-varying methane concentrations from year 1850 to 2005. (For the purposes of this study, 1850 is used to define the beginning of the industrial era and 2005 is used to define the present.) CanESM2 consists of coupled dynamical atmosphere and ocean models with full marine and terrestrial carbon cycle components. The first set of simulations is the ensemble of five standard historical simulations, which contributed to the set of coordinated experiments (http://cmip-pcmdi.llnl.gov/cmip5/) performed for phase 5 of the coupled model intercomparison project (CMIP5), that is, with specified concentrations of all greenhouse gases increasing over the historical 1850–2005 period, together with changing land cover and emissions of aerosols. In these simulations, methane concentration increased from 791 to 1754 ppb between 1850 and 2005. The global-mean surface air temperature increase modeled over the 1850–2005 period (calculated as the difference between the 1851–1865 and 1991–2005 periods) amounts to 0.81°C and compares well to the observation-based estimate reported by the Intergovernmental Panel on Climate Change in its Fifth Assessment report (IPCC AR5). According to the IPCC (Hartmann et al. 2013), the globally averaged combined land and ocean surface temperature data show a warming of 0.85°C (0.65–1.06°C) over the period 1880–2012, when multiple independently produced datasets exist. The total increase between the average of the 1850–1900 and 2003–2012 periods is 0.78°C (0.72–0.85°C), and between the average of the 1850–1900 and 1986–2005 periods is 0.61°C (0.55–0.67°C), based on the single longest dataset available.

In the second set of simulations, also a five-member ensemble, the methane concentration was fixed at its year 1850 level (791 ppb) throughout the 1850–2005 period, while all other forcings remained the same as in the first simulations. Thus, the difference in climate between the two sets of simulations represents the climate response due to changes in methane concentration from 1850 to present-day.

To quantify the effect of historical changes in methane concentration on present-day climate, the assessment focuses on the average over the 15-year period 1991–2005. Due to the inertia in the climate system, present-day climate is influenced not only by present-day greenhouse gas concentrations but also by their concentrations in the past. Figure 8.1 shows the temperature change calculated from the difference between the two sets of simulations described in the previous paragraph. The analysis suggests that the effect of changes in methane concentration since the pre-industrial period has been to enhance warming by around 0.31±0.02°C (mean ± standard deviation) when averaged globally, and by 0.58±0.11°C when averaged over the Arctic (north of 60°N). The standard deviation of the sampling distribution of the differences in means of the temperatures, for the period 1991–2005, for the simulation with all forcings (S1) and the simulation with methane concentration at its 1850 value (S2) is calculated as:

$$\sqrt{\left(\sigma_{S1}^{2} + \sigma_{S2}^{2} \right)/n} \qquad \text{Eq. 8.1}$$

where σ_{S1}^{2} the variance of the temperatures for the S1 case, and similarly for the S2 case, and n=5.

The larger response in the Arctic compared to the global response is associated with the Arctic amplification of greenhouse gas-induced warming, caused by various factors including feedbacks in snow- and ice-albedo, ocean heat transport, cloudiness and longwave radiation (Collins et al. 2013; Pithan and Mauritsen 2014). The Arctic amplification factor is generally accepted to be

Change in global average surface air temperature caused by methane, °C
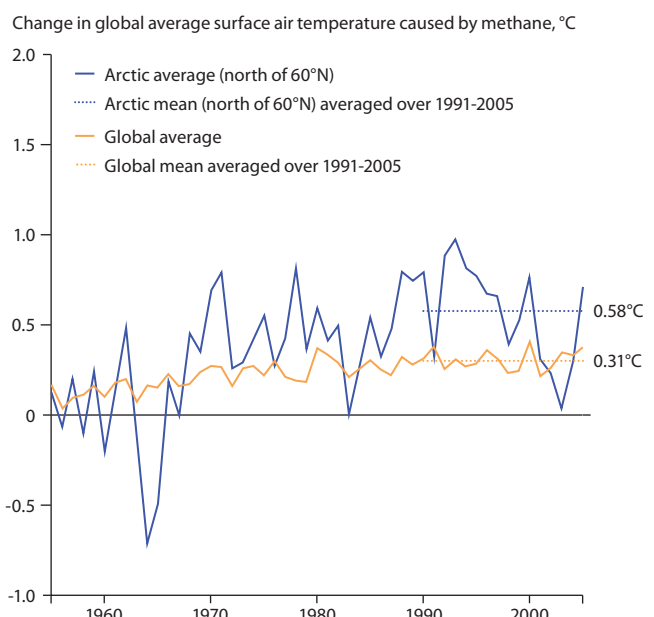
Fig. 8.1 Surface air temperature change caused by the increase in methane concentrations since 1850, as calculated by the Earth System model CanESM2. Temperature change is calculated as the difference between the model simulations with varying (historical) methane concentrations and the model simulations where methane was fixed at its year 1850 concentrations.

around two, meaning that the Arctic region has warmed more than twice as fast as the global average (Cohen et al. 2014). For CanESM2 this value is 0.58/0.31=1.87.

Figure 8.1 also shows that the simulated climate response to methane is more variable in time over the Arctic. This is expected, given the inherent higher natural climate variability in the Arctic but also the smaller area (compared to the whole globe) over which the response is averaged.

In this context it is worth noting that increases in emissions of methane since 1850 have also affected other climate forcers such as ozone, carbon dioxide and stratospheric water vapor. The radiative forcings of those climate forcers is not taken into account in the approach applied here, which looks at the climate response to methane *concentration* change only. Nevertheless, this approach is able to identify the warming response to greenhouse gases and is typically used for climate detection and attribution studies (e.g. Gillett et al. 2012).

8.3 Effects of changing anthropogenic and natural methane emissions

Ideally the effect of future changes in methane emissions on climate would be addressed using Earth System Models (ESMs) that treat methane as a prognostic variable (see definition in Box 8.1) and take into account all relevant feedbacks between the atmosphere and other components of the Earth System as well as interactions between climate change and atmospheric chemistry. Simulating atmospheric methane concentration as a prognostic variable in ESMs requires to model a range of processes that calculate its surface-atmosphere exchange (including emissions from wetlands and fires, and the soil sink) and atmospheric chemistry processes that determine methane's loss rates in the atmosphere (e.g. Collins et al., 2011). As a result of this complexity, only a handful of ESMs currently have this ability. Only few ESMs currently simulate atmospheric methane concentration as a prognostic variable with chemistry-climate interactions (e.g. Collins et al. 2011; Shindell et al. 2013) although efforts are underway to include this functionality in other such models. In the absence of this functionality, a combination of various modeling approaches were chosen for the present study. A Box model and a Chemistry Transport Model (CTM) were used to calculate changes in methane concentration in response to emission scenarios based on earlier chapters of this report. The concentrations were then used in different ESMs to calculate the climate response. For a short description of the different types of model see Box 8.2. A summary table of all ESM simulations performed for this assessment is provided in Sect. 8.4.1. It should be noted that the climate response to abatement of emissions of non-methane climate forcers is not addressed in this report. For aspects on mitigation of SLCFs in relation to carbon dioxide mitigation, readers are referred to other publications in the recent literature (e.g. Shoemaker and Schrag 2013; Pierrehumbert 2014; Rogelj et al. 2014).

8.3.1 Box model – Earth System Model calculations

To assess the future impact of changes in methane emissions on climate, a Box model was run to calculate the time-dependent

Box 8.2 Types of model

A *Box model*, in the context of this study, is a globally-averaged representation of atmospheric concentration of a given trace gas. More specifically, the Box model employed by the Methane Expert Group uses global methane emissions as input and calculates the temporal evolution of the resulting global-mean methane concentration. Alternatively, the globally-averaged methane concentration can be specified as an input, and the model can be used to calculate the emissions that would have led to a given methane concentration pathway. In both applications, the Box model takes into account the effect of changes in methane concentration on methane lifetime (Ch. 2).

Chemistry Transport Models (CTMs) are used to calculate three-dimensional distributions of chemical species in the atmosphere, using spatially resolved emission data. They usually include detailed atmospheric chemistry calculations, represent the transport and removal of various chemical species and are typically driven by meteorological data specified via external sources (e.g. reanalyses or climate model output). In their typical application, CTMs do not allow for any feedback from chemistry to meteorology.

Earth System Models (ESMs) represent the interactions between the physical components of the climate system (land, atmosphere and ocean in three dimensions) but also include interactions between the physical climate system and the terrestrial and oceanic carbon cycles, nitrogen cycles and other biogeochemical cycles. Other interactions and processes may also be included, such as representation of aerosols and atmospheric chemistry. Due to the high computational demand, ESMs are typically run at a grid resolution of 1° to 2° (~100–200 km) and many processes must be parameterized.

global average concentration of methane. The concentrations were then used in two ESMs: the Canadian Earth System Model CanESM2 (see Sect. 8.2) and the Community Earth System Model CESM1-CAM5 (Neale et al. 2012), hereafter referred to as 'CESM1', to calculate the climate response in terms of changes in average surface air temperature. CESM1 consists of coupled land (CLM4), ocean (POP), and atmosphere (CAM5) models.

8.3.1.1 Response to changes in anthropogenic emissions

The International Institute for Applied Systems Analysis (IIASA) has provided three anthropogenic methane emission scenarios calculated by the GAINS integrated assessment model to year 2050, referred to as 'ECLIPSE (2012) scenarios' (see Sect. 5.5):

- The current legislation scenario ('CLE') describes the most likely future anthropogenic emission pathway when the current state of technology prevails and any further emission reductions are limited to those prescribed by currently adopted legislation.

- The maximum technically feasible reduction scenario ('MFR') describes the future emission pathway when existing mitigation technology is applied with current effectiveness to a maximum feasible extent globally.

- The 'MFR-AC8' scenario describes the case where these mitigation options are applied in the eight Arctic nations only, while all other countries follow CLE.

See Ch. 5 for detailed descriptions of the three anthropogenic methane emissions scenarios used as input for modeling the climate benefits from methane mitigation.

Table 8.1 lists the global total methane emissions for these scenarios (see also Fig. 5.9), as well as other scenarios used later in this chapter (see Sect. 8.3.1.2 and 8.3.2.3). In CLE, anthropogenic methane emissions increase from 323 to 439 Tg CH_4/y between 2005 and 2050, while in MFR they decrease from 323 to 222 Tg CH_4/y in 2030, then rise slightly to reach 234 Tg CH_4/y in 2050. In MFR-AC8 the total global emissions increase, because the maximum technically feasible reduction that can be achieved in the Arctic nations cannot compensate for the increase in emissions in the rest of the world in this scenario. Nevertheless, the emissions in 2050 in MFR-AC8 amount to 396 Tg CH_4/y, which is 43 Tg CH_4/y lower than the emissions in 2050 in the CLE case. As shown in Fig. 5.9, the CLE, MFR, and MFR-AC8 scenarios are identical until 2015 and start differing only thereafter.

For natural emissions, a global source of 202 Tg CH_4/y was used, with a specified uncertainty (±28 Tg CH_4/y) following Prather et al. (2012) and references therein. When assessing the effect of reductions in anthropogenic methane emissions, it was assumed that natural emissions remain constant at this level. The sensitivity of changes in atmospheric methane concentration for the CLE and MFR-AC8 scenarios to different assumptions about increase in natural emissions was also tested, in order to compare the effect of changes in natural emissions to the effect of maximum technically feasible reductions in anthropogenic emissions by the eight Arctic nations. These experiments are described in Sect. 8.3.1.2.

A crucial step for performing future climate simulations is to translate the changes in emissions to changes in concentrations, which can then be used in ESMs to assess the potential climate benefits of reductions in anthropogenic methane emissions. A Box model was used by the Methane Expert Group. The one-box model for global-mean atmospheric

methane concentration was developed at the Canadian Centre for Climate Modelling and Analysis and is described in the appendix to this chapter. To evaluate the Box model, it was first necessary to calculate anthropogenic methane emissions over the historical period that are consistent with the observed historical increase in atmospheric methane concentration and observation-based estimates of methane life time from Prather et al. (2012). It was found that the calculated historical anthropogenic emissions compared well with other inventory-based estimates. For 2005, the Box model-calculated methane anthropogenic emissions are 314±33 Tg CH_4/y (mean ± standard deviation) compared to an observation-based estimate of 352±45 Tg CH_4/y (Prather et al. 2012). It is also within the range of estimates listed in Table 5.3. For estimates of future methane concentration, the application of the Box model was reversed: The anthropogenic methane emissions from the three GAINS scenarios were used as input, and the resulting atmospheric methane concentrations were calculated.

Figure 8.2 shows observed methane concentrations for the historical period together with the Box model-calculated concentrations for future emissions under the three GAINS scenarios. By 2050, the difference in concentrations between the CLE and MFR scenarios is around 840 ppb. If maximum technically feasible reductions are applied only in Arctic nations (MFR-AC8) then global-mean methane concentrations continue to increase, but at a lower rate compared to the CLE scenario. The 2050 global-mean methane concentration for MFR-AC8 is calculated to be about 200 ppb lower than for the CLE scenario.

The future methane concentrations calculated by the Box model were then used in the CanESM2 and CESM1 to calculate the climate response in terms of average surface air temperature change to maximum technically feasible reductions in global anthropogenic emissions. ESMs need concentrations of all

Table 8.1 Total global methane emission values used in this assessment.

Scenario		Emissions, Tg CH_4/y		
		2005	2030	2050
Anthropogenic emissions	CLE[a]	323	414	439
	MFR[a]	323 (=CLE)	222	234
	MFR-AC8	323 (=CLE)	371	396
	Arctic205	323 (=CLE)	-	439 (=CLE)
Natural emissions	Baseline	202	202	202
Assumed *increase* in natural emissions since 2005	'low'	-	14	25
	'high'	-	28	50
	'extreme'	-	56	100

[a] Referred to as 'CLE, 2012ii' and 'MFR, 2012ii' in Table 5-6 (ECLIPSE 2012). When the model calculations for this assessment had to start, these were the latest emission data sets. The mitigation potential in ECLIPSE 2012 is estimated at 192 Tg CH_4/y for 2030 and 205 Tg CH_4/y for 2050, consistent with the anthropogenic emission totals listed for CLE and MFR in this table.

Global mean CH_4, ppb

Fig. 8.2 Evolution of global-mean methane concentrations. The emission data used from 2005 are from ECLIPSE 2012 (see Sect. 5.5). Uncertainty in future atmospheric methane concentrations is the result of uncertainties in methane lifetime and in natural emissions.

Box 8.3 Blending scenarios

The Box model-calculated methane concentrations for the CLE and MFR scenarios are not sufficient to explore the climate impact of reductions in methane emissions in a coupled atmosphere-ocean model. For that purpose, concentrations of other greenhouse gases (carbon dioxide, nitrous oxide, chlorofluorocarbons) and, if treated prognostically, emissions of aerosol species and ozone precursors are also needed. The complete set of forcings is available for the Representative Concentration Pathway scenarios (RCPs) (Meinshausen et al. 2011) used for CMIP5 but not for the CLE and MFR scenarios. On the other hand, the GAINS scenarios are needed to study the individual impact of methane mitigation. The methane concentrations in the RCP6.0 scenario were therefore replaced by those corresponding to the CLE and MFR scenarios while the concentrations of all other greenhouse gases and emissions of aerosols were retained, resulting in two blended scenarios – RCP6.0-CLE and RCP6.0-MFR – which differ *only* in terms of methane emissions. (Emissions of ozone precursors other than methane were not used in the CanESM2 and CESM1 models. However, the temperature change due to methane-induced ozone change was estimated through a scaling approach (see Box 8.4), and calculated by NorESM (Sect. 8.3.2.2).) The RCP6.0 scenario was chosen among the RCPs because it is most consistent with the GAINS scenarios (being based on similar assumptions regarding population growth, GDP growth, energy intensity, etc.).

The assumption with this blended scenario approach is that, regardless of the climate change caused by non-methane greenhouses gases, the difference between the RCP6.0-CLE and RCP6.0-MFR scenarios should provide an estimate of the potential benefit of the maximum technically feasible reduction in methane emissions. Nevertheless, in order to test the validity of this assumption, methane concentrations from the CLE and MFR scenarios were also blended with the RCP8.5 scenario giving two additional scenarios – RCP8.5-CLE and RCP8.5-MFR.

This blending approach is further justified by the fact that methane mitigation in the MFR scenario does not affect the emissions of other radiatively important species (see Sect. 5.5).

greenhouse gases and, if aerosols are treated prognostically, emissions of aerosol species and their precursors. Since the GAINS data sets do not provide information for non-methane greenhouse gases and other climate forcers, simulated methane concentrations for the CLE and MFR scenarios from the Box model were blended with non-methane forcings from two future climate change scenarios (RCP6.0 and RCP8.5), resulting in four blended scenarios (for details see Box 8.3).

The simulated changes in globally-averaged surface air temperature are shown in Fig. 8.3 for the period 2006–2050, using the blended scenarios RCP6.0-CLE, RCP6.0-MFR, RCP8.5-CLE and RCP8.5-MFR, along with the estimated uncertainty based on three ensemble members that were run by both ESMs and for each of the scenarios. All simulations were initialized from the end of the 1850–2005 CMIP5 simulations. Temperature change is plotted with respect to the 2006–2010 average. As reported in the Working Group I Contribution to the IPCC AR5 (Flato et al. 2013 their table 9.5), the transient climate response (TCR; which is a measure of the temperature response to a doubling in carbon dioxide based on the simulation in which carbon dioxide increases at a rate of 1% per year) is model-dependent. The TCR values for CanESM2 (2.4°C) and CESM1 (2.3°C) are similar. For the scenarios considered here, the simulated temperature increase over the 2006–2050 period (reflected by the general slope of the curves in this graphic) is therefore also similar in the two ESMs, with about 1°C warming in the RCP6.0 cases and about 1.5°C in the RCP8.5 cases. The difference between the RCP6.0 and RCP8.5 cases is consistent with the higher concentrations of non-methane greenhouse gases in RCP8.5, as compared to RCP6.0. The increase in temperature of about 1.0 and 1.5°C in the RCP6.0 and RCP8.5 scenarios, respectively, compares well to the near-term climate change projections for the same scenarios in IPCC AR5 (Kirtman et al. 2013 their fig. 11.24a).

The difference between the dark red and blue lines in Fig. 8.3 represents the effect of maximum feasible reductions in methane emissions, when implemented globally. In CanESM2, the MFR scenario yields a global-mean temperature that is 0.18±0.05°C (mean ($\bar{x}$) ± standard deviation[6] (σ_x)) lower than that in the CLE scenario, when using RCP6.0 as the background scenario, and 0.18±0.03°C lower when using RCP8.5, averaged over the period 2036–2050. The temperature benefit of maximum feasible reductions in methane emissions based on CESM1 simulations is smaller: 0.07±0.04°C and 0.11±0.05°C when using the RCP6.0 and RCP8.5 as background scenarios, or averaged equal to 0.09±0.03°C based on both scenarios for the same period. The $\bar{x} + 1.385\,\sigma_x$ range, which corresponds to 83.4% confidence intervals, from CanESM2 and CESM1 overlap, for the respective background RCP scenarios, so the estimates of reduced warming from the two models are not statistically different at the 95% confidence level (Knol et al. 2011).

Since the prescribed methane concentration data were the same in the CanESM2 and CESM1 simulations, differences may be related to the calculations of radiative forcing due to methane (e.g. Collins et al. 2006) and of the climate response to that change in radiative forcing. The global-mean climate response to a given amount of radiative forcing varies for different greenhouse gases, according to their efficacy (Hansen et al. 2005). A much deeper analysis would be needed to fully resolve the sources of difference between the model results. As a first step, the radiative forcing caused by the methane change should be diagnosed. However, this would require additional model runs, which were not possible within the time frame of this study.

---

6 The standard deviation of the sampling distribution of the differences in means of the temperatures corresponding to CLE and MFR scenarios for the period 2036–2050, which is in fact the standard error, is calculated as $\sqrt{(\sigma^2_{CLE} + \sigma^2_{MFR})/n}$ where σ_{CLE} is the variance of the temperatures for the CLE scenario, and similarly for the MFR scenario, and n=3. In order to increase the signal-to-noise ratio, more than three simulations should have been performed for each of the CLE and MFR versions of the RCP6.0 and RCP8.5 scenarios but this was not possible owing to limited time and computing resources.

Change in global average surface air temperature, °C

Change in global average surface air temperature, °C

Change in global average surface air temperature, °C

Change in global average surface air temperature, °C

— CLE CH$_4$ emissions   — MFR CH$_4$ emissions
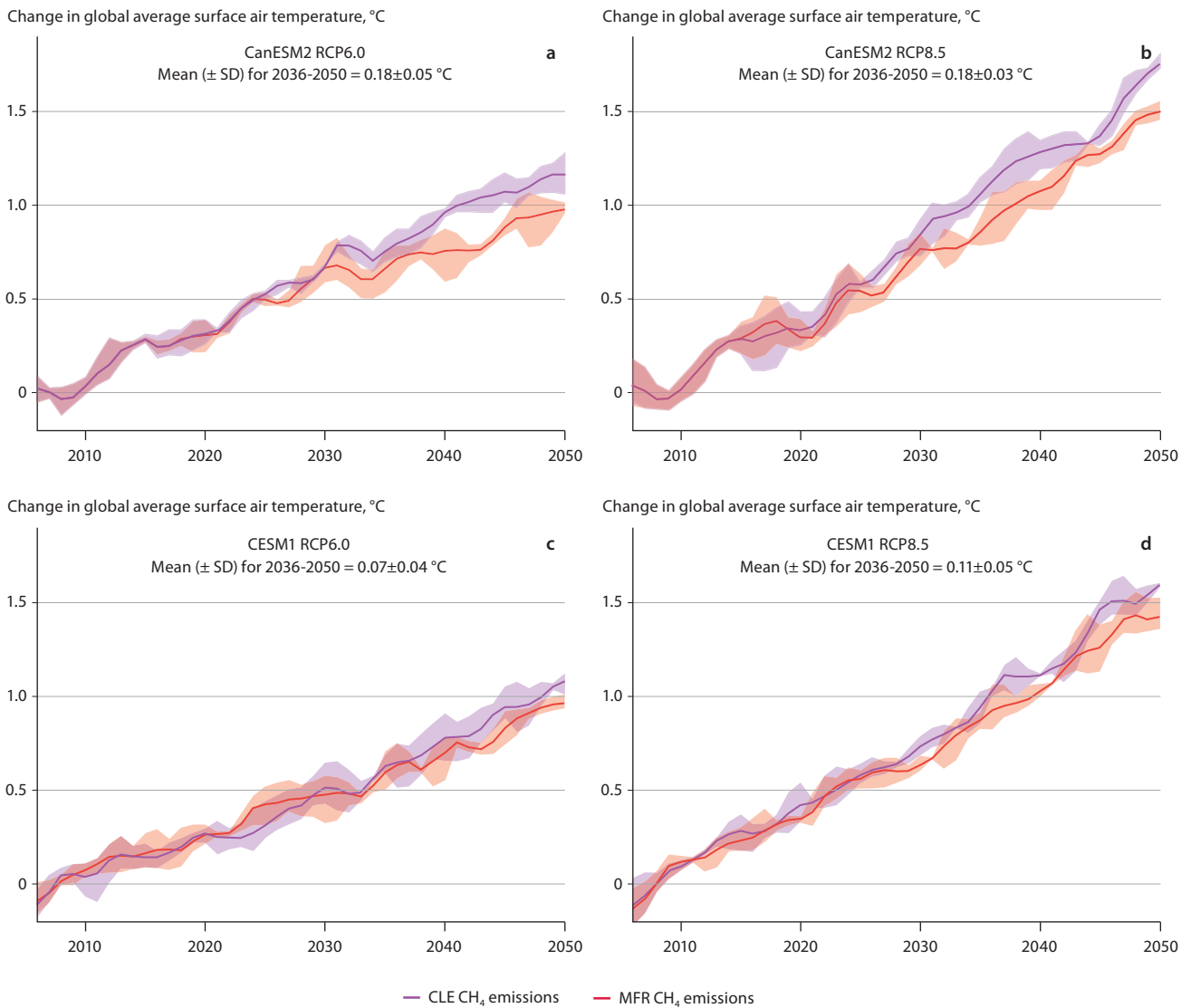
Fig. 8.3 Modelled global-mean surface air temperature increase, with respect to the 2006–2010 average, as calculated by CanESM2 (a and b) and CESM1 (c and d). The bold lines and shaded areas show, respectively, the means and range across the three ensemble members that have been run for each scenario. As described in Box 8.3, the models use climate forcers other than methane from the RCP6.0 and RCP8.5 scenarios, while methane is based on either CLE (purple lines) or MFR (red lines). Note that climate change is mainly driven by the carbon dioxide increase prescribed by the RCP scenarios. The difference between the red and purple lines represents the effect of maximum technically feasible reductions in methane emissions, when implemented globally. It should be noted that in the case of CanESM2 this difference does not include the ozone and stratospheric water vapor effects, while in the case of CESM1 only the ozone effect is not included.

Nevertheless, results from both models give a clear indication that maximum technically feasible reduction in global methane emissions will lead to a reduction in global warming. When judging the magnitude of this reduction, it should be remembered that this is the result of abatement of one greenhouse gas only, and that the effects of ozone (CanESM2, CESM1) and stratospheric water vapor (CanESM2) are not included. Scaled results taking into account these effects are presented at the end of this section.

Figure 8.4 shows the zonally-averaged temperature response to maximum technically feasible reduction in methane emissions, that is, the difference between the RCP6.0-CLE and RCP6.0-MFR simulations (blue curves) and between the RCP8.5-CLE and RCP8.5-MFR simulations (green curves), based on the three ensemble members by each of the two models for each of the scenarios. The reduced warming due to maximum technically feasible reduction in methane is predominant almost everywhere, although the variability (indicated by the ± standard deviation range) in the temperature difference

between the CLE and MFR simulations is very large in northern high latitudes since the Arctic temperature is inherently more variable. When averaged over the Arctic region (north of 60°N), CanESM2 calculates a reduction in warming of 0.40±0.14°C and 0.35±0.17°C over the period 2036–2050, when using the RCP6.0 and RCP8.5 as background scenarios, respectively. In the CESM1 these numbers are 0.26±0.26°C and 0.33±0.25°C. The Arctic temperature response is a net outcome of many different processes and feedbacks (such as changes in ocean currents, atmospheric circulation, ice/snow albedo feedback, etc.), and explaining the difference between the CanESM2 and CESM1 results in this regard is beyond the scope of this work.

Given the large variability across the ESMs in the climate response to changes in methane emissions, especially in the Arctic, the additional simulation of the MFR-AC8 scenario did not seem worthwhile. The difference between the CLE and MFR-AC8 emissions is much smaller than between the CLE and MFR emissions, so that the climate response would have been even more difficult to model with reasonable accuracy.

Near-surface temperature change, °C

Near-surface temperature change, °C
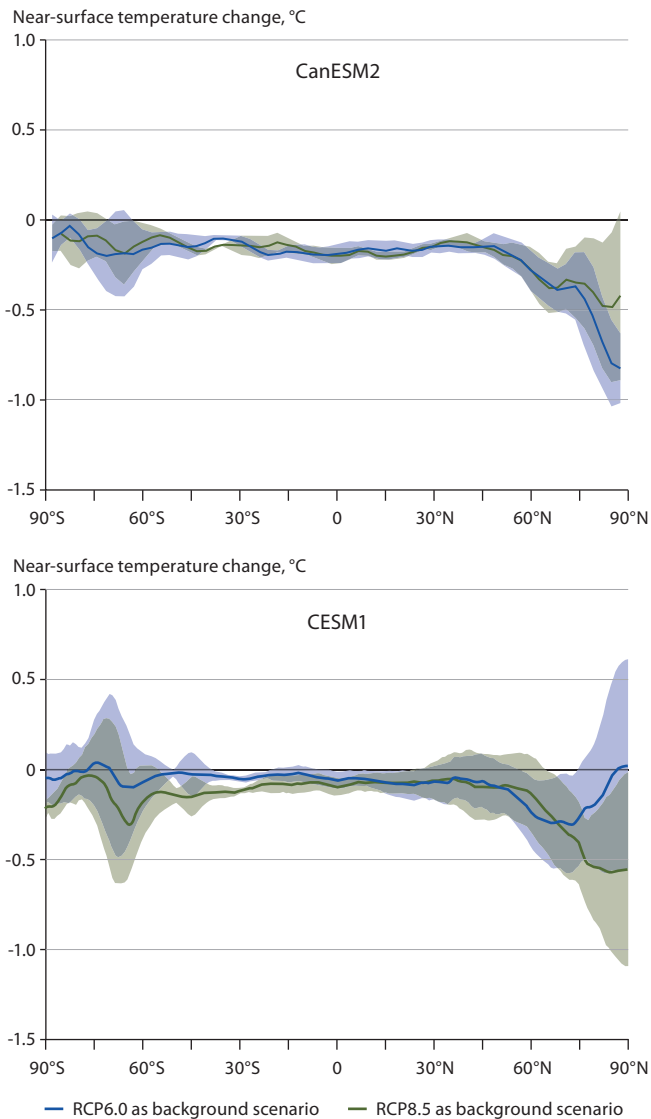
Fig. 8.4 Changes in zonal-mean surface air temperature due to reduction in anthropogenic methane emissions (i.e. MFR minus CLE), as calculated by CanESM2 (upper) and CESM1 (lower). Shaded areas indicate standard deviations[6] based on three ensemble members. It should be noted that in the case of CanESM2 this difference does not include the ozone and stratospheric water vapor effects, while in the case of CESM1 only the ozone effect is not included.

However, as the methane concentration in the MFR-AC8 scenario falls between those for CLE and MFR, but closer to CLE, it may be assumed with confidence that the climate response would fall somewhere between those modelled for CLE and MFR, but closer to CLE (i.e. the blue lines in Fig. 8.3). A simple scaling method, based on the numbers for global-mean methane concentrations given in Fig. 8.2 and the results for climate response given above, suggests that the reduction in global-mean surface air temperature due to changes in methane emissions in the MFR-AC8 scenario would be less than one tenth of a degree.

As previously mentioned, the ensemble-based estimates of reduced climate warming in response to maximum feasible global reductions in global anthropogenic methane emissions for the 2036–2050 period do not take into account the effect of reduced methane on changes in tropospheric ozone, because neither CanESM2 nor CESM1 include the interactive chemistry that would be necessary to represent this feedback. Regarding the effect of methane change on stratospheric

water vapor, the CESM1 includes a parameterization of this effect, while CanESM2 does not. The concentration of ozone and stratospheric water vapor will decrease with reductions in methane emissions since methane is a precursor to the production of both these greenhouse gases.

Scaling factors are derived to account for changes in the concentration of ozone, and the stratospheric water vapor effect, or both, that are associated with changes in atmospheric concentration of methane, based on radiative forcing estimates reported in the IPCC AR5 (Myhre et al. 2013 their table 8.SM.6). For CanESM2 and CESM1 these factors are 1.485 and 1.339, respectively (see Box 8.4). The potential reduced warming due to maximum technically feasible reduction in anthropogenic methane emissions is thus calculated to be 0.27±0.07°C (RCP6.0) and 0.26±0.04°C (RCP8.5) based on CanESM2

Box 8.4 Scaling factors for temperature response

Radiative forcing due to methane emissions is caused by increases in concentrations of methane itself, but also by the enhanced ozone and stratospheric water vapor concentrations that are caused by the methane emissions. Because the Earth System models used here do not include all three effects, scaling factors were applied in the present study.

According to the IPCC, indirect effects on ozone and stratospheric water vapor can be accounted for by increasing the effect of methane concentration change by 50% and 15%, respectively (Myhre et al. 2013 their section 8.7.2.1). These values correspond to the ratios between the radiative forcings of ozone and stratospheric water vapor caused by methane emissions since pre-industrial times (0.241 W/m² and 0.070 W/m², respectively) and the radiative forcing due to methane concentration change over the same period (0.484 W/m²). The radiative forcing of methane change since the pre-industrial period is, however, a net result of methane emissions and of changes in nitrogen oxides and other chemical species. Without these latter effects, the radiative forcing of methane would have been 0.641 W/m² (Myhre et al. 2013 their table 8.SM.6). As future scenarios are equivalent to such a case (i.e. nitrogen oxides and other chemical species being the same in the CLE and MFR scenarios), the scaling factors were calculated here based on the radiative forcing of 0.641 W/m² due to methane emission change (Myhre et al. 2013 their table 8.SM.6). Accounting for the ozone effect alone would thus require an increase by (0.241/0.641)×100%, and similarly (0.070/0.641)×100% for water vapor, or ((0.241+0.070)/0.641)×100% for both (CanESM2). For CESM1, which does include the water vapor effect, the increase is (0.241/(0.641+0.070))×100%, and for NorESM (Sect. 8.3.2), which includes the ozone effect but not the water vapor effect, it is (0.070/(0.641+0.241))×100%. The use of simple scaling factors is a relatively crude method because these depend, among other things, on the chemical regime, which is not the same for past and future periods. Ideally, transient ESM simulations with full atmospheric chemistry should have been performed for the climate benefit of reduction in methane emissions to be calculated more accurately (Sect. 8.4.2).

— RCP6.0 as background scenario   — RCP8.5 as background scenario

results, and 0.10±0.05°C (RCP6.0) and 0.15±0.06°C (RCP8.5) based on CESM1 results. The scaling factors are here applied only to the global-mean results. The distribution of regional climate response is more complex to calculate and depends on the climate forcer (e.g. Shindell 2007). As methane-induced changes in ozone and stratospheric water vapor are not evenly distributed (see Sect. 8.3.2.2), the Arctic climate response (north of 60°N) should not be multiplied by scaling factors derived on the basis of global-mean radiative forcing values.

8.3.1.2 Impact of future changes in natural emissions

Although Ch. 3 (terrestrial) and 4 (marine) on natural sources present some examples of possible future changes in emissions, uncertainty on the magnitude of these sources remains very high. While terrestrial monitoring is improving and many of the underlying processes are known, the large spatial variability in wetlands leads to substantial uncertainty when upscaling fluxes. Upscaling fluxes from the marine environment is even more challenging, as the location, magnitude and temporal evolution of emissions are not well known, and many critical processes are not fully understood. In light of the large uncertainties, it is difficult to define precise scenarios for future changes in natural methane emissions to 2050 for use in the modeling projections. Instead, in order to evaluate the impact of potential future changes in natural methane emissions from the Arctic region, three scenarios were developed for use with the Box model of atmospheric methane to assess changes in global-mean atmospheric methane concentration associated with the scenarios. The three scenarios do not represent specific quantitative assessments but rather, given the current understanding presented in Ch. 3 and 4, represent a span of possible future outcomes for changes in Arctic natural methane emissions. Even though all scenarios are hypothetical, they do represent a reasonable range of possibilities, and are valuable tools to investigate the climate response to changes in natural methane emissions from the Arctic.

The three scenarios are described as 'low', 'high', and 'extreme', with natural emissions assumed to be 25 Tg CH_4/y (low), 50 Tg CH_4/y (high) or 100 Tg CH_4/y (extreme) larger in 2050 than in 2005. To illustrate these numbers, an increase of 25 Tg CH_4/y could represent a large increase in methane emissions from the tundra, but a small change from the ocean, while an increase of 50 Tg CH_4/y could represent a major increase in both. Additionally, the 'extreme' scenario of 100 Tg CH_4/y would be the result of catastrophic feedback processes enhancing emissions (see Ch. 3 and 4 for more details and examples). This last scenario would amount to an increase of almost one fifth of the current global total (i.e. anthropogenic plus natural) methane emission rate into the atmosphere (Table 8.1). Although an increase to such an extreme emission from Arctic sources by 2050 is highly unlikely, it cannot be ruled out entirely.

The natural emission increase is implemented linearly over the period from 2006 to 2050. For example, in the 'high' scenario the total natural emission in 2005 amounts to 202 Tg CH_4/y and increases linearly to 252 Tg CH_4/y by the year 2050 (numbers for natural emissions are listed in Table 8.1). Using a Box model means that the spatial distribution of emissions is not taken into account. Thus, only the *magnitude* of the Arctic methane

emission change is used, and the response in global mean methane concentration calculated.

If climate change induces increases in natural methane emissions in the Arctic region, it must be acknowledged that changes in natural methane emissions in other parts of the globe may also occur. However, changes in natural methane emissions outside the Arctic region were not assessed by the Methane Expert Group and so are not taken into account in the model experiments described here. Figure 8.5 shows the evolution of global-mean methane concentrations for the three cases for the CLE and MFR-AC8 scenarios over the 2006–2050 period. (It should be noted that, since the natural emissions increase is implemented globally in the Box model, the results presented in this section can be applied to any spatial distribution of changes in natural methane emissions, that is, including either Arctic or non-Arctic emissions, or a combination of both.) Total anthropogenic and changes in

Global mean CH₄ concentration, ppb

Global mean CH₄ concentration, ppb
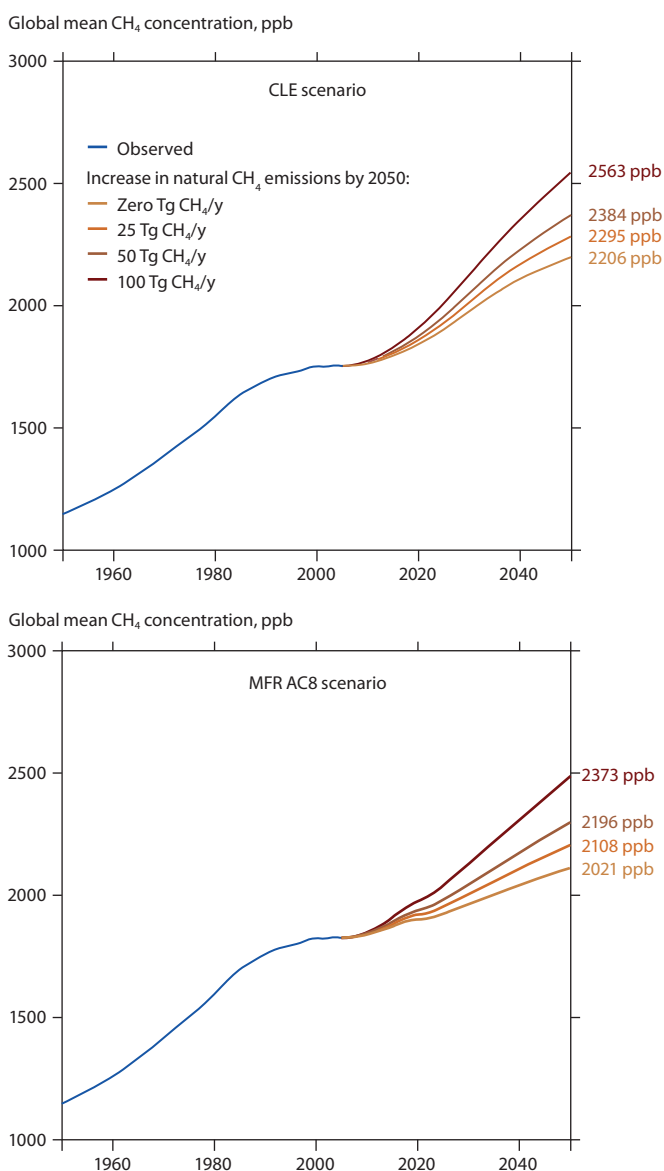
Fig. 8.5 Global-mean concentrations until 2050 assuming different scenarios for anthropogenic and natural emissions. Future concentrations are calculated by a Box model, using the current legislation (CLE; upper) or maximum technically feasible reduction in the eight Arctic nations (MFR-AC8; lower) scenarios for anthropogenic emissions, and different (linear) increases in natural emissions, in addition to the baseline natural emissions of 202 Tg CH_4/y (see Table 8.1).

natural emissions are listed in Table 8.1. For example, the Box model results for the MFR-AC8 simulation with *no* increase in natural emissions (lowermost curve in the lower panel of Fig. 8.5) correspond to anthropogenic and natural emissions of 396 and 202 Tg CH_4/y, respectively, for year 2050. In the scenarios with a 100 Tg CH_4/y increase in natural emissions, natural emissions increase linearly from 202 Tg CH_4/y in 2005 to 302 Tg CH_4/y in 2050.

Within the time frame of the present study, it was not feasible to perform ESM simulations with the three scenarios of natural emission increase. If it is assumed that, due to the relatively long lifetime of methane with respect to time scales of atmospheric circulation, the location of emissions does not matter significantly to global concentrations of methane, then the amount of total emissions should determine the global climate response to a large extent. As indicated by Fig. 8.5 (upper panel), natural emission change in the 'extreme' case would lead to a 357 ppb increase in global-mean methane on top of the increase that is due to anthropogenic methane emissions in the CLE scenario. This corresponds to about 40% of the 840 ppb difference between the CLE and MFR scenarios in year 2050 (Sect. 8.3.1.1). Using a simple scaling argument, this additional increase would probably lead to an increase of about one tenth of a degree in global-mean surface air temperature. Anisimov (2007) performed a similar calculation focusing on Russian permafrost thaw only – the additional natural source of methane by the mid-21st century amounted to 6–8 Tg CH_4/y. This is less than one tenth of the increase in the 'extreme' estimate (which is for the entire Arctic) used in the present assessment. However, taking this lower emission rate into account, Anisimov's result of a 0.012°C global temperature rise is consistent with the present assessment.

As discussed in Sect. 8.3.1.1, maximum technically feasible reduction in anthropogenic methane emissions by only the Arctic nations will reduce methane concentrations in year 2050 by about 200 ppb compared to the CLE scenario, if natural emissions do not increase. This decrease in atmospheric methane concentration reflects a decrease in total methane emissions of about 43 Tg CH_4/y in the MFR-AC8 scenario compared to the CLE scenario. As Fig. 8.5 shows, this case would yield a global-mean methane concentration of 2196 ppb in 2050, compared to 2206 ppb for the CLE scenario with no changes in natural emissions.

It is important to note, however, that changes in natural emissions will depend on how climate continues to evolve, and on the interactions between various components of the climate system (including permafrost), which are also influenced by changes in methane concentration. For the calculations performed here the *same* set of natural methane emission increases ('zero', 'low', 'high', and 'extreme') on top of two different scenarios of anthropogenic methane emissions (CLE and MFR-AC8) were used. With the tools available in this study, the effect of climate change mitigation through abatement of anthropogenic methane emissions on natural emission sources could not be taken into account. Since climate warming is mainly caused by the increase in carbon dioxide, the MFR-AC8 scenario with large natural emission increase could be interpreted as a hypothetical case where all efforts are made to reduce methane emissions, while no progress is made

in reducing emissions of carbon dioxide and other greenhouse gases. Conversely, it could be assumed that near-term methane mitigation may avoid some fraction (albeit perhaps very small) of natural methane increases, thus giving near-term methane mitigation 'extra credit'.

8.3.2 Chemical Transport Model – Earth System Model calculations

The calculations described in Sect. 8.3.1.1 take account of changes in global-mean methane concentrations, and estimate the effect of changes in ozone (caused by the methane change) through a scaling approach. Although methane is relatively well-mixed in the atmosphere, it does exhibit some spatial variation geographically and in height, which might alter in response to non-uniform changes in emissions. The changes in radiative forcing are not only due to changes in methane, but also to concurrent changes in ozone which can also exhibit spatial variability. As a result, changes in regional climate may occur that are different from what may be expected due to change in the global-mean methane concentration. In an additional study (see Sect. 8.3.2.1), the chemistry transport model Oslo CTM3 (Søvde et al. 2012) was therefore used to calculate the *three-dimensional* global distributions of monthly-mean methane and ozone concentrations for year 2005 and 2050 conditions, corresponding to the cases with and without maximum technically feasible reduction of methane emissions. The results were then used as input to the Norwegian Earth System Model (NorESM; Bentsen et al. 2013) to calculate the climate response, providing an independent assessment of the impact of methane mitigation through changes in both methane and ozone. An additional sensitivity experiment was performed to assess the importance of the location of methane emission change.

8.3.2.1 Changes in concentrations of methane and ozone

The year 2005 is, in the context of the long-term changes investigated here, considered 'present-day'. Two separate simulations with the Oslo CTM3 model were performed for 2050, using methane emissions corresponding to the CLE and MFR scenarios (for emission totals see Table 8.1). The emissions of air pollutants such as nitrogen oxides, carbon monoxide and volatile organic compounds (which also influence climate through their chemical interaction with several climate gases and aerosols) were specified according to the CLE scenario in both simulations in order to isolate the effect of methane mitigation alone. Anthropogenic halocarbon and biomass burning emissions are not represented in the CLE and MFR scenarios so these were specified based on the SRES-A1B (Nakicenovic et al. 2000) and GFED-v3 (van der Werf et al. 2010) data, respectively. These emissions were also the same in the CLE and the MFR simulations. Halocarbon and biomass burning emissions were required in these experiments because of their importance for ozone concentrations in the stratosphere and troposphere, respectively.

The reason for using SRES-A1B data, rather than the RCPs, in regard to ozone-depleting substances is that RCP data were not ready for use in the Oslo CTM3 model at the time

the experiments for this study had to start. However, this does not imply any noteworthy inconsistencies because (i) data used for ozone-depleting substances in the CLE and MFR simulations are the same and will thus cancel out when differencing these simulations, and (ii) the main interest of the present study in terms of methane impact is tropospheric ozone change for which ozone-depleting substances are of minor relevance.

Owing to the large computational requirement of CTM calculations, simulations were only done for present-day and year 2050 conditions, and not for the intervening years. Yet, the Oslo CTM3 model was run for 25 years with constant emissions (for 2005, and for 2050 with anthropogenic emissions corresponding to CLE and MFR scenarios) in order to obtain concentrations that are close (within ~90%) to equilibrium with the chosen emissions and the loss mechanisms for methane. As the difference in methane emissions between CLE and MFR is already largely achieved by year 2030 (see Table 8.1 and Fig. 5.9) it is reasonable to assume that by 2050 the methane concentration change would be close to the equilibrium response to that difference.

The Oslo CTM3 calculations indicate that, from 2005 to 2050, global-mean methane will increase by 454 ppb in the CLE scenario, and decrease by about 283 ppb in the MFR scenario. By the year 2050, methane concentrations in the MFR scenario are thus about 740 ppb lower than in the CLE scenario. In the Box model this benefit due to maximum technically feasible reduction amounted to about 840 ppb (Sect. 8.3.1.1). The reason why this value is lower in Oslo CTM3 than in the Box model is related to the relatively high OH concentrations in the Oslo CTM3, which lead to a slightly lower lifetime of methane (the reaction with OH being the main loss mechanism for methane in the atmosphere). However, these OH concentrations, and thus the modelled methane lifetime are within the uncertainty range of methane lifetime (9.1±0.9 years for present-day conditions, according to Prather et al. 2012). The uncertainty in the concentration change in methane due to MFR is thus a result of the uncertainty in OH levels, and adds to the uncertainty in later calculations of the climate response.

Figure 8.6 shows the geographical distribution of the modelled changes in methane and ozone between present-day and 2050 for the CLE scenario (left panels). Both methane and ozone abundances are projected to increase in the CLE scenario. In the case of methane this is mainly due to the increase in methane emissions, while ozone is strongly affected also by changes in other chemical species, such as nitrogen oxides, volatile organic compounds, and ozone-depleting substances in the stratosphere. The range of methane increases is narrow, which is consistent with methane being well-mixed throughout the troposphere. The modelled increase in tropospheric ozone (middle left panel) is greatest in regions where ozone precursor emissions, mainly nitrogen oxides are projected to increase. In some areas in North America and Europe, tropospheric ozone is modelled to decrease, as a result of reductions in ozone precursor emissions. The increases in total ozone (bottom left panel) reflect changes in both tropospheric and stratospheric ozone, and thus include the response to reductions in ozone-depleting substances in the stratosphere (recovery of the ozone layer). Related to this, the largest increase (in absolute terms) is seen over Antarctica.

The right panels in Fig. 8.6 show the differences between the MFR and CLE scenarios with regard to tropospheric methane and ozone in 2050. As the two CTM simulations for CLE and MFR differ only in regard to anthropogenic methane emissions, the differences seen in these three panels reflect the change due to methane mitigation only. Methane abundances are lower in the MFR case than in the CLE case throughout the globe. Again, the range of change is narrow as a result of the relatively long lifetime of methane. Since methane is a precursor of ozone, reductions in methane also lead to reductions in ozone. However, the pattern is different because methane-induced ozone change is also a function of photochemical production, which in turn depends on the local chemical regime (e.g. concentrations of other ozone precursors), physical parameters (e.g. humidity and vertical mixing of air), and the availability of sunlight. Many of the peak reductions in ozone are linked to areas of fossil fuel extraction (large mitigation potential per unit area, such as the Middle East). In addition, ozone in areas with strong emissions of nitrogen oxides is particularly sensitive to changes in methane, such as in India. The geographical distribution of total (tropospheric plus stratospheric) ozone, and of changes therein, is also controlled by meridional (north-south) transport of ozone from low (and middle) to high latitudes. The peak reduction in total ozone in high latitudes is mainly due to increased ozone formation in the lower stratosphere in mid-latitudes combined with meridional transport to high latitudes.

8.3.2.2 Climate response to changes in concentrations of methane and ozone

The three-dimensional fields of monthly-mean methane and ozone concentrations, as calculated by the Oslo CTM3, were used as input in the NorESM to calculate the climate response to changes in methane and ozone. NorESM is an Earth System model based on version 4 of the Community Climate System Model (CCSM4; Gent et al. 2011) and uses here a combination of the aerosol scheme described by Kirkevåg et al. (2013) and Mozart-4 tropospheric chemistry (Emmons et al. 2010). In the NorESM simulations performed for this assessment, the atmosphere was fully coupled to a three-dimensional ocean model.

In contrast to the CanESM2 and CESM1 experiments discussed in Sect. 8.2 and 8.3.1, the NorESM projections were run as 'constant perturbation' simulations (in regard to methane and ozone) rather than transient simulations. This means that concentrations of methane and ozone in the multi-year simulations of NorESM were fixed either at their year 2005 or year 2050 levels as provided by Oslo CTM3, rather than varying over time. The reason for this approach is that the methane and ozone concentrations from Oslo CTM3 are based on time slice experiments for 2005 and 2050 and so do not provide concentrations for the period in between.

An advantage of using a constant perturbation in methane and ozone is that statistically significant results can be obtained with only one ensemble member, provided that the ESM is integrated for a sufficient amount of time. In these simulations, NorESM was initiated with present-day conditions from a historical simulation. The model was run for 15 years of spin-up, and the following 45 consecutive years were used for the analysis (this is equal to the number of years used for the analysis in the ensemble approach of Sect. 8.3.1, where the

ΔCH₄ (ppb), CLE, 2050 vs 2005
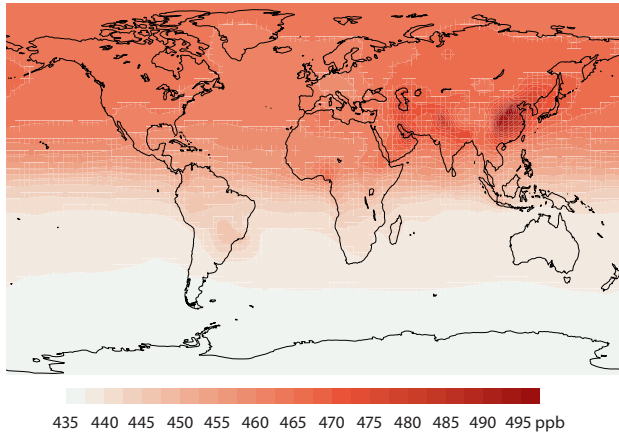
ΔCH₄ (ppb), MFR-CLE, 2050
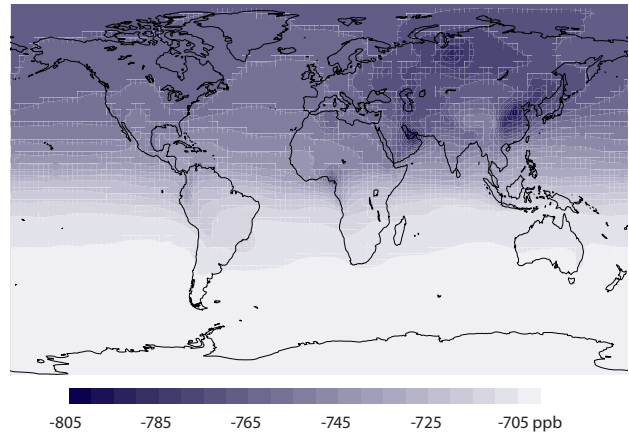
ΔO₃ (DU, trop), CLE, 2050 vs 2005
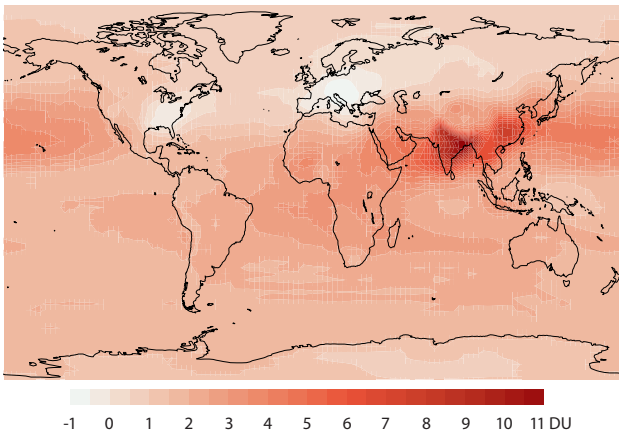
ΔO₃ (DU, trop), MFR-CLE, 2050
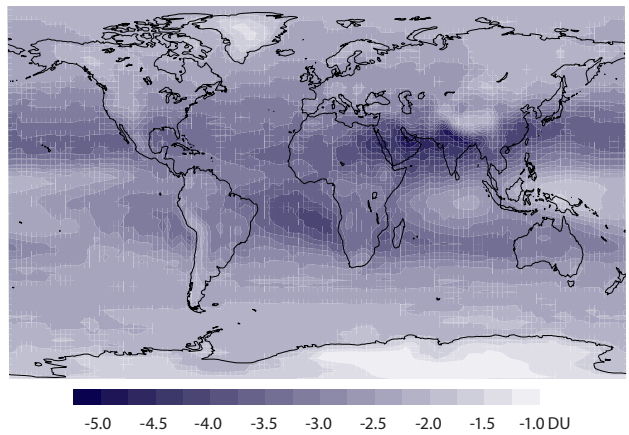
ΔO₃ (DU, trop+strat), CLE, 2050 vs 2005
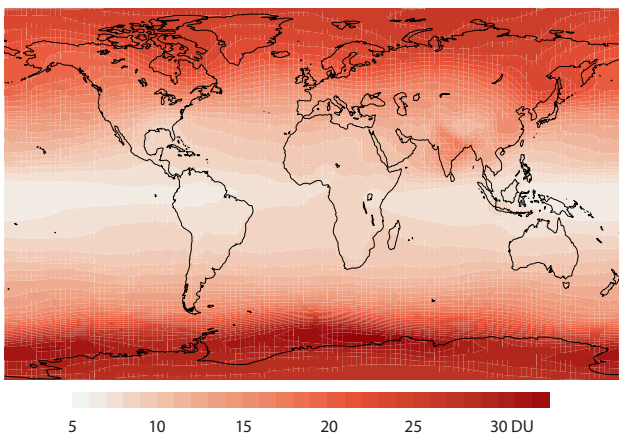
ΔO₃ (DU, trop+strat), MFR-CLE, 2050
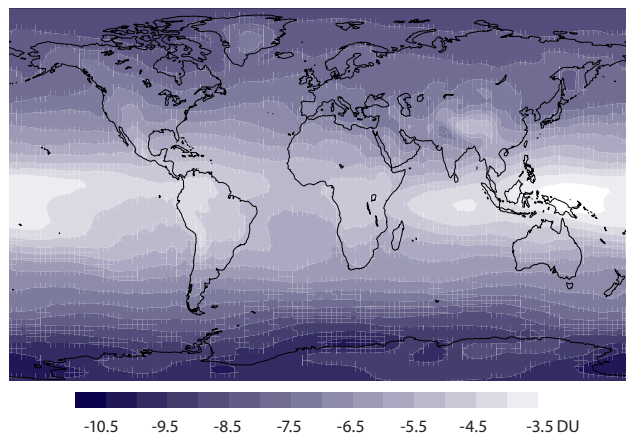
Fig. 8.6 The left panels show changes in concentration for tropospheric methane (upper), tropospheric ozone (middle), and total ozone (lower) from present-day conditions to 2050, modelled by the Oslo CTM3 for the current legislation (CLE) scenario. The changes are a response to changes in emissions of methane, ozone precursors and ozone-depleting substances from present-day to 2050. The right panels show the reductions in tropospheric methane (upper), tropospheric ozone (middle), and total ozone (lower), due to global maximum technically feasible reduction (MFR) of methane emissions only, as represented by the difference between two Oslo CTM3 simulations for 2050, using the CLE and MFR methane emissions, respectively. The reductions reflect the change in methane emissions only. For methane (top panels), the average concentration between the surface and 500 hPa is shown. In regions with surface pressures below 500 hPa (e.g. Himalaya or Andes) surface concentration is shown. For ozone (middle and lower panels), the tropospheric column or total (tropospheric plus stratospheric) column is displayed in Dobson Units (DU). Dobson Units are a measure of column-integrated ozone abundance per unit area (1 DU corresponds to $2.67e16$ molecules of ozone per cm^2). Here, the ozone abundance is integrated from the surface to the tropopause, to give tropospheric ozone abundance. Note the different color scales in the graphic.

last 15 years of three ensemble members were averaged). The tropospheric chemistry scheme of the model was used to calculate the spatial and temporal variations of chemical species other than methane and ozone. The time evolution of gas species which are not treated by the tropospheric chemistry scheme was specified based on the RCP6.0 scenario (see Box 8.3). As the atmosphere in these runs was fully coupled to a three-dimensional ocean model, the climate system in the model, as in the real world, is not initially in equilibrium with the greenhouse gas forcings. However, the surface air temperature response to the perturbation (i.e. the changes in methane and ozone), as represented by the difference between the MFR and CLE simulations, is expected to be close to equilibrium after a spin-up period of 15 years.

The NorESM results show that the global-mean temperature increase in the MFR scenario is about 0.20±0.03°C (mean ± standard deviation) lower than in the CLE scenario (or 0.33±0.14°C lower when averaged over the Arctic). This calculated reduction in global warming is a result of the reductions in methane and ozone combined. Scaling to include the water vapor effect (see Box 8.4) gives a reduction in global warming of 0.22±0.04°C, lying in between the corresponding results obtained from the CanESM2 and CESM1 calculations (Sect. 8.3.2).

Figure 8.7 shows the benefit of MFR in terms of reduced zonal-mean warming, as represented by the difference between MFR and CLE temperatures in 2050. As was the case in the CanESM2 and CESM1 results (see Fig. 8.4), zonal variability is large, and again greatest in the Arctic. Nevertheless, all ESM results agree in that there is reduced warming at almost all latitudes, due to MFR.

8.3.2.3 Does the location of methane emissions matter?

The Methane Expert Group was also tasked with investigating the importance of the location of methane emissions and their abatement. The background for this is that, for many SLCFs (e.g. black carbon), the location of emissions is highly relevant for the spatial distribution of the pollutant in the atmosphere and its effects on climate change. The effects of methane mitigation, or of changes in natural sources due to climate change, would thus also depend on where the mitigation is implemented or where changes in natural emissions occur. However, since the methane lifetime (about 9 years) is considerably longer than the typical time scales of inter-hemispheric mixing (about 1 to 2 years), it is a common assumption that the location of emissions, or the location of emission change, is of limited importance in the case of methane. For example, Fiore et al. (2008) found that the climate benefits from methane mitigation do not depend strongly on the location of the mitigation, so that the lowest-cost emission controls can be targeted.

For the present study, one additional Oslo CTM3 simulation was made to address this issue more quantitatively. The amount of methane emissions that corresponds to the difference between the total global emissions in 2050 for the CLE and MFR scenarios (i.e. 205 Tg CH_4/y) was added to the MFR scenario, but emitted in a confined region of the Arctic[7]. The region of enhanced emissions in this model simulation corresponds, in good approximation, to the East Siberian Arctic Shelf. The total global emission in this new scenario (labeled 'Arctic205' and listed in Table 8.1) is thus equal to the one in CLE, but its spatial distribution is very different, with much larger emissions occurring in the Arctic and much lower emissions in land areas further south. As in the simulations described in Sect. 8.3.2.1, the Oslo CTM3 model was run for 25 years with constant emissions.

Change in surface air temperature,°C
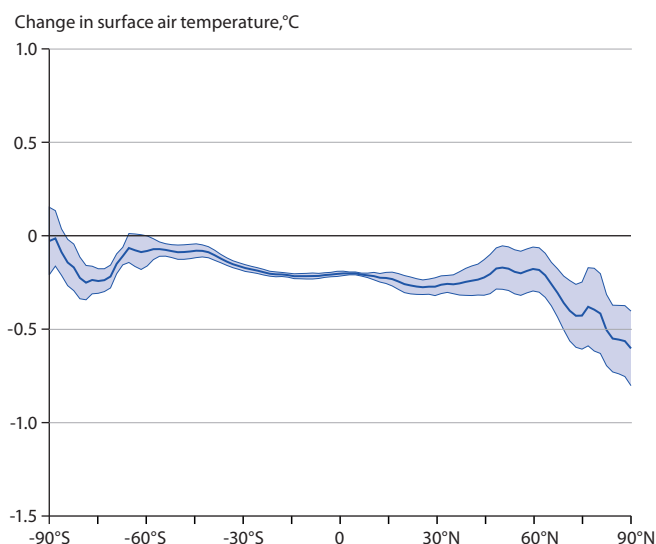
Fig. 8.7 Changes in zonal-mean surface air temperature due to maximum technically feasible reduction in anthropogenic methane emissions (i.e. MFR minus CLE), as calculated by the Earth System model NorESM. The middle curve represents the mean of the 45 years of simulation that have been analyzed, while the two other curves define the standard deviation.

The uncertainty is given as standard deviation and has been calculated for NorESM in the same way as for the CanESM2 and CESM1 results shown in Fig. 8.4[6]. The 45 years of the NorESM run that were used for the analysis, were split into three periods of equal length and then treated as three 15-year ensemble members. This was also the rationale behind the choice of analyzing 45 years. In this context it should be noted that, while the difference between MFR and CLE simulations was relatively stable during this 45-year period, there was an overall trend in temperature due to the increase in greenhouse gases. For the calculation of standard deviation, this trend had to be statistically removed from the data.

Given the drastic nature of this prescribed change in emission distribution, its effect on methane and ozone concentrations, as represented by the difference between the Arctic205 and CLE simulations for 2050, is relatively small. Figure 8.8 shows the percentage difference in methane concentration up to 500 hPa (representative of methane change in the troposphere), and in tropospheric and total ozone burden between the Arctic205 and CLE scenarios in 2050. The modelled change in methane is fairly stationary, but due to its long lifetime the change is also transported over long distances. Still, as indicated in Fig. 8.8, less methane is transported to the lower troposphere of the southern hemisphere than in the CLE case. Tropospheric zonal-mean methane in the Arctic205 simulation is up to 10% higher than in CLE in high northern latitudes. In absolute values this amounts to about 200–250 ppb, compared to background levels of about 2170 ppb.

The total methane burden in the atmosphere (not shown) is slightly higher in Arctic205 than in CLE, with increases in global mean concentration of about 3 ppb. In a scenario where emissions increase mainly at high latitudes, but decrease by an equal amount at lower latitudes, a higher global mean concentration of methane may be expected, because its lifetime is longer at high latitudes related to the lower OH levels found there.

In terms of tropospheric and total ozone, the shift of methane emissions to the Arctic leads to small reductions in parts of the

---

7   The simulation was performed in coordination with the GAME project (see Acknowledgments), which investigated the effects of emissions from the East Siberian Arctic Shelf. However, the purpose of the analysis for this assessment is to look at the impact of emissions from sources strictly confined to the Arctic rather than from emissions distributed across the globe. No assumption is made here as to whether the East Siberian Arctic Shelf could be an area of large increase in natural emissions in the future.
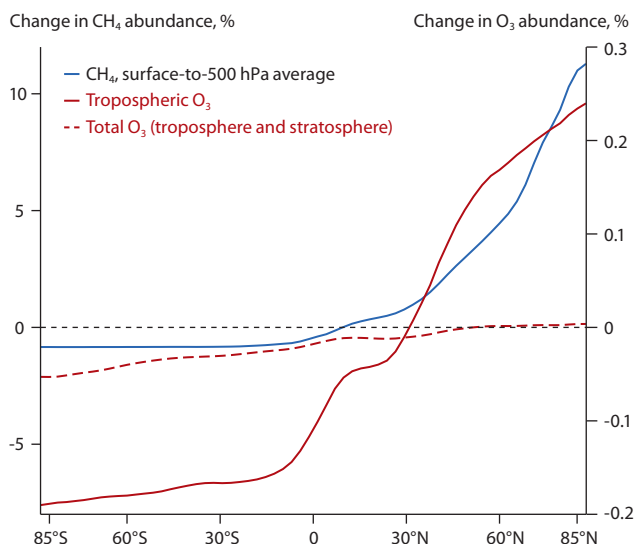
Fig. 8.8 Zonal-mean change in methane and ozone abundance due to a prescribed change in the spatial distribution of methane emissions, plotted as the difference 'Arctic205 minus CLE'.

southern hemisphere, consistent with the methane reduction there (methane being a precursor of ozone). The increases in tropospheric ozone in the northern hemisphere stay within a few tenths of a percent even at high latitudes. The relatively small ozone change is related to the modest methane change due to the shift of methane emissions prescribed in the Arctic205 scenario.

Judging by these changes, and in view of the drastic nature of the considered emission scenario (more than 200 Tg CH_4/y emissions being moved from low- and mid-latitude regions to high-latitude regions), it can be concluded that the emission location is important for a relatively long-lived species such as methane. Nevertheless, the different latitude distributions of methane and ozone in the Arctic205 scenario (compared to the CLE case) may lead to a different climate response. For example, the regional climate response, in particular to the column increase in methane in the Arctic may be noticeable. Hence, an additional NorESM simulation was performed with the methane and ozone concentrations calculated for the Arctic205 scenario, to be compared with the results from the CLE scenario presented in Sect. 8.3.2.2. Apart from the methane and ozone concentrations, the setup of this simulation was exactly the same as for the CLE simulation.

The calculated global-mean surface air temperature in the Arctic205 scenario is calculated to be 0.04±0.04°C (mean ± standard deviation) higher than in the CLE scenario. In the Arctic the difference is greater (0.16±0.26°C). The small global temperature increase is consistent with an increase in total atmospheric methane abundance. However, while the relatively large response in the Arctic is likely to be related to the large change in the latitudinal gradient of methane (with largest methane concentration increases modelled for the Arctic in this scenario) it is clear that the low signal-to-noise ratio in these calculations makes it impossible to draw any firm conclusions. All that can be said based on this additional study is that the change in the spatial distribution of anthropogenic methane emissions in the Arctic205 scenario does not lead to any large change in global-mean methane concentration.

8.4 Conclusions

8.4.1 Key findings

This chapter has used sophisticated climate modeling systems, and the emission data based on Ch. 3, 4 and 5, to address the questions raised in Ch. 1. These include how methane changes in the past have affected climate and to what extent mitigation measures for anthropogenic methane emissions can reduce climate warming in the future. Scenarios of natural emission change have also been explored. Table 8.2 summarizes the ESM experiments performed in this assessment.

Q1: What is the contribution of historical changes in global atmospheric methane to Arctic climate warming?

The historical Earth System model simulations performed with CanESM2 suggest that changes in methane concentration until present-day have warmed the Arctic (global) climate by 0.58°C (0.31°C) since 1850. Results from the same simulation are also reported by Fyfe et al. (2013), who reported a 0.04°C per decade warming trend in the Arctic over the 1900–2005 period due to radiative forcing of methane. These numbers need to be compared with the overall global warming calculated by CanESM2 for the 1850–2005 period (calculated as the difference between the 1851–1865 and 1991–2005 periods) amounting to 1.29°C (0.81°C) over the Arctic region (whole globe), indicating that historical changes in methane concentration have contributed just over one third of the global warming, and

Table 8.2 Summary of Earth System Model experiments performed for this assessment. Details of anthropogenic methane emissions are given in Table 8.1 and Ch. 5.

Simulation	Model(s)	Time period	Methane concentrations	No. of ensemble members
Control simulation	CanESM2	1850–2005	Constant at year 1850 value (=791 ppb)	5
Historical simulation[a]	CanESM2	1850–2005	Based on observations (increasing from 791 to 1854 ppb over the time period)	5
CLE	CanESM2 and CESM1	2005–2050	Based on box model results for the entire time period, based on CLE emissions	3[b]
	NorESM	2005, 2050	Oslo CTM3 results for 2005 and 2050, based on CLE emissions	1
MFR	CanESM2 and CESM1	2005–2050	Based on box model results for the entire time period, based on MFR emissions	3[b]
	NorESM	2050	Oslo CTM3 results for 2050, based on MFR emissions	1
Arctic205	NorESM	2050	Oslo CTM3 results for 2050, based on MFR emissions and an additional large source in the Arctic	1

[a]The CanESM2 historical simulation was performed as part of CMIP5; [b]both CanESM2 and CESM1 performed two ensemble simulations (with three members in each ensemble) using non-methane climate forcers either from RCP6.0 or RCP8.5.

over 40% of the Arctic warming, until present-day. However, this simple scaling is somewhat misleading since the historical warming is the *net* result of the warming caused by increases in the concentrations of greenhouse gases and the cooling caused by increase in the concentration of aerosols.

Q2: What impact will increasing atmospheric concentrations of methane have on climate and will Arctic nations have the ability to influence that impact through mitigation of anthropogenic methane emissions?

If the current state of technology prevails, and any further emission reductions are limited to those prescribed by already adopted current legislation (CLE scenario), methane concentrations will continue to rise and thus induce further warming. The increase in methane from present-day to 2050 in the CLE scenario will amount to about 450 ppb, which is almost half of the increase from the pre-industrial period to present-day. Using the result of methane having induced global warming of about 0.3°C until present-day (see Q1), a rough estimate of further global warming due to methane would be between one and two tenths of a degree in this scenario. This needs to be compared with the overall warming of about 1 to 1.7°C caused by all climate forcers over the same period (see Fig. 8.3).

If maximum technically feasible reduction (MFR) in anthropogenic methane emissions is implemented in the Arctic nations only, with rest-of-world emissions changing according to the CLE scenario, global-mean methane concentrations will still continue to rise.

On the other hand, if maximum technically feasible reduction in anthropogenic methane emissions is implemented globally, then by 2050 the difference in global-mean methane concentration between the CLE and MFR scenarios is about 800 ppb. Three different ESMs – CanESM2, CESM1, and NorESM – were used to calculate the potential benefits of MFR in terms of reduced climate warming. Table 8.3 summarizes the results for reduction in near surface air temperature.

Averaging results based on the 26 transient climate model simulations that have been performed for the future yield a temperature benefit of about 0.20°C degrees globally, due to maximum technically feasible reduction in global anthropogenic methane emissions. This estimate of reduced climate warming is similar to those from the UNEP (2011b) and Shindell et al. (2012) studies (both based on time slice experiments of comprehensive climate models with chemistry), which estimate reduced warming of around 0.4–0.5°C in response to methane *and* black carbon emission reductions, half of which is attributed to reduction in methane emissions. Smith and Mizrahi (2013) estimated the climate change mitigation potential of methane and black carbon (and co-emitted species) to lie between 0.04 and 0.35°C in 2050. Their calculated climate mitigation potential from methane reductions is around 0.15°C in 2050 (their figure 1).

Results from CMIP5 concentration-driven experiments that contributed to the IPCC AR5 show that the mean-model warming in globally-averaged surface air temperature over the period 2006–2050 varies from about 0.7°C in the RCP2.6 scenario to around 1.5°C in the RCP8.5 scenario as a result of all forcings including greenhouse gases, aerosols and land use change (Collins et al. 2013 their fig. 12.5). For the present study, the potential reduced warming of about 0.20°C, due to maximum technically feasible reduction in global anthropogenic methane emissions, corresponds to about 10–15% of the warming expected over the 2006–2050 period in globally-averaged surface air temperature, due to all climate forcers in the RCP8.5 scenario.

Regarding the climate response in the Arctic, the present model results show larger effects of methane mitigation on surface air temperature, but also larger variability. Averaged over the Arctic (north of 60°N) and using RCP6.0 as the background scenario, CanESM2, CESM1, and NorESM calculate a reduction of surface air temperature warming by 0.40±0.14°C, 0.26±0.26°C, and 0.33±0.14°C, respectively, for the period 2036–2050

Table 8.3 Summary of results for the *reduction* in global warming for the 2036–2050 period, due to maximum technically feasible reduction in anthropogenic methane emissions, calculated as the difference in surface air temperature between the MFR and CLE scenarios (CLE minus MFR), averaged either globally or over the Arctic region. 'Background scenario' refers to the scenario according to which non-methane climate forcers were specified. As listed in Table 8.2, CanESM2 and CESM1 simulations were performed for both RCP6.0 and RCP8.5 scenarios, while NorESM performed simulations for the RCP6.0 scenario only. ΔT is the result from the ESM simulations, while $\Delta T_{O3,H2O}$ takes into account the effects of changes in ozone and stratospheric water vapor due to changes in methane emissions. The ratio between $\Delta T_{O3,H2O}$ and ΔT depends on the ESM and is calculated based on numbers of radiative forcing given by IPCC AR5 (Myhre et al. 2013), as described in Sect. 8.3.1.1. This ratio could, in the present work, only be defined for global-mean values; therefore $\Delta T_{O3,H2O}$ is not calculated for the Arctic region. The *mean* reduction in warming is not calculated for ΔT because different models include different processes related to changes in methane (either the corresponding changes in ozone, or stratospheric water vapor, or none) so averaging of raw model results is not appropriate.

Model	Background scenario	Reduction in warming simulated by the model (ΔT), °C		Reduction in warming after taking into account the associated changes in ozone and stratospheric water vapor ($\Delta T_{O3,H2O}$), °C
		Global	Arctic	Global
CanESM2	RCP6.0	0.18 ± 0.05	0.40 ± 0.14	0.27 ± 0.07
	RCP8.5	0.18 ± 0.03	0.35 ± 0.17	0.26 ± 0.04
CESM1	RCP6.0	0.07 ± 0.04	0.26 ± 0.26	0.10 ± 0.05
	RCP8.5	0.11 ± 0.05	0.33 ± 0.25	0.15 ± 0.06
NorESM	RCP6.0	0.20 ± 0.03	0.33 ± 0.14	0.22 ± 0.04
Mean		-	-	0.20 ± 0.02[a]

[a]The error bar of ±0.02°C reported here is the statistical uncertainty of the mean over the five model simulations. It is not representative of the level of scientific understanding, as it does not take into account any systematic errors in the models (model biases, missing processes, etc.) or uncertainties in the emission estimates.

due to maximum technically feasible reduction in methane emissions. However, in these estimates for the Arctic, only the NorESM result takes into account the effect of changes in ozone concentration. The results suggest that methane mitigation will reduce warming in the Arctic by a few tenths of a degree. However, it should be noted that effects of mitigation measures are in general small whenever they are considered in isolation. This fact in itself does *not* imply that such measures would not be important as a part of climate change policies.

Furthermore, it should be mentioned that the estimate used here for the methane mitigation potential (205 Tg CH_4/y) was adjusted upward (to about 285 Tg CH_4/y) in the ECLIPSE 2014 data set (see Fig. 5.9). Using a simple scaling argument, the ECLIPSE 2014 estimate would probably increase the calculated reduction in global-mean surface air temperature from two to almost three tenths of a degree. Also, the difference between the CLE and MFR scenarios used here does not include changes in energy scenario or behavioral changes, which would further increase the mitigation potential and thus the temperature response, although some of those effects would already result from carbon dioxide mitigation (Rogelj et al. 2014).

Q3: How will atmospheric methane concentrations change in response to potential changes in natural methane emissions and how do these changes compare to those that might result from mitigation of anthropogenic methane emissions?

As discussed in Ch. 3 and 4, natural emissions may increase in the future due to climate warming (caused by all climate forcers, including methane), but the size and rate of this increase are very uncertain. Within the framework of Ch. 8 it was not possible to calculate changes in natural emission as a result of climate warming. Rather, expert estimates from Ch. 3 and 4 were used as input to the one box model of atmospheric methane to calculate future changes in methane concentration for three different scenarios; 'low', 'high', and 'extreme' (in terms of natural emission change).

The results indicate that, in these scenarios, changes in natural methane emission will cause an increase in global-mean methane concentration in the range of about 85 ppb ('low') to 350 ppb ('extreme') over the 2006–2050 period. The increase in the 'extreme' case corresponds to roughly half the difference between the CLE and MFR scenarios by 2050. A simple scaling method, based on the results reported for Q2, suggests that this 'extreme' scenario would lead to about one tenth of a degree of global warming attributable to changes in natural methane emissions.

In the absence of dynamic calculations of changes in natural methane emission it was not possible to estimate how much of the increase in natural emissions can be avoided through maximum feasible reductions in anthropogenic methane emissions. However, it is possible to draw broad conclusions on the basis of the magnitude of possible changes in natural and anthropogenic emissions. Maximum feasible reductions, when applied globally, will by year 2050 lead to methane concentrations that are about 800 ppb lower than in the CLE scenario, thus outweighing additional methane inputs from natural sources in the Arctic even in the 'extreme' scenario. Maximum feasible reductions when implemented by the Arctic nations only (leading to a 43 Tg CH_4/y emission

decrease by 2050), would still compensate for a large part of the increases in natural emissions in the Arctic region in the 'high' scenario (natural emissions increase of 50 Tg CH_4/y by 2050).

Q4: Does the location of anthropogenic methane emissions matter?

The model experiment performed to address this question, effectively moved 205 Tg CH_4/y (about two-fifths of the total global emission rate) from low and mid-latitude regions to the Arctic region. This led to only a very small (<0.2%) increase in the global-mean methane concentration, suggesting that the location of methane emissions is of limited importance to its global-mean level. This is expected because methane is relatively well-mixed in the atmosphere. In contrast, the latitudinal gradients of methane and ozone concentrations do change noticeably in this simulation. However, it has not been possible within the scope of this study to accurately model global or regional climate responses to these changes.

8.4.2 Recommendations

As the chemistry of methane and its radiative properties are relatively well-known (in contrast to black carbon) a large part of the uncertainty in the present calculations of changes in methane concentration and its radiative forcing lies in the estimate of the magnitude of emission reductions. However, with regard to the climate response, the uncertainties in the ESMs are probably at least as large. The uncertainty in modelling the climate response is reflected by the difference between the results from the multiple ESM simulations presented in this chapter. In order to obtain more robust projections of the climate response to changes in anthropogenic methane emissions, the following recommendations are made for model development and future work:

- Although progress is being made, most current-generation ESMs do not yet include processes that are necessary to model feedbacks specific to methane and the Arctic region. A representation of wetlands, permafrost, the soil sink of methane, wildfires, expansion of shrubs, and ocean-atmosphere methane flux (together with atmospheric chemistry) would make it possible to model atmospheric methane concentration as a dynamic variable and the bi-directional coupling between climate change and natural methane emissions.

- Coupled chemistry-climate models are computationally very expensive to run. Yet, inclusion of processes representing the oxidation of methane, and other climate-chemistry interactions, is crucial for modelling atmospheric methane concentration dynamically and for making a complete assessment of the effect of changes in anthropogenic methane emissions. Climate-chemistry interactions not only include those related to changes in ozone and stratospheric water vapor that are caused by changes in methane emissions, but also feedbacks such as the increase in methane oxidation in a warming climate (e.g. Denisov et al. 2013).

- Regarding the effects of ozone produced from methane, uncertainties lie both in the ozone change itself (e.g. Fry et al. 2012, and discussion in Sect. 8.3.2.1) and in the climate response to ozone change. The latter will also depend on

feedbacks involving the biosphere (e.g. Sitch et al. 2007b; Collins et al. 2010), which have not been taken into account in the present study. Further research is needed for a more accurate assessment of the climate response to future ozone changes.

- Uncertainty in the calculated temperature response to the maximum technically feasible reduction of methane is relatively large, especially in the Arctic, as reflected by the difference between the results from the three ESMs used in this study. A detailed investigation of the various factors contributing to this variability in model results is also likely to contribute to a better understanding of the effect of the changes in natural and anthropogenic methane emissions on the Arctic climate.

- Annual-mean surface air temperature is not the only relevant climate parameter. For the Arctic region in particular, changes in other high-impact climate variables including sea-ice extent, snow cover, evaporation and precipitation, and ocean circulation are also relevant. Additional analyses that focus on the benefit of reduction in SLCFs including methane will benefit from an assessment of the response of these other high-impact climate variables.

- On a more general note, uncertainties with respect to modelling the regional climate response remain large, and this is of particular relevance for studies aimed at the Arctic region. Improved regional climate modelling with a focus on the Arctic region deserves increased attention in this respect.

Acknowledgments

Appendix: One-box model of atmospheric methane

A one-box model of atmospheric methane is used to obtain globally-averaged methane concentrations corresponding to global emissions for the CLE and the MFR scenarios. The model describes the change in burden of atmospheric methane (H) as a balance of surface emissions ($E = E_N + E_A$, consisting of natural E_N and anthropogenic emissions E_A) and the atmospheric and surface sinks (S).

$$\frac{dH}{dt} = E - S \qquad\qquad \text{Eq. A1}$$

The sink S is calculated as a first-order loss process from methane's atmospheric lifetime in the atmosphere (τ_{CH_4}) as $S = H\,[1 - \exp(-1 / \tau_{CH_4})] \cdot \tau_{CH_4}$ is calculated as:

$$\frac{1}{\tau_{CH_4}} = \frac{1}{\tau_{OH}} + \frac{1}{\tau_{strat}} + \frac{1}{\tau_{soil}} + \frac{1}{\tau_{trop\text{-}Cl}} \qquad \text{Eq. A2}$$

where τ_{OH} (present-day value of 11.17 years), τ_{strat} (120 years), $\tau_{trop\text{-}cl}$ (200 years) and τ_{soil} (150 years) are the lifetimes associated with the destruction of methane by tropospheric OH radicals, its loss in the stratosphere, and its reaction with tropospheric chlorine and uptake by soils, respectively, following Prather et al. (2012). This yields a present-day value of $\tau_{CH_4} = 9.1 \pm 0.9$ years in Eq. A2. For the pre-industrial period, Prather et al. (2012) estimated τ_{CH_4} as 9.5 ± 1.3 years assuming τ_{OH} to be equal to 11.76 years, based on Atmospheric Chemistry and Climate Model Intercomparison Project (ACCMIP) results (Voulgarakis et al. 2013) and lifetimes associated with other processes assumed to stay the same. In the present study, the value of τ_{CH_4} for the future 2006–2050 period is calculated by changing τ_{OH} based on changes in methane concentration but τ_{strat}, $\tau_{trop\text{-}cl}$ and τ_{soil} are assumed to stay the same. For τ_{OH} the approach used in the MAGICC IAM (http://wiki.magicc.org/index.php?title=Non-CO2_Concentrations) and by Prather et al. (2012) is followed, which results in a decrease in loss frequency $f_{OH} = 1/\tau_{CH}$ of 0.32% (and hence an increase in methane lifetime) for every 1% increase in methane concentration. This approach takes into account the positive feedback where methane affects its own lifetime but the effects of changes in nitrogen oxides emissions or tropospheric water vapor are not taken into account.

The one-box atmospheric methane model is first evaluated over the historical period using observation-based methane concentrations (or H in Eq. A1), the estimates of pre-industrial and present day τ_{CH_4} and natural emissions E_N (202±28 Tg CH$_4$/y, assumed to stay constant), together with their uncertainties, from Prather et al. (2012) to calculate anthropogenic methane emissions E_A. The calculated anthropogenic methane emissions for 2005 are 314±33 Tg CH$_4$/y (mean ± standard deviation, with a range of 239 to 399) as mentioned in Sect. 8.3.1.1. The one-box model of atmospheric methane is then driven for the 2006–2050 period with anthropogenic emissions from the CLE and MFR scenarios. The uncertainty range in calculated anthropogenic emissions for 2005 is also applied to the emissions for CLE and the MFR scenarios, and the emissions are reduced by 11 Tg CH$_4$/y to be consistent with the box model's mean estimate of 314 Tg CH$_4$/y for 2005. The resulting methane concentrations for the CLE and MFR scenarios are shown in Fig. 8.2.

9. Conclusions and Recommendations

AUTHORS: J. MICHAEL KUPERBERG, MARJORIE SHEPHERD, VIVEK K. ARORA, LORI BRUHWILER, ELIZABETH BUSH, TORBEN R. CHRISTENSEN, LENA HÖGLUND-ISAKSSON, MICHAEL GAUSS, FRANS-JAN W. PARMENTIER, DAVID A. PLUMMER, CARRIE TAYLOR

9.1 Context

The overarching context for this assessment is the concern of the Arctic nations about the consequences of large and rapid climate change in the Arctic region that is evident in both observational records and modeled projections of future change.

From pre-industrial time (around 1750), the global average atmospheric concentration of methane has risen from 700 to around 1820 ppb. Methane concentrations over the Arctic are slightly higher, currently about 1895 ppb (2013/14), reflecting regional differences in the relative strength of sources and sinks. Over the period 1950–2012, mean annual surface temperature (combined land and sea surface temperatures) for the region north of 60°N increased by about 1.6°C. Winter temperature, over the same period, increased by about 2.0°C while summer mean temperature rose by about 1.1°C. This warming is due primarily to increased atmospheric carbon dioxide concentration. Changes in methane concentration (resulting primarily from increases in anthropogenic methane emissions) during a somewhat shorter period (1950–2005) contributed to the warming by about 0.5°C in the Arctic.

Among the risks associated with warming of the Arctic is the potential for positive feedbacks between the Arctic ecosystems (both terrestrial and marine) and climate, which can increase the rate at which carbon is released from ecosystems. These positive feedbacks are likely to more than offset negative feedbacks thereby exacerbating global and Arctic warming.

A key process in this context is the production and release of carbon dioxide and methane as a result of changes in Arctic ecosystems, particularly rising temperatures and changing precipitation patterns. Large reservoirs of methane and organic carbon compounds (decomposition of which can lead to the emission of carbon dioxide and/or methane) exist in oceans, sediments and soils of the Arctic. A large fraction of these reservoirs are currently frozen or experience conditions where the surface–air exchange is partially mediated by ice cover. Rapid changes in Arctic ecosystems, including higher surface temperatures, create the potential for significant additional release of carbon dioxide and methane. As methane is a much more powerful greenhouse gas than carbon dioxide and knowing that the magnitude of methane emissions could impact on climate on a global scale, climate feedback risks associated with methane are of potential concern.

Given the relatively short atmospheric lifetime of methane, actions to reduce methane emissions could have a much faster impact on global and Arctic warming than similar efforts to reduce emissions of the much longer-lived carbon dioxide. It is these factors that focused the attention of the Arctic Council on short-lived climate forcing agents (also known as short-lived climate forcers or SLCFs), and methane in particular. This report provides a scientific review[8] that answers two major questions concerning mitigation of anthropogenic methane emissions:

What is the potential benefit, in terms of reduced Arctic warming, of methane emissions mitigation by Arctic nations?

How does the magnitude of potential emission reductions from anthropogenic sources compare to potential changes in methane emissions from natural sources in the Arctic?

The AMAP Methane Expert Group approached this challenge by developing more-specific policy-relevant science questions which guided each chapter. The responses to those questions are provided here as conclusions to this Technical Report.

Q1: What are the current and potential future natural emissions from the Arctic region? (Chapters 3 & 4)

Natural methane emissions globally result from the following sources: wetlands, freshwaters, wild animals, wildfires, termites, geological seeps, gas hydrates, and permafrost. While significant uncertainty exists in the estimates of emissions from natural systems, the relative order of magnitude of annual natural global emissions is robust, although top-down estimates based on atmospheric observations and modeling are lower than bottom-up estimates derived by adding estimates of individual natural methane-generating processes.

Current understanding concerning the processes that generate, consume, store and release methane in Arctic terrestrial and marine systems is summarized in Ch. 3 and 4, and emission estimates are developed for the Arctic region based on flux measurements, process studies, model simulations, and estimates of carbon stores.

For Arctic terrestrial systems, it is clear that tundra regions, inclusive of wetland areas, common to the Arctic, are the major natural sources of methane emission. Current estimates of natural methane emission from Arctic tundra fall in the range 10–30 Tg CH_4/y. Constraining this estimate is limited by key uncertainties, namely the limited measurements in time (few long-term records, and very limited measurements during winter) and in spatial coverage (very few measurement sites). Other limitations relate to gaps in understanding the controlling biological and physical processes that release methane from these ecosystems to the atmosphere. In addition to the terrestrial wetland emissions, the freshwaters of the Arctic are estimated to contribute as much as 13 Tg CH_4/y, yielding total terrestrial and freshwater emissions as large as 43 Tg CH_4/y.

Future methane release from Arctic tundra depends on how changes in Arctic temperature and precipitation affect the controlling processes (leading to a change in methane production or consumption) as well as on the extent/magnitude of available

---

8   This chapter does not include references as all results are derived from the underlying chapters and reference therein.

carbon pools in Arctic soils. It is estimated that 1400–1850 Pg of carbon is frozen in Arctic soils (although there is significant uncertainty in these estimates). The potential release of this permafrost carbon to the atmosphere is by consequence also uncertain. The quantification of this uncertainty is further exacerbated by the limited (or non-existent) representation of carbon and other biogeochemical cycle processes specific to the Arctic region and methane in Earth System models (ESMs). Despite these uncertainties, it is reasonable to conclude that significant stocks of frozen carbon do exist in permafrost with the potential to thaw and decay, releasing methane and/or carbon dioxide in a warming Arctic. The extent of future Arctic terrestrial methane release is intrinsically tied to changes in spatial extent of wetlands and changes in the rate of wetland methane production. Future emissions from Arctic tundra are estimated to increase by 50% or more by 2050.

For Arctic marine systems, it is likely that gas hydrates are the largest potential source of marine methane release to the atmosphere due to the large amounts of methane contained within these deposits. However, many other source types (e.g. geological) also contribute. Current methane emissions from the Arctic Ocean to the atmosphere are estimated to range from as low as 1 Tg CH_4/y to as high as 17 Tg CH_4/y. These emissions emanate primarily from shallow waters of the Arctic Ocean, since methane release from the deeper seabed is subject to significant oxidative loss (i.e. consumption) during the ascent through the water column. Future projections of release will depend on estimates of the methane stocks in these marine reservoirs and the impact of changing temperatures and sea-ice coverage on the controlling biological and physical processes. While estimates of gas hydrate inventory in the Arctic vary widely, a recent estimate put the quantity of carbon frozen in gas hydrates at 116 Pg. This is the basis for estimating a potential increase of 1.9 Tg CH_4/y in the release of methane into the Arctic Ocean over the next 100 years which translates into a much smaller release to the atmosphere due to oxidative loss as methane rises through the water column. Overall, this is a relatively small additional contribution; however this conclusion is tempered by significant uncertainty in the understanding of marine processes and the magnitude of marine hydrate carbon that is potentially vulnerable.

Understanding and quantifying marine methane sources, sinks and processes is more limited than for terrestrial systems, and so estimated ranges are larger and more uncertain. The nature, distribution and vulnerability of marine methane hydrate deposits are poorly understood. The processes that produce, consume and release methane from the ocean floor, through the water column, and ultimately to the atmosphere, are diverse and inadequately quantified. As a result, the release of methane from oceans to the atmosphere is extremely uncertain and the associated processes are difficult to model for future projections.

Regardless of the limitations and uncertainties in characterizing Arctic natural (terrestrial and marine) methane emissions, there is considerable interest in estimating their impact on global and Arctic climate now and in the future. Hence, values up to the year 2050 were selected based on the expert judgment of the author team. These future emissions values represent three scenarios judged by the team to characterize the span of possible future outcomes for changes in Arctic natural methane

emissions. The three methane emission scenarios used to estimate the climate response are described as 'low' (+25 Tg CH_4/y), 'high' (+50 Tg CH_4/y), and 'extreme' (+100 Tg CH_4/y) increases to the 202 Tg CH_4/y global natural emissions baseline by 2050.

Ideally, the sum of all process-based bottom-up estimates of natural emissions should reconcile with emissions estimated from the atmospheric budget for methane. Current comparisons based on the available albeit limited process-based emission estimates and the limited atmospheric observations do show the two to be roughly similar indicating progress in estimating the magnitudes of these sources, but highlighting that ability to constrain natural source emissions values is at an early stage, and that further research is required to characterize these natural sources, and their extrapolation to the larger Arctic region spatial scale.

Q2: What are the current and potential future anthropogenic emissions of Arctic and non-Arctic nations? (Chapter 5)

Chapter 5 summarizes existing inventories and projections of future anthropogenic methane emissions at a global scale as well as for the Arctic nations. The chapter focuses on how anthropogenic methane emissions in the Arctic nations compare to global emissions and the relative importance of various emission sectors within the Arctic nations in terms of their contribution to current and potential future emissions and reduction potentials.

The evaluation of current (and past) global anthropogenic methane emissions is based on review of eight global inventories, with a focus on three of the most recent and sector-detailed inventories: the USEPA, IIASA (GAINS), and the European Commission (EDGAR). Emissions inventories are rarely based on direct measurements, and generally rely on the use of emissions factors that can differ in range by nation and/or sector. Each of the approaches leads to different levels of uncertainty. There is noticeable and important year-to-year variability in the reporting of methane emissions. Despite the fact that most estimates of total global emissions agree within a narrow range of values, there is important uncertainty among the various sectoral estimates, suggesting that inventories may not be as good as the agreement in the overall totals suggest. The most recent estimates for which multiple, detailed, sector-specific data are available are for 2005. This provides an estimate of global anthropogenic emissions in the range of 319 to 346 Tg CH_4/y. Currently the eight Arctic nations release about a fifth of global anthropogenic methane emissions, or about 66 Tg CH_4/y, although not all of these are emitted above 60°N. The emissions are attributed (in descending order) to fossil fuel production, transmission and distribution; agriculture; and waste/wastewater sectors.

The projections of future anthropogenic methane emission are based on assumptions about future developments in major socio-economic sectors and assumptions about the nature and extent of future climate policies. For the Arctic nations, it is estimated that maximum feasible reductions (based on the IIASA GAINS derived estimates of maximum technically achievable reductions with no consideration of economic cost – MFR) could result in emissions that are 63% below currently legislated emissions (CLE), or about one quarter of

the entire global technical reduction potential estimated for anthropogenic methane in 2030. The largest technical abatement potentials for Arctic nations are found from oil and gas systems, specifically reduced venting of waste gas primarily associated with oil extraction and management of unintended leakage during oil and gas production, transmission and distribution. As a single world region, the eight Arctic nations emit more anthropogenic methane and have a larger technical abatement potential, than any other major world region.

Q3: Are the current monitoring activities (of atmospheric concentrations and fluxes) sufficient to capture anticipated source changes? (Chapters 6 & 7)

Chapter 6 presents the first pan-Arctic synthesis of long-term atmospheric methane concentrations. Chapter 7 applies these observations using atmospheric inverse modeling techniques to estimate emissions and sources of methane, with a specific focus on wetland sources.

Over the past five to six years the number of surface monitoring sites for methane has increased in the Arctic. This report includes data from eighteen long-term Arctic and sub-Arctic sites which are now (or recently have been) in operation, and for which the data are accessible and of known quality. Only a handful of these sites span time periods back to the mid-1980s, and most extend back only about ten years. With these observations, it is now possible to undertake analyses directed towards characterizing interannual variability, as well as seasonal and diurnal patterns. This report is the first time that these Arctic methane observations have been compiled in an integrated pan-Arctic analysis; consequently, the results are preliminary and the focus is on presenting the temporal patterns (trends and variability). The authors were unable to conduct an in-depth analysis of the spatial adequacy of the current observations to detect changes in atmospheric concentrations resulting from human activities or climate change within the timeframe of this study.

Overall, the trends in Arctic atmospheric concentrations of methane mirror the global trends. In winter, Arctic sites are strongly influenced by transport from mid-latitude source regions. During the warmer summer period there is much more day-to-day variability, which is indicative of near surface source influences attributed to wetlands. Methane isotopic data provide additional confirmation that the higher atmospheric concentrations observed during summer can be attributed to wetland sources, and during winter to regional fossil fuel sources.

It is anticipated that Arctic terrestrial ecosystems will undergo significant changes as warming continues. The positive (warming) feedback from such changes may be large, although to date, no significant changes in Arctic atmospheric methane concentrations related to natural sources have been detected by the observational network. Given the large year-to-year variability in the Arctic and the relatively short methane observational record, with only three Arctic measurement sites having records of 30 years or more, it is not possible to detect an atmospheric signal (i.e. change in atmospheric methane concentrations) related to long-term changes in natural sources such as wetlands, permafrost or marine environments that may be associated with climate change. As these observational records continue and atmospheric transport modeling capability

continues to evolve, a detailed assessment of the adequacy of the observational network to detect future atmospheric change and to support the characterization of sources could be undertaken.

Continuation of the existing long-term observational network, as well as evaluating the adequacy of spatial and temporal coverage of Arctic atmospheric methane measurements will be essential to improve ability to assess the overall impact of changes in regional and global methane sources and to detect corresponding changes in the atmospheric concentrations of methane.

The integration of surface observations with atmospheric transport modeling, through the use of atmospheric inverse modeling techniques, has demonstrated the usefulness of the existing observations in providing an alternate approach to estimating methane emissions. Arctic region natural and anthropogenic emission estimates from atmospheric inverse modeling studies agree reasonably well over the period 2000–2010 suggesting total emissions of 25 Tg CH_4/y. The atmospheric concentrations of methane provide an upper bound or envelope for estimating source contributions. This suggests that the higher estimates for natural emissions are unlikely.

Methane-related biogeochemical processes, including those in wetlands, are being progressively included in ESMs. This includes the capability to dynamically simulate the spatial extent of wetlands and the corresponding methane emissions based on wetland sub-modules of terrestrial ecosystem models. Process model estimates of methane emissions from wetlands were systematically compared with global atmospheric observations using atmospheric inverse modeling approaches. The process-based models appear to overestimate the natural source strength globally and for the Arctic region, in so far as the specification of anthropogenic methane emissions in inverse modeling studies is realistic. Models generally appear to capture the latitudinal and seasonal patterns expected according to the observations. Expanded observational coverage and increased length of data records, will have the dual contribution of improving quantification of the current emissions, but also in providing the opportunities to assess the performance of the ESMs used to project climate change and the future behavior of various biogeochemical processes.

Q4: What is the historical and future Arctic climate response to changes in methane emissions, from Arctic and from global sources? (Chapter 8)

Chapter 8 presents model-based projections of the impacts of future change in methane emissions, both from anthropogenic and natural sources, on concentrations of atmospheric methane and climate globally and for the Arctic region.

Results from 26 model simulations using three different ESMs indicate that global implementation of available maximum technically feasible reductions in global anthropogenic methane emissions (the MFR scenario, relative to the CLE scenario) would reduce the future average warming of global climate by 0.2°C for the 2036–2050 period (including corresponding contributions from ozone and stratospheric water vapor). For the Arctic region, the ESM results show larger air temperature responses related to this methane mitigation, but also greater variability. The three model simulations undertaken for this analysis estimate a reduction in annual mean warming in the range 0.26–0.40°C for the Arctic region. Given the

large variability in the Arctic climate response to changes in methane emission (Fig. 8.4), additional simulation of the rather unrealistic implementation of MFR by the eight Arctic nations only was not undertaken, but simple scaling of the global response suggests it would reduce warming, both global and Arctic, on the order of one tenth of a degree. However, this does not imply that such measures by the Arctic nations would not be important as a part of climate change policies. It should also be noted that more recent emission scenarios (e.g. ECLIPSE 2014) and implications of various energy scenarios or behavioral changes, suggest that the estimate of reductions in warming in the present report may be conservative.

Over a similar time period (to 2050), Arctic warming driven by all climate forcers, primarily carbon dioxide, can potentially increase natural emissions from terrestrial and marine ecosystems. The maximum technically feasible (MFR) emission reduction scenario for the eight Arctic nations, which reduces anthropogenic emissions by 43 Tg CH_4/y by 2050, is comparable to the magnitude of the potential increase by 50 Tg CH_4/y in natural emissions in the 'high' scenario due to climate warming. As ESMs progressively include methane-related biogeochemical processes it will be possible to gain a better understanding of the effect of climate warming on methane-related feedbacks and to quantify the effect of mitigating anthropogenic methane emissions in a consistent framework.

It is well recognized that the location of black carbon emissions, another short-lived climate forcing agent, is relevant to determining its impact on Arctic climate. While commonly accepted that geographic location of emissions of longer-lived atmospheric species such as methane are not relevant, a limited investigation of this issue was undertaken. The analysis indicates that although there are latitudinal gradients in methane distribution, drastic changes in the spatial distribution of methane emissions will not significantly affect the global-mean concentration of methane, and need not be a major consideration in mitigation strategies.

Q5: What are the uncertainties in understanding the Arctic climate response to methane? (Various chapters)

Uncertainty was a cross-cutting theme through all chapters and is summarized here. The climate response to methane is influenced by the breadth of spatial scales across source types and atmospheric transport distances, as well as by the breadth of time scales from seasonal variability in emission sources to the near decadal atmospheric lifetime of methane and related warming impact. Uncertainty exists in all aspects, from mechanistic or process understanding, to observational and monitoring data, to models and model results, and includes application of expert judgment. The multiple layers of uncertainty make it difficult to precisely quantify the Arctic climate response to changing methane emissions. In light of this, uncertainties are discussed below as a basis for the subsequent recommendations to improve scientific confidence in both estimating the Arctic climate response to methane, and in tracking the atmospheric response to changing methane emissions over time.

Atmospheric monitoring: For methane, standardized protocols exist for atmospheric monitoring of greenhouse gases as established by the World Meteorological Organization Global Atmosphere Watch (WMO-GAW) program, and the resulting

values for a given site can be specified with great precision and accuracy. Uncertainty in observations generally arises as short-term, site-specific results are scaled up to be representative of larger areas and longer time periods.

Ecosystem processes: Our uncertainty in understanding processes can be grouped into areas that are thought to be generally and widely understood, processes that may be well understood in limited areas, processes that are thought to be poorly understood and processes that are not recognized or appreciated (the unknown unknowns). The ecological, biological and physical processes that control Arctic systems and the response of those systems to change range in scales from molecular to landscape, regional and global. A major source of uncertainty results from the scaling of small-scale or point measurements and related understanding of the underlying processes, to the larger regional and global scales of the climate response to changing atmospheric methane concentrations.

Modeling: Uncertainty in model projections is associated with the capability of a model to represent the variability associated with the natural Earth system (Internal variability); the ability to represent the biological, chemical and physical processes within the atmosphere, oceans and biosphere based on imperfect understanding of those processes (Model uncertainty); and the socio-economic story lines that describe various futures and related emission pathways that are used to 'force' ESMs (Scenario uncertainty). Socio-economic assumptions are generally thought to represent the largest source of uncertainty in future emission projections and becomes more important as the time perspective of the simulation increases.

9.2 Recommendations for research and monitoring

Each chapter of this report made detailed recommendations for research and monitoring that warrant attention specific to the challenge of estimating the impact of methane on Arctic climate, and detecting that impact in the atmosphere. The recommendations are summarized as follows.

9.2.1 Natural emissions

Maintain and expand existing methane flux time series measurements in order to improve understanding of the terrestrial ecosystem processes that control methane emissions and so improve their representation in ecosystem models. In particular: i**ncrease flux measurements during winter, add more sites in representative ecosystems/areas, and expand efforts to better characterize (especially in terms of carbon contents) Arctic soils, sediments and water bodies** so that emerging process understanding can be better extrapolated across the Arctic region. Addressing these recommendations requires an overall enhancement of Arctic research and monitoring infrastructure to make measurements possible in all seasons and across challenging Arctic locales.

Continue and significantly enhance current efforts to characterize the distribution, extent and stability of methane hydrates as well as to **understand the processes associated with ocean methane production, consumption, transport, and**

release in order to improve the understanding and representation of marine methane emissions. Likewise, **further investigate sources in subsea permafrost areas and the effect of sea-ice decline**. Recognizing the obvious difficulty in monitoring natural marine source contributions to the atmosphere (e.g. using shipboard platforms), there is a need to **develop new techniques to determine the sea-to-air flux of methane**. In addition, **extensive analysis of high-resolution paleo records** would put current and projected future releases into context. **Apply the newly obtained knowledge in process-based models** to better assess current and future methane release from the Arctic Ocean.

9.2.2 Anthropogenic emissions

Undertake additional direct or on-site source measurements (at scales that support extrapolation), **harmonize development and application of emission factors internationally, and improve the temporal (interannual) resolution of reported emissions** in order to improve estimation of anthropogenic methane emissions. Subsequent assessment efforts should **focus on fugitive emissions from all aspects of oil and gas systems** from exploration through production and distribution.

9.2.3 Observations and inverse modeling

Continue existing long-term monitoring sites on decadal timeframes, and make all data consistent and accessible through international data archives, addressing obvious large spatial gaps. This is essential in order to assess the overall impact of regional and global, and anthropogenic and natural, source influences on atmospheric concentrations, and the related Arctic climate response. The existing observations support preliminary investigation of the spatial adequacy of observations for detecting changes in natural and anthropogenic sources as reflected by atmospheric concentrations of methane, and it is recommended this work be done to guide the ongoing network design and optimization.

Continue efforts to reconcile top-down and bottom-up estimates, which include improvements related to surface observations, anthropogenic inventories and characterization of natural source processes; total column measurements; and improved atmospheric transport models particularly regarding their spatial resolution.

9.2.4 Earth system modeling

Continue and enhance ongoing efforts to improve the representation of Arctic specific land-surface processes and atmospheric chemistry processes related to methane in ESMs in order to improve the representation of regional Arctic climate and methane-related feedbacks. Arctic-specific processes include representation of shrubs, their expansion in response to climate warming, permafrost and wetlands. Processes required for modelling the atmospheric concentration of methane as a dynamic variable require wildfires and wetlands, the soil sink of methane, the ocean-atmosphere methane flux, and atmospheric chemistry processes. The atmospheric chemistry processes include the linkages between methane and ozone, representation of the OH–methane sink and the ozone and water vapor radiative forcing contributions.

9.3 Final comments

This report contributes to the growing number of studies focused specifically on the Arctic climate response to short-lived climate forcing agents, confirming the relevance of Arctic nations and global action on methane to Arctic climate. In summary, the Arctic is both a region sensitive to climate change and an important source of natural methane emissions. At this time, there is insufficient scientific understanding and data to provide a precise quantitative estimate of the Arctic climate response to changing emissions of the Arctic nations. However, it is clear that global action to reduce anthropogenic emissions of methane would reduce the magnitude of anticipated warming in the Arctic. More specifically, in response to the two overarching questions posed as the basis for this report:

What is the potential benefit, in terms of reduced Arctic warming, of methane emissions mitigation by Arctic nations? Examining scenarios with a focus on methane only, indicates that global anthropogenic methane emissions mitigation would reduce Arctic warming by a few tenths of a degree. Simple scaling of the global response suggests that implementation of maximum technically feasible reduction by Arctic nations only, according to the scenarios analyzed in this report, would reduce warming by less than one tenth of a degree. Methane-specific mitigation actions, if implemented globally, would contribute to addressing global and Arctic region warming, and correspond to about 10–15% of the global average warming expected over the 2006–2050 period due to all climate forcers (carbon dioxide, methane, nitrous oxides, hydrofluorocarbons and aerosols) in a future where there is no additional mitigation, as in the business-as-usual RCP8.5 scenario.

How does the magnitude of potential emission reductions from anthropogenic sources compare to potential changes in methane emissions from natural sources in the Arctic? Given the large uncertainty in estimates of current and potential future natural sources, absolute conclusions are not possible. Changes in natural emissions will depend upon how climate continues to change. Mitigation of anthropogenic methane, as a complement to action on carbon dioxide, will contribute to reducing the potential for increased release of methane from natural sources related to a warming climate. The maximum feasible emission reductions globally in year 2050 (MFR scenario) result in reductions in atmospheric methane concentration which are roughly comparable to the increase projected in the 'extreme' natural emissions scenario.

It must be noted that climate warming over the near and longer term will continue to be driven primarily by increases in atmospheric concentrations of carbon dioxide. Correspondingly, the capacity to mitigate greenhouse-gas driven warming will require efforts on all fronts and methane mitigation has a clear contribution to make in this effort.

Annex: Modeling the climate response – A summary

AUTHORS: TERJE K. BERNTSEN, MICHAEL GAUSS

A1 Introduction

This Annex is a common contribution to the AMAP assessments on methane (the present report) and black carbon and ozone (AMAP 2015) and has been produced to facilitate an integrated understanding of the separate climate modelling exercises undertaken by the two AMAP expert groups on short-lived climate forcers (SLCFs).

The objective for modeling studies in the two expert groups has been to quantify the potential reduction in global and Arctic warming by mitigation of methane (CH_4), black carbon (BC) or non-methane ozone precursors (nmOP). The nmOP include nitrogen oxides (NO_X), carbon monoxide (CO) and non-methane volatile organic carbons (nmVOC).

To address this objective, the two expert groups chose different modeling strategies due to the different nature of methane versus BC/nmOP. Although these species are commonly referred to as short-lived climate forcers it is important to distinguish two different interpretations of the term 'short-lived'.

1. *Short-lived* in the sense that the residence time is shorter than the typical mixing time in the atmosphere on a hemispheric scale (i.e. shorter than about one month). Only BC/nmOP is short-lived in this context. With this short lifetime, the location and seasonal cycle of emissions can have direct effect on the climate response in the Arctic, so that sources and regions must be treated individually. These compounds are denoted here as very-SLCFs (VSLCF).

2. *Short-lived* in the sense that the residence time is shorter than for typical long-lived greenhouse gases (such as carbon dioxide, CO_2; nitrous oxide, N_2O; or sulfur hexafluoride, SF_6) and that the compound is amenable to mitigation for which a climate response would be evident in the near term (decades). Both methane and BC/nmOP are short-lived in this context.

A2 Modeling approach

Coupled chemistry-climate models (CCMs) are now available, so the ideal approach for estimating the effect of reductions in both methane and BC/OP emissions would be through fully coupled transient CCM simulations. However, for BC/nmOP emissions (including co-emitted species like organic carbon, OC, and sulfur dioxide, SO_2) this is not feasible due to the very small forcing signals from individual regions/sources, which would require extremely long simulations (or a very high number of ensembles) to obtain a statistically robust result for the climate response. In the case of methane, due its relatively long lifetime (about nine years) and thus its relatively small spatial variability in the atmosphere, it is common in climate models to prescribe concentrations rather than emissions. For the AMAP methane assessment, methane concentrations were calculated with a box model and a chemical transport model (CTM), and then used in Earth System Models (ESMs) to calculate the climate response.

A2.1 VSLCFs

In the black carbon and ozone assessment the main outcome of the modelling simulations is a quantification of the contribution to Arctic equilibrium warming by *current* emissions from *seven regions, six emission sectors*, and by the *components BC, OC, SO_2, and nmOP*. From each experiment and model the zonally average radiative forcings in broad latitude bands were diagnosed. To obtain an estimate of the Arctic surface air temperature response, the AMAP BC/O3 Expert Group used regional temperature potentials (RTPs) pre-calculated by the Goddard Institute for Space Studies Earth System Model (GISS ESM, Shindell and Faluvegi 2010). RTPs relate equilibrium regional temperature response to radiative forcing in different latitude bands and thus offer an efficient way to obtain regional temperature change for a multitude of scenarios.

In parallel to the modeling efforts of the AMAP expert groups, the EU-project ECLIPSE has undertaken similar modeling efforts. ECLIPSE developed and used a global mitigation scenario with focus on optimal BC/nmOP reductions, including all regions and sectors. For this global scenario, transient CCM simulations were performed, and some results are reported in the AMAP assessment on black carbon and ozone (AMAP 2015: Sect. 11.5).

A2.2 SLCFs

For methane the reductions in emissions from all regions and sectors were considered together since the location and annual cycle of the emissions are of minor importance. In addition, since the radiative forcing due to reduction in methane emissions is greater than that for other SLCFs, fewer experiments were needed. Transient simulations performed with three different ESMs (see Sect. 8.3) were used to calculate the climate response to reductions in anthropogenic methane emissions, averaged over the 2036–2050 period, with respect to the 2006–2010 period. Methane emissions from the ECLIPSE 2012 data set were used (see Fig. 5.9 and Table 8.1), as this was the most recent version at the time.

A3 Summary of main results

Table A1 provides a summary of the potential for reduced warming in the Arctic (and globally) around year 2050 if emissions of SLCFs are reduced according to the mitigation scenario established within the ECLIPSE project. The numbers given are from the AMAP Expert Groups, and from the ECLIPSE project (see Sect. A4.2).

Table A1 Summary of ESM and RTP-based modelling estimates of the potential reduction in Arctic (and global) warming around 2050[a], by mitigation of SLCFs.

	Predicted total warming[b]	Reduction potential by mitigation of SLCF emissions			
Arctic	About 2°C	Net of all SLCFs			
		°C		Model	
		0.40		RTP-based	
		0.29		ECLIPSE, CESM-CAM5	
		0.42		ECLIPSE, NorESM	
		0.54		ECLIPSE, CESM-CAM4	
		0.49		ECLIPSE, HadGCM	
		Non-methane only		Methane only	
		°C	Model	°C	Model
		0.23	RTP-based	0.40±0.14	CanESM2, RCP6.0
		0.14	ECLIPSE, ECHAM[c]	0.35±0.17	CanESM2, RCP8.5
				0.26±0.26	CESM1, RCP6.0
				0.33±0.25	CESM1, RCP8.5
				0.33±0.14	NorESM, RCP6.0
				0.17	RTP-based
Global	About 0.7–1.5°C[d]	Net of all SLCFs		Methane only	
		°C	Model	°C	Model
		-0.05	ECLIPSE, CESM-CAM5	0.27±0.07	CanESM2, RCP6.0
		0.20	ECLIPSE, NorESM	0.26±0.04	CanESM2, RCP8.5
		0.22	ECLIPSE, CESM-CAM4	0.10±0.05	CESM1, RCP6.0
		0.29	ECLIPSE, HadGCM	0.15±0.06	CESM1, RCP8.5
				0.22±0.04	NorESM, RCP6.0

[a]The model results and RTP-based values in this table are given as multi-year averages, representative for the 2040s; [b]with respect to present day; [c]results from ECHAM (an ESM used in the assessment on black carbon and ozone, see AMAP 2015) are for BC, OC and SO_4 only; ECHAM does not include the impact of BC on snow; [d]Collins et al. (2013, their figure 12.5).

A4 Results from the Expert Group on Black Carbon and Ozone

To identify the mitigation potential for BC/nmOP, for combinations of regions and sectors, the individual contributions by current emissions to equilibrium Arctic warming were calculated first (Fig. A1). In absolute terms, emissions from domestic combustion (e.g. heating, cooking, waste burning – with BC as the main component) make the largest contribution. The impact of nmOP is relatively small.

While the results shown in Fig. A1 provide a tool to identify the potential for impact on Arctic temperature from mitigation by region and sector, the results in Fig. A2 provide a basis for estimating the Arctic temperature response for any given combination of compounds, regions and sectors. The numbers in Fig. A2 also provide the basis for estimating cost-efficacy if the cost for each source is known.

A4.1 Ozone

Ozone is a secondary gas formed through oxidation of methane, nmVOC, CO and NO_X in the presence of sunlight. For the assessment on black carbon and ozone (AMAP 2015),

model simulations were performed where the emissions of the three ozone precursors NO_X, CO and nmVOC were removed *simultaneously*. Methane concentrations were kept constant at the 2010 level in all simulations. With this model set-up it was possible to estimate the effect on Arctic temperture from these ozone precursors combined, but not their individual contributions. The CTMs were used to calculate concentration changes and radiative forcings. Emissions of NO_X, CO and nmVOCs do not only change ozone, but also the oxidizing capacity of the atmosphere and thus impact methane concentrations. RTPs were applied to estimate the impact on Arctic temperature as shown in Fig. A3, giving a net Arctic warming of about 0.05°C. Note that the net impact of the ozone precursors (NO_X, CO and nmVOCs) is much lower than the impact of aerosols (BC, OC, and SO_4) (Fig. A2).

Increased methane emissions also lead to increased ozone formation. Neither of the AMAP expert groups performed model simulations to quantify the Arctic warming that is due only to changes in ozone concentration associated with increases in anthropogenic methane emissions. To derive an estimate of this effect, simulations of ozone changes due to current anthropogenic emissions of all ozone precursors (NO_X, CO, nmVOC and methane) were used in the ACCMIP

Arctic Ts response, °C
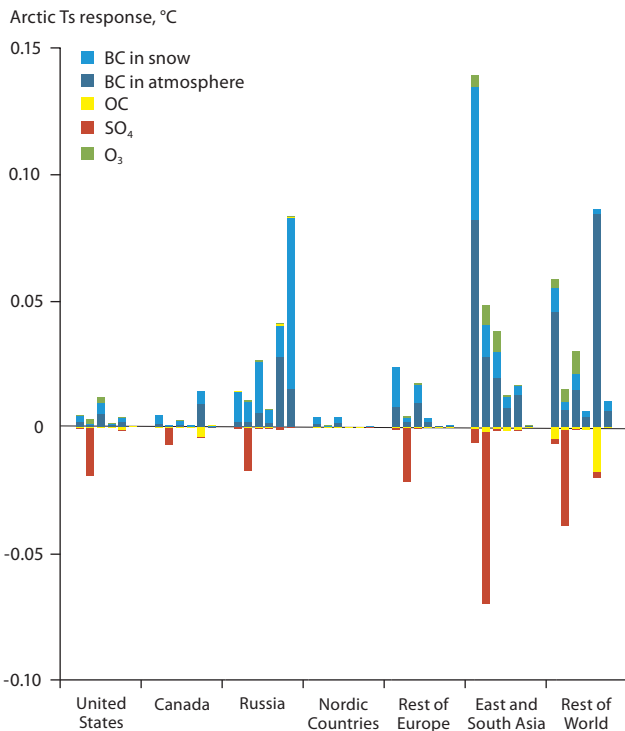
Fig. A1 Arctic equilibrium surface temperature response due to direct forcing by black carbon (BC), organic carbon (OC), sulfate (SO$_4$) and ozone (O$_3$) averaged over the models CESM, NorESM, SMHI-MATCH and Oslo-CTM. Each bar represents the different emission sectors for each source region specified on the X-axis. The sectors for each emission region are 1) Domestic, 2) Energy+Industry+Waste, 3) Transport, 4) Agricultural waste burning, 5) Forest fires and, 6) Flaring. The temperature changes were derived by translating the radiative forcings with the use of climate sensitivity parameters.

Arctic Ts response per unit emission, °C per Tg/y
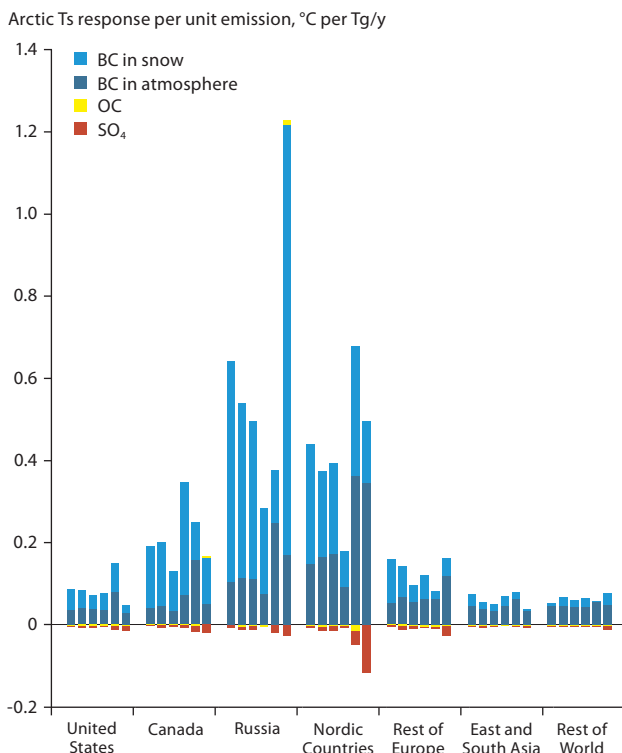
Fig. A2 Arctic equilibrium surface temperature response per emissions due to direct forcing of black carbon (BC), BC in snow, organic carbon (OC) and sulfate (SO$_4$) (in (°C (Tg/y)$^{-1}$) averaged over the models CESM, NorESM, SMHI-MATCH and Oslo-CTM. The sectors for each emission region are (from left to right): 1) Domestic, 2) Energy+Industrial+Waste, 3) Transport, 4) Agricultural waste burning, 5) Forest fires and, 6) Flaring. The temperature changes were derived by translating the radiative forcings with the use of climate sensitivity parameters.

Arctic Ts response, °C

Fig. A3 Arctic equilibrium surface temperature response due to the net impact of emission of ozone (O$_3$) precursors in the Oslo-CTM model. The temperature changes were derived by translating the radiative forcings with the use of climate sensitivity parameters.

experiment (Lamarque et al. 2013). Calculating the radiative forcing and using the RTP approach, resulted in an estimated total Arctic warming by these emissions of 0.12°C. Assuming that the difference can be assigned to ozone produced from methane, it may be concluded that ozone produced by current methane oxidation gives an equilibrium Arctic warming of about 0.07°C. This crude estimate neglects non-linear chemical effects and has substantial uncertainty through the RTP coefficients for ozone which have only been calculated by one model (GISS) so far.

A4.2 Results from the ECLIPSE transient simulations

Within the ECLIPSE project a future emission mitigation scenario of SLCFs has been established, taking into account that mitigation of compounds (e.g. BC) that lead to warming will, to a certain extent, also reduce emissions of cooling compounds (co-emitted species). The scenario assumes that for all sources the emission reductions are phased in linearly over 15 years (2015–2030), and kept constant after that. The scenario includes mitigation of all SLCFs, including methane, OC and SO$_2$. It should be noted that the total emission reductions in this scenario are quite high. By 2050, according to version 5 of the ECLIPSE data set (in the present report referred to as 'ECLIPSE 2014'), the maximum technically feasible reductions with respect to the CLE (Current LEgislation) scenario are 76% or 4.7 Tg/y (BC), 54% or 285 Tg/y (CH$_4$), 48% or 270 Tg/y (CO) and 63% or 79 Tg/y for VOC. For OC the reduction is 71% (9.8 Tg/y), while for SO$_2$ it is only 1%.

Transient model simulations for the period 2015–2050 have been performed with four ESMs. The response to the SLCF

Table A2 Effects of maximum technically feasible reduction in all SLCF emissions on ensemble-mean climate states, averaged over 2041–2050, following the ECLIPSE version 5 scenario. Changes significant at p=0.05 are shown in bold.

	Model	Reduction in surface air temperature, °C	Increase in sea-ice area, km²
Global	CESM-CAM5	-0.05	8.8×10⁴
	NorESM	**0.20**	**4.4×10⁵**
	CESM-CAM4	**0.22**	**5.0×10⁵**
	HadGEM	**0.29**	**9.5×10⁵**
Arctic (60–90°N)	CESM-CAM5	**0.29**	**1.6×10⁵**
	NorESM	**0.42**	**2.3×10⁵**
	CESM-CAM4	**0.54**	2.8×10⁵
	HadGEM	**0.49**	**2.9×10⁵**
	RTP-based	0.40	

The MITIGATE scenario assumes the full implementation of a portfolio of SLCF measures by 2030 and 2050 designed to achieve large reductions in temperature response in the short term at the global scale. The BASELINE scenario includes all presently agreed legislation and adopted policies affecting air pollutant emissions (see Ch. 5 in AMAP 2015).

mitigation scenario mentioned above can also be estimated with an RTP-based approach using the climate sensitivities given in Fig. A2 (and from the literature for NO$_X$, CO, nmVOC and methane). Table A2 summarizes the net global and Arctic responses (averaged over the period 2041–2050) for the ESMs and for the RTP-based method.

The forcing and responses given in Table A2 are for the combined effect of mitigation of all SLFCs. Without additional costly simulations it is not possible to attribute the impacts to individual components. However, this can be done using the more simple RTP-based approach (Shindell and Faluvegi 2010) described in Section A2.1. Using the Arctic RTPs for the aerosols (BC, OC, and SO$_4$) from Fig. A2, and RTPs for the ozone precursors (including methane) from Collins et al. (2013) it was possible to calculate the transient response to the mitigation scenario. For the 2040–2050 period, methane mitigation accounts for 42% of the signal in the reduced Arctic surface warming. Figure A4 shows the contributions from the different components as a function of time using the RTP-based method.

A5 Results from the Expert Group on Methane

The Expert Group on Methane used emissions from the ECLIPSE 2012 data set (see Fig. 5.9 and Table 8.1) to calculate the effect of methane emissions mitigation on surface air temperature. It was possible to calculate the effect of methane in isolation from other SLCFs because the methane mitigation measures considered in the ECLIPSE scenario do not affect the emissions of other species to a significant degree. The methane emissions mitigation potential by year 2050 in this version amounts to 205 Tg CH$_4$/y, compared to year 2005. This is lower than in the more recent ECLIPSE 2014 data set (285 Tg CH$_4$/y, Fig. 5.9), which was used by the Expert Group on Black Carbon and Ozone. The reason why ECLIPSE 2012 was used in the
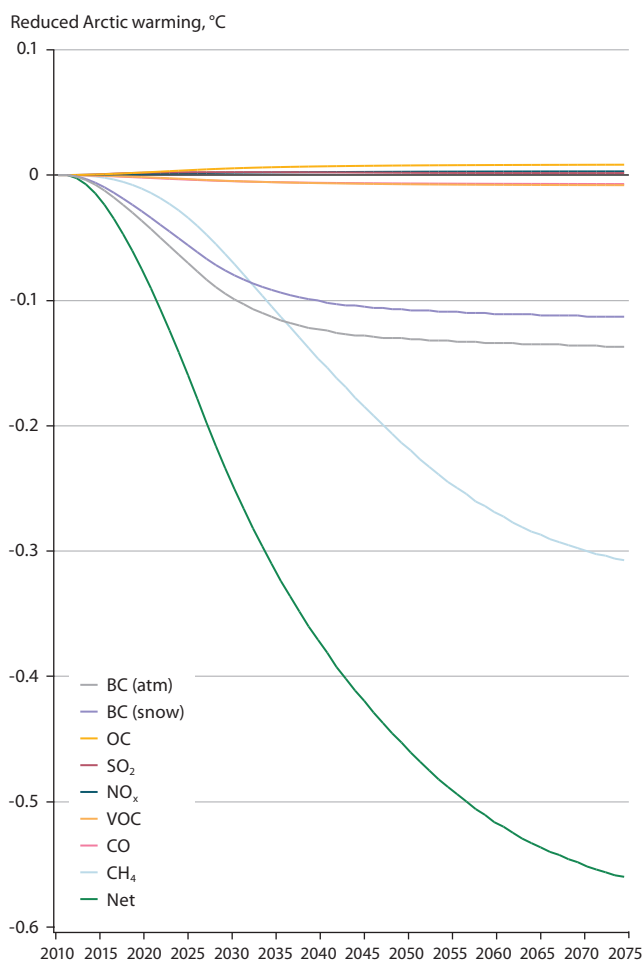
Fig. A4 RTP-based estimate of reduced warming in the Arctic in response to ECLIPSE mitigation scenario.

present assessment is because this was the most recent data set at the time the model calculations began.

Three different ESMs (CanESM2, CESM1, NorESM) were used to calculate the climate response to maximum technically feasible reductions (MFR) in anthropogenic methane emissions. The climate response was calculated over the period 2036–2050 as the difference between simulations that used methane concentrations corresponding to the MFR scenario and simulations that used concentrations corresponding to the CLE scenario. In the CLE scenario, the anthropogenic methane emissions continue to increase as the current state of technology prevails and any further emission reductions are limited to those prescribed by currently adopted legislation.

Since the ECLIPSE 2012 data did not contain all climate gases that are needed to run the ESMs, some components (notably CO$_2$) were taken from the RCP (representative concentration pathways) scenarios used by the Intergovernmental Panel on Climate Change in its Fifth Assessment (IPCC AR5). This approach of blending ECLIPSE and RCP data is explained in Box 8.3. It is important to note that methane emissions used in the present calculation were derived solely from the MFR and CLE scenarios of the ECLIPSE data set. Methane data from the RCP scenarios were not used.

The methane concentrations corresponding to the two emissions scenarios (MFR and CLE) were obtained using two approaches:

Table A3 Summary of results for the *reduction* in global warming for the 2036–2050 period, due to maximum technically feasible reduction in anthropogenic methane emissions, diagnosed as the difference in surface air temperature between the MFR and CLE scenarios, averaged either globally or over the Arctic region. (This table corresponds to Table 8.3 but with the RTP-based result added for comparison.)

Model	Background scenario	Reduction in warming simulated by the model (ΔT), °C		Reduction in warming after taking into account the associated changes in ozone and stratospheric water vapor ($\Delta T_{O3,H2O}$), °C
		Global	Arctic	Global
CanESM2	RCP6.0	0.18±0.05	0.40±0.14	0.27±0.07
	RCP8.5	0.18±0.03	0.35±0.17	0.26±0.04
CESM1	RCP6.0	0.07±0.04	0.26±0.26	0.10±0.05
	RCP8.5	0.11±0.05	0.33±0.25	0.15±0.06
NorESM	RCP6.0	0.20±0.03	0.33±0.14	0.22±0.04
Mean		-	-	0.20±0.02[a]
RTP-based		0.17		

'Background scenario' refers to the scenario according to which non-methane climate forcers (e.g. CO_2) were specified. ΔT is the result from the ESM simulations, while $\Delta T_{O3,H2O}$ takes into account the effects of changes in ozone and stratospheric water vapor due to changes in methane emissions. The ratio between $\Delta T_{O3,H2O}$ and ΔT depends on the ESM and is calculated based on numbers of radiative forcing given by IPCC AR5 (Myhre et al. 2013), as described in Box 8.4.

[a]The error bar of ±0.02°C is the statistical uncertainty of the mean over the five model simulations. It is not representative of the level of scientific understanding, as it does not take into account any systematic errors in the models (model biases, missing processes, etc.) or uncertainties in the emission estimates.

1. A one-box model of atmospheric methane calculated annually-averaged global-mean concentrations of methane and these were used by CanESM2 and CESM1.

2. A chemical transport model calculated monthly-averaged 3-D fields of methane and ozone concentration and these were used by NorESM.

Table A3 summarizes the temperature reduction due to maximum technically feasible reduction in anthropogenic emissions of methane, averaged over the Arctic region and globally, based on 26 simulations. Averaging over the results of all models generates a reduction in global-mean temperature of 0.20°C. The models calculate Arctic temperature reductions of between 0.26 and 0.40°C, which compares well with the ECLIPSE results. Given the different capabilities of the ESMs, the effects of ozone and stratospheric water vapor due to changes in methane emissions are not included in all models. However, the effects of ozone and stratospheric water vapor are accounted for through scaling methods, although only for the *global mean* values. The distribution of *regional* climate response is more complex to calculate and depends on the climate forcer (e.g. Shindell 2007). As methane-induced changes in ozone and stratospheric water vapor are not evenly distributed (see Sect. 8.3.2.2), the Arctic climate response (north of 60°N) should not be multiplied by scaling factors derived on the basis of global-mean radiative forcing values.

As seen in Table A3, the spread of calculated reductions for the Arctic is considerable and reflects the uncertainty in modelling climate response over small regions, especially in the Arctic given its inherent climatic variability. This uncertainty should also be kept in mind when estimating temperature change based on RTPs used above, which are derived from one model only (GISS ESM).

References

ACIA, 2004. Impacts of a Warming Arctic: Arctic Climate Impact Assessment. Cambridge University Press.

ACIA, 2005. Arctic Climate Impact Assessment. Cambridge University Press.

Alberta Energy Regulator, 1998. Alberta Environmental Protection: Code of Practice for Landfills. Government of Alberta, Canada.

Alberta Energy Regulator, 2013. Upstream Petroleum Industry Flaring and Venting Report, 2012. Government of Alberta, Canada.

Alberta Energy Regulator, 2014. Directive 060: Upstream Petroleum Industry Flaring, Incinerating and Venting. Government of Alberta, Canada.

Alberta Environment, 2007. Quantification Protocol for the Anaerobic Decomposition of Agricultural Materials. Government of Alberta, Canada.

Alexandratos, N. and J. Bruinsma, 2012. World Agriculture towards 2030/2050: The 2012 Revision. ESA Working Paper No. 12-03. United Nations Food and Agricultural Organization.

Allan, W., H. Struthers and D.C. Lowe, 2007. Methane carbon isotope effects caused by atomic chlorine in the marine boundary layer: Global model results compared with Southern Hemisphere measurements. Journal of Geophysical Research, 112, D04306, doi:10.1029/2006JD007369.

Allen, D.T., V.M. Torres, J. Thomas, D.W. Sullivan, M. Harrison, A. Hendler, S.C. Herndon, C.E. Kolb, M.P. Fraser, A.D. Hill, B.K. Lamb, J. Miskimins, R.F. Sawyer and J.H. Seinfeld, 2013. Measurements of methane emissions at natural gas production sites in the United States. Proceeding of the National Academy of Sciences of the United States of America, 110:17768-17773.

Amann, M., I. Bertok, J. Borken-Kleefeld, J. Cofala, C. Heyes, L. Höglund-Isaksson, Z. Klimont, B. Nguyen, M. Posch, P. Rafaj, R. Sandler, W. Schöpp, F. Wagner and W. Winiwarter, 2011. Cost-effective control of air quality and greenhouse gases in Europe: Modelling and policy applications. Environmental Modeling and Software, 26:1489-1501.

AMAP, 2011a. Snow, Water, Ice and Permafrost in the Arctic (SWIPA): Climate Change and the Cryosphere. Arctic Monitoring and Assessment Programme (AMAP), Oslo, Norway.

AMAP, 2011b. The Impact of Black Carbon on Arctic Climate. By: Quinn, P.K., A. Stohl, A. Arneth, T. Berntsen, J. Burkhart, J. Christensen, M. Flanner, K. Kupiainen, H. Lihavainen, M. Shepherd, V. Schevchenko, H. Skov and V. Vestreng. AMAP Technical report No. 4. Arctic Monitoring and Assessment Programme (AMAP), Oslo.

AMAP, 2015. AMAP Assessment 2015: Black Carbon and Ozone as Arctic Climate Forcers. Arctic Monitoring and Assessment Programme (AMAP), Oslo.

Andreae, M.O. and P. Merlet, 2001. Emission of trace gases and aerosols from biomass burning. Global Biogeochemical Cycles, 15:955-966.

Andrews, A.E., J.D. Kofler, M.E. Trudeau, J.C. Williams, D.H. Neff, K.A. Masarie, D.Y. Chao, D.R. Kitzis, P.C. Novelli, C.L. Zhao, E.J. Dlugokencky, P.M. Lang, M.J. Crotwell, M.L. Fischer, M.J. Parker, J.T. Lee, D.D. Baumann, A.R. Desai, C.O. Stanier, S.F.J. de Wekker, D.E. Wolfe, J.W. Munger and P.P. Tans, 2013. CO_2, CO and CH_4 measurements from the NOAA Earth System Research Laboratory's Tall Tower Greenhouse Gas Observing Network: instrumentation, uncertainty analysis and recommendations for future high-accuracy greenhouse gas monitoring efforts. Atmospheric Measurement Techniques Discussions, 6:1461-1553.

Anisimov, O.A., 2007. Potential feedback of thawing permafrost to the global climate system through methane emission. Environmental Research Letters, 2, doi:10.1088/1748-9326/2/4/045016.

Archer, D., 2007. Methane hydrate stability and anthropogenic climate change. Biogeosciences, 4:521-544.

Archer, D., B. Buffett and V. Brovkin, 2009. Ocean methane hydrates as a slow tipping point in the global carbon cycle. Proceedings of the National Academy of Sciences, 106:20596-20601.

Arora, V.K., J.F. Scinocca, G.J. Boer, J.R. Christian, K.L. Denman, G.M. Flato, V.V. Kharin, W.G. Lee and W.J. Merryfield, 2011. Carbon emission limits required to satisfy future representative concentration pathways of greenhouse gases. Geophysical Research Letters, 38:L05805, doi:10.1029/2010GL046270.

Arrhenius, S., 1896. On the influence of carbonic acid in the air upon the temperature on the ground. Philosophical Magazine (Ser. 5), 41:237-276.

Arrhenius, S., 1908. Worlds in the Making. Harper, New York.

Aydin, M., K.R. Verhulst, E.S. Saltzman, M.O. Battle, S.A. Montzka, D.R. Blake, Q. Tang and M.J. Prather, 2011. Recent decreases in fossil-fuel emissions of ethane and methane derived from firn air. Nature, 476:198-201.

Barnier, B., G. Madec, T. Penduff, J.-M. Molines, A.-M. Treguier, J. Le Sommer, A. Beckmann, A. Biastoch, C. Böning, J. Dengg, C. Derval, E. Durand, S. Gulev, E. Remy, C. Talandier, S. Theetten, M. Maltrud, J. McClean and B. De Cuevas, 2006. Impact of partial steps and momentum advection schemes in a global ocean circulation model at eddy-permitting resolution. Ocean Dynamics, 56:543-567.

Bartlett, K.B. and R.C. Harriss, 1993. Review and assessment of methane emissions from wetlands. Chemosphere, 26:261-320.

Bartlett, K.B., P. Crill, R.C. Sass, R.S. Harriss and N.B. Dise, 1992. Methane emissions from tundra environments in the Yukon-Kuskokwim Delta, Alaska. Journal of Geophysical Research: Atmospheres, 97:16,645-16,660.

Bastviken, D., L.J. Tranvik, J.A. Downing, P. Crill and A. Enrich-Prast, 2011. Freshwater marine emissions offset the continental carbon sink. Science, 331:50, doi:10.1126/science.1196808.

Bates, T.S., K.C. Kelly, J.E. Johnson and R.H. Gammon, 1996. A re-evaluation of the open ocean source of methane to the atmosphere. Journal of Geophysical Research: Atmospheres, 101:6953-6961.

BC Ministry of Environment, 2008. Landfill Gas Management Regulation. Government of British Columbia, Canada.

BC Oil and Gas Commission, 2013. Flaring and Venting Reduction Guideline. Government of British Columbia, Canada.

Behrens, E., A. Biastoch and C.W. Böning, 2013. Spurious AMOC trends in global ocean sea-ice models related to subarctic freshwater forcing. Ocean Modelling, 69:39-49.

Bekryaev, R.V., I.V. Polyakov and V.A. Alexeev, 2010. Role of polar amplification in long-term surface air temperature: variations and modern Arctic warming. Journal of Climate, 23:3888-3906.

Bellisario, L.M., J.L. Bubier, T.R. Moore and J.P. Chanton, 1999. Controls on CH_4 emissions from a northern peatland. Global Biogeochemical Cycles, 13:81-91.

Bentsen, M., I. Bethke, J.B. Debernard, T. Iversen, A. Kirkevåg, Ø. Seland, H. Drange, C. Roelandt, I.A. Seierstad, C. Hoose and J.E. Kristjánsson, 2013. The Norwegian Earth System Model, NorESM1-M – Part 1: Description and basic evaluation of the physical climate. Geoscientific Model Development, 6:687-720.

Bergamaschi, P., M. Krol, F. Dentener, A. Vermeulen, F. Meinhardt, R. Graul, M. Ramonet, W. Peters and E.J. Dlugokencky, 2005. Inverse modeling of national and European CH_4 emissions using the atmospheric zoom model TM5. Atmospheric Chemistry and Physics, 5:2431-2460.

Bergamaschi, P., C. Frankenberg, J.F. Meirink, M. Krol, F. Dentener, T. Wagner, U. Platt, J.O. Kaplan, S. Korner, M. Heimann, E.J. Dlugokencky and A. Goede, 2007. Satellite chartography of atmospheric methane from SCIAMACHY on board ENVISAT: 2. Evaluation based on inverse model simulations. Journal of Geophysical Research, 112:D02304, doi:10.1029/2006JD007268.

Bergamaschi, P., C. Frankenberg, J.F. Meirink, M. Krol, M.G. Villani, S. Houweling, F. Dentener, E J. Dlugokencky, J.B., L.V. Gatti, A. Engel and I. Levin, 2009. Inverse modeling of global and regional CH_4 emissions using SCIAMACHY satellite retrievals. Journal of Geophysical Research, 114:D22301, doi:10.1029/2009JD012287.

Bergamaschi, P., S. Houweling, A. Segers, M. Krol, C. Frankenburg, R.A. Scheepmaker, E. Dlugokencky, S.C. Wofsy, E.A. Kort, C. Sweeney, T. Schuck, C. Brenninkmeijer, H. Chen, V. Beck and C. Gerbig, 2013. Atmospheric CH_4 in the first decade of the 21st century: Inverse modeling analysis using SCIAMACHY satellite retrievals and NOAA surface measurements. Journal of Geophysical Research: Atmospheres, 118:7350-7369.

Berndt, C., T. Feseker, T. Treude, S. Krastel, V. Liebetrau, H. Niemann, V.J. Bertics, I. Dumke, K. Dünnbier, B. Ferré, C. Graves, F. Gross, K. Hissmann, V. Hühnerbach, S. Krause, K. Lieser, J. Schauer and L. Steinle, 2014. Temporal constraints on hydrate-controlled methane seepage off Svalbard. Science, 343:284-287.

Berntsen, T.K., I.S.A. Isaksen, G. Myhre, J.S. Fuglestvedt, F. Stordal, T.A. Larsen, R.S. Freckleton and K.P. Shine, 1997. Effects of anthropogenic emissions on tropospheric ozone and its radiative forcing. Journal of Geophysical Research: Atmospheres, 102:28101-28126.

Bhatt, U.S., D.A. Walker, J. Walsh, E. Carmack, K.E. Frey, W. Meier, S. Moore, F.-J.W. Parmentier, E. Post, V. Romanovsky and W. Simpson, 2014. Implications of Arctic sea ice decline for the Earth system. Annual Review of Environment and Resources, 39:57-89.

Biastoch, A., T. Treude, L.H. Rüpke, U. Riebesell, C. Roth, E.B. Burwicz, W. Park, M. Latif, C.W. Böning, G. Madec and K. Wallmann, 2011. Rising Arctic Ocean temperatures cause gas hydrate destabilization and ocean acidification. Geophysical Research Letters, 38:L08602, doi:10.1029/2011GL047222.

Bindoff, N.L., P.A. Stott, K.M. AchutaRao, M.R. Allen, N. Gillett, D. Gutzler, K. Hansingo, G. Hegerl, Y. Hu, S. Jain, I.I. Mokhov, J. Overland, J. Perlwitz, R. Sebbari and X. Zhang, 2013. Detection and attribution of climate change: From global to regional. In: Stocker, T.F., D. Qin, G-K. Plattner, M. Tignor, S.K. Allen, J. Boschun, A. Nauels, Y. Xia, V. Bex and P.M. Midgley (eds.), Climate Change 2013: The Physical Science Basis. Contribution of Working Group I to the Fifth Assessment Report of the Intergovernmental Panel on Climate Change. Cambridge University Press.

Blunier, T., J.A. Chappellaz, J. Schwander, J.-M. Barnola, T. Desperts, B. Stauffer and D. Raynaud, 1993. Atmospheric methane, record from a Greenland ice core over the last 1000 year. Geophysical Research Letters, 20:2219-2222.

Boetius, A. and F. Wenzhöfer, 2013. Seafloor oxygen consumption fuelled by methane from cold seeps. Nature Geoscience, 6:725-734.

Boetius, A., K. Ravenschlag, C.J. Schubert, D. Rickert, F. Widdel, A. Gieseke, R. Amann, B.B. Jørgensen, U. Witte and O. Pfannkuche, 2000. A marine microbial consortium apparently mediating anaerobic oxidation of methane. Nature, 407:623-626.

Bolin, B. and C.D. Keeling, 1963. Large-scale atmospheric mixing as deduced from seasonal and meridional variations of carbon dioxide. Journal of Geophysical Research, 68:3899-3920.

Bosiö, J., M. Johansson, T.V. Callaghan, B. Johansen and T.R. Christensen, 2012. Future vegetation changes in thawing subarctic mires and implications for greenhouse gas exchange-a regional assessment. Climatic Change, 115:379-398.

Bourassa, M.A., S.T. Gille, C. Bitz, D. Carlson, I. Cerovecki, C.A. Clayson, M.F. Cronin, W.M. Drennan, C.W. Fairall, R.N. Hoffman, G. Magnusdottir, R.T. Pinker, I.A. Renfrew, M. Serreze, K. Speer, L.D. Talley and G.A. Wick, 2013. High-latitude ocean and sea ice surface fluxes: challenges for climate research. Bulletin of the American Meteorological Society, 94:403-423.

Bousquet, P., P. Ciais, J.B. Miller, E.J. Dlugokencky, D.A. Hauglustaine, C. Prigent, G.R. Van der Werf, P. Peylin, E.-G. Brunke, C. Carouge, R.L. Langenfelds, J. Lathière, F. Papa, M. Ramonet, M. Schmidt, L.P. Steele, S.C. Tyler and J. White, 2006. Contribution of anthropogenic and natural sources to atmospheric methane variability. Nature, 443:439-443.

Bousquet, P., B. Ringeval, I. Pison, E.J. Dlugokencky, E.-G. Brunke, C. Carouge, F. Chevallier, A. Fortems-Cheiney, C. Frankenberg, D.A. Hauglustaine, P.B. Krummel, R.L. Langenfelds, M. Ramonet, M. Schmidt, L.P. Steele, S. Szopa, C. Yver, N. Viovy and P. Ciais, 2011. Source attribution of the changes in atmospheric methane for 2006-2008. Atmospheric Chemistry and Physics, 11:3689-3700.

Brandt, A.R., G.A. Heath, E.A. Kort, F.O'Sullivan, G. Petron, S.M. Jordaan, P. Tans, J. Wilcox, A.M. Gopstein, D. Arent, S. Wofsy, N.J. Brown, R. Bradley, G.D. Stucky, D. Eardley and R. Harriss, 2014. Methane leaks from North American natural gas systems. Science, 343:733-735.

Brown, M., 1993. Deduction of emissions of source gases using an objective inversion algorithm and a chemical transport model. Journal of Geophysical Research: Atmospheres, 98:12,639-12,660.

Brown, M., 1995. The singular value decomposition method applied to the deduction of the emissions and the isotopic composition of atmospheric methane. Journal of Geophysical Research: Atmospheres, 100:11,425-11,446.

Brown, J., O. Ferrians, J.A. Heginbottom and E. Melnikov, 2014. Circum-Arctic Map of Permafrost and Ground-Ice Conditions. National Snow and Ice Data Center, Boulder, Colorado USA.

Bruhwiler, L., E. Dlugokencky, K. Masarie, M. Ishizawa, A. Andrews, J. Miller, C. Sweeney, P. Tans and D. Worthy, 2014a. CarbonTracker-CH4: an assimilation system for estimating emissions of atmospheric methane. Atmospheric Chemistry and Physics, 14:8269-8293.

Bruhwiler, L.M., E. Dlugokencky, K. Masarie, M. Ishizawa, A. Andrews, J. Miller, C. Sweeney, P. Tans and D. Worthy, 2014b. Carbon tracker-CH4: an assimilation system for estimating emissions of atmospheric methane. Atmospheric Chemistry and Physics Discussions, 14:2175-2233.

Buffett, B.A., 2000. Clathrate hydrates. Annual Review of Earth and Planetary Sciences, 28:477-507.

Bünz, S., S. Polyanov, S. Vadakkepuliyambatta, C. Consolaro and J. Mienert, 2012. Active gas venting through hydrate-bearing sediments on the Vestnesa Ridge, offshore W-Svalbard. Marine Geology, 332-334:189-197.

Burwicz, E.B., L.H. Rüpke and K. Wallmann, 2011. Estimation of the global amount of submarine gas hydrates formed via microbial methane formation based on numerical reaction-transport modeling and a novel parameterization of Holocene sedimentation. Geochimica et Cosmochimica Acta, 75:4562-4576.

Callaghan, T.V., D. Dahl-Jensen, M. Johansson, R. Kallenorn, J.R. Key, R. Macdonald, T. Prowse, M. Sharp, K. Steffen and W.F. Vincent, 2011. Cross-cutting Scientific Issues. In: Snow, Water, Ice and Permafrost in the Arctic (SWIPA): Climate Change and the Cryosphere. Arctic Monitoring and Assessment Programme, Oslo, Norway.

Canadell, J.G., P. Ciais, K. Gurney, C. Le Quéré, S. Piao, M.R. Raupach and C.L. Sabine, 2011. An international effort to quantify regional carbon fluxes. EOS, 92:81-82.

Canadian Minister of Justice, 2009. Newfoundland Offshore Petroleum Drilling Production Regulations. Government of Canada, Canada.

Cao, M., S. Marshall and K. Gregson, 1996. Global carbon exchange and methane emissions from natural wetlands: Application of a process-based model. Journal of Geophysical Research, 101:14,399-14,414.

CAPP, 2002. Estimation of Flaring and Venting Volumes from Upstream Oil and Gas Facilities. Canadian Association of Petroleum Producers (CAPP), Calgary.

Capros, P., A. De Vita, N. Tasios, D. Papadopoulos, P. Siskos, E. Apostolaki, M. Zampara, L. Höglund-Isaksson, W. Winiwarter, P. Purohit, H. Böttcher, S. Frank, P. Havlik, M. Gusti and H.P. Witzke, 2013. EU Energy, Transport and GHG emissions – Trends to 2050. Reference Scenario 2013. European Commission.

Carbon Limits, 2013. Associated Petroleum Gas Flaring Study for Russia, Kazakhstan, Turkmenistan and Azerbaijan – Final Report. Carbon Limits AS, Oslo.

Carini, P., A.E. White, E.O. Campbell and S.J. Giovannoni, 2014. Methane production by phosphate-starved SAR11 chemoheterotrophic marine bacteria. Nature Communications, 5:4346, doi:10.1038/ncomms5346.

Cathles, L.M., L. Brown, M. Taam and A. Hunter, 2012. A commentary on "The greenhouse-gas footprint of natural gas in shale formations" by Howarth, R.W., R. Santoro and A. Ingraffea. Climatic Change, 113:525-535.

Caulton, D., P.B. Shepson, R.L. Santoro, J.P Sparks, R.W. Howarth, A.R. Ingraffea, M.O.L. Cambaliza, C. Sweeney, A. Karion, K.J. Davis, B.H. Stirm, S.A. Montzka and B.R. Miller, 2014. Toward a better understanding and quantification of methane emissions from shale gas development. Proceedings of the National Academy of Sciences of the United States of America, 111:6237-6242.

Chan, E. and R.J. Vet, 2010. Baseline levels and trends of ground level ozone in Canada and the United States. Atmospheric Chemistry and Physics, 10:8629-8647.

Chappellaz, J.A., I.Y. Fung and A.M. Thompson, 1993a. The atmospheric CH_4 increase since the Last Glacial Maximum: 1. Source Estimates. Tellus, 45B:228-241.

Chappellaz, J., T. Bluniert, D. Raynaud, J.M. Barnola, J. Schwander and B. Stauffert, 1993b. Synchronous changes in atmospheric CH_4 and Greenland climate between 40 and 8 kyr BP. Nature, 366:443-445.

Chen, Y.-H. and R.G. Prinn, 2006. Estimation of atmospheric methane emissions between 1996 and 2001 using a three-dimensional global chemical transport model. Journal of Geophysical Research, 111:D10307, doi:10.1029/2005JD006058.

Christensen, T.R., 2014. Climate science: Understand Arctic methane variability. Nature, 509:279-281.

Christensen, T.R. and P. Cox, 1995. Response of methane emission from Arctic tundra to climatic change: results from a model simulation. Tellus, 47B:301-310.

Christensen, T.R., S. Jonasson, T.V. Callaghan and M. Havström, 1995. Spatial variation in high latitude methane flux along a transect across Siberian and Eurasian tundra environments. Journal of Geophysical Research: Atmospheres, 100:21035-21045.

Christensen, T.R., I.C. Prentice, J. Kaplan, A. Haxeltine and S. Sitch, 1996. Methane flux from northern wetlands and tundra: an ecosystem source modelling approach. Tellus B, 48:651-660.

Christensen, T.R., A. Michelsen, S. Jonasson and I.K. Schmidt, 1997. Carbon dioxide and methane exchange of a subarctic heath in response to climate change related environmental manipulations. Oikos 79:34-44.

Christensen, T.R., A. Michelsen and S. Jonasson, 1999. Exchange of CH_4 and N_2O in a subarctic heath soil: effects of inorganic N and P amino acid addition. Soil Biology and Biochemistry, 31:637-641.

Christensen, T.R., A. Joabsson, L. Ström, N. Panikov, M. Mastepanov, M. Öquist, B.H. Svensson, H. Nykänen, P. Martikainen and H. Oskarsson, 2003. Factors controlling large scale variations in methane emissions from wetlands. Geophysical Research Letters, 30:1414, doi:10.1029/2002GL016848.

Christensen, J.H., K. Krishna Kumar, E. Aldrian, S.-I. An, I.F.A. Cavalcanti, M. de Castro, W. Dong, P. Goswami, A. Hall, J.K. Kanyanga, A. Kitoh, J. Kossin, N.-C. Lau, J. Renwick, D.B. Stephenson, S.-P. Xie and T. Zhou, 2013. Climate phenomena and their relevance for future regional climate change. In: Stocker, T.F., D. Qin, G.-K. Plattner, M. Tignor, S.K. Allen, J. Boschung, A. Nauels, Y. Xia, V. Bex and P.M. Midgley (eds.), Climate Change 2013: The Physical Science Basis. Contribution of Working Group I to the Fifth Assessment Report of the Intergovernmental Panel on Climate Change, pp. 1217-1308. Cambridge University Press.

Christian, T.J., B. Kleiss, R.J. Yokelson, R. Holzinger, P.J. Crutzen, W.M. Hao, B.H. Saharjo and D.E. Ward, 2003. Comprehensive laboratory measurements of biomass-burning emissions: 1. Emissions from Indonesian, African, and other fuels. Journal of Geophysical Research, 108:4719, doi:10.1029/2003JD003704.

Ciais, P., C. Sabine, G. Bala, L. Bopp, V. Brovkin, J. Canadell, A. Chhabra, R. DeFries, J. Galloway, M. Heimann, C. Jones, C. Le Quéré, R.B. Myneni, S. Piao and P. Thornton, 2013. Carbon and other biogeochemical cycles. In: Stocker, T.F., D. Qin, G.-K. Plattner, M. Tignor, S.K. Allen, J. Boschung, A. Nauels, Y. Xia, V. Bex and P.M. Midgley (eds.), Climate Change 2013: The Physical Science Basis. Contribution of Working Group I to the Fifth Assessment Report of the Intergovernmental Panel on Climate Change, pp. 465-570. Cambridge University Press.

Cicerone, R.J. and R.S. Oremland, 1988. Biogeochemical aspects of atmospheric methane. Global Biogeochemical Cycles, 2:299-327.

Clymo, R.S. and E.J.F. Reddaway, 1971. Productivity of Sphagnum (bog-moss) and peat accumulation. Hydrobiologia, 12:181-192.

Cohen, J., J.A. Screen, J.C. Furtado, M. Barlow, D. Whittleston, D. Coumou, J. Francis, K. Dethloff, D. Entekhabi, J. Overland and J. Jones, 2014. Recent Arctic amplification and extreme mid-latitude weather. Nature Geoscience, 7:627-637.

Cole, J.J. and N.F. Caraco, 1998. Atmospheric exchange of carbon dioxide in a low-wind oligotrophic lake measured by the addition of SF6. Limnology and Oceanography, 43:647-656.

Collins, W.D., V. Ramaswamy, M.D. Schwarzkopf, Y. Sun, R.W. Portmann, Q. Fu, S.E. Casanova, J.L Dufresne, D.W. Fillmore, P.M. Forster, V.Y. Galin, L.K. Gohar, W.J. Ingram, D.P. Kratz, M.P. Lefebvre, J. Li, P. Marquet, V. Oinas, Y. Tsushima, T. Uchiyama and W.Y. Zhong, 2006. Radiative forcing by well-mixed greenhouse gases: Estimates from climate models in the Intergovernmental Panel on Climate Change (IPCC) Fourth Assessment Report (AR4). Journal of Geophysical Research, 111:D14317, doi:10.1029/2005JD006713.

Collins, W.J., S. Sitch and O. Boucher, 2010. How vegetation impacts affect climate metrics for ozone precursors. Journal of Geophysical Research, 115:D23308, doi:10.1029/2010JD014187.

Collins, W.J., N. Bellouin, M. Doutriaux-Boucher, N. Gedney, P. Halloran, T. Hinton, J. Hughes, C.D. Jones, M. Joshi, S. Liddicoat, G. Martin, F. O'Connor, J. Rae, C. Senior, S. Sitch, I. Totterdell, A. Wiltshire and S. Woodward, 2011. Development and evaluation of an Earth-System model – HadGEM2. Geoscientific Model Development, 4:1051-1075.

Collins, M., R. Knutti, J. Arblaster, J.-L. Dufresne, T. Fichefet, P. Friedlingstein, X. Gao, W.J. Gutowski, T. Johns, G. Krinner, M. Shongwe, C. Tebaldi, A.J. Weaver and M. Wehner, 2013. Long-term climate change: Projections, commitments and irreversibility. In: Stocker, T.F., D. Qin, G.-K. Plattner, M. Tignor, S.K. Allen, J. Boschung, A. Nauels, Y. Xia, V. Bex and P.M. Midgley (eds.), Climate Change 2013: The Physical Science Basis. Contribution of Working Group I to the Fifth Assessment Report of the Intergovernmental Panel on Climate Change, pp. 1029-1136. Cambridge University Press.

Conrad, R., 1996. Soil microorganisms as controllers of atmospheric trace gases (H_2, CO, CH_4, OCS, N_2O and NO). Microbiological Reviews, 60:609-640.

Conrad, R., 2009. The global methane cycle: recent advances in understanding the microbial processes involved. Environmental Microbiology Reports, 1:285-292.

Conrad, R. and W. Seiler, 1988. Methane and hydrogen in seawater (Atlantic Ocean). Deep-Sea Research, 35:1903-1917.

Cooper, O.R., D.D. Parrish, J. Ziemke, N.V. Balashov, M. Cupeiro, I.E. Galbally, S. Gilge, L. Horowitz, N.R. Jensen, J.-F. Lamarque, V. Naik, S.J. Oltmans, J. Schwab, D.T. Shindell, A.M. Thompson, V. Thouret, Y. Wang and R.M. Zbinden, 2014. Global distribution and trends of tropospheric ozone: an observations-based review. Elementa, 2, 000029, doi:10.12952/journal.elementa.000029.

Corradi, C., O. Kolle, K. Walter, S.A. Zimov and E.D. Schulze, 2005. Carbon dioxide and methane exchange of a north-east Siberian tussock tundra. Global Change Biology, 11:1910-1925.

Cory, R.M., C.P. Ward, B.C. Crump and G.W. Kling, 2014. Sunlight controls water column processing of carbon in arctic fresh waters. Science, 345:925-928.

Crabeck, O., B. Delille, D.N. Thomas, N.X. Geilfus, S. Rysgaard and J.L. Tison, 2014. CO_2 and CH_4 in sea ice from a subarctic fjord. Biogeosciences Discussions, 11:4047-4083.

Crill, P., K. Bartlett and N. Roulet, 1992. Methane flux from boreal peatlands. Suo, 43:173-182.

Crosson, E.R., 2008. A cavity ring-down analyzer for measuring atmospheric levels of methane, carbon dioxide, and water vapor. Journal of Applied Physics B, 92:403-408.

Crusius, J. and R. Wanninkhof, 2003. Gas transfer velocities measured at low wind speed over a lake. Limnology and Oceanography, 48:1010-1017.

Crutzen, P.J., 1974. Photochemical reactions initiated by and influencing ozone in unpolluted tropospheric air. Tellus, 26:47-57.

Crutzen, P.J. and P.H. Zimmermann, 1991. The changing photochemistry of the troposphere. Tellus B, 43:136-151.

Curry, C.L., 2007. Modeling the soil consumption of atmospheric methane at the global scale. Global Biogeochemical Cycles, 21, GB4012, doi:10.1029/2006GB002818.

D'Hondt, S., S. Rutherford and A.J. Spivack, 2002. Metabolic activity of subsurface life in deep-sea sediments. Science, 295:2067-2070.

Damm, E., E. Helmke, S. Thoms, U. Schauer, E. Noethig, K. Bakker and R.P. Kiene, 2010. Methane production in aerobic oligotrophic surface water in the central Arctic Ocean. Biogeosciences, 7:1099-1108.

Davidson, E.A. and J.P. Schimel, 1995. Microbial processes of production and consumption of nitric oxide, nitrous oxide, and methane. In: Matson, P. and R. Harriss (eds.), Methods in Ecology: Trace Gases, pp. 327-357. Blackwell Scientific.

De Angelis, M.A. and C. Lee, 1994. Methane production during zooplankton grazing on marine phytoplankton. Limnology and Oceanography, 39:1298-1308.

DeConto, R.M., S. Galeotti, M. Pagani, D. Tracy, K. Schaefer, T. Zhang, D. Pollard and D.J. Beerling, 2012. Past extreme warming events linked to massive carbon release from thawing permafrost. Nature, 484:87-91.

Denisov, S.N., M.M. Arzhanov, A.V. Eliseev and I.I. Mokhov, 2011. Assessment of the response of subaqueous methane hydrate deposits to possible climate change in the twenty-first century. Doklady Earth Sciences, 441:1706-1709.

Denisov, S.N., A.V. Eliseev and I.I. Mokhov, 2013. Climate change in IAP RAS global model taking account of interaction with methane cycle under anthropogenic scenarios of RCP family. Russian Meteorology and Hydrology, 38:741-749.

Denman, K.L., G. Brasseur, A. Chidthaisong, P. Ciais, P.M. Cox, R.E. Dickinson, D. Hauglustaine, C. Heinze, E. Holland, D. Jacob, U. Lohmann, S Ramachandran, P.L. da Silva Dias, S.C. Wofsy and X. Zhang, 2007. Couplings between changes in the climate system and biogeochemistry. In: Solomon, S., D. Qin, M. Manning, Z. Chen, M. Marquis, K.B. Averyt, M.Tignor and H.L. Miller (eds.), Climate Change 2007: The Physical Science Basis. Contribution of Working Group I to the Fourth Assessment Report of the Intergovernmental Panel on Climate Change. Cambridge University Press.

Dickens, G.R., 1999. Carbon cycle: The blast in the past. Nature, 401:752-755.

Dickens, G.R., 2011. Down the Rabbit Hole: toward appropriate discussion of methane release from gas hydrate systems during the Paleocene-Eocene thermal maximum and other past hyperthermal events. Climate of the Past, 7:831-846.

Dickens, G.R., J.R. O'Neil, D.K. Rea and R.M. Owen, 1995. Dissociation of oceanic methane hydrate as a cause of the carbon isotope excursion at the end of the Paleocene. Paleoceanography, 10:965-971.

Dillon, T.J. and J.N. Crowley, 2008. Direct detection of OH formation in the reactions of HO_2 with $CH_3C(O)O_2$ and other substituted peroxy radicals. Atmospheric Chemistry and Physics, 8:4877-4889.

Divins, D.L., 2003. Total sediment thickness of the world's oceans and marginal seas. NOAA National Geophysical Data Centre, Boulder. Colorado.

Dlugokencky, E.J., K.A. Masaire, P.M. Lang, P.P. Steele and E.G. Nisbet, 1994. A dramatic decrease in the growth rate of atmospheric methane in the Northern Hemisphere during 1992. Geophysical Research Letters, 21:45-48.

Dlugokencky, E.J., E.G. Dutton, P.C. Novelli, P.P. Tans, K.A. Masarie, K.O. Lantz and S. Madronich, 1996. Changes in CH_4 and CO growth rates after the eruption of Mt. Pinatubo and their link with changes in tropical tropospheric UV flux. Geophysical Research Letters, 23:2761-2764.

Dlugokencky, E.J., S. Houweling, L. Bruhwiler, K.A. Masarie, P.M. Lang, J.B. Miller and P.P. Tans, 2003. Atmospheric methane levels off: Temporary pause or a new steady-state? Geophysical Research Letters, 30:1992, doi:10.1029/2003GL018126.

Dlugokencky, E.J., R.C. Myers, P.M. Lang, K.A. Masarie, A.M. Crotwell, K.W. Thoning, B.D. Hall, J.W. Elkins and L.P. Steele, 2005. Conversion of NOAA atmospheric dry air CH_4 mole fractions to a gravimetrically prepared standard scale. Journal of Geophysical Research, 110:D18306, doi:10.1029/2005JD006035.

Dlugokencky, E.J., L. Bruhwiler, J.W.C. White, L.K. Emmons, P.C. Novelli, S.A. Montzka, K.A. Masarie, P.M. Lang, A.M. Crotwell, J.B. Miller and L.V. Gatti, 2009. Observational constraints on recent increases in the atmospheric CH_4 burden. Geophysical Research Letters, 36:L18803, doi:10.1029/2009GL039780.

Dlugokencky, E.J., E.G. Nisbet, R. Fisher and D. Lowry, 2011. Global atmospheric methane: Budget, changes and dangers. Philosophical Transactions of the Royal Society A, 369:2058-2072.

Dmitrenko, I.A., S.A. Kirillov, L.B. Tremblay, H. Kassens, O.A. Anisimov, S.A. Lavrov, S.O. Razumov and M.N. Grigoriev, 2011. Recent changes in shelf hydrography in the Siberian Arctic: Potential for subsea permafrost instability. Journal of Geophysical Research, 116:C10027, doi:10.1029/2011JC007218.

Dorling, S.R. and T.D. Davies, 1992. Cluster analysis: A technique for estimating the synoptic meteorological controls on air and precipitation chemistry – method and applications. Atmospheric Environment, 26A:2575-2581.

Dorling, S.R., T.D. Davies and C.E. Pierce, 1992. Cluster analysis: A technique for estimating the synoptic meteorological controls on air and precipitation chemistry – results from Eskdalemuir, South Scotland. Atmospheric Environment. 26A:2583-2602.

Dorrepaal, E., S. Toet, R.S.P. Van Logtestijn, E. Swart, M.J. Van de Weg, T.V. Callaghan and R. Aerts, 2009. Carbon respiration from subsurface peat accelerated by climate warming in the subarctic. Nature, 460:616-620.

Duncan, B.N., J.A. Logan, I. Bey, I.A. Megretskaia, R.M. Yantosca, P.C. Novelli, N.B. Jones and C.P. Rinsland, 2007. Global budget of CO, 1988-1997: Source estimates and validation with a global model. Journal of Geophysical Research, 112, D22301, doi:10.1029/2007JD008459.

EC, 2009. The 2020 Climate and Energy Package. European Commission. http://ec.europa.eu/clima/policies/package/index_en.htm.

EC, 2014. 2030 framework for climate and energy policies. http://ec.europa.eu/clima/policies/2030/index_en.htm.

ECLIPSE, 2012. ECLIPSE v.4a scenarios on air pollution by the Greenhouse Gas and Air Pollution Interactions and Synergies (GAINS) model. International Institute for Applied Systems Analysis, Laxenburg, Austria. Scenarios produced for the Evaluating the CLimate and air quality ImPacts of Short-livEd pollutants (ECLIPSE) project coordinated by the Norwegian Institute for Air Research (NILU).

ECLIPSE, 2014. ECLIPSE v.5 scenarios on air pollution by the Greenhouse Gas and Air Pollution Interactions and Synergies (GAINS) model. International Institute for Applied Systems Analysis, Laxenburg, Austria. Scenarios produced for the Evaluating the CLimate and air quality ImPacts of Short-livEd pollutants (ECLIPSE) project coordinated by the Norwegian Institute for Air Research (NILU).

EDGAR, 2010. EDGAR version 4.1. Emission Database for Global Atmospheric Research. Joint Research Centre of the European Commission and the Netherlands Environmental Assessment Agency (PBL).

EDGAR, 2012. EDGAR version 4.2. Emission Database for Global Atmospheric Research. Joint Research Centre of the European Commission and the Netherlands Environmental Assessment Agency (PBL).

EDGAR, 2013. EDGAR version 4.2FT2010. Emission Database for Global Atmospheric Research. Joint Research Centre of the European Commission and the Netherlands Environmental Assessment Agency (PBL).

Ehhalt, D.H., 1974. The atmospheric cycle of methane. Tellus, 26:58-70.

EIA, 2009. International Energy Outlook. US Energy Information Administration, US Department of Energy, Washington D.C.

EIA, 2011a. International Energy Statistics and Country Analysis Briefs. US Energy Information Administration, US Department of Energy, Washington D.C.

EIA, 2011b. World Shale Gas Resources: An Initial Assessment of 14 Regions Outside the United States. US Energy Information Administration, US Department of Energy, Washington D.C.

EIA, 2013. International Energy Outlook. US Energy Information Administration, US Department of Energy, Washington D.C.

Elberling, B., C. Nordstrøm, L. Grøndahl, H. Søgaard, T. Friborg, T.R. Christensen, L. Ström, F. Marchand and I. Nijs, 2008. High-Arctic soil CO_2 and CH_4 production controlled by temperature, water, freezing and snow. In: Meltofte, H., T.R. Christensen, M.C. Forchhammers and M. Rasch (eds.), High-Arctic Ecosystem Dynamics in a Changing Climate, pp. 441-472. Academic Press.

Emmerton, C.A., V.L. St. Louis, I. Lehnherr, E.R. Humphreys, E. Rydz and H.R. Kosolofski, 2014. The net exchange of methane with high Arctic landscapes during the summer growing season. Biogeosciences, 11:3095-3106.

Emmons, L.K., S. Walters, P.G. Hess, J.-F. Lamarque, G.G. Pfister, D. Fillmore, C. Granier, A. Guenther, D. Kinnison, T. Laepple, J. Orlando, X. Tie, G. Tyndall, C. Wiedinmyer, S.L. Baughcum and S. Kloster, 2010. Description and evaluation of the Model for Ozone and Related chemical Tracers, version 4 (MOZART-4). Geoscientific Model Development, 3:43-67.

Enting, I.G. and J.V. Mansbridge, 1989. Seasonal sources and sinks of atmospheric CO_2 Direct inversion of filtered data. Tellus, 41B:111-126.

Etheridge, D.M., G.I. Pearman and P.J. Fraser, 1992. Changes in tropospheric methane between 1841 and 1978 from a high accumulation-rate Antarctic ice core. Tellus, 44B:282-294.

Etiope, G. and B. Sherwood Lollar, 2013. Abiotic methane on Earth. Reviews of Geophysics, 51:276-299.

European Commission, 2009. European Commission, Joint Research Centre (JRC)/Netherlands Environmental Assessment Agency (PBL). Emission Database for Global Atmospheric Research (EDGAR), release version 4.0. http://edgar.jrc.ec.europa.eu.

Evans, M. and V. Roshchanka, 2014. Russian policy on methane emissions in the oil and gas sector: A case study in opportunities and challenges in reducing short-lived forcers. Atmospheric Environment, 92:199-206.

FAO, 2003. World Agriculture: Towards 2015/2030. Summary report. Food and Agricultural Organization of the United Nations.

FAO, 2006. Livestock's Long Shadow: Environmental Issues and Options. Food and Agricultural Organization of the United Nations.

FAPRI, 2010. U.S. and World Agricultural Outlook. Food and Agricultural Policy Research Institute (FAPRI), Iowa State University and University of Missouri-Columbia. Ames, Iowa.

Fiore, A.M., J.J. West, L.W. Horowitz, V. Naik and M.D. Schwarzkop, 2008. Characterizing the tropospheric ozone response to methane emission controls and the benefits to climate and air quality. Journal of Geophysical Research, 113:D08307, doi:10.1029/2007JD009162.

Fiore, A.M., F.J. Dentener, O. Wild, C. Cuvelier, M.G. Schultz, P. Hess, C. Textor, M. Schulz, R.M. Doherty, L.W. Horowitz, I.A. MacKenzie, M.G. Sanderson, D.T. Shindell, D.S. Stevenson, S. Szopa, R. Van Dingenen, G. Zeng, C. Atherton, D. Bergmann, I. Bey, G. Carmichael, W.J. Collins, B.N. Duncan, G. Faluvegi, G. Folberth, M. Gauss, S. Gong, D. Hauglustaine, T. Holloway, I.S.A. Isaksen, D.J. Jacob, J.E. Jonson, J.W. Kaminski, T.J. Keating, A. Lupu, E. Marmer, V. Montanaro, R.J. Park, G. Pitari, K.J. Pringle, J.A. Pyle, S. Schroeder, M.G. Vivanco, P. Wind, G. Wojcik, S. Wu and A. Zuber, 2009. Multimodel estimates of intercontinental source-receptor relationships for ozone pollution. Journal of Geophysical Research, 114:D04301, doi:10.1029/2008JD010816.

Fischer, M., A. Biastoch, E. Behrens and J. Baehr, 2013. Simulations of a Line W-based observing system for the Atlantic meridional overturning circulation. Ocean Dynamics, 63:865-880.

Fisher, R.E., S. Sriskantharajah, D. Lowry, M. Lanoisellé, C.M.R. Fowler, R.H. James, O. Hermansen, C. Lund Myhre, A. Stohl, J. Greinert, P.B.R. Nisbet and E.G. Nisbet, 2011. Arctic methane sources: isotopic evidence for atmospheric inputs. Geophysical Research Letters, 38:L21803, doi:10.1029/2011GL049319.

Flato, G., J. Marotzke, B. Abiodun, P. Braconnot, S.C. Chou, W. Collins, P. Cox, F. Driouech, S. Emori, V. Eyring, C. Forest, P. Gleckler, E. Guilyardi, C. Jakob, V. Kattsov, C. Reason and M. Rummukainen, 2013. Evaluation of climate models. In:

Stocker, T.F., D. Qin, G.-K. Plattner, M. Tignor, S.K. Allen, J. Boschung, A. Nauels, Y. Xia, V. Bex and P.M. Midgley (eds.), Climate Change 2013: The Physical Science Basis. Contribution of Working Group I to the Fifth Assessment Report of the Intergovernmental Panel on Climate Change. Cambridge University Press.

Fleming, E.L., C.H. Jackman, R.S. Stolarski and A.R. Douglass, 2011. A model study of the impact of source gas changes on the stratosphere for 1850–2100. Atmospheric Chemistry and Physics, 11:8515-8541.

Forster, P.M.D. and K.P. Shine, 1997. Radiative forcing and temperature trends from stratospheric ozone changes. Journal of Geophysical Research, 102:10841-10855.

Fraser, A., P.I. Palmer, L. Feng, H. Boesch, A. Cogan, R. Parker, E.J. Dlugokencky, P.J. Fraser, P.B. Krummel, R.L. Langenfelds, S. O'Doherty, R.G. Prinn, L.P. Steele, M. van der Schoot and R.F. Weiss, 2013. Estimating regional methane surface fluxes: the relative importance of surface and GOSAT mole fraction measurements. Atmospheric Chemistry and Physics, 13:5697-5713.

Frederick, J.M. and B.A. Buffett, 2014. Taliks in relict submarine permafrost and methane hydrate deposits: Pathways for gas escape under present and future conditions. Journal of Geophysical Research: Earth Surface, 119:106-122.

Friborg, T., T.R. Christensen, B.U. Hansen, C. Nordstroem and H. Soegaard, 2000. Trace gas exchange in a high-arctic valley 2. Landscape CH_4 fluxes measured and modeled using eddy correlation data. Global Biogeochemical Cycles, 14:715-723.

Frolking, S. and P. Crill, 1994. Climate controls on temporal variability of methane flux from a poor fen in southeastern New Hampshire - measurement and modeling. Global Biogeochemical Cycles, 8:385-397.

Fry, M.M., V. Naik, J.J. West, M.D. Schwarzkopf, A.M. Fiore, W.J. Collins, F.J. Dentener, D.T. Shindell, C. Atherton, D. Bergmann, B.N. Duncan, P. Hess, I.A. MacKenzie, E. Marmer, M.G. Schultz, S. Szopa, O. Wild and G. Zeng, 2012. The influence of ozone precursor emissions from four world regions on tropospheric composition and radiative climate forcing. Journal of Geophysical Research, 117:D07306, doi:10.1029/2011JD017134.

Fuchs, J., A. Hofzumahaus, F. Rohrer, B. Bohn, T. Brauers, H-P. Dorn, R. Häseler, F. Holland, M. Kaminski, X. Li, K. Lu, S. Nehr, R. Tillmann, R.Wegener and A.Wahner, 2013. Experimental evidence for efficient hydroxyl radical regeneration in isoprene oxidation. Nature Geoscience, 6:1023-1026.

Fung, I., J. John, J. Lerner, E. Matthews, M. Prather, L.P. Steele and P.J. Fraser, 1991. Three-dimensional model synthesis of the Global methane cycle. Journal of Geophysical Research: Atmospheres, 96:13,033-13,065.

Fyfe, J.C., K. von Salzen, N.P. Gillett, V.K. Arora, G.M. Flato and J.R. McConnel, 2013. One hundred years of Arctic surface temperature variation due to anthropogenic influence. Scientific Reports, 3:2645, doi:10.1038/srep02645.

G8, 2009. Declaration of the Leaders. Major Economies Forum on Energy and Climate. L'Aquila, Italy, 9 July 2009. Online at: www.g8italia2009.it/static/G8_Allegato/MEF_Declarationl.pdf

Garcia, J.-L., B.K.C. Patel and B. Ollivier, 2000. Taxonomic, phylogenetic and ecological diversity of methanogenic Archaea. Anaerobe, 6:205-226.

Garnett, T., 2009. Livestock-related greenhouse gas emissions: impacts and options for policy makers. Environmental Science and Policy, 12:491-503.

Gauss, M., G. Myhre, I.S.A. Isaksen, V. Grewe, G. Pitari, O. Wild, W.J. Collins, F.J. Dentener, K. Ellingsen, L.K. Gohar, D.A. Hauglustaine, D. Iachetti, J.-F. Lamarque, E. Mancini, L.J. Mickley, M.J. Prather, J.A. Pyle, M.G. Sanderson, K.P. Shine, D.S. Stevenson, K. Sudo, S. Szopa and G. Zeng, 2006. Radiative forcing since preindustrial times due to ozone change in the troposphere and the lower stratosphere. Atmospheric Chemistry and Physics, 6:575-599.

GCAM, 2009. Data from GCAM model results for RCPs version 2.0 received from A. Thomson, 17 January 2014. Global Change Assessment Model, Joint Global Change Research Institute, Pacific Northwest National Laboratory and University of Maryland, College Park, USA.

Gent, P.R., G. Danabasoglu, L.J. Donner, M.M. Holland, E.C. Hunke, S.R. Jayne, D.M. Lawrence, R.B. Neale, P.J. Rasch, M. Vertenstein, P.H. Worley, Z.-L. Yang and M. Zhang, 2011. The community climate system model version 4. Journal of Climate, 24:4973-4991.

Giglio, L., G.R. van der Werf, J.T. Randerson, G.J. Collatz and P. Kasibhatla, 2006. Global estimation of burned area using MODIS active fire observations. Atmospheric Chemistry and Physics, 6:957-974.

Gillett, N.P., V.K. Arora, G.M. Flato, J.F. Scinocca and K. von Salzen, 2012. Improved constraints on 21st-century warming derived using 160 years of temperature observations. Geophysical Research Letters, 39:L01704, doi:10.1029/2011GL050226.

Giustiniani, M., U. Tinivella, M. Jakobsson and M. Rebesco, 2013. Arctic Ocean gas hydrate stability in a changing climate. Journal of Geological Research, 2013:1-10.

GMI and EC, 2013. European Commission Global Methane Reduction Actions. Ref. Ares (2013)2843722-06/08/2013. Global Methane Initiative and European Commission. Online at: www.globalmethane.org/documents/EC_GMI_reduction_actions.pdf

Goodrich, J.P., R.K. Varner, S. Frolking, B.N. Duncan and P.M. Crill, 2011. High-frequency measurements of methane ebullition over a growing season at a temperate peatland site. Geophysical Research Letters, 38:L07404, doi:10.1029/2011GL046915.

Granberg, G., M. Ottosson-Lofvenius, H. Grip, I. Sundh and M. Nilsson, 2001. Effect of climatic variability from 1980 to 1997 on simulated methane emission from a boreal mixed mire in northern Sweden. Global Biogeochemical Cycles, 15:977-991.

Grant, R.F., 1998. Simulation of methanogenesis in the mathematical model ecosys. Soil Biology and Biochemistry, 30:883-896.

Grant, R.F., 1999. Simulation of methanotrophy in the mathematical model ecosys. Soil Biology and Biochemistry, 31:287-297.

Griffies, S.M., A. Biastoch, C. Böning, F. Bryan, G. Danabasoglu, E.P. Chassignet, M.H. England, R. Gerdes, H. Haak, R.W. Hallberg, W. Hazeleger, J. Jungclaus, W.G. Large, G. Madec, A. Pirani, B.L. Samuels, M. Scheinert, A.S. Gupta, C.A. Severijns, H.L. Simmons, A.-M. Treguier, M. Winton, S. Yeager and J. Yin, 2009. Coordinated Ocean-ice Reference Experiments (COREs). Ocean Modelling, 26:1-46.

Grossart, H.-P., K. Frindte, C. Dziallas, W. Eckert and K.W. Tang, 2011. Microbial methane production in oxygenated water column of an oligotrophic lake. Proceedings of the National Academy of Sciences of the United States of America, 108:19,657-19,661.

Grosse, G., J. Harden, M. Turetsky, A.D. McGuire, P. Camill, C. Tarnocai, S. Frolking, E.A.G. Schuur, T. Jorgenson, S. Marchenko, V. Romanovsky, K.P. Wickland, N. French, M. Waldrop, L. Bourgeau Chavez and R.G. Striegl, 2011. Vulnerability of high latitude soil organic carbon in North America to disturbance. Journal of Geophysical Research, 116:G00K06, doi:10.1029/2010JG001507.

Hampton, M.A., H.J. Lee and J. Locat, 1996. Submarine landslides. Reviews of Geophysics, 34:33-59.

Hamza, V.M., R.R. Cardoso and C.F.P. Neto, 2007. Spherical harmonic analysis of earth's conductive heat flow. International Journal of Earth Sciences, 97:205-226.

Handel, M.D. and J.S. Risbey, 1992. An annotated-bibliography on the greenhouse-effect and climate change. Climatic Change, 21:97-253.

Hansen, J., M. Sato, R. Ruedy, L. Nazarenko, A. Lacis, G.A. Schmidt, G. Russell, I. Aleinov, M. Bauer, S. Bauer, N. Bell, B. Cairns, V. Canuto, M. Chandler, Y. Cheng, A. Del Genio, G. Faluvegi, E. Fleming, A. Friend, T. Hall, C. Jackman, M. Kelley, N. Kiang, D. Koch, J. Lean, J. Lerner, K. Lo, S. Menon, R. Miller, P. Minnis, T. Novakov, V. Oinas, Ja. Perlwitz, Ju. Perlwitz, D. Rind, A. Romanou, D. Shindell, P. Stone, S. Sun, N. Tausnev, D. Thresher, B. Wielicki, T. Wong, M. Yao and S. Zhang, 2005. Efficacy of climate forcings. Journal of Geophysical Research, 110:D18104, doi:10.1029/2005JD005776.

Hanson, R.S. and T.E. Hanson, 1996. Methanotrophic bacteria. Microbiological Reviews, 60:439-471.

Harder, S.L., D.T. Shindell, G.A. Schmidt and E.J. Brook, 2007. A global climate model study of CH_4 emissions during the Holocene and glacial-interglacial transitions constrained by ice core data. Global Biogeochemical Cycles, 21:GB1011, doi:10.1029/2005GB002680.

Harrison, M.R., K.E. Galloway, A. Hendler, T.M. Shires, D. Allen, M. Foss, J. Thomas and J. Spinhirne, 2011. Natural Gas Industry Methane Emission Factor Improvement Study. Final Report prepared under Cooperative Agreement No. XA-83376101. U.S. Environmental Protection Agency.

Harriss, R., K. Bartlett, S. Frolking and P. Crill, 1993. Methane emissions from northern high-latitude wetlands. In: R.S. Oremland (ed.), Biogeochemistry of Global Change: Radiatively Active Trace Gases. Chapman & Hall.

Hartley, D. and R. Prinn, 1993. Feasibility of determining surface emissions of trace gases using an inverse method in a three-dimensional chemical transport model. Journal of Geophysical Research, 98:5183-5197.

Hartmann, D.L., A.M.G. Klein Tank, M. Rusticucci, L.V. Alexander, S. Brönnimann, Y. Charabi, F.J. Dentener, E.J. Dlugokencky, D.R. Easterling, A. Kaplan, B.J. Soden, P.W. Thorne, M. Wild and P.M. Zhai, 2013. Observations: atmosphere and surface. In: Stocker, T.F., D. Qin, G.-K. Plattner, M. Tignor, S.K. Allen, J. Boschung, A. Nauels, Y. Xia, V. Bex and P.M. Midgley (eds.), Climate Change 2013: The Physical Science Basis. Contribution of Working Group I to the Fifth Assessment Report of the Intergovernmental Panel on Climate Change. Cambridge University Press.

Hedenus, F., S. Wirsenius and D.J.A. Johansson, 2014. The importance of reduced meat and dairy consumption for meeting stringent climate change targets. Climatic Change, 124:79-91.

Hein, R. and M. Heimann, 1994. Determination of global scale emissions of atmospheric methane using an inverse modeling method. In: J. van Ham et al. (eds.), Non-CO_2 Greenhouse Gases, pp. 271-281. Kluwer Academic Publishers.

Hein, R., P.J. Crutzen and M. Heimann, 1997. An inverse modeling approach to investigate the global atmospheric methane cycle. Global Biogeochemical Cycles, 11:43-76.

Hesselbo, S.P., D.R. Gröcke, H.C. Jenkyns, C.J. Bjerrum, P. Farrimond, H.S. Morgans Bell and O.R. Green, 2000. Massive dissociation of gas hydrate during a Jurassic oceanic anoxic event. Nature, 406:392-395.

Hester, K.C. and P.G. Brewer, 2009. Clathrate hydrates in nature. Annual Review of Marine Science, 1:303-327.

Hodson, E.L., B. Poulter, N.E. Zimmermann, C. Prigent and J.O. Kaplan, 2011. The El Niño–Southern Oscillation and wetland methane interannual variability. Geophysical Research Letters, 38:L08810, doi:10.1029/2011GL046861.

Höglund-Isaksson, L., 2012. Global anthropogenic methane emissions 2005-2030: technical mitigation potentials and costs. Atmospheric Chemistry and Physics, 12:9079-9096.

Höglund-Isaksson, L., W. Winiwarter, P. Purohit, P. Rafaj, W. Schöpp and Z. Klimont, 2012. EU low carbon roadmap 2050: Potentials and costs for mitigation of non-CO_2 greenhouse gas emissions. Energy Strategy Reviews, 1:97-108.

Holmes, C.D., M.J. Prather, O.A. Sovde and G. Myhre, 2013. Future methane, hydroxyl, and their uncertainties: key climate and emission parameters for future predictions. Atmospheric Chemistry and Physics, 13:285-302.

Hopcroft, P.O., P.J. Valdes and D.J. Beerling, 2011. Simulating idealized Dansgaard-Oeschger events and their potential impacts on the global methane cycle. Quarterly Science Review, 30:3258-3268.

Hope, C., J. Anderson and P. Wenman, 1993. Policy analysis of the greenhouse effect: An application of the PAGE model. Energy Policy, 21:327-338.

Houghton, J.T., G.J. Jenkins and J.J. Ephraums (eds.), 1990. Climate Change. The IPCC Scientific Assessment. Cambridge University Press.

Houweling, S., F. Dentener and J. Lelieveld, 1998. The impact of nonmethane hydrocarbon compounds on tropospheric photochemistry. Journal of Geophysical Research: Atmospheres, 103:10673-10696.

Houweling, S., T. Kaminski, F. Dentener, J. Lelieveld and M. Heimann, 1999. Inverse modeling of methane sources and sinks using the adjoint of a global transport model. Journal of Geophysical Research: Atmospheres, 104:26,137-26,160.

Houweling, S., M. Krol, P. Bergamaschi, C. Frankenberg, E.J. Dlugokencky, I. Morino, J. Notholt, V. Sherlock, D. Wunch, V. Beck, C. Gerbig, H. Chen, E.A. Kort, T. Röckmann and I. Aben, 2014. A multi-year methane inversion using SCIAMACHY, accounting for systematic errors using TCCON measurements. Atmospheric Chemistry and Physics, 14:3991-4012.

Howarth, R.W., R. Santoro and A. Ingraffea, 2011. Methane and the greenhouse-gas footprint of natural gas from shale formations. Climatic Change, 106:679-690.

Hovland, M. and A.G. Judd, 1988. Seabed Pockmarks and Seepages. Graham and Trotham, London.

Hristov, A.N., J. Oh, C. Lee, R. Meinen, F. Montes, T. Ott, J. Firkins, A. Rotz, C. Dell, A. Adesogan, W. Yang, J. Tricarico, E. Kebreab, G. Waghorn, J. Dijkstra and S. Oosting, 2013. Mitigation of Greenhouse Gas Emissions in Livestock Production. Gerber, P.J., B. Henderson and H.P.S. Makkar (eds.). United Nations Food and Agricultural Organization.

Hugelius, G., C. Tarnocai, G. Broll, J.G. Canadell, P. Kuhry and D.K. Swanson, 2013. The northern circumpolar soil carbon database: spatially distributed datasets of soil coverage and soil carbon storage in the northern permafrost regions. Earth System Science Data, 5:3-13.

Hugelius, G., J. Strauss, S. Zubrzycki, J.W. Harden, E.A.G. Schuur, C.L. Ping, L. Schirrmeister, G. Grosse, G.J. Michaelson, C.D. Koven, J.A. O'Donnel, B. Elberling, U. Mishra, P. Camill, Z. Yu, J. Palmtag and P. Kuhry, 2014. Estimated stocks of circumpolar permafrost carbon with quantified uncertainty ranges and identified data gaps. Biogeosciences, 11:6573-6593.

Hulbak Røland, T., 2010. Associated Petroleum Gas in Russia: Reasons for Non-utilization. FNI Report 13/2010, Fridtjof Nansen Institute, Lysaker, Norway.

Hunt, T.S., 1863. On the Earth's climate in Palaeozoic times. Philosophical Magazine, IV:323-324.

IEA, 2009. IEA World Energy Outlook 2009. International Energy Agency, Paris.

IEA, 2011a. IEA World Energy Outlook 2011. International Energy Agency, Paris.

IEA, 2011b. IEA World Energy Outlook 2011: Special Report. Are we entering a Golden Age of Gas? International Energy Agency, Paris.

IEA, 2012. Energy Strategy Perspectives 2012: Pathways to a Clean Energy System. International Energy Agency, Paris.

IIASA, 2009. The RCP Database (version 2.0). International Institute for Applied Systems Analysis. Online at: http://tntcat.iiasa.ac.at:8787/RcpDb/dsd?Action=htmlpage&page=welcome

IIASA, 2013. The Greenhouse Gas and Air Pollution Interactions and Synergies (GAINS) model. International Institute for Applied Systems Analysis. Online at: http://gains.iiasa.ac.at

Ijima, Y., A.N. Fedorov, H. Park, K. Suzuki, H. Yabuki, T.C. Maximov and T. Ohata, 2010. Abrupt increases in soil temperatures following increased precipitation in a permafrost region, Central Lena River Basin, Russia. Permafrost and Periglacial Processes, 21:30-41.

Ijima, Y., T. Ohta, A. Kotani, A.N. Fedorov, Y. Kodama and T.C. Maximov, 2014. Sap flow changes in relation to permafrost degradation under increasing precipitation in an eastern Siberian larch forest. Ecohydrology, 7:177-187.

IPCC, 2006. IPCC Guidelines for National Greenhouse Gas Inventories, Prepared by the National Greenhouse Gas Inventories Programme, Eggleston H.S., Buendia L., Miwa K., Ngara T. and Tanabe K. (eds). Intergovernmental Panel on Climate Change (IPPC), Institute for Global Environmental Strategies, Japan.

IPCC, 2013a. Summary for Policymakers. In: Stocker, T.F., D. Qin, G.-K. Plattner, M. Tignor, S.K. Allen, J. Boschung, A. Nauels, Y. Xia, V. Bex and P.M. Midgley (eds.), Climate Change 2013: The Physical Science Basis. Contribution of Working Group I to the Fifth Assessment Report of the Intergovernmental Panel on Climate Change. Cambridge University Press.

IPCC, 2013b. Climate Change 2013: The Physical Science Basis. Contribution of Working Group I to the Fifth Assessment Report of the Intergovernmental Panel on Climate Change. Stocker, T.F., D. Qin, G.-K. Plattner, M. Tignor, S.K. Allen, J. Boschung, A. Nauels, Y. Xia, V. Bex and P.M. Midgley (eds.). Cambridge University Press.

IPCC, 2013c. Annex I: Atlas of Global and Regional Climate Projections [van Oldenborgh, G.J., M. Collins, J. Arblaster, J.H. Christensen, J. Marotzke, S.B. Power, M. Rummukainen and T. Zhou (eds.)]. In: Stocker, T.F., D. Qin, G.-K. Plattner, M. Tignor, S.K. Allen, J. Boschung, A. Nauels, Y. Xia, V. Bex and P.M. Midgley (eds.), Climate Change 2013: The Physical Science Basis. Contribution of Working Group I to the Fifth Assessment Report of the Intergovernmental Panel on Climate Change, pp. 1311-1394. Cambridge University Press.

IPCC, 2014. Climate Change 2014: Mitigation of Climate Change. Contribution of Working Group III to the Fifth Assessment Report of the Intergovernmental Panel on Climate Change. Edenhofer, O., R. Pichs-Madruga, Y. Sokona, E. Farahani, S. Kadner, K. Seyboth, A. Adler, I. Baum, S. Brunner, P. Eickemeier, B. Kriemann, J. Savolainen, S. Schlömer, C. von Stechow, T. Zwickel and J.C. Minx (eds.). Cambridge University Press.

Ite, A.E. and U.J. Ibok, 2013. Gas flaring and venting associated with petroleum exploration and production in the Nigeria's Niger Delta. American Journal of Environmental Protection, 1:70-77.

Iversen, N. and B.B. Jørgensen, 1985. Anaerobic methane oxidation rates at the sulfate-methane transition in marine sediments from Kattegat and Skagerrak (Denmark). Limnology and Oceanography, 30:944-955.

Jackowicz-Korczyński, M., T.R. Christensen, K. Bäckstrand, P. Crill, T. Friborg, M. Mastepanov and L. Ström, 2010. Annual cycle of methane emission from a subarctic peatland. Journal of Geophysical Research, 115:G02009, doi: 10.1029/2008JG000913.

Jakobsson, M., 2002. Hypsometry and volume of the Arctic Ocean and its constituent seas. Geochemistry, Geophysics, Geosystems, 3:1-18.

Jeffries, M.O. and J. Richter-Menge (eds.), 2013. Arctic. In: State of the Climate in 2012. Special issue, Bulletin of the American Meteorological Society, 94(8):S111-S146.

Jenkins, L.K, L.L. Bourgeau-Chavez, N.H.F. French, T.V. Loboda and B.J. Thelen, 2014. Development of methods for detection and monitoring of fire disturbance in the Alaskan tundra using a two-decade long record of synthetic aperture radar satellite images. Remote Sensing, 6:6347-6364.

Joabsson, A. and T.R. Christensen, 2001. Methane emissions from wetlands and their relationship with vascular plants: an Arctic example. Global Change Biology, 7:919-932.

Joabsson, A., T.R. Christensen and B. Wallén, 1999. Vascular plant controls on methane emissions from northern peatforming wetlands. Trends in Ecology and Evolution, 14:385-388.

Johansson, T., N. Malmer, P.M. Crill, T. Friborg, J.H. Akerman, M. Mastepanov and T.R. Christensen, 2006. Decadal vegetation changes in a northern peatland, greenhouse gas fluxes and net radiative forcing. Global Change Biology, 12:2352-2369.

Johnson, M.R. and A.R. Coderre, 2011. An analysis of flaring and venting activity in the Alberta upstream oil and gas industry. Journal of Air and Waste Management, 61:190-200.

Johnson, M.R. and A.R. Coderre, 2012. Opportunities for CO_2 equivalent emissions reductions via flare and vent mitigation: A case study for Alberta, Canada. International Journal of Greenhouse Gas Control, 8:121-131.

Jones, B.M., G. Grosse, C.D. Arp, M.C. Jones, K.M. Walter Anthony and V.E. Romanovsky, 2011. Modern thermokarst lake dynamics in the continuous permafrost zone, northern Seward Peninsula, Alaska. Journal of Geophysical Research, 116:G00M03, doi:10.1029/2011JG001666.

Jonsson, P.K., 2014. Personal information received from Paal Kolka Jonsson, Environmental Agency of Iceland on 24 April 2014.

Jorgenson, M.T., Y.L. Shur and E.R. Pullman, 2006. Abrupt increase in permafrost degradation in arctic Alaska. Geophysical Research Letters, 33: L02503, doi: http://dx.doi.org/10.1029/2005GL024960.

Judd, A.G., 2004. Natural seabed gas seeps as sources of atmospheric methane. Environmental Geology, 46:988-996.

Kai, F.M., S.C. Tyler, J.T. Randerson and D.R. Blake, 2011. Reduced methane growth rate explained by decreased Northern Hemisphere microbial sources. Nature, 476:194-197.

Kaiser, C., H. Meyer, C. Biasi, O. Rusalimova, P. Barsukov and A. Richter, 2007. Conservation of soil organic matter through cryoturbation in arctic soils in Siberia. Journal of Geophysical Research, 112:G02017, doi:10.1029/2006JG000258.

Kaplan, J.O., 2002. Wetlands at the last glacial maximum: Distribution and methane emissions. Geophysical Research Letters, 29:1079, doi:10.1029/2001GL013366.

Karion, A., C. Sweeney, G. Pétron, G. Frost, R.M. Hardesty, J. Kofler, B.R. Miller, T. Newberger, S. Wolter, R. Banta, A. Brewer, E. Dlugokencky, P. Lang, S.A. Montzka, R. Schnell, P. Tans, M. Trainer, R. Zamora and S. Conley, 2013. Methane emissions estimate from airborne measurements over a western United States natural gas field. Geophysical Research Letters, 40:4393-4397.

Karl, D.M., L. Beversdorf, K.M. Björkman, M.J. Church, A. Martinez and E.F. Delong, 2008. Aerobic production of methane in the sea. Nature Geoscience, 1:473-478.

Kelly, D.L. and C.D. Kolstad, 1999. Integrated Assessment Models for Climate Change Control. In: Folmer H. and T. Tietenberg (eds.), International Yearbook of Environmental and Resource Economics 1999/2000: A Survey of Current Issues. Edward Elgar, Cheltenham, UK.

Kennett, J.P. and L.D. Stott, 1991. Abrupt deep-sea warming, palaeoceanographic changes and benthic extinctions at the end of the Palaeocene. Nature, 353:225-229.

Kennett, J.P., K.G. Cannariato, I.L. Hendy and R.J. Behl, 2000. Carbon isotopic evidence for methane hydrate instability during Quaternary interstadials. Science, 288:128-133.

Kennett, J.P., K.G. Cannariato, I.L. Hendy and R.J. Behl, 2003. Methane Hydrates in Quaternary Climate Change. American Geophysical Union, Washington, D.C.

Kiene, R.P., 1991. Production and consumption of methane in aquatic systems. In: Microbial Production and Consumption of Greenhouse Gases: Methane, Nitrogen Oxides, and Halomethanes, pp. 111-146. American Society for Microbiology, Washington D.C.

Kiene, R.P., L.J. Linn and J.A. Bruton, 2000. New and important roles for DMSP in marine microbial communities. Journal of Sea Research, 43:209-224.

Kip, N., J.F. van Winden, Y. Pan, L. Bodrossy, G.-J. Reichart, A.J.P. Smolders, M.S.M. Jessen, J.S. Simminghe Damste and H.J.M. Op den Camp, 2010. Global prevalence of methane oxidation by symbiotic bacteria in peat-moss ecosystems. Nature Geoscience, 3617-621.

Kirchgessner, D.A., R.A. Lott, R.M. Cowgill, M.R. Harrison and T.M. Shires, 1997. Estimate of methane emissions from the U.S. natural gas industry. Chemosphere, 35:1365-1390.

Kirkevåg, A., T. Iversen, Ø. Seland, C. Hoose, J.E. Kristjánsson, H. Struthers, A.M.L. Ekman, S. Ghan, J. Griesfeller, E.D. Nilsson and M. Schulz, 2013. Aerosol-climate interactions in the Norwegian Earth System Model – NorESM1-M. Geoscientific Model Development, 6:207-244.

Kirschke, S., P. Bousquet, P. Ciais, M. Saunois, J.G. Canadell, E.J. Dlugokencky, P. Bergamaschi, D. Bergmann, D.R. Blake, L. Bruhwiler, P. Cameron-Smith, S. Castaldi, F. Chevallier, L. Feng, A. Fraser, M. Heimann, E.L. Hodson, S. Houweling, B. Josse, P.J. Fraser, P.B. Krummel, J.-F. Lamarque, R.L. Langenfelds, C. Le Quéré, V. Naik, S. O'Doherty, P.L. Palmer, I. Pison, D. Plummer, B. Poulter, R.G. Prinn, M. Rigby, B. Ringeval, M. Santini, M. Schmidt, D.T. Shindell, I.J. Simpson, R. Spahni, L.P. Steele, S.A. Strode, K. Sudo, S. Szopa, G.R. van der Werf, A. Voulgarakis, M. van Weele, R.F. Weiss, J.E. Williams and G. Zeng, 2013. Three decades of global methane sources and sinks. Nature Geoscience, 6:813-823.

Kirtman, B., S.B. Power, J.A. Adedoyin, G.J. Boer, R. Bojariu, I. Camilloni, F.J. Doblas-Reyes, A.M. Fiore, M. Kimoto, G.A. Meehl, M. Prather, A. Sarr, C. Schär, R. Sutton, G.J. van Oldenborgh, G. Vecchi and H.J. Wang, 2013. Near-term climate change: Projections and predictability. In: Stocker, T.F., D. Qin,

G.-K. Plattner, M. Tignor, S.K. Allen, J. Boschung, A. Nauels, Y. Xia, V. Bex and P.M. Midgley (eds.), Climate Change 2013: The Physical Science Basis. Contribution of Working Group I to the Fifth Assessment Report of the Intergovernmental Panel on Climate Change. Cambridge University Press.

Klapstein, S.J., M.R. Turetsky, A.D. McGuire, J.W. Harden, C.I. Czimczik, X. Xu, J.P. Chanton and J.M. Waddington, 2014. Controls on methane released through ebullition in peatlands affected by permafrost degradation. Journal of Geophysical Research: Biogeosciences, 119:418-431.

Klauda, J.B. and S.I. Sandler, 2005. Global distribution of methane hydrate in ocean sediment. Energy Fuels, 19:459-470.

Knittel, K. and A. Boetius, 2009. Anaerobic oxidation of methane: progress with an unknown process. Annual Review of Microbiology, 63:311-334.

Knol, M.J., W.R. Pestman and D.E. Grobbee, 2011. The (mis)use of overlap of confidence intervals to assess effect modification. European Journal of Epidemiology, 26:253-254.

Kohnert, K., A. Serafimovich, J. Hartmann and T. Sachs, 2014. Airborne measurements of methane fluxes in Alaskan and Canadian tundra with the research aircraft Polar 5, Reports on polar and marine research. [online] Available from: http://epic.awi.de/35358/ (Accessed 9 April 2014).

Kort, E.A., S.C. Wofsy, B.C. Daube, M. Diao, J.W. Elkins, R.S. Gao, E.J. Hintsa, D.F. Hurst, R. Jimenez, F.L. Moore, J.R. Spackman and M.A. Zondlo, 2012. Atmospheric observations of Arctic Ocean methane emissions up to 82 degrees north. Nature Geoscience, 5:318-321.

Koven, C., P. Friedlingstein, P. Ciais, D. Khvorostyanov, G. Krinner and C. Tarnocai, 2009. On the formation of high-latitude soil carbon stocks: Effects of cryoturbation and insulation by organic matter in a land surface model. Geophysical Research Letters, 36:L21501, doi:10.1029/2009GL040150.

Kretschmer, K., A. Biastoch, L. Rüpke and E. Burwicz, 2015. Modeling the fate of methane hydrates under global warming. Global Biogeochemical Cycles, 29, doi:10.1002/2014GB005011.

Krol, M., S. Houweling, B. Bregman, M. van den Broek, A. Segers, P. van Velthoven, W. Peters, F. Dentener and P. Bergamaschi, 2005. The two-way nested global chemistry-transport zoom model TM5: algorithm and applications. Atmospheric Chemistry and Physics, 5:417-432.

Krull, E.S. and G.J. Retallack, 2000. δ^{13}C depth profiles from paleosols across the Permian-Triassic boundary: Evidence for methane release. Geological Society of America Bulletin, 112:1459-1472.

Kuhlmann, A.J., D.E.J. Worthy, N.B.A. Trivett and I. Levin, 1998. Methane emissions from a wetland region within the Hudson bay Lowland: An atmospheric approach. Journal of Geophysical Research:Atmospheres, 103:16,009-16,016.

Kvenvolden, K.A., 1988a. Methane hydrate – A major reservoir of carbon in the shallow geosphere? Chemical Geology, 71:41–51.

Kvenvolden, K.A., 1988b. Methane hydrates and global climate. Global Biogeochemical Cycles, 2:221-229.

Kvenvolden, K.A., 1993. Gas hydrates – geological perspective and global change. Reviews of Geophysics, 31:173-187.

Kvenvolden, K.A., M.D. Lilley, T.D. Lorenson, P.W. Barnes and E. McLaughlin, 1993. The Beaufort Sea continental shelf as a seasonal source of atmospheric methane. Geophysical Research Letters, 20:2459-2462.

Lamarque, J.F., T. Bond, V. Erying, C. Granier, A. Heil, Z. Klimont, D. Lee, C. Liousse, A. Mieville, B. Owen, M. Schultz, D. Shindell, S. Smith, E. Stehfest, J. Van Ardenne, O. Cooper, M. Kainuma, N. Mahowald, J. McConnell, V. Naik, K. Riahi and D. Van Vuuren, 2010. Historical (1850–2000) gridded anthropogenic and biomass burning emissions of reactive gases and aerosols: methodology and application. Atmospheric Chemistry and Physics, 10:7017-7039.

Lamarque, J.F., D.T Shindell, B. Josse, P.J Young, I. Cionni, V. Eyring, D. Bergmann, P. Cameron-Smith, W.J Collins, R. Doherty, S. Dalsoren, G. Faluvegi, G. Folberth, S.J Ghan, L.W Horowitz, Y.H Lee, I.A MacKenzie, T. Nagashima, V. Naik, D. Plummer, M. Righi, S.T Schulz, R.B Skeie, D.S Stevenson, S. Strode, K. Sudo, S. Szopa, A. Voulgarakis, G. Zeng, 2013. The Atmospheric Chemistry and Climate Model Intercomparison Project (ACCMIP): Overview and description of models, simulations and climate diagnostics. Geoscientific Model Development, 6:179-206.

Lamontagne, R.A., J.W. Swinnerton, V.J. Linnenbom and W.D. Smith, 1973. Methane concentrations in various marine environments. Journal of Geophysical Research, 78:5317-5324.

Large, W.G. and S.G. Yeager, 2008. The global climatology of an interannually varying air–sea flux data set. Climate Dynamics, 33:341-364.

Laske, G. and G. Masters, 1997. A global digital map of sediment thickness. Eos, Transactions, American Geophysical Union, 78, F483.

Leifer, I. and R.K. Patro, 2002. The bubble mechanism for methane transport from the shallow sea bed to the surface: A review and sensitivity study. Gas in Marine Sediments: Contributions from the 5th International Conference organized by the Shallow Gas Group, Bologna, Italy, September 1998, 22:2409-2428.

Lelieveld, J., F.J. Dentener, W. Peters and M.C. Krol, 2004. On the role of hydroxyl radicals in the self-cleansing capacity of the troposphere. Atmospheric Chemistry and Physics, 4:2337-2344.

Lelieveld, J., S. Lechtenböhmer, S.S. Assonov, C.A.M. Brenninkmeijer, C. Dienst, M. Fischedick and T. Hanke, 2005. Low methane leakage from gas pipelines. Nature, 434:841-842.

Lelieveld, J., T.M. Butler, J.N. Crowley, T.J. Dillon, H. Fischer, L. Ganzeveld, H. Harder, M.G. Lawrence, M. Martinez, D. Taraborrelli and J. Williams, 2008. Atmospheric oxidation capacity sustained by a tropical forest. Nature, 452:737-740.

Levin, I., C. Veidt, B.H. Vaughn, G. Brailsford, T. Bromley, R. Heinz, D. Lowe, J.B. Miller, C. Poß and J.W.C. White, 2012. No inter-hemispheric $\delta^{13}CH_4$ trend observed. Nature, 486:E3-E4, doi:10.1038/nature11175.

Levitus, S., T.P. Boyer, T.D. O'Brien, J. Antonov, C. Stephens, L. Stathoplos, D. Johnson and R. Gelfield, 1998. World Ocean Database 1998.

Locatelli, R., P. Bousquet, F. Chevallier, A. Fortems-Cheney, S. Szopa, M. Saunois, A. Agusti-Panareda, D. Bergmann, H. Bian, P. Cameron-Smith, M.P. Chipperfield, E. Gloor, S. Houweling, S.R. Kawa, M. Krol, P.K. Patra, R.G. Prinn, M. Rigby, R. Saito and C. Wilson, 2013. Impact of transport model errors on the global and regional methane emissions estimated by inverse modelling. Atmospheric Chemistry and Physics, 13:9917-9937.

Loulergue, L., A. Schilt, R. Spahni, V. Masson-Delmotte, T. Blunier, B. Lemieux, J.M. Barnola, D. Raynaud, T.F. Stocker and J. Chappellaz, 2008. Orbital and millennial-scale features of atmospheric CH_4 over the past 800,000 years. Nature, 453:383-386.

MacDonald, G.M., D.W. Beilman, K.V. Kremenetski, Y. Sheng, L.C. Smith and A.A. Velichko, 2006. A rapid early development of circumarctic peatlands and atmospheric CH_4 and CO_2 variations. Science, 314:285-288.

MacIntyre, S., A. Jonsson, M. Jansson, J. Aberg, D.E. Turney and S.D. Miller, 2010. Buoyancy flux, turbulence, and the gas transfer coefficient in a stratified lake. Geophysical Research Letters, 37:L24604, doi:10.1029/2010GL044164.

Madec, G., 2008. NEMO Ocean Engine. Institut Pierre-Simon Laplace (IPSL), France.

Manitoba Ministry of Conservation and Water Stewardship, 2009. Prescribed Landfills Regulation. Government of Manitoba, Canada.

Marín-Moreno, H., T.A. Minshull, G.K. Westbrook, B. Sinha and S. Sarkar, 2013. The response of methane hydrate beneath the seabed offshore Svalbard to ocean warming during the next three centuries. Geophysical Research Letters, 40:5159-5163.

Marty, D.G., 1993. Methanogenic bacteria in seawater. Limnology and Oceanography, 38:452-456.

Masarie, K.A., R.L. Langenfelds, C.E. Allison, T.J. Conway, E.J. Dlugokencky, R.J. Francey, P.C. Novelli, L.P. Steele, P.P. Tans, B. Vaughn and J.W.C. White, 2001. NOAA/CSIRO Flask Air Intercomparison Experiment: A strategy for directly assessing consistency among atmospheric measurements made by independent laboratories. Journal of Geophysical Research, 106:20445-20464.

Mastepanov, M., C. Sigsgaard, E.J. Dlugokencky, S. Houweling, L. Strom, P.P. Tamstorf and T.R. Christensen, 2008. Large tundra methane burst during onset of freezing. Nature, 456:628-631.

Mastepanov, M., C. Sigsgaard, T. Tagesson, L. Ström, M. Tamstorf, M. Lund and T.R. Christensen, 2013. Revisiting factors controlling methane emissions from high-Arctic tundra. Biogeosciences, 10:5139-5158.

Masui, T., K. Matsumoto, Y. Hijioka, T. Kinoshita, T. Nozawa, S. Ishiwatari, E. Kato, P.R. Shukla, Y. Yamagata and M. Kainuma, 2011. An emission pathway for stabilization at 6 Wm^{-2} radiative forcing. Climatic Change, 109:59-76.

Matthews, E., 1989. Global Data Bases on Distribution, Characteristics and Methane Emission of Natural Wetlands: Documentation of Archived Data Tape. NASA TM-4153. National Aeronautics and Space Administration.

Matthews, E. and I. Fung, 1987. Methane emission from natural wetlands: global distribution, area, and environmental characteristics of sources. Global Biogeochemical Cycles, 1:61-86.

Mauldin, R.L. III, F.L. Eisele, C.A. Cantrell, E. Kosciuch, B.A. Ridley, B. Lefer, D.J. Tanner, J.B. Nowak, G. Chen, L. Wang and D. Davis, 2001. Measurements of OH aboard the NASA P-3 during PEM-Tropics B. Journal of Geophysical Research, 106:32657-32666.

McCarthy, M.C., K.A. Boering, A.L. Rice, S.C. Tyler, P. Connell and E. Atlas, 2003. Carbon and hydrogen isotopic compositions of stratospheric methane: 2. Two-dimensional model results and implications for kinetic isotope effects. Journal of Geophysical Research, 108:4461, doi:10.1029/2002JD003183.

McGinnis, D.F., J. Greinert, Y. Artemov, S.E. Beaubien and A. Wüest, 2006. Fate of rising methane bubbles in stratified waters: How much methane reaches the atmosphere? Journal of Geophysical Research, 111:C09007, doi:10.1029/2005JC003183.

McGuire, A.D., L.G. Anderson, T.R. Christensen, S. Dallimore, L. Guo, D.J. Hayes, M. Heimann, T.D. Lorenson, R.W. Macdonald and N. Roulet, 2009. Sensitivity of the carbon cycle in the Arctic to climate change. Ecological Monographs, 79:523-555.

McGuire, A.D., R.W. Macdonald, E.A.G. Schuur, J.W. Harden, P. Kuhry, D.J. Hayes, T.R. Christensen and M. Heimann, 2010. The carbon budget of the northern cryosphere region. Current Opinion in Environmental Sustainability, 2:231-236.

McGuire, A.D., T.R. Christensen, D. Hayes, A. Heroult, E. Euskirchen, J.S. Kimball, C. Koven, P. Lafleur, P.A. Miller, W. Oechel, P. Peylin, M. Williams and Y. Yi, 2012. An assessment of the carbon balance of Arctic tundra: comparisons among observations, process models, and atmospheric inversions. Biogeosciences, 9:3185-3204.

McInerney, F.A. and S.L. Wing, 2011. The Paleocene-Eocene thermal maximum: A perturbation of carbon cycle, climate, and biosphere with implications for the future. Annual Review of Earth and Planetary Sciences, 39:489-516.

Meinshausen, M., S.J. Smith, K.V. Calvin, J.S. Daniel, M.L.T. Kainuma, J.-F. Lamarque, K. Matsumoto, S.A. Montzka, S.C.B. Raper, K. Riahi, A.M. Thomson, G.J.M. Velders and D. van Vuuren, 2011. The RCP Greenhouse Gas Concentrations and their Extension from 1765 to 2300. Climatic Change (Special Issue).

Melton, J.R., R. Wania, E.L. Hodson, B. Poulter, B. Ringeval, R. Spahni, T. Bohn, C.A. Avis, D.J. Beerling, G. Chen, A.V. Eliseev, S.N. Denisov, P.O. Hopcroft, D.P. Lettenmaier, W.J. Riley, J.S. Singarayer, Z.M Subin, H.Tian, S. Zurcher, V. Brovkin, P.M. van Bodegom, T. Kleinen, Z.C. Yu and J.O. Kaplan, 2013. Present state of global wetland extent and wetland methane modelling: conclusions from a model intercomparison project (WETCHIMP). Biogeosciences, 10:753-788.

MESSAGE, 2009. Data from MESSAGE model results received from S. Rao-Skirbekk on 30 January 2014. International Institute for Applied Systems Analysis, Laxenburg, Austria.

Migeotte, M.V., 1948. Spectroscopic evidence of methane in the Earth's atmosphere. Physical Review, 73:519-520.

Mikaloff Fletcher, S.E., P.P. Tans, L.M. Bruhwiler, J.B. Miller and M. Heimann, 2004a. CH_4 sources estimated from atmospheric observations of CH_4 and its $^{13}C/^{12}C$ isotopic ratios: 1. Inverse modeling of source processes. Global Biogeochemical Cycles, 18:GB4004, doi:10.1029/2004GB002223.

Mikaloff Fletcher, S.E., P.P. Tans, L.M. Bruhwiler, J.B. Miller and M. Heimann, 2004b. CH_4 sources estimated from atmospheric observations of CH_4 and its $^{13}C/^{12}C$ isotopic ratios: 2. Inverse modeling of CH_4 fluxes from geographical regions. Global Biogeochemical Cycles, 18:GB4005, doi:10.1029/2004GB002224.

Milkov, A.V., 2003. Global estimates of hydrate-bound gas in marine sediments: how much is really out there? Earth-Science Reviews, 66:183-197.

Milkov, A.V., 2005. Molecular and stable isotope compositions of natural gas hydrates: A revised global dataset and basic interpretations in the context of geological settings. Organic Geochemistry, 36:681-702.

Miller, S.D., C. Marandino and E.S. Saltzman, 2010. Ship-based measurement of air-sea CO_2 exchange by eddy covariance. Journal of Geophysical Research, 115:D02304, doi:10.1029/2009JD012193.

Miller, S.M., D.E.J. Worthy, A.M. Michalak, S.C. Wofsy, E.A. Kort, T.C. Havice, A.E. Andrews, E.J. Dlugokencky, J.O. Kaplan, P.J. Levi, H.T. Tian and B. Zhang, 2014. Observational constraints on the distribution, seasonality, and environmental predictors of North American boreal methane emissions. Global Biogeochemical Cycles, 28:146-160.

Montzka, S.A., M. Krol, E. Dlugokencky, B. Hall, P. Jöckel and J. Lelieveld, 2011. Small interannual variability of global atmospheric hydroxyl. Science, 331:67-69.

Moore, T.R. and N.T. Roulet, 1993. Methane flux – water-table relations in northern wetlands. Geophysical Research Letters, 20:587-590.

Moosavi, S.C. and P.M. Crill, 1997. Controls on CH_4 and CO_2 emissions along two moisture gradients in the Canadian boreal zone. Journal of Geophysical Research: Atmospheres, 102:29,261-29,277.

Moss, R., M. Babiker, S. Brinkman, E. Calvo, T. Carter, J. Edmonds, I. Elgizouli, S. Emori, L. Erda, K. Hibbard, R. Jones, M. Kainuma, J. Kelleher, J.F. Lamarque, M. Manning, B. Matthews, J. Meehl, L. Meyer, J. Mitchell, N. Nakicenovic, B. O'Neill, R. Pichs, K. Riahi, S. Rose, P. Runci, R. Stouffer, D. van Vuuren, J. Weyant, T. Wilbanks, J.P. van Ypersele and M. Zurek, 2008. Towards New Scenarios for Analysis of Emissions, Climate Change, Impacts and Response Strategies. Technical Summary. Intergovernmental Panel on Climate Change.

Moss, R.H., J.A. Edmonds, K.A. Hibbard, M.R. Manning, S.K. Rose, D.P. van Vuuren, T.R. Carter, S. Emori, M. Kainuma, T. Kram, G.A. Meehl, J.F.B. Mitchell, N. Nakicenovic, K. Riahi, S.J. Smith, R.J. Stouffer, A.M. Thomson, J.P. Weyant and T. Wilbanks, 2010. The next generation of scenarios for climate change research and assessment. Nature, 463:747-756.

Murrell, J.C., 2010. The aerobic methane oxidizing bacteria (Methanotrophs). In: K.N. Timmis (ed.), Handbook of Hydrocarbon and Lipid Microbiology, pp. 1953-1966. Springer.

Myhre, G., D. Shindell, F.-M. Bréon, W. Collins, J. Fuglestvedt, J. Huang, D. Koch, J.-F. Lamarque, D. Lee, B. Mendoza, T. Nakajima, A. Robock, G. Stephens, T. Takemura and H. Zhang, 2013. Anthropogenic and natural radiative forcing. In: Stocker, T.F., D. Qin, G.-K. Plattner, M. Tignor, S.K. Allen, J. Boschung, A. Nauels, Y. Xia, V. Bex and P.M. Midgley (eds.), Climate Change 2013: The Physical Science Basis. Contribution of Working Group I to the Fifth Assessment Report of the Intergovernmental Panel on Climate Change. Cambridge University Press.

Naik, V., A. Voulgarakis, A.M. Fiore, L.W. Horowitz, J.-F. Lamarque, M. Lin, M.J. Prather, P. J. Young, D. Bergmann, P. J. Cameron-Smith, I. Cionni, W.J. Collins, S.B. Dalsøren, R. Doherty, V. Eyring, G. Faluvegi, G.A. Folberth, B. Josse, Y.H. Lee, I.A. MacKenzie, T. Nagashima, T.P.C. van Noije, D.A. Plummer, M. Righi, S.T. Rumbold, R. Skeie, D.T. Shindell, D.S. Stevenson, S. Strode, K. Sudo, S. Szopa and G. Zeng, 2013. Preindustrial to present-day changes in tropospheric hydroxyl radical and methane lifetime from the Atmospheric Chemistry and Climate Model Intercomparison Project (ACCMIP). Atmospheric Chemistry and Physics, 13:5277-5298.

Nakazawa, T., M. Ishizawa, K. Higuchi and N.B.A. Trivett, 1997. Two curve fitting methods applied to CO_2 Flask data. Environmetrics, 8:197-218.

Nakicenovic, N., J. Alcamo, G. Davis, B. de Vries, J. Fenhann, S. Gaffin, K. Gregory, A. Grübler, T. Yong Jung, T. Kram, E. Lebre La Rovere, L. Michaelis, S. Mori, T. Morita, W. Pepper, H. Pitcher, L. Price, K. Riahi, A. Roehrl, H.-H. Rogner, A. Sankovski, M. Schlesinger, P. Shukla, S. Smith, R. Swart, S. van Rooijen, N. Victor and Z. Dadi, 2000. Special Report on Emissions Scenarios: A Special Report of Working Group III of the Intergovernmental Panel on Climate Change, Cambridge University Press.

Natali, S., E.A.G. Schuur, E.E. Webb, C.E. Hicks Pries and K.G. Crummer, 2014. Permafrost degradation stimulates carbon loss from experimentally warmed tundra. Ecology, 95:602-608.

Neale, R.B., C.-C. Chen, A. Gettelman, P.H. Lauritzen, S. Park, D.L. Williamson, A.J. Conley, R. Garcia, D. Kinnison, J.-F. Lamarque, D. Marsh, M. Mills, A.K. Smith, S. Tilmes, F. Vitt, H. Morrison, P. Cameron-Smith, W.D. Collins, M.J. Iacono, R.C. Easter, S.J. Ghan, X. Liu, P.J. Rasch, P.J. and M.A. Taylor, 2012. Description of the NCAR community atmosphere model (CAM 5.0), NCAR Tech. Note NCAR/TN-486+ STR.

New Brunswick Department of Energy and Mines, 2013. Responsible environmental management of oil and natural gas activities in New Brunswick: Rules for industry. Government of New Brunswick, Canada.

Nicolsky, D.J., V.E. Romanovsky, N.N. Romanovskii, A.L. Kholodov, N.E. Shakhova and I. Semiletov, 2012. Modeling sub-sea permafrost in the East Siberian Arctic Shelf: The Laptev Sea region. Journal of Geophysical Research, 117:F03028, doi:10.1029/2012JF002358.

Niemann, H., P. Linke, K. Knittel, E. MacPherson, A. Boetius, W. Brückmann, G. Larvik, K. Wallmann, U. Schacht, E. Omoregie, D. Hilton, K. Brown and G. Rehder, 2013. Methane-carbon flow into the benthic food web at cold seeps – A case study from the Costa Rica subduction zone. PLoS ONE, 8:e74894, doi:10.1371/journal.pone.0074894.

Nisbet, E.G., 1989. Some northern sources of atmospheric methane: production, history and future implications. Canadian Journal of Earth Sciences, 26:1603-1611.

Nisbet, E.G. (ed.), 2001. Russian emissions of atmospheric methane: Study of sources. Final Report INTAS 97-2055, European Commission, Brussels, Belgium.

Nisbet, E.G., 2002. Have sudden large releases of methane from geological reservoirs occurred since the Last Glacial Maximum, and could such releases occur again? Philosophical Transactions of the Royal Society A, 360:581-607.

Nisbet, E.G., E.J. Dlugokencky and P. Bousquet, 2014. Methane on the rise – again. Science, 343:493-495.

NOAA, 2010. Global Gas Flaring Estimates Database. National Geophysical Data Centre, Boulder.

Notz, D., V. Brovkin and M. Heimann, 2013. Arctic: Uncertainties in methane link. Nature, 500:529.

NRC, 2013. Committee on Understanding and Monitoring Abrupt Climate Change and its Impacts; Board on Atmospheric Climate and Sciences; Division of Earth and Life Studies. Abrupt Impacts of Climate Change: Anticipating Surprises. National Research Council (NRC), National Academies Press.

O'Keefe, A., J.J. Scherer and J.B. Paul, 1999. cw Integrated cavity output spectroscopy. Chemical Physics Letters, 307:343-349.

Olefeldt, D., M.R. Turetsky, P.M. Crill and A.D. McGuire, 2013. Environmental and physical controls on northern terrestrial methane emissions across permafrost zones. Global Change Biology, 19:589-603.

Olivier, J.G.J., G. Janssens-Maenhout and J.A.H.W. Peters, 2012. Trends in global CO_2 emissions – 2012 Report. Joint Research Centre of the European Commission and the Netherlands Environmental Assessment Agency (PBL), Netherlands.

Ontario Ministry of Energy, 2009. FIT and MicroFIT Program. Government of Ontario, Canada.

Ontario Ministry of Environment, 2007. Landfill gas collection and control regulation. Government of Ontario, Canada.

Oremland, R.S., 1979. Methanogenic activity in plankton samples and fish intestines: A mechanism for in situ methanogenesis in oceanic surface waters. Limnology and Oceanography, 24:1136-1141.

Overland, J.E., K.R. Wood and M. Wang, 2011a. Warm Arctic-cold continents: Impacts of the newly open Arctic Sea. Polar Research, 30:15787, doi:10.3402/polar.v30i0.15787.

Overland, J.E., M. Wang, J.E. Walsh, J.H. Christensen, V. Kattsov and W.L. Chapman, 2011b. Climate model projections for the Arctic. In: Snow, Water, Ice and Permafrost in the Arctic (SWIPA): Climate Change and the Cryosphere. Arctic Monitoring and Assessment Programme, Oslo, Norway.

Panieri, G., R.H. James, A. Camerlenghi, G.K. Westbrook, C. Consolaro, I. Cacho, V. Cesari and C.S. Cervera, 2014. Record of methane emissions from the West Svalbard continental margin during the last 23.500 yrs revealed by $\delta^{13}C$ of benthic foraminifera. Global and Planetary Change, 122:151-160.

Panikov, N.S., 1995. Microbial Growth Kinetics. Chapman & Hall.

Panikov, N.S. and S.N. Dedysh, 2000. Cold season CH_4 and CO_2 emission from boreal peat bogs (West Siberia): Winter fluxes and thaw activation dynamics. Global Biogeochemical Cycles, 14:1071-1080.

Park, W., N. Keenlyside, M. Latif, A. Ströh, R. Redler, E. Roeckner and G. Madec, 2010. Tropical Pacific climate and its response to global warming in the Kiel Climate Model. Journal of Climate, 22:71-92.

Parmentier, F.-J.W. and T.R. Christensen, 2013. Arctic: Speed of methane release. Nature, 500:529-529.

Parmentier, F.J.W., J. van Huissteden, N. Kip, H.J.M. Op den Camp, M.S.M. Jetten, T.C. Maximov and A.J. Dolman, 2011. The role of endophytic methane-oxidizing bacteria in submerged *Sphagnum* in determining methane emissions of Northeastern Siberian tundra. Biogeosciences, 8:1267-1278.

Parmentier, F.-J.W., T.R. Christensen, L.L. Sørensen, S. Rysgaard, A.D. McGuire, P.A. Miller and D.A. Walker, 2013. The impact of lower sea-ice extent on Arctic greenhouse-gas exchange. Nature Climate Change, 3:195-202.

Patra, P.K., S. Houweling, M. Krol, P. Bousquet, D. Belikov, D. Bergmann, H. Bian, P. Cameron-Smith, M.P. Chipperfield, K. Corbin, A. Fortems-Cheiney, A. Fraser, E. Gloor, P. Hess, A. Ito, S.R. Kawa, R.M. Law, Z. Loh, S. Maksyutov, L. Meng, P.I. Palmer, R.G. Prinn, M. Rigby, R. Saito and C. Wilson, 2011. TransCom model simulations of CH_4 and related species: linking transport, surface flux and chemical loss with CH_4 variability in the troposphere and lower stratosphere. Atmospheric Chemistry and Physics, 11:12813-12837.

Paull, C.K., W. Ussler and W.S. Holbrook, 2007a. Assessing methane release from the colossal Storegga submarine landslide. Geophysical Research Letters, 34:L04601, doi:10.1029/2006GL028331.

Paull, C.K., W. Ussler, S.R. Dallimore, S.M. Blasco, T.D. Lorenson, H. Melling, B.E. Medioli, F.M. Nixon and F.A. McLaughlin, 2007b. Origin of pingo-like features on the Beaufort Sea shelf and their possible relationship to decomposing methane gas hydrates. Geophysical Research Letters, 34:L01603, doi:10.1029/2006GL027977.

Pavelin, E.G., C.E. Johnson, S. Rughooputh and R. Toumi, 1999. Evaluation of pre-industrial surface ozone measurements made using Schönbein's method. Atmospheric Environment, 33:919-929.

Pedersen, J.A., M.A. Simpson, J.G. Bockheim and K. Kumar, 2011. Characterization of soil organic carbon in drained thaw-lake basins of Arctic Alaska using NMR and FTIR photoacoustic spectroscopy. Organic Geochemistry, 42:947-954.

PEI Ministry of Environment, Labour and Justice, 2009. Waste resource management regulations (article 22). Government of Prince Edward Island, Canada.

Petrescu, A.M.R., E.J.R. van Beek, J. van Huissteden, C. Prigent, T. Sachs, C.A.R. Corradi, F.J.W. Parmentier and A.J. Dolman, 2010. Modeling regional to global CH_4 emissions of boreal and arctic wetlands. Global Biogeochemical Cycles, 24: GB4009, doi:10.1029/2009GB003610.

Pétron, G., G. Frost, B.R. Miller, A.I. Hirsch, S.A. Montzka, A. Karion, M. Trainer, C. Sweeney, A.E. Andrews, L. Miller, J. Kofler, A. Bar-Ilan, E.D. Dlugokencky, L. Patrick, C.T. Moore Jr., T.B. Ryerson, K. Masarie, B. Hall, D. Guenther, D. Kitzis, J. Miller, D. Welsh, D. Wolfe, W. Neff and P. Tans, 2012. Hydrocarbon emissions characterization in the Colorado Front Range: A pilot study. Journal of Geophysical Research, 111:1-19.

PFC Energy, 2007. Using Russia's Associated Gas. Report prepared for the Global Gas Flaring Reduction Partnership and the World Bank, PFC Energy, Washington D.C.

Pickett-Heaps, C.A., D.J. Jacob, K.J. Wecht, E.A. Kort, S.C. Wofsy, G.S. Diskin, D.E.J. Worthy, J.O. Kaplan, I. Bey and J. Drevet, 2011. Magnitude and seasonality of wetland methane emissions from the Hudson Bay lowlands (Canada). Atmospheric Chemistry and Physics, 11:3773-3779.

Pierrehumbert, R.T., 2014. Short-lived climate pollution. Annual Review of Earth and Planetary Sciences, 42:341-379.

Pison, I., P. Bousquet, F. Chevallier, S. Szopa and D. Hauglustaine, 2009. Multi-species inversion of CH_4, CO and H_2 emissions from surface measurements. Atmospheric Chemistry and Physics, 9:5281-5297.

Pithan, F. and T. Mauritsen, 2014. Arctic amplification dominated by temperature feedbacks in contemporary climate models. Nature Geoscience, 7:181-184.

Portmann, R.W. and S. Solomon, 2007. Indirect radiative forcing of the ozone layer during the 21st century. Geophysical Research Letters, 34:L02813, doi:10.1029/2006GL028252.

Portnov, A., A.J. Smith, J. Mienert, G. Cherkashov, P. Rekant, P. Semenov, P. Serov and B. Vanshtein, 2013. Offshore permafrost decay and massive seabed methane escape in water depths >20 m at the South Kara Sea shelf. Geophysical Research Letters, 40:3962-3967.

Potter, C.S. and S.A. Klooster, 1997. Global model estimates of carbon and nitrogen storage in litter and soil pools: response to changes in vegetation quality and biomass allocation. Tellus, 49B:1-17.

Plug, L.J., C. Walls and B.M. Scott, 2008. Tundra lake changes from 1978 to 2001 on the Tuktoyaktuk Peninsula, western Canadian Arctic. Geophysical Research Letters, 35:L03502, doi:10.1029/2007GL032303.

Prather, M.J., C.D. Holmes and J. Hsu, 2012. Reactive greenhouse gas scenarios: Systematic exploration of uncertainties and the role of atmospheric chemistry. Geophysical Research Letters, 39:L09803, doi:10.1029/2012GL051440.

Prinn, R.G., J. Huang, R.F. Weiss, D.M. Cunnold, P.J. Fraser, P.G. Simmonds, A. McCulloch, C. Harth, S. Reimann, P. Salameh, S. O'Doherty, R.H.J. Wang, L.W. Porter, B.R. Miller and P.B. Krummel, 2005. Evidence for variability of atmospheric hydroxyl radicals over the past quarter century. Geophysical Research Letters, 32:L07809, doi:10.1029/2004GL022228.

Proskurowski, G., M.D. Lilley, J.S. Seewald, G.L. Früh-Green, E.J. Olson, J.E. Lupton, S.P. Sylva and D.S. Kelley, 2008. Abiogenic hydrocarbon production at Lost City hydrothermal field. Science, 319:604-607.

Québec MDDELCC, 2009. Issuance of offsets credits protocol 1: Covered manure storage facilities – CH_4 destruction. Québec Ministère du Développement durable, de l'Environnement et de la Lutte contre les changements climatiques, Gouvernement du Québec, Canada.

Québec MDDELCC, 2011. Règlement sur l'enfouissement et l'incinération de matières Résiduelles. Québec Ministère du Développement durable, de l'Environnement et de la Lutte contre les changements climatiques, Gouvernement du Québec, Canada.

Rajan, A., J. Mienert, S. Bünz and S. Chand, 2012. Potential serpentinization, degassing, and gas hydrate formation at a young (<20 MA) sedimented ocean crust off the Arctic Ocean ridge system. Journal of Geophysical Research: 117:B03102, doi:10.1029/2011JB008537.

Rajan, A., S. Bünz, J. Mienert and A.J. Smith, 2013. Gas hydrate systems in petroleum provinces of the SW-Barents Sea. Marine and Petroleum Geology, 46:92-106.

Reeburgh, W.S., 2007. Oceanic methane biogeochemistry. Chemical Reviews, 107:486-513.

Reeburgh, W.S., N.T. Roulet and B. Svensson, 1994. Terrestrial biosphere-atmosphere exchange in high latitudes. In: Prinn R.G. (ed.), Global Atmospheric-Biospheric Chemistry. Plenum Press.

Reed, D.L., E.A. Silver, J.E. Tagudin, T.H. Shipley and P. Vrolijk, 1990. Relations between mud volcanoes, thrust deformation, slope sedimentation, and gas hydrate, offshore north Panama. Marine and Petroleum Geology, 7:44-54.

Rehder, G., I. Leifer, P.G. Brewer, G. Friederich and E.T. Peltzer, 2009. Controls on methane bubble dissolution inside and outside the hydrate stability field from open ocean field experiments and numerical modeling. Marine Chemistry, 114:19-30.

Rhee, T.S., A.J. Kettle and M.O. Andreae, 2009. Methane and nitrous oxide emissions from the ocean: A reassessment using basin-wide observations in the Atlantic. Journal of Geophysical Research, 114:D12304, doi:10.1029/2008JD011662.

Riahi, K., S. Rao, V. Krey, C. Cho, V. Chirkov, G. Fischer, G. Kindermann, N. Nakicenovic and P. Rafaj, 2011. RCP 8.5 – A scenario of comparatively high greenhouse gas emissions. Climatic Change, 109:33-57.

Ridgwell, A.J., S.J. Marshall and K. Gregson, 1999. Consumption of atmospheric methane by soils: A process-based model. Global Biogeochemical Cycles, 13:59-70.

Riley, W.J., Z.M. Subin, D.M. Lawrence, S.C. Swenson, M.S. Torn, L. Meng, N.M. Mahowald and P. Hess, 2011. Barriers to predicting changes in global terrestrial methane fluxes: analyses using CLM4Me, a methane biogeochemistry model integrated in CESM. Biogeosciences, 8:1925-1953.

Ringeval, B., P. Friedlingstein, C. Koven, P. Ciais, N. de Noblet-Ducoudré, B. Decharme and P. Cadule, 2011. Climate-CH4 feedback from wetlands and its interaction with the climate-CO_2 feedback. Biogeosciences, 8:2137-2157.

Rinsland, C., J.S. Levine and T. Miles, 1985. Concentration of methane in the troposphere deduced from 1951 infrared solar spectra. Nature, 318:245-249.

Ritter, J., J. Barrick, G. Sachse, G. Gregory, M. Woerner, C. Watson, G. Hill and J. Collins, 1992. Airborne flux measurements of trace species in an Arctic boundary-layer. Journal of Geophysical Research: Atmospheres, 97:16,601-16,625.

Ritter, J.A., J.D.W. Barrick, C.E. Watson, G.W. Sachse, G.L. Gregory, B.E. Anderson, M.A. Woerner and J.E. Collins, 1994. Airborne boundary layer flux measurements of trace species over Canadian boreal forest and northern wetland regions. Journal of Geophysical Research: Atmospheres, 99:1671-1685.

Roach, J., B. Griffith, D. Verbyla and J. Jones, 2011. Mechanisms influencing changes in lake area in Alaskan boreal forest. Global Change Biology, 17:2567-2583.

Roeckner, E., 2003. The atmospheric general circulation model ECHAM5.

Rogelj, J., M. Schaeffer, M. Meinshausen, D.T. Shindell, W. Harec, Z. Klimont, G.J.M. Velders, M. Amann and H.J. Schellnhuber, 2014. Disentangling the effects of CO_2 and short-lived climate forcer mitigation. Proceedings of the National Academy of Sciences, 111:16325-16330.

Romankevich, E.A., A.A. Vetrov and V.I. Peresypkin, 2009. Organic matter of the World Ocean. Russian Geology and Geophysics, 50:299-307.

Romanovskii, N.N., H.W. Hubberten, A.V. Gavrilov, A.A. Eliseeva and G.S. Tipenko, 2005. Offshore permafrost and gas hydrate stability zone on the shelf of East Siberian Seas. Geo-Marine Letters, 25:167-182.

Roulet, N., T. Moore, J. Bubier and P. Lafleur, 1992. Northern fens: Methane flux and climatic change. Tellus, 44:100-105.

Roulet, N.T., A. Jano, C.A. Kelly, L.F. Klinger, T.R. Moore, R. Protz, J.A. Ritter and W.R. Rouse, 1994. The role of the Hudson Bay Lowland as a source of atmospheric methane. Journal of Geophysical Research, 99:1439-1454.

Rühs, S., J.V. Durgadoo, E. Behrens and A. Biastoch, 2013. Advective timescales and pathways of Agulhas leakage. Geophysical Research Letters, 40:3997-4000.

Ruppel, C.D., 2011. Methane hydrates and contemporary climate change. Nature Education Knowledge, 3:29 [online] Available from: www.nature.com/scitable/knowledge/library/methane-hydrates-and-contemporary-climate-change-24314790 (Accessed 19 November 2013).

Ruppel, C., 2014. Permafrost-associated gas hydrate: Is it really approximately 1% of the global system? Journal of Chemical and Engineering Data, 60:429-436.

Russ, P, J-C, Ciscar, B. Saveyn, A. Soria, L. Szabo, T. van Ierland, D. van Regemorter and R. Virdis, 2009. Economic Assessment of Post-2012 Global Climate Policies – Analysis of Gas Greenhouse Gas Emission Reduction Scenarios with the POLES and GEM-E3models. Joint Research Centre of the European Community, Seville, Spain.

Sachs, T., C. Wille, J. Boike and L. Kutzbach, 2008. Environmental controls on ecosystem-scale CH_4 emission from polygonal tundra in the Lena River Delta, Siberia. Journal of Geophysical Research, 113:G00A03, doi:10.1029/2007JG000505.

Sachs, T., M. Giebels, J. Boike and L. Kutzbach, 2010. Environmental controls on CH_4 emission from polygonal tundra on the microsite scale in the Lena river delta, Siberia. Global Change Biology, 16:3096-3110.

Sachs, T., A. Serafimovich and J. Hartmann, 2012. Airborne eddy covariance measurements of methane on the North Slope of Alaska and in the Mackenzie Delta, Canada. Abstract B24C-04. 2012 Fall Meeting, AGU, San Francisco, CA, 3-7 Dec.

Sanderson, M.G., 1996. Biomass of termites and their emissions of methane and carbon dioxide: A global database. Global Biogeochemical Cycles, 10:543-557.

Saskatchewan Ministry for Energy and Resources, 2011. Upstream Petroleum Industry Associated Gas. Conservation Directives S-10 and S-20. Government of Saskatchewan, Canada.

Schädel, C., E.A.G. Schuur, R. Bracho, B. Elberling, C. Knoblauch, H. Lee, Y. Luo, G.R. Shaver and M. Turetsky, 2014. Circumpolar assessment of permafrost C quality and its vulnerability over time using long-term incubation data. Global Change Biology, 20:641-652.

Schimel, J., 2004. Playing scales in the methane cycle: From microbial ecology to the globe. Proceedings of the National Academy of Sciences of the United States of America, 101:12400-12401.

Schirrmeister, L., V. Kunitsky, G. Grosse, S. Wetterich, H. Meyer, G. Schwamborn, O. Babiy, A. Derevyagin and C. Siegert, 2010. Sedimentary characteristics and origin of the Late Pleistocene Ice Complex on north-east Siberian Arctic coastal lowlands and islands. A review. Quaternary International, 241:3-25.

Schirrmeister, L., G. Grosse, S. Wetterich, P.P. Overduin, J. Strauss, E.A.G. Schuur and H.W. Hubberten, 2011. Fossil organic matter characteristics in permafrost deposits of the northeast Siberian Arctic. Journal of Geophysical Research, 116:G00M02, doi:10.1029/2011JG001647.

Schneider von Deimling, J., G. Rehder, J. Greinert, D.F. McGinnnis, A. Boetius and P. Linke, 2011. Quantification of seep-related methane gas emissions at Tommeliten, North Sea. Continental Shelf Research, 31:867-878.

Schuur, E.A.G., J. Bockheim, J.G. Canadell, E. Euskirchen, C.B. Field, S.V. Goryachkin, S. Hagemann, P. Kuhry, P.M. Lafleur, H. Lee, G. Mazhitova, F.E. Nelson, A. Rinke, V.E. Romanovsky, N. Shiklomanov, C. Tarnocai, S. Venevsky, J.G. Vogel and S.A. Zimov, 2008. Vulnerability of permafrost carbon to climate change: Implications for the global carbon cycle. BioScience, 58:701-714.

Schuur, E.A.G., B.W. Abbott, W.B. Bowden, V. Brovkin, P. Camill, J.G. Canadell, J.P. Chanton, F.S. Chapin III, T.R. Christensen, P. Ciais, B.T. Crosby, C.I. Czimczik, G. Grosse, J. Harden, D.J. Hayes, G. Hugelius, J.D. Jastrow, J.B. Jones, T. Kleinen, C.D. Koven, G. Krinner, P. Kuhry, D.M. Lawrence, A.D. McGuire, S.M. Natali, J.A. O'Donnell, C.L. Ping, W.J. Riley, A. Rinke, V.E. Romanovsky, A.B.K. Sannel, C. Schädel, K. Schaefer, J. Sky, Z.M. Subin, C. Tarnocai, M.R. Turetsky, M.P. Waldrop, K.M. Walter Anthony, K.P. Wickland, C.J. Wilson and S.A. Zimov, 2013. Expert assessment of vulnerability of permafrost carbon to climate change. Climatic Change, 119:359-374.

Schwietzke, S., W.M. Griffin, H.S. Matthews and L.M.P. Bruhwiler, 2014. Natural gas fugitive emissions rates constrained by global atmospheric methane and ethane. Environmental Science and Technology, 48:7714-7722.

Scranton, M.I. and P.G. Brewer, 1977. Occurrence of methane in the near-surface waters of the western subtropical North-Atlantic. Deep-Sea Research, 24:127-138.

Segers, R. and P.A. Leffelaar, 2001a. Modeling methane fluxes in wetlands with gas-transporting plants 3. Plot scale. Journal of Geophysical Research: Atmospheres, 106:3541-3558.

Segers, R. and P.A. Leffelaar, 2001b. Modeling methane fluxes in wetlands with gas-transporting plants 1. Single-root scale. Journal of Geophysical Research: Atmospheres, 106:3511-3528.

Seiter, K., C. Hensen, J. Schröter and M. Zabel, 2004. Organic carbon content in surface sediments – defining regional provinces. Deep Sea Research I, 51:2001-2026.

Serafimovich, A., S. Metzger, J. Hartmann, K. Kohnert and T. Sachs, 2013. The airborne measurements of methane fluxes (AIRMETH) Arctic Campaign. Abstract B43G-07. 2013 Fall Meeting, AGU, San Francisco, CA, 9-13 Dec.

Shakhova, N., I. Semiletov, A. Salyuk, V. Yusupov, D. Kosmach and O. Gustafsson, 2010. Extensive methane venting to the atmosphere from sediments of the East Siberian Arctic Shelf. Science 327:1246-1250.

Shakhova, N., I. Semilitov, I. Leifer, V. Sergienko, A., Salyuk, D. Kosmach, D. Chernykh, C. Stubbs, D. Nicolsky, V. Tumskoy and O. Gustafsson, 2014. Ebullition and storm-induced methane release from the East Siberian Arctic Shelf. Nature Geoscience, 7:64-70.

Shindell, D., 2007. Local and remote contributions to Arctic warming. Geophysical Research Letters, 34:L14704, doi:10.1029/2007GL030221.

Shindell, D.T., 2012. Evaluation of the absolute regional temperature potential. Atmospheric Chemistry and Physics, 12:7955-7960.

Shindell D. and G. Faluvegi, 2010. The net climate impact of coal-fired power plant emissions. Atmospheric Chemistry and Physics, 10:3247-3260.

Shindell, D. and J.C.I. Kuylenstierna, E. Vignati, R. van Dingenen, M. Amann, Z. Klimont, S.C. Anenberg, N. Muller, G. Janssens-Maenhout, F. Raes, J. Schwartz, G. Faluvegi, L. Pozzoli, K. Kupiainen, L. Höglund-Isaksson, L. Emberson, D. Streets, V. Ramanathan, K. Hicks, N.T. Kim Oanh, G. Milly, M. Williams, V. Demkine and D. Fowler, 2012. Simultaneously mitigating near-term climate change and improving human health and food security. Science, 335:183-189.

Shindell, D.T., O. Pechony, A. Voulgarakis, G. Faluvegi, L. Nazarenko, J.-F. Lamarque, K. Bowman, G. Milly, B. Kovari, R. Ruedy and G.A. Schmidt, 2013. Interactive ozone and methane chemistry in GISS-E2 historical and future climate simulations. Atmospheric Chemistry and Physics, 13:2653-2689.

Shine, K., J. Fuglestvedt, K. Hailemariam and N. Stuber, 2005: Alternatives to the global warming potential for comparing climate impacts of emissions of greenhouse gases. Climatic Change, 68:281-302.

Shirakova, L.S., O.S. Pokrovsky, S.N. Kirpotin, C. Desmukh, B.G. Pokrovsky, S. Audry and J. Viers, 2013. Biogeochemistry of organic carbon, CO_2, CH_4 and trace elements in thermokarst water bodies in discontinuous permafrost zones of Western Siberia. Biogeochemistry, 113:573-593.

Shoemaker, J.K. and D.P. Schrag, 2013. The danger of overvaluing methane's influence on future climate change. Climatic Change, 120:903-914.

Simpson, I.J., M.P. Sulbaek Andersen, S. Meinardi, L. Bruhwiler, N.J. Blake, D. Helmig, F.S. Rowland and D.R. Blake, 2012. Long-term decline of global atmospheric ethane concentrations and implications for methane. Nature, 488:490-494.

Singh, H.B., G.L. Gregory, B. Anderson, E. Browell, G.W. Sachse, D.D. Davis, J. Crawford, J.D. Bradshaw, R. Talbot, D.R. Blake, D. Thornton, R. Newell and J. Merill, 1996. Low ozone in the marine boundary layer of the tropical Pacific Ocean: Photochemical loss, chlorine atoms and entrainment. Journal of Geophysical Research, 101:1907-1917.

Sitch, S., A.D. McGuire, J. Kimball, N. Gedney, J. Gamon, R. Emgstrom, A. Wolf, Q. Zhuang and J. Clein, 2007a. Assessing the circumpolar carbon balance of arctic tundra with remote sensing and process-based modeling approaches. Ecological Applications, 17:213-234.

Sitch, S., P.M. Cox, W.J. Collins and C. Huntingford, 2007b. Indirect radiative forcing of climate change through ozone effects on the land-carbon sink. Nature, 448:791-794.

Skarke, A., C. Ruppel, M. Kodis, D. Brothers and E. Lobecker, 2014. Widespread methane leakage from the sea floor on the northern US Atlantic margin. Nature Geoscience, doi:10.1038/ngeo2232.

Slater, A.G. and D.M. Lawrence, 2013. Diagnosing present and future permafrost from climate models. Journal of Climate, 26:5608-5623.

Sluijs, A., S. Schouten, M. Pagani, M. Woltering, H. Brinkhuis, J.S.S. Damsté, G.R. Dickens, M. Huber, G.-J. Reichart, R. Stein, J. Matthiessen, L.J. Lourens, N. Pedentchouk, J. Backman, K. Moran and the Expedition 302 Scientists, 2006. Subtropical Arctic Ocean temperatures during the Palaeocene/Eocene thermal maximum. Nature, 441:610-613.

Smith, S.J. and A. Mizrahi, 2013. Near-term climate mitigation by short-lived forcers. Proceedings of the National Academy of Science, 110:14202-14206.

Smith, B., I. Prentice and M. Sykes, 2001. Representation of vegetation dynamics in modelling of terrestrial ecosystems: comparing two contrasting approaches within European climate space. Global Ecology and Biogeography, 10:621-637.

Solomon, E.A., M. Kastner, I.R. MacDonald and I. Leifer, 2009. Considerable methane fluxes to the atmosphere from hydrocarbon seeps in the Gulf of Mexico. Nature Geoscience, 2:561-565.

Søvde, O.A., M.J. Prather, I.S.A. Isaksen, T.K. Berntsen, F. Stordal, X. Zhu, C.D. Holmes and J. Hsu, 2012. The chemical transport model Oslo CTM3. Geoscientific Model Development, 5:1441-1469.

Sowers, T., 2006. Late Quaternary atmospheric CH_4 isotope record suggests marine clathrates are stable. Science, 311:838-840.

Spahni, R., R. Wania, L. Neef, M. Van Weele, L. Pison, P. Bousquet, C. Frankenberg, P.N. Foster, F. Joos, I.C. Prentice and P. van Velthoven, 2011. Constraining global methane emissions and uptake by ecosystems. Biogeosciences, 8:1643-1665.

SPARC, 2013. SPARC Report on the Lifetimes of Stratospheric Ozone-Depleting Substances, their Replacements, and Related Species. M.K.W. Ko, P.A. Newman, S. Reimann and S.E. Strahan (eds.), SPARC (Stratospheric Processes And Their Role in Climate) Report No. 6, WCRP-15/2013 (www.sparc-climate.org/publications/sparc-reports/sparc-report-no6).

Sriskantharajah, S., R.E. Fisher, D. Lowry, T. Aalto, J. Hatakka, M. Aurela, T. Laurila, A. Lohila, E. Kuitunen and E.G. Nisbet, 2012. Stable carbon isotope signatures of methane from a Finnish subarctic wetland. Tellus, 64B, 18818, 8p.

Steele, M., R. Morley and W. Ermold, 2001. PHC: A global ocean hydrography with a high-quality Arctic Ocean. Journal of Climate, 14:2079-2087.

Stefels, J., 2000. Physiological aspects of the production and conversion of DMSP in marine algae and higher plants. Journal of Sea Research, 43:183-197.

Stevenson, D.S., P.J. Young, V. Naik, J.-F. Lamarque, D.T. Shindell, A. Voulgarakis, R.B. Skeie, S.B. Dalsoren, G. Myhre, T.K. Berntsen, G.A. Folberth, S.T. Rumbold, W.J. Collins, I.A. MacKenzie, R.M. Doherty, G. Zeng, T.P.C. van Noije, A. Strunk D. Bergmann, P. Cameron-Smith, D.A. Plummer, S.A. Strode, L. Horowitz, Y.H. Lee, S. Szopa, K. Sudo, T. Nagashima, B. Josse, I. Cionni, M. Righi, V. Eyring, A. Conley, K.W. Bowman, O. Wild and A. Archibald, 2013. Tropospheric ozone changes, radiative forcing and attribution to emissions in the Atmospheric Chemistry and Climate Model Intercomparison Project (ACCMIP). Atmospheric Chemistry and Physics, 13:3063-3085.

Strauss, J., L. Schirrmeister, G. Grosse, S. Wetterich, M. Ulrich, U. Herzschuh and H.W. Hubberten, 2013. The deep permafrost carbon pool of the Yedoma region in Siberia and Alaska. Geophysical Research Letters, 40:6165-6170.

Ström, L., A. Ekberg and T.R. Christensen, 2003. Species-specific effects of vascular plants on carbon turnover and methane emissions from a tundra wetland. Global Change Biology, 9:1185-1192.

Svensson, B.H., 1976. Methane production in tundra peat. In: Schlegel, H.G., G. Gottschalk and N. Pfennig (eds.), Microbial Production and Utilization of Gases (H_2, CH_4, CO), pp. 135-139. E. Goltze.

Talling, P., M. Clare, M. Urlaub, E. Pope, J. Hunt and S. Watt, 2014. Large submarine landslides on continental slopes: geohazards, methane release, and climate change. Oceanography, 27:32-45.

Tans, P.P., I.Y. Fung and T. Takahashi, 1990. Observational constraints on the global atmospheric CO_2 budget. Science, 247:1431-1438.

Tarnocai, C., J.G. Canadell, E.A.G. Schuur, P. Kuhry, G. Mazhitova and S. Zimov, 2009. Soil organic carbon pools in the northern circumpolar permafrost region. Global Biogeochemical Cycles, 23:GB2023, doi:10.1029/2008GB003327.

Thatcher, K.E., G.K. Westbrook, S. Sarkar and T.A. Minshull, 2013. Methane release from warming-induced hydrate dissociation in the West Svalbard continental margin: Timing, rates, and geological controls. Journal of Geophysical Research: Solid Earth, 118:22-38.

Thomson, A.M., K.V. Calvin, S.J. Smith, G.P. Kyle, A. Volke, P. Patel, S. Delgado-Arias, B. Bond-Lamberty, M.A. Wise, L.E. Clarke and J.A. Edmonds, 2011. RCP4.5: a pathway for stabilization of radiative forcing by 2100. Climatic Change, 109:77-94.

Thoning, K.W., P.P. Tans and W.D. Komhyr, 1989. Atmospheric carbon dioxide at Mauna Loa Observatory, 2. Analysis of the NOAA/GMCC data, 1974-1985. Journal of Geophysical Research: Atmospheres, 94:8549-8565.

Tian, H., X. Xu, M. Liu, W. Ren, C. Zhang, G. Chen and C. Lu, 2010. Spatial and temporal patterns of CH_4 and N_2O fluxes in terrestrial ecosystems of North America during 1979-2008: application of a global biogeochemistry model. Biogeosciences, 7:2673-2694.

Tian, H., X. Xu, C. Lu, M. Liu, W. Ren, G. Chen, J.M. Melillo and J. Liu, 2011. Net exchanges of CO_2, CH_4, and N_2O between China's terrestrial ecosystems and the atmosphere and their contributions to global climate warming. Journal of Geophysical Research: Atmospheres, 116:1-13.

Tishchenko, P., C. Hensen, K. Wallmann and C.S. Wong, 2005. Calculation of the stability and solubility of methane hydrate in seawater. Chemical Geology, 219:37-52.

Treat, C., S.M. Natali, J. Ernakovich, C.M. Iversen, M. Lupascu, A.D. McGuire, R.J. Norby, T. Roy Chowdhury, A. Richter, H. Santruckova, C. Schädel, E.A.G. Schuur, V.L. Sloan, M.R. Turetsky and M. Waldrop, 2015. A pan-Arctic synthesis of potential CH_4 and CO_2 production from anoxic soil incubations. Global Change Biology doi/10.1111/gcb.12875.

Trenberth, K.E., P.D. Jones, P. Ambenje, R. Bojariu, D. Easterlinhg, A. Klein Tank, D. Parker, F. Rahimzadeh, J.A. Renwisk, M. Rusticucci, B. Soden and P. Zhai, 2007. Observations: Surface and atmospheric climate change. In: Solomon, S., D. Qin, M. Manning, Z. Chen, M. Marquis, K.B. Averyt, M. Tignor and H.L. Miller (eds.), Climate Change 2007: The Physical Science Basis, Contribution of Working Group I to the Fourth Assessment Report of the Intergovernmental Panel on Climate Change. Cambridge University Press.

Treude, T., A. Boetius, K. Knittel, K. Wallmann and B.B. Jørgensen, 2003. Anaerobic oxidation of methane above gas hydrates at Hydrate Ridge, NE Pacific Ocean. Marine Ecology Progress Series, 264:1-14.

Tripati, A. and H. Elderfield, 2005. Deep-sea temperature and circulation changes at the Paleocene-Eocene thermal maximum. Science, 308:1894-1898.

Turetsky, M.R., R.K. Wieder, D.H. Vitt, R.J. Evans and K.D. Scott, 2007. The disappearance of relict permafrost in boreal North America: Effects on peatland carbon storage and fluxes. Global Change Biology, 13:1922-1934.

Tyndall, J., 1861. On the absorbtion and radiation of heat by gases and vapours, and on the physical connexion of radiation, absorption and conduction – The Bakerian Lecture. Philosophical Magazine, 169-194.

Udo, H.M.J., H.A. Aklilu, L.T. Phong, R.H. Bosma, I.G.S. Budisatria, B.R. Patil, T. Samdup and B.O. Bebe, 2011. Impact of intensification of different types of livestock production in smallholder crop-livestock systems. Livestock Science 139:22-29.

UNEP, 2011a. Near-term Climate Protection and Clean Air Benefits: Actions for Controlling Short-lived Climate Forcers. United Nations Environment Programme (UNEP), Nairobi, Kenya.

UNEP, 2011b. Integrated Assessment of Black Carbon and Tropospheric Ozone. United Nations Environment Programme (UNEP), Nairobi, Kenya.

UNEP and WMO, 2011. Integrated Assessment of Black Carbon and Tropospheric Ozone. United Nations Environment Programme (UNEP) and World Meteorological Organization (WMO). UNON/Publishing Services Section/Nairobi.

UNFCCC, 2013. Common Reporting Format (CRF) tables and National Inventory Reports (NIRs). United Nations Framework Convention on Climate Change. Online at: http://unfccc.int/national_reports

USEPA, 2006. Global anthropogenic non-CO_2 greenhouse gas emissions: 1990-2020. United States Environmental Protection Agency, Washington D.C.

USEPA, 2011. Draft: Global Anthropogenic Non-CO_2 Greenhouse Gas Emissions: 1990-2030. EPA 430-R-03-002, United States Environmental Protection Agency, Washington D.C.

USEPA, 2012. Global Anthropogenic Non-CO_2 Greenhouse Gas Emissions: 1990-2030. EPA 430-R-12-006, US Environmental Protection Agency, Washington D.C.

USEPA, 2013. Integrated science assessment for ozone and related photochemical oxidants. EPA Report 600/R-10/076F, United States Environmental Protection Agency (US EPA).

USEPA, 2014. Overview of Greenhouse Gases – Methane Emissions. US Environmental Protection Agency. Online at: http://epa.gov/climatechange/ghgemissions/gases/ch4.html (accessed 2014-04-07).

Valentine, D.L., D.C. Blanton, W.S. Reeburgh and M. Kastner, 2001. Water column methane oxidation adjacent to an area of active hydrate dissociation, Eel river Basin. Geochimica et Cosmochimica Acta, 65:2633-2640.

van der Werf, G.R., J.T. Randerson, L. Giglio, G.J. Collatz, P.S. Kasibhatla and A.F. Arellano Jr., 2006. Interannual variability in global biomass burning emissions from 1997 to 2004. Atmospheric Chemistry and Physics, 6:3423-3441.

Van der Werf, G.R., J.T. Randerson, L. Giglio, G.J. Collatz, M. Mu, P.S. Kasibhatla, D.C. Morton, R.S. DeFries, Y. Jin and T.T. van Leeuwen, 2010. Global fire emissions and the contribution of deforestation, savanna, forest, agricultural, and peat fires (1997-2009). Atmospheric Chemistry and Physics, 10:11707-11735.

Van Huissteden, J. and A.J. Dolman, 2013. Soil carbon in the Arctic and the permafrost carbon feedback. Current Opinions in Environmental Sustainability, 4:545-551.

Van Huissteden, J., C. Berrittella, F.J.W. Parmentier, Y. Mi, T.C. Maximov and A.J. Dolman, 2011. Methane emissions from permafrost thaw lakes limited by lake drainage. Nature Climate Change, 1:119-123.

Van Huissteden, J., J. Vandenberghe, P.L. Gibbard and J. Lewin, 2013. Periglacial fluvial sediments and forms. Encyclopedia of Quaternary Science, 3:440-499.

van Vuuren, D.P., J. Edmonds, M. Kainuma, K. Riahi, A. Thomson, K. Hibbard, G.C. Hurtt, T. Kram, V. Krey, J.-F. Lamarque, T. Masui, M. Meinshausen, N. Nakicenovic, S.J. Smith and S.K. Rose, 2011a. The representative concentration pathways: An overview. Climatic Change, 109:5-31.

van Vuuren, D.P., E. Stehfest, M.G.J. den Elzen, T. Kram, J. van Vliet, S. Deetman, M. Isaac, K.K. Goldewijk, A. Hof, A. Mendoza Beltran, R. Oostenrijk and B. van Ruijven, 2011b. RCP2.6: exploring the possibility to keep global mean temperature increase below 2°C. Climatic Change, 109:95-116.

Volz, A. and D. Kley, 1988. Evaluation of the Montsouris series of ozone measurements made in the 19th century. Nature, 332:240-242.

Vonk, J. and Ö. Gustafsson, 2013. Permafrost-carbon complexities. Nature Geoscience, 6:675-676.

Voulgarakis, A., O. Wild, N.H. Savage, G.D. Carver and J.A. Pyle, 2009. Clouds, photolysis and regional tropospheric ozone budgets. Atmospheric Chemistry and Physics, 9:8235-8246.

Voulgarakis, A., V. Naik, J. Lamarque, D. Shindell, P. Young, M. Prather, O. Wild, R. Field, D. Bergmann, P. Cameron-Smith, I. Cionni, W. Collins, S. Dalsoren, R. Doherty, V. Eyring, G. Faluvegi, G. Folberth, L. Horowitz, B. Josse, I. MacKenzie, T. Nagashima, D. Plummer, M. Righi, S. Rumbold, D. Stevenson, S. Strode, K. Sudo, S. Szopa and G. Zeng, 2013. Analysis of present day and future OH and methane lifetime in the ACCMIP simulations. Atmospheric Chemistry and Physics, 13:2563-2587.

Wahlen, M., 1993. The global methane cycle. Annual Review of Earth and Planetary Science, 21:407-426.

Wallmann, K., E. Pinero, E. Burwicz, M. Haeckel, C. Hensen, A. Dale and L. Ruepke, 2012. The global inventory of methane hydrate in marine sediments: A theoretical approach. Energies, 5:2449-2498.

Walsh, J.E., J.E. Overland, P.Y. Groisman and B. Rudolf, 2011. Arctic climate: Recent variations. In: Snow, Water, Ice and Permafrost in the Arctic (SWIPA): Climate Change and the Cryosphere. Arctic Monitoring and Assessment Programme, Oslo, Norway.

Walter, B.P. and M. Heimann, 2000. A process-based, climate-sensitive model to derive methane emissions from natural wetlands: Application to five wetland sites, sensitivity to model parameters, and climate. Global Biogeochemical Cycles, 14:745-766.

Walter, B.P., M. Heimann and E. Matthews, 2001. Modeling modern methane emissions from natural wetlands 1. Model description and results. Journal of Geophysical Research: Atmospheres, 106:34,189-34,206.

Walter, K.M., S.A. Zimov, J.P. Chanton, D. Verbyla and F.S. Chapin, 2006. Methane bubbling from Siberian thaw lakes as a positive feedback to climate warming. Nature, 443:71-75.

Walter, K.M., M.E. Edwards, G. Grosse, S.A. Zimov and F.S. Chapin, 2007. Thermokarst lakes as a source of atmospheric CH_4 during the last deglaciation. Science, 318:633-636.

Walter Anthony, K.M. and P. Anthony, 2013. Constraining spatial variability of methane ebullition seeps in thermokarst lakes using point process models. Journal of Geophysical Research: Biogeosciences, 118:1015-1034.

Walter Anthony, K., L.C. Smith and F.S. Chapin III, 2007. Methane bubbling from northern lakes: present and future contributions to the global methane budget. Philosophical Transactions of the Royal Society A, 365:1657-1676.

Walter Anthony, K., P. Anthony, G. Grosse and J. Chanton, 2012. Geologic methane seeps along boundaries of Arctic permafrost thaw and melting glaciers. Nature Geoscience, 5:419-426.

Walter Anthony, K.M., S.A. Zimov, G. Grosse, M.C. Jones, P.M. Anthony, F.S. Chapin III, J.C. Finlay, M.C. Mack, S. Davydov, P. Frenzel and S. Frolking, 2014. A shift of thermokarst lakes from carbon sources to sinks during the Holocene epoch. Nature, 511:452-456.

Wang, Y. and D.J. Jacob, 1998. Anthropogenic forcing on tropospheric ozone and OH since preindustrial times. Journal of Geophysical Research D, 103:31123-31135.

Wang, X.L. and V.R. Swail, 2001. Changes of extreme wave heights in northern hemisphere oceans and related atmospheric circulation regimes. Journal of Climate, 14:2204-2221.

Wania, R., 2007. Modelling northern peatland land surface processes, vegetation dynamics and methane emissions. PhD thesis, University of Bristol, UK.

Wania, R., I. Ross and I.C. Prentice, 2010a. Implementation and evaluation of a new methane model within a dynamic global vegetation model: LPJ-WHyMe v1.3.1. Geoscientific Model Development, 3:565-584.

Wania, R., I. Ross and I. C. Prentice, 2010b. Implementation and evaluation of a new methane model within a dynamic global vegetation model LPJ-WHyMe v1.3. Geoscientific Model Development Discussions, 3:1-59.

Wania, R. J.R. Melton, E.L. Hodson, B. Poulter, B. Ringeval, R. Spahni, T. Bohn, C.A. Avis, G. Chen, A.V. Eliseev, P.O. Hopcroft, W.J. Riley, Z.M. Subin, H. Tian, P.M. van Bodegom, T. Kleinen, Z.C. Yu, J.S. Singarayer, S. Zürcher, D.P. Lettenmaier, D.J. Beerling, S.N. Denisov, C. Prigent, F. Papa and J.O. Kaplan, 2013. Present state of global wetland extent and wetland methane modelling: methodology of a model inter-comparison project (WETCHIMP). Geoscientific Model Development, 6:617-641.

Wanninkhof, R., 1992. Relationship between wind speed and gas exchange over the ocean. Journal of Geophysical Research: Oceans, 97:7373-7382.

Wanninkhof, R., 2014. Relationship between wind speed and gas exchange over the ocean revisited. Limnology and Oceanography: Methods, 12:351-362.

Wanninkhof, R., W.E. Asher, D.T. Ho, C. Sweeney and W.R. McGillis, 2009. Advances in quantifying air-sea gas exchange and environmental forcing. Annual Review of Marine Science, 1:213-244.

Watts, J.D., J.S. Kimball, F.J.W. Parmentier, T. Sachs, J. Rinne, D. Zona, W. Oechel, T. Tagesson, M. Jackowicz-Korczyński and M. Aurela, 2014. A satellite data driven biophysical modeling approach for estimating northern peatland and tundra CO_2 and CH_4 fluxes. Biogeosciences, 11:1961-1980.

Wennberg, P.O., T.F. Hanisco, R.C. Cohen, R.M. Stimpfle, L.B. Lapson and J.G. Anderson, 1995. In situ measurements of OH and HO_2 in the upper troposphere and stratosphere. Journal of the Atmospheric Sciences, 52:3413-3420.

Westbrook, G., K. Thatcher, E.J. Rohling, A.M. Piotrowski, H. Palike, A.H. Osborne, E.G. Nisbet, T.A. Minshull, M. Lanoisellé, R.H. James, V. Huhnerbach, D. Green, R.E. Fisher, A.J. Crocker, A. Chabert, C. Bolton, A. Beszcynska-Moller, C. Berndt and A. Aquilina, 2009. Escape of methane gas from the seabed along the West Spitsbergen continental margin. Geophysical Research Letters, 36, L15608, doi:10.1029/2009GL039191.

Whalen, S.C. and W.S. Reeburgh, 1990a. A methane flux transect along the trans-Alaska pipeline haul road. Tellus, 42B:237-249.

Whalen, S.C. and W.S. Reeburgh, 1990b. Consumption of atmospheric methane by tundra soils. Nature, 346:160-162.

Whalen, S.C. and W.S. Reeburgh, 1992. Interannual variations in tundra methane emissions: A four-year time-series at fixed sites. Global Biogeochemical Cycles, 6:139-159.

Wik, M., P.M. Crill, D. Bastviken, Å. Danielsson and E. Norbäck, 2011. Bubbles trapped in arctic lake ice: Potential implications for methane emissions. Journal of Geophysical Research, 116: G03044, doi:10.1029/2011JG001761.

Wik, M., B.F. Thornton, D. Bastviken, S. MacIntyre, R.K. Varner and P.M. Crill, 2014. Energy input is primary controller of methane bubbling in subarctic lakes, Geophysical Reseach Letters, 41:555-560.

Wild, O. and P.I. Palmer, 2008. How sensitive is tropospheric oxidation to anthropogenic emissions? Geophysical Research Letters, 35:L22802, doi:10.1029/2008GL035718.

Wille, C., L. Kutzbach, T. Sachs, D. Wagner and E.-M. Pfeiffer, 2008. Methane emission from Siberian arctic polygonal tundra: eddy covariance measurements and modeling. Global Change Biology, 14:1395-1408.

WMO, 2005. Thirteenth WMO/IAEA Meeting of Experts on Carbon Dioxide Concentration and Related Tracers Measurement Techniques. Boulder, Colorado, USA, 19-22 September 2005. J.B. Miller (ed.), World Meteorological Organization (WMO), WMO TD No. 1336.

WMO, 2014. WMO statement on the status of the global climate in 2013. WMO-No. 1130, World Meteorological Organization, Geneva, Switzerland.

Wolf, A., T.V. Callaghan and K. Larson, 2008. Future changes in vegetation and ecosystem function of the Barents Region. Climatic Change, 87:51-73.

Worthy, D.E.J., N.B.A. Trivett, J.F. Hopper, J.W. Bottenheim and I. Levin, 1994. Analysis of long range transport events at Alert, N.W.T., during the Polar Sunrise Experiment. Journal of Geophysical Research, 99:25329-25344.

Worthy, D.E.J., I. Levin, N.B.A. Trivett, A.J. Kuhlmann, J.F. Hopper and M.K. Ernst, 1998. Seven years of continuous methane observations at a remote boreal site in Ontario, Canada. Journal of Geophysical Research: Atmospheres, 103:15,995-16,007.

Worthy, D E.J., A. Platt, R. Kessler, M. Ernst, C. Audette and S, Racki, 2005. An update on the Canadian GHG measurement program. In: Report of the 12th WMO/IAEA Meeting of Experts on Carbon Dioxide Concentration and Related Tracer Measurement Techniques, Toronto, Canada, September 2003. D. Worthy and L. Huang (eds.), World Meteorological Organization Global Atmosphere Watch, Report 162, pp. 220-231.

Worthy, D.E.J., E. Chan, M. Ishizawa, D. Chan, C. Poss, E.J. Dlugokencky, S. Maksyutov and I. Levin, 2009. Decreasing anthropogenic methane emissions in Europe and Siberia inferred from continuous carbon dioxide and methane observations at Alert, Canada. Journal of Geophysical Research, 114:D10301, doi:10.1029/2008JD011239.

Young, P.J., A.T. Archibald, K.W. Bowman, J.-F. Lamarque, V. Naik, D.S. Stevenson, S. Tilmes, A. Voulgarakis, O. Wild, D. Bergmann, P. Cameron-Smith, I. Cionni, W.J. Collins, S.B. Dalsøren, R.M. Doherty, V. Eyring, G. Faluvegi, L.W. Horowitz, B. Josse, Y.H. Lee, I.A. MacKenzie, T. Nagashima, D.A. Plummer, M. Righi, S.T. Rumbold, R.B. Skeie, D.T. Shindell, S.A. Strode, K. Sudo, S. Szopa and G. Zeng, 2013. Pre-industrial to end 21st century projections of tropospheric ozone from the Atmospheric Chemistry and Climate Model Intercomparison Project (ACCMIP). Atmospheric Chemistry and Physics, 13:2063-2090.

Yvon-Durocher, G., A.P. Allen, D. Bastviken, R. Conrad, C. Gudasz, A. St-Pierre, N. Thanh-Duc and P.A. Del Giorgio, 2014. Methane fluxes show consistent temperature dependence across microbial to ecosystem scales. Nature, 507:488-491.

Zachos, J., M. Pagani, L. Sloan, E. Thomas and K. Billups, 2001. Trends, rhythms, and aberrations in global climate 65 Ma to present. Science, 292:686-693.

Zachos, J.C., U. Röhl, S.A. Schellenberg, A. Sluijs, D.A. Hodell, D.C. Kelly, E. Thomas, M. Nicolo, I. Raffi, L.J. Lourens, H. McCarren and D. Kroon, 2005. Rapid acidification of the ocean during the Paleocene-Eocene thermal maximum. Science, 308:1611-1615.

Zhang, Y., C.S. Li, C.C. Trettin, H. Li and G. Sun, 2002. An integrated model of soil, hydrology, and vegetation for carbon dynamics in wetland ecosystems. Global Biogeochemical Cycles, 16:9.1-9.17.

Zhang, Y., T. Sachs, C. Li and J. Boike, 2012. Upscaling methane fluxes from closed chambers to eddy covariance based on a permafrost biogeochemistry integrated model. Global Change Biology, 18:1428-1440.

Zhang, W., P. Miller, B. Smith, R. Wania, T. Koenigk and R. Doscher, 2013. Tundra shrubification and tree-line advance amplify arctic climate warming: results from an individual-based dynamic vegetation model. Environmental Research Letters, 8:034023, doi:10.1088/1748-9326/8/3/034023.

Zhou, J., J.L. Tison, G. Carnat, N.X. Geilfus and B. Delille, 2014. Physical controls on the storage of methane in landfast sea ice. The Cryosphere Discussions, 8:121-147.

Zhuang, Q., J.M. Melillo, D.W. Kicklighter, R.G. Prinn, A.D. McGuire, P.A. Steudler, B.S. Felzer and S. Hu, 2004. Methane fluxes between terrestrial ecosystems and the atmosphere at northern high latitudes during the past century: A retrospective analysis with a process-based biogeochemistry model. Global Biogeochemical Cycles, 18:GB3010, doi: 10.1029/2004GB002239.

Zimov, S.A., S.P. Davydov, G.M. Zimova, A.I. Davydova, E.A.G. Schuur, K. Dutta and F.S. Chapin III, 2006. Permafrost carbon: Stock and decomposability of a globally significant carbon pool. Geophysical Research Letters, 33:L20502, doi:10.1029/2006GL027484.

Acronyms and abbreviations

τ_{CH4}	Atmospheric methane lifetime
$\delta\,^{13}C_{CH4}$	Methane isotope, carbon isotope of methane
ACCMIP	Atmospheric Chemistry Climate Model Intercomparison Project
AIM	Asia-Pacific Integrated Model
AMAP	Arctic Monitoring and Assessment Programme
AR5	The Fifth Assessment Report (of the IPCC)
CanESM2	Canadian Earth System Model
CARVE	Carbon in Arctic Reservoirs Vulnerability Experiment (NASA)
CESM1	Community Earth System Model CESM1-CAM5
CH_4	Methane
CIE	Carbon Isotope Excursion
CLE	Current LEgislation scenario
CMIP5	Phase 5 of the coupled model intercomparison project
CO	Carbon monoxide
CO_2	Carbon dioxide
CO_2eq	Carbon dioxide equivalent
CTM	Chemistry Transport Model
EC-JRC	European Commission - Joint Research Centre
EDGAR	Emissions Database for Global Atmospheric Research (EC-JRC)
ESAS	East Siberian Arctic Shelf
ESM	Earth System Model
GAINS	Greenhouse gas and Air pollutant Interactions and Synergies model (IIASA)
GAW	Global Atmosphere Watch program (of the WMO)
GCAM	Global Change Assessment Model
GHSZ	Gas hydrate stability zone
IAM	Integrated Assessment Model
IEA	International Energy Agency
IIASA	International Institute for Applied Systems Analysis (Austria)
IMAGE	Integrated Model to Assess the Greenhouse Effect (PBL)
INSTAAR	Institute of Arctic and Alpine Research
IPCC	Intergovernmental Panel on Climate Change
LST	Local standard time
MACC	Marginal abatement cost curve
MESSAGE	Model of Energy Supply Systems and the General Environmental Impacts (IIASA)
MFR	Maximum technically Feasible Reductions scenario
N_2	Molecular nitrogen
N_2O	Nitrous oxide
nmOP	Non-methane ozone precursors
nmVOC	Non-methane volatile organic compound

NO	Nitrogen monoxide
NO_2	Nitrogen dioxide
NOAA	National Oceanic and Atmospheric Administration (US)
NorESM	Norwegian Earth System Model
NOx	Nitrogen oxides
$O(^1D)$	Excited atomic oxygen
O_2	Molecular oxygen
O_3	Ozone
OH	Hydroxyl radical
PBL	Environmental Assessment Agency (Netherlands)
ppb	Parts per billion, 10^9
RCP	Representative Concentration Pathway (IPCC)
RHUL	Royal Holloway, University of London
SLCF	Short-lived climate forcer
SOM	Soil organic matter
TF-HTAP	Task Force on Hemispheric Transport of Air Pollution
UNFCCC	United Nations Framework Convention on Climate Change
USEPA	United States Environmental Protection Agency
WETCHIMP	Wetland and Wetland CH4 Inter-comparison of Models Project
WMO	World Meteorological Organization

ARCTIC COUNCIL

AMAP
Arctic Monitoring and
Assessment Programme